Strategies to improve the efficiency of oxidation reactions of the enzyme Cytochrome P450Bm3

Shaghayegh Dezvarei

Supervisors

Assoc. Prof. Stephen G. Bell

Prof. Christian Doonan

Thesis submitted for the degree of Doctor of Philosophy

Department of Chemistry

School of Physical Sciences

University of Adelaide

May 2019

Content

Table of Figures, Tables and Equations

Citations

1. Munday, S. D.; Dezvarei, S.; Bell, S. G., Increasing the Activity and Efficiency of Stereoselective Oxidations by using Decoy Molecules in Combination with Rate-Enhancing Variants of P450Bm3. ChemCatChem 2016, 8 (17), 2789-2796.

2. Munday, S. D.; Dezvarei, S.; Lau, I. C. K.; Bell, S. G., Examination of Selectivity in the Oxidation of ortho- and meta-Disubstituted Benzenes by CYP102A1 (P450 Bm3) Variants. ChemCatChem 2017, 9 (13), 2512-2522.

3. Dezvarei, S.; Lee, J. H. Z.; Bell, S. G., Stereoselective hydroxylation of isophorone by variants of the cytochromes P450 CYP102A1 and CYP101A1. Enzyme Microb Technol 2018, 111, 29-37.

4. Dezvarei, S.; Onoda, H.; Shoji, O.; Watanabe, Y.; Bell, S. G., Efficient hydroxylation of cycloalkanes by co-addition of decoy molecules to variants of the cytochrome P450 CYP102A1. J Inorg Biochem 2018, 183, 137-145.

5. Dezvarei, S.; Shoji, O.; Watanabe, Y.; Bell, S. G., The effect of decoy molecules on the activity of the P450Bm3 holoenzyme and a heme domain peroxygenase variant. Catal Commun 2019, 124, 97-102.

Abstract

Selective and efficient C-H bond oxidation using conventional organic methods is a challenging task. As biocatalysts, cytochrome P450 enzymes provide an enzymatic route for the oxidation of unreactive carbon-hydrogen (C-H) bonds. CYP102A1 (P450Bm3) from the *Bacillus megaterium* bacterium is one of the most studied members of the P450 superfamily because of its solubility and high activity towards fatty acids (C12-15). P450Bm3 is a self-sufficient enzyme and only needs NADPH (as a source of electrons) and O_2 for oxidation reactions.

The primary subject of this thesis is exploring the regio- and stereoselectivity of four rate accelerating variants of P450Bm3: KT2 (A191T/N239H/I259V/A276T/L353I), R19 (R47L/Y51F/H171L/Q307H/N319Y), RLYFIP (R47L/Y51F/I401P) and RLYFAP (R47L/Y51F/A330P), in the oxidation of substituted benzenes that contain different alkyl and vinyl groups. Whereas wild type (WT) P450Bm3 showed low activity for the oxidation of these substrates, the mutated variants showed high product formation rates and maintained the regioselectivity of WT P450Bm3. However, the RLYFAP variant, which contains an alanine330 (A330) to proline mutation (A330P) resulted in different regioselectivity. For example, oxidation of 3-ethyltoluene with RLYFAP occurred at the benzene ring and generated a phenol product (2-ethyl-4-methylphenol, 92 %) in contrast to the WT, R19, KT2 and RLYFIP variants, which oxidised the alkyl side chain and the aromatic ring with equal yields.

The effects of polyfluorinated fatty acids (PFCs) on the activity and selectivity of P450Bm3 variants were also studied. Decoy molecules are dummy substrates with a similar structure to fatty acids. Therefore, the carboxylate group interacts with key residues of P450Bm3 (Arg47 and Tyr51) and places the enzyme in a catalytically ready state while leaving enough space for

non-native species to get close to the haem centre. The addition of decoy molecules to the variants increased the range of the substrates along with providing higher productivity. The regioselectivity of the enzyme that catalysed oxidations was maintained and the stereoselectivity slightly improved. For example, the addition of PFC10 to the WT Bm3 in the oxidation of ethylbenzene enhanced the enantiomeric excess from 48 % to 68% (*R*).

4-Hydroxyisophorone is a flavour and fragrance compound and the selective oxidation of isophorone to (*R*)-4-hydroxyisophorone with RLYFIP, R19, WT and GVQ (A74G/F87V/L188Q) variants was studied. GVQ and RLYFIP showed a 280-fold increase in oxidation activity over WT. Addition of decoy molecules further increased oxidation activity with the majority of the variants. However, decoy molecules reduced the activity of the GVQ variant for the reaction. The product distributions with the variants were almost identical and (*R*)-4-hydroxyisophorone was the main product with > 90 % ee.

The decoy molecules (PFC3-PFC10) were employed in the hydroxylation of cycloalkanes (C5-C10) to investigate how the combination of different sizes of substrates and decoy molecules changes the oxidation activity of the WT P450Bm3 and its variants. The highest product formation was observed with cyclooctane. The combination of decoy molecules with WT P450Bm3 and other variants increased productivity. By increasing the size of the decoy molecule, higher activity was achieved, and PFC10 was the best decoy molecules in all variants, excluding the GVQ variant, which showed lower activity with decoy molecules. Second generation decoy molecules, which are a combination of first-generation decoy molecules (PFC9) and amino acids were also employed in the hydroxylation of cycloalkanes as well and significantly improved the activity of P450Bm3WT in the oxidation of smaller substrates (cyclopentane and cyclohexane) to the corresponding cyclic alcohol (cyclopentanol

and cyclohexanol). It is hypothesised that the incorporation of amino acid into the decoy molecules better-allowed interaction with the active site of the P450Bm3.

A single mutation of threonine 268, which is involved in dioxygen activation, to glutamic acid (T268E) was made to the haem domain of P450Bm3 WT. This mutant was found to convert WT Bm3 into an H_2O_2-dependent variant (Bm3T268E or Bm3TE). The activity of Bm3TE in the oxidation of styrene, ethylbenzene and methylthiobenzene in the presence of H_2O_2 was tested and compared with the holoenzymes (WT and R19 variants). While no activity was observed with WT and R19 variants, Bm3TE successfully oxidised the substrates above. The addition of the second generation decoy molecules to holoenzymes enhanced the oxidation activity, but they did not significantly improve the activity of Bm3TE. The regioselectivity was maintained with the Bm3TE variant although stereoselectivity of ethylbenzene oxidation changed and was more in favour of the (*S*) enantiomer.

Finally, encapsulation of Bm3TE in metal-organic frameworks (MOFs) was studied. Since Zeolitic imidazolate frameworks (ZIFs) can be synthesised under mild conditions, ZIF-8 and ZIF-90 crystals were the candidates MOFs for in-situ encapsulation of Bm3TE to increase thermal and chemical stability. It was found that Bm3TE lost almost all its activity in the process of encapsulation. Therefore, ZIF-8 and ZIF-90 crystals were pre-synthesised to study immobilisation of Bm3TE on the surface. But again, no activity was observed.

Given that organic ligands and MOF surface were a challenge during the immobilisation of Bm3TE, bacterial compartments were used for encapsulation of P450Bm3. Two encapsulin compartments from *Thermotoga maritima* (Tm) and *Myxococcus xanthus* (Mx) were employed for capsid formation around the P450Bm3 R19 variant. Bm3 R19 was used as a cargo protein after being tagged with short targeting peptides (TPs) of the natural cargo of Tm and Mx encapsulins. Encapsulated P450Bm3 R19 in Tm encapsulin showed almost no activity but low

level of product formation were observed with the P450Bm3 R19 in the Mx encapsulin. Future studies will include modification of the encapsulin plasmids and conditions of protein expression for more efficient packaging of P450Bm3 R19 and other P450 systems.

Declaration

I certify that this work contains no material which has been accepted for the award of any other degree or diploma in my name, in any university or other tertiary institution and, to the best of my knowledge and belief, contains no material previously published or written by another person, except where due reference has been made in the text. In addition, I certify that no part of this work will, in the future, be used in a submission in my name, for any other degree or diploma in any university or other tertiary institution without the prior approval of the University of Adelaide and where applicable, any partner institution responsible for the joint-award of this degree.

I acknowledge that copyright of published works contained within this thesis resides with the copyright holder(s) of those works.

I also give permission for the digital version of my thesis to be made available on the web, via the University's digital research repository, the Library Search and also through web search engines, unless permission has been granted by the University to restrict access for a period of time.

I acknowledge the support I have received for my research through the provision of a Scholarship by the Univeristy of Adelaide.

Shaghayegh Dezvarei

May 2019

Acknowledgment

Firstly, I would like to thank my supervisor Stephen Bell for his continuous support and patience during my PhD. I could not be able to finish my thesis without his help.

I would like to thank Christian Doonan and Chris Sumby and Dumby group members Weibin, Natasha and Oliver for the MOFs work.

I would like to thank our collaborators at the University of Nagoya in particular, Osami Shoji and Yoshihito Watanabe and their group with the hydrogen peroxide-dependent variant work. I am grateful to Dr Yu Heng Lau from the University of Sydney for providing encapsulin plasmids.

Special thanks to Kathrine, Stella, Tom, Joel, Natasha and Weibin for proofreading parts of this document.

Thanks to all my friends in Badger building: Stella, Katherine, Stefania, Tom, Raihan, Heba Joel, Matthew, Saurabh, Daniel, Henery, Ossama, Rouven, Micheal, BJ, and Ruth.

Thanks to all my friends for all the good times: Shahdad, Mahsa, Muslih, Gail, Daryl, Afsoon, Melody, Nick, Dee, Jelena and Hanieh.

Thanks to the lovely people in the Chemistry department for being supportive and helpful.

Finally, a big thanks to my lovely family for their motivation, support, and dealing with grumpy Sherry: Ehsan, Amir, Ali, Mahsa, Afi, Nazi, Enza, Stephen and Charles. Special thanks to my parents, the most special people in my life for all their support and endless love.

Abbreviations

BMCs: bacterial microcompartments

BID: barrier discharge ionisation detector

bpydc:2,2′-bipyridine 5,5′-dicarboxylate

CCMV: Chlorotic Mottle virus

CLSM: confocal laser microscopy

CPR: cytochrome P450 reductase

CYP: cytochrome P450

Cyt c: cytochrome c

DTT: dithiothreitol

Dyp: dye-decolorizing peroxidase

DFT: density functional theory

ee: enantiomeric excess

EGFP: enhanced green fluorescent protein

FAD: flavine adenine dinucleotide

FITC: fluorescein isothiocyanate

Flp: ferritin-like proteins

FMN: flavine mononucleotide

Fr: fraction

FPLC: fast protein liquid chromatography

GC: gas chromatography

HAT: H-atom Abstraction

HOF: hydrogen bonded organic framework

HPLC: high performance liquid chromatography

HRP: horseradish peroxidase

HS: high spin

IEx: ion exchange

IPTG: isopropyl-b-D-thiogalactopyranoside

kan: kanamycin

KIE: kinetic isotope effect

LB: luria-Bertani broth

LS: low spin

MOF: metal organic framework

MP-11: Microperoxidase-11

Mx: Myxococcus xanthus

NAD(P)H: nicotinamide adenine dinucleotide phosphate (H: reduced form)

NH_2-bdc: 2-amino-1,4-benzene dicarboxylic acid

NIH: national institutes of health

NPG: N-palmitoyl glycine

pda: 1,4-phenylenediacetate

PFR: product formation rate

PVP: polyvinylpyrrolidon

SEC: size exclusion chromatography

SET: single electron transfer

SB: substrate bound

SF: substrate free

TE: trace elements solution

TIC: total ion count

Tm: thermotoga maritima

TPs: targeting peptides

Tris: tris(hydroxylmethyl)aminomethane

WT: wild-type

2xYT: yeast extract tryptone medium

ZIF: zeolitic imidazolate frameworks

Chapter 1

1 Introduction

1.1 Background

Cytochrome P450 enzymes are a superfamily of haem monooxygenases that can be found in almost all living creatures from prokaryotes to eukaryotes[1]. The name "P450" originates from the red pigmentation of the enzyme when the haem moiety in its reduced ferrous form binds carbon monoxide, resulting in a Soret band absorption at 450 nm[2-4]. As of 2018, more than 41000 members of this superfamily have been named according to the family and subfamily nomenclature of Nebert et al.[5]. A P450 family is defined such that its members have at least 40 percent similarity in their amino acid sequences; these are denoted by a number after the CYP prefix. When the amino acid sequence similarity is above 55 percent, genes are grouped into subfamilies which are represented by a letter after the family name and following by the gene identifier number[5-8]. For example, the P450 CYP102A1 from *Bacillus megaterium* belongs to family 102 and is the first member of subfamily A.

The first cytochrome P450 structure characterized was P450cam (CYP101A1) which was reported by Poulos in the 1980s[9, 10]. By comparing the structures of P450s from different families, it has been observed that this class of enzymes has a highly conserved general fold. The structure is more conserved around the haem centre, especially in the L and I helices[11], which contain several catalytically essential residues. The metal centre in cytochrome P450 enzymes consists of a central iron (III) atom coordinated to four nitrogen ligand donors from a porphyrin ring, a proximal cysteine (Cys) residue and a water molecule as the sixth ligand in

the resting state. In this resting state, the low-spin iron is in the ferric oxidation state (Figure 1. 1)[12].

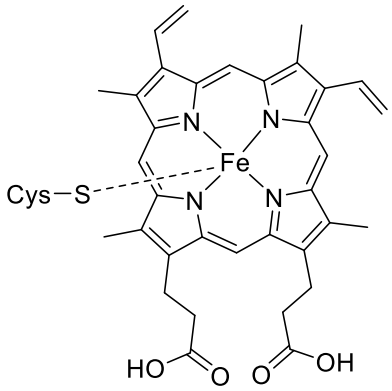

Figure 1. 1 All P450 haem-thiolate enzymes consist of iron (III) protoporphyrin IX linked to a Cys ligand[12].

1.2 Catalytic cycle of P450 enzymes

P450 enzymes catalyse a diverse range of reactions such as heteroatom dealkylation, heteroatom oxygenation, epoxide formation, and aromatic oxidation[13, 14]. Nonetheless, the most common reaction catalysed by P450 enzymes is the hydroxylation of C-H bonds. As monooxygenases, cytochrome P450 enzymes utilise atmospheric dioxygen to insert a single oxygen atom into the substrate with a concomitant reduction of the other oxygen atom to a molecule of water[15] (Equation 1. 1). However, there are some exceptions like the peroxygenase family of P450, CYP152, which employ H_2O_2 instead of molecular oxygen for the hydroxylation of fatty acids[11, 16, 17].

Equation 1. 1 Hydroxylation of a C-H bond by a P450 enzyme.

$$R\text{-}H + O_2 + 2e^- + 2H^+ \rightarrow R\text{-}OH + H_2O$$

The source of electrons required for this reaction is generally nicotinamide adenine dinucleotide phosphate NAD(P)H, (H: reduced form).

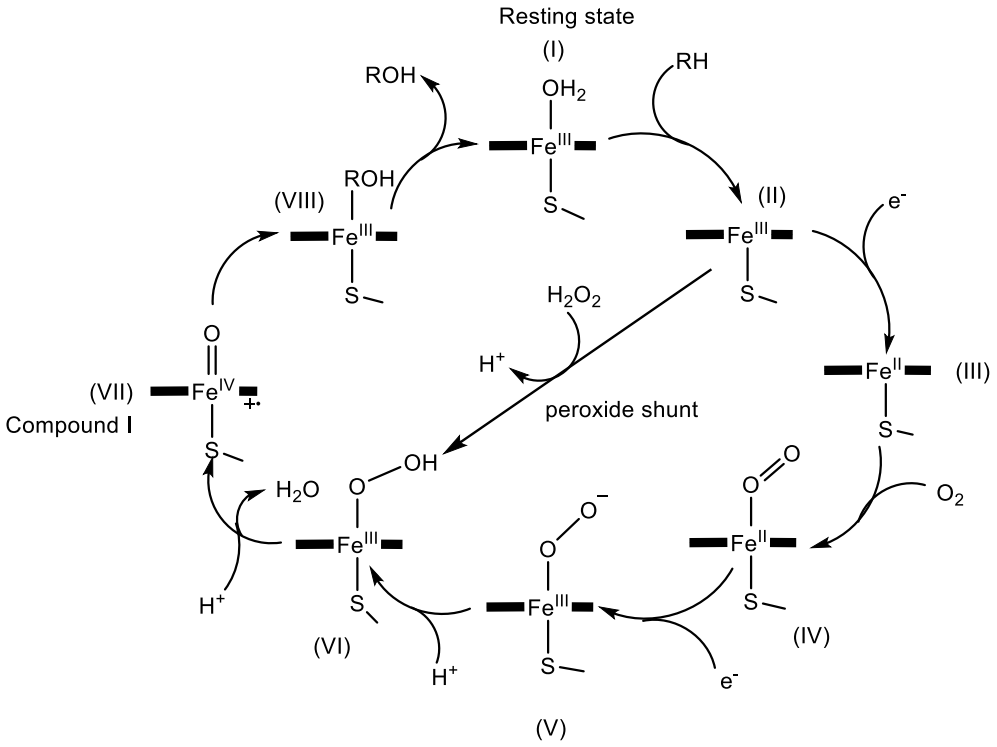

Figure 1. 2 The catalytic cycle of a P450 enzyme shows the substrate binding, electron transfer, oxygen binding and activation steps. Compound I (VII) is the active oxidant.

Upon substrate binding, the distal water ligand of the resting state (I) is displaced, yielding a five-coordinated ferric species (II). The first electron transfer then occurs, and the ferric iron is reduced to the ferrous state (III). This reduction facilitates the binding of the molecular oxygen as the sixth ligand to yield an oxy-bound species (IV). The second electron is then transferred, followed by protonation of the distal oxygen atom to form a hydroperoxy complex (V-VI). The next protonation leads to O-O bond cleavage with the release of one molecule of water, generating the iron-oxo radical cation intermediate (VII, Compound I). This highly reactive oxygen species abstracts a proton from the substrate to form a radical and Compound II (Figure 1. 3). This radical attacks the Fe-OH group of Compound II, allowing for homolytic O-Fe cleavage and producing a ferric complex (VII-VIII). The oxidised substrate is released, and a molecule of water binds to the ferric centre to reform the resting state (I)[18-23].

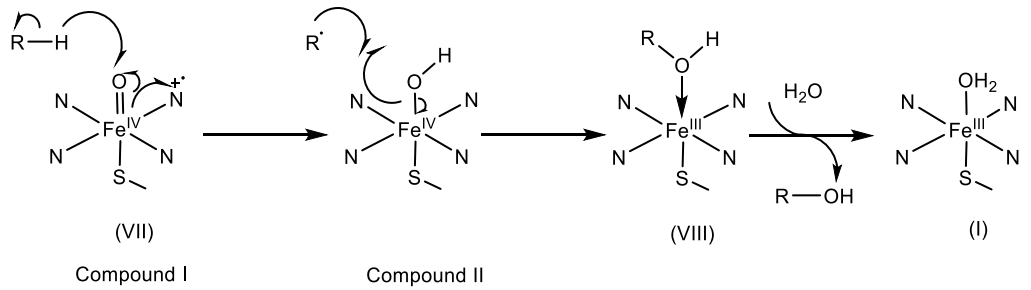

Figure 1. 3 The radical rebound mechanism of Compound I to hydroxylate the substrate.

The catalytic cycle of P450 enzymes (Figure 1. 2) requires an auxiliary electron transfer protein to provide electrons from NAD(P)H to the reduced ferric haem (II) and ferrous-dioxy (III) complexes. There are different electron transfer systems. Initial classification of electron transfer systems of P450 enzymes consisted of two major types (Figure 1. 4). However, subsequent studies have identified that electron transfer systems are more diverse and can be classified into ten groups[24-26]. The first class contains most of the bacterial P450 systems and the mitochondrial P450s from eukaryotes. Systems in this class require three proteins; the P450, an FAD (flavin adenine dinucleotide)-containing ferredoxin reductase and an iron-sulphur ferredoxin. Generally in a class I system, the electron is transferred from the NAD(P)H electron source to the FAD source, then through the FAD to the Fe_2S_2 cluster and finally to the haem centre in P450 enzymes. In bacterial P450 systems, all three proteins are typically water soluble; however, in eukaryote mitochondrial systems, only the ferredoxin is water-soluble[27, 28 29]. Examples of class I systems include the bacterial system P450cam (CYP101) from *Pseudomonas putida* and mitochondrial P450scc (CYP11A1)[30].

The class II system is found with mammalian P450s and includes a P450 and a diflavin reductase. This species contains both the organic cofactors FAD and FMN (flavin mononucleotide), which transfer electrons to the P450 enzyme. Both enzymes in these class II systems are membrane-bound (Figure 1. 4, b and c); therefore, they have a lower solubility in aqueous solution compared to bacterial class I enzymes.

P450Bm3 (CYP102A1) is from class VIII and was the first self-sufficient P450 that was discovered. In P450Bm3, the reductase domain is fused to the haem domain, and the enzyme only needs oxygen and NADPH as a source of electrons (Figure 1. 4 d). P450Bm3 has been reported as a dimer in solution[30]. Studies by Munro et al. showed that Bm3 was required to be in its dimeric form to be catalytically active[31]. The reductase domain contains FAD and FMN, and since these are bound in the same enzyme as the haem, a reorientation of FMN is required to allow it to dock to the haem for successful electron transfer. The flexible nature of these regions of this protein is hypothetically one of the reasons that no crystal structure of full-length P450Bm3 has been reported[32].

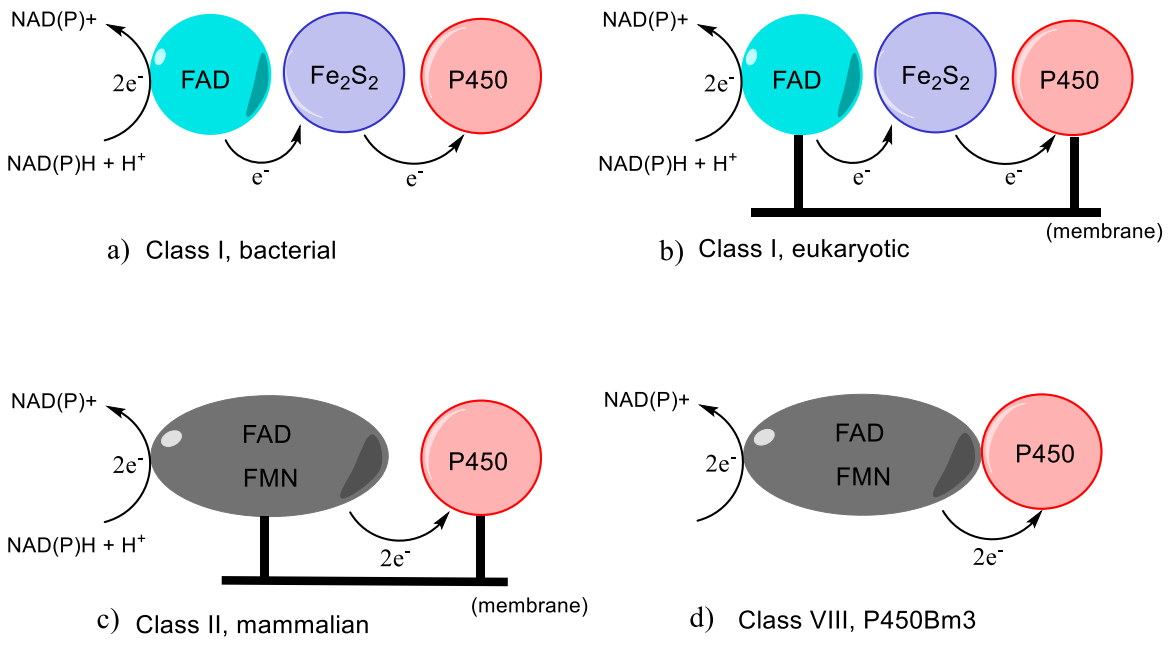

Figure 1. 4 Electron transfer system in P450 enzymes. a) bacterial class I and b) eukaryotic class I, c) mammalian class II and d) the P450Bm3 system. In eukaryotic systems, proteins are membrane-bound (Black tick lines) and poorly soluble in water.

1.3 P450 reactions

Compound I is widely believed to be responsible for the C-H bond oxidation in P450 enzymes, and its role in hydroxylation has been extensively studied[33-35]. However, other intermediates have been suggested for specific P450 enzymes reactions because of their different reactivity profiles. For example, the electrophilic Compound 0 has been reported to be able to catalyse alkene epoxidation[34, 36-38]. The most common reactions catalysed by P450 enzymes are briefly described below[14, 39-42].

1.3.1 Hydroxylation

C-H bond oxidation is one of the most challenging chemical reactions due to the high stability of this bond. This unreactive bond often requires harsh reaction conditions like high temperature and pressure. Enzymatic approaches, specifically, using monooxygenase enzymes, have emerged as an alternative method for C-H bond oxidation. The initially proposed mechanism for C-H oxidation by Groves et al. involved hydrogen abstraction from the substrate by Compound I, followed by rebounding of the radical to generate the ferric (III) complex (Figure 1. 3)[43-45]. Experiments determining the kinetic isotope effect (KIE) for many P450-catalysed transformations, supported the radical mechanism[46], but the existence of a radical intermediate was cast into doubt using ultrafast radical clocks[47-49]. The lifetime of the substrates as intermediates calculated using the ultrafast radical clock was closer to that expected for a transition state than a reaction intermediate[50-52].

Based on DFT calculations, the spin state of Compound I has been suggested to control whether the hydroxylation proceeds via a carbocation or a radical state[53] (Figure 1. 5). Using these calculations, the short radical lifetime observed in certain experiment is explained by the barrier-free radical rebound pathway when Compound I is low spin (doublet), and the longer

lifetime attributed to the high energy barrier in the high spin state (quartet). The high energy barrier in the radical rebound mechanism for the high spin pathway leads to an alternative reaction involving a cationic intermediate, while this barrier for the low spin state is negligible. Therefore when Compound I is low spin, the radical rebound mechanism is favoured (Figure 1. 5)[53].

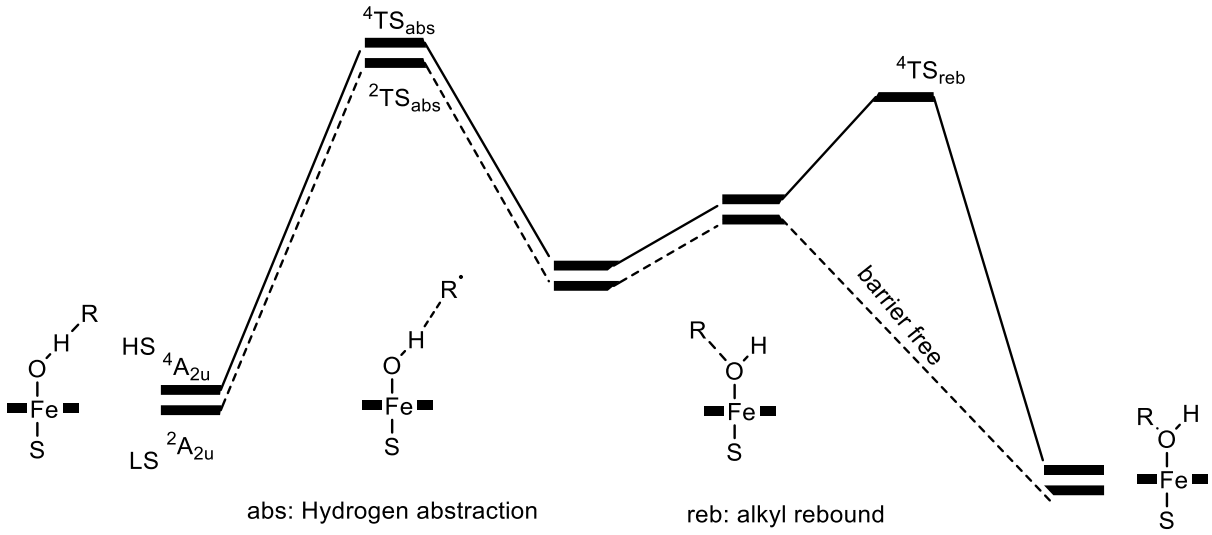

Figure 1. 5 The DFT-based mechanism for hydroxylation from high spin (HS: $^4A_{2u}$, solid line) and low spin states (LS: $^2A_{2u}$, dashed line) of Compound I. TS refers to the transition state.

1.3.2 Epoxidation of alkenes

Epoxidation of alkenes by cytochrome P450 enzymes usually display some stereoselectivity, which originally suggested a concerted mechanism by the enzyme[47, 54] (Figure 1. 6).

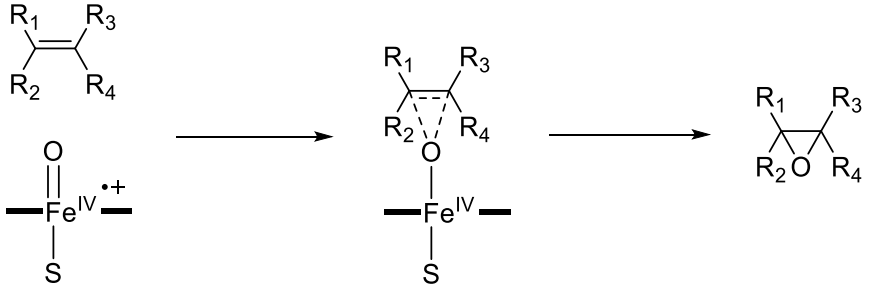

Figure 1. 6 The concerted mechanism of alkene epoxidation by P450 enzymes.

Subsequently, two species have been reported to be responsible for epoxidation by the haem domain, Compound I and Compound 0. The pathway using Compound I is again proposed to use a two-state reactivity model (TSR) of the low and high spin states[55] (Figure 1. 7). The low spin state has a low energy barrier and generates a radical intermediate. The high spin state has a higher energy barrier and generates a carbocation. This larger barrier for the high spin state increases its lifetime, which leads to a more stereoselective product[56-59]. Compound 0 was calculated to have single state reactivity (SSR), and its energy barrier for epoxidation was larger than for Compound I[55]. Therefore, based on DFT calculations, Compound 0 was proposed to not be an oxidant by itself [55].

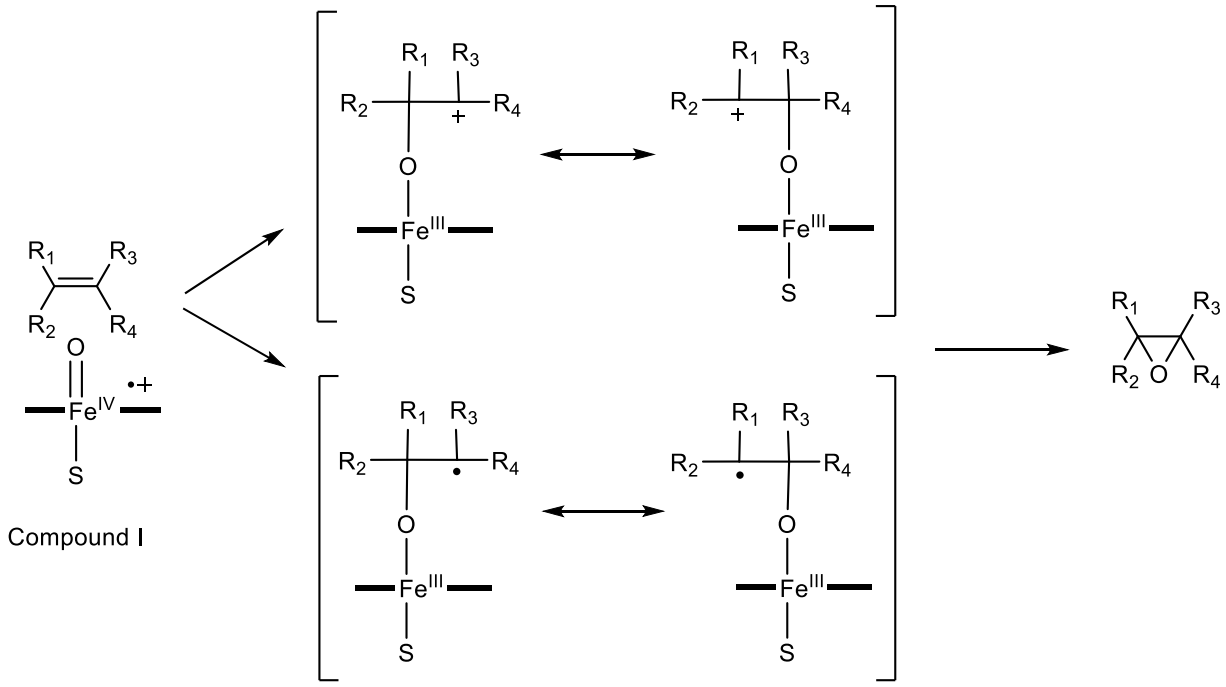

Figure 1. 7 The epoxidation of alkanes by Compound I through radical (top) and cationic (bottom) pathways.

Another pathway reported from the oxidation of alkenes by P450 enzymes is the formation of aldehydes. Aldehyde formation can be explained by an electron transfer between a C-radical and Fe (IV) with the generation of a carbocation intermediate. The Fe(IV)-oxyl then binds to

the less substituted C, and one of the substitutions migrate to generate an aldehyde (Figure 1. 8)[55].

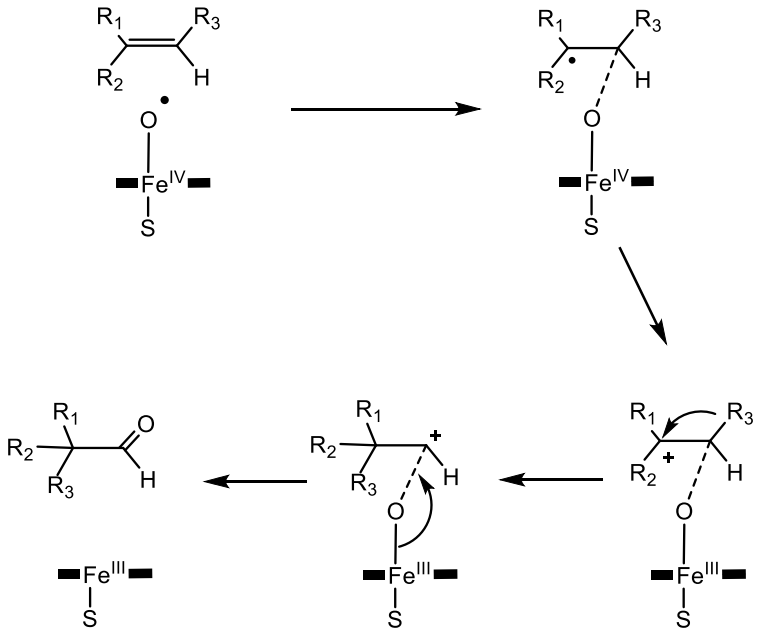

Figure 1. 8 Mechanism of aldehyde formation instead of epoxidation by P450 enzymes.

1.3.3 Aromatic oxidation

The aromaticity and high dissociation energy of the C-H bonds of benzene (111 kcal/mol) impede its abstraction by P450 enzymes, in contrast to the aliphatic alkanes[60, 61]. The first pathway for hydroxylation of benzene was reported by Jerina et al. in 1969 and involves an arene oxide intermediate followed by a hydrogen migration in the aromatic system and phenol formation[62]. This hydrogen migration was reported by the National Institutes of Health and is subsequently known as the NIH shift[62]. The oxidation reaction with P450 enzymes proceeds via the addition of iron (IV)-oxyl to the benzene ring (Figure 1. 9)[63]. Epoxidation after iron (IV)-oxyl addition to the ring could proceed by two pathways, one includes a radical formation (Figure 1. 9), while the other is derived via a cationic state[64, 65] (Figure 1. 9). The formation of the cation from the radical complex via an internal electron transfer is plausible, and

calculations show that the cationic and radical intermediates could also be generated independently[63,66]. Both pathways generate a phenol product. The radical complex generates the epoxide before an NIH shift (Figure 1. 9) and is followed by a tautomerisation to form the phenol. In the cationic pathway, the direct proton transfer to the oxygen (Figure 1. 9 b) results in the formation of phenol.

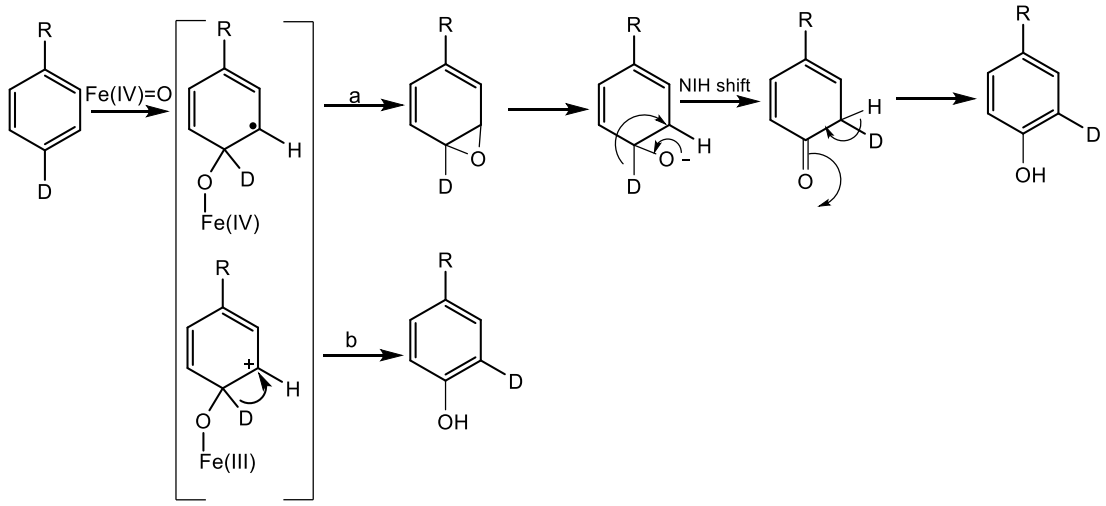

Figure 1. 9 Hypothesised mechanism of aromatic oxidation by P450 enzymes. a) the radical pathway followed by an NIH shift and tautomerisation; b) direct proton transfer in the cation mechanism, which generates phenol.

1.3.4 Sulfoxidation

The mutation of threonine, which is essential for molecular oxygen activation and proton delivery (see 1.7 Hydrogen peroxide dependent variants) decrease the rate of the hydroxylation reaction because of a reduction in the formation of Compound I. However, the sulfoxidation rate increases[67]. This indicates that there could be another oxidant besides Compound I for sulfoxidation[67]. Sulfoxidation is hypothesised to proceed via a concerted mechanism that includes the nucleophilic attack of the sulphur on the oxygen of distal H_2O_2 (Figure 1. 10), where the heterolytic O-O bond cleavage is following by a proton transfer to form Fe^{III}-OH_2[67].

It has been shown that the cleavage of O-O is the rate determine step, which could be heterolytic or homolytic. The comparison of heterolytic and homolytic cleavage showed that the former pathway is more energetically favoured[67].

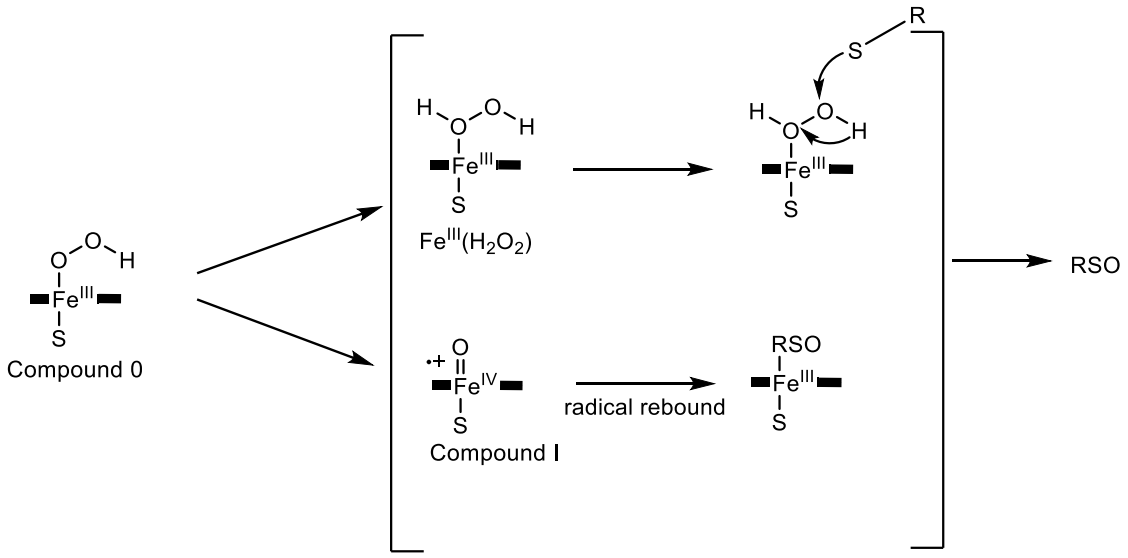

Figure 1. 10 The concerted mechanism of sulfoxidation via Fe^{III} (H_2O_2) oxidant.

1.3.5 Dehydrogenation

P450 enzymes can function as oxidase-dehydrogenases and catalyse the desaturation of saturated hydrocarbons to unsaturated hydrocarbons (Figure 1. 11). The first step is similar to the hydroxylation mechanism, with an initial hydrogen abstraction by Compound I yielding a carbon radical[35]. At this point, the mechanism can branch: either a second hydrogen abstraction forms the unsaturated product (Figure 1. 11 bottom) or a single electron transfer from the radical to the iron yields a carbocation, followed by proton transfer to generate the unsaturated hydrocarbon (Figure 1. 11 top)[68-70].

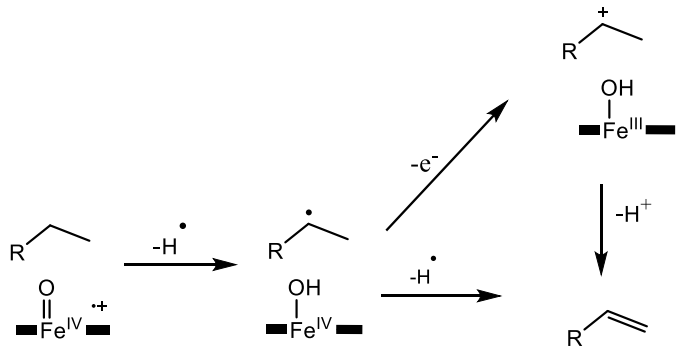

Figure 1. 11 The proposed mechanisms of desaturation of hydrocarbons by P450 enzymes. Hydrogen abstraction and oxygen rebound in Fe species followed by; single electron transfer (top) or a second hydrogen abstraction (bottom).

1.4 CYP102A1/ P450Bm3

CYP102A1 was discovered by Fulco in 1970s[71]. This protein is the third enzyme isolated from *Bacillus megaterium*, which gave rise to its name, P450Bm3[71-74]. This enzyme is the P450 most commonly utilised for chemical reactions because of its self-sufficient nature. This 119 kDa monooxygenase is a holoenzyme consisting of a 55 kDa haem domain covalently connected to a 65 kDa reductase domain, which contains FAD and FMN flavin groups (1.2 Catalytic cycle of P450); therefore, it only requires NADPH (as a source of electrons) and molecular oxygen to initiate monooxygenase reactions[75-77]. The significance of the covalent linkage of these domains was demonstrated in experiments, where individual expression of the haem and the reductase domains showed little affinity for one another[77-80]. P450Bm3 is a dimer in solution, and its catalytic activity arises from its dimeric form[30]. Studies by Munro et al. showed that at low concentrations, P450Bm3 exhibits less activity because of the prevalence of the monomeric form[31].

A wide variety of fatty acids have been reported as substrates for P450Bm3, and it was found that a chain length of 12-15 carbon atoms in a substituted fatty acid is favoured for optimal

binding and activity. The oxidation of these fatty acids by P450Bm3 takes place at the ω-n (n= 1-3) positions in different ratios depending on the orientation in the active site (Figure 1. 12)[75, 81-83].

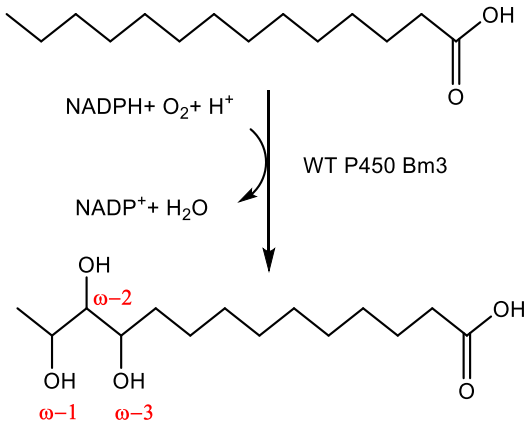

Figure 1. 12 Oxidation of fatty acids by P450Bm3 is regioselective and occurs at the ω-n (n=1-3) positions.

Proteolysis of the reductase domain yields two sub-domains, an FAD/ NADPH and an FMN region[84, 85], and neither is active in the absence of the other[86]. The formation of semiquinone intermediates from the flavins provides a single electron to the haem before oxidising the substrate. In microsomal cytochrome P450 reductase (CPR), electrons are transferred from NADPH to FAD and then to FMN to form $FMNH_2$. These electrons are shuttled from $FMNH_2$ to the haem to yield the FMNH semiquinone and the reduced haem intermediate. The electron transfer mechanism in P450Bm3 is similar to that of mammalian CPR, although in P450Bm3 the electrons are shuttled from FMNH instead of $FMNH_2$ (Figure 1. 13), which illustrating the difference in reduction potential of CPR and P450Bm3[87-89]. It is thought that the different preferences for electron transfer partners are a result of changes in the FMN binding loop of CPR versus P450Bm3[89].

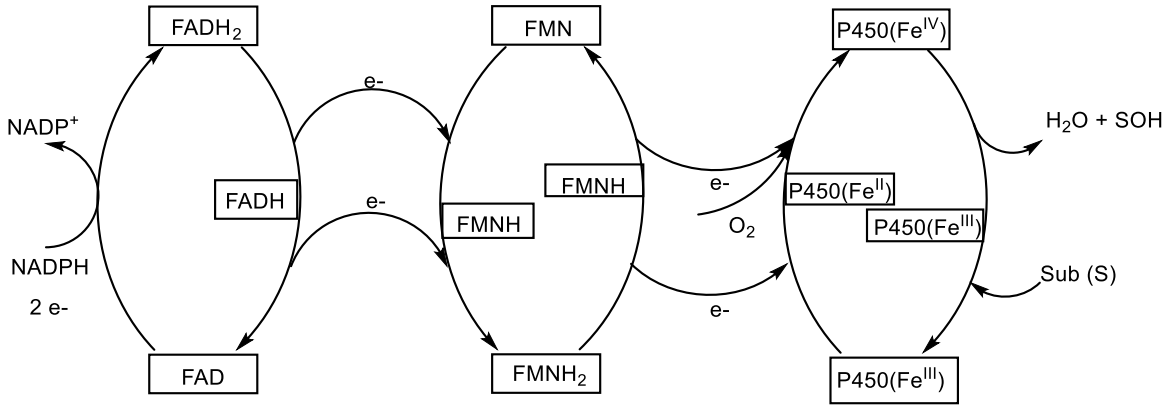

Figure 1. 13 A schematic representation of electron transfer in P450Bm3. The electron from NADPH forms FAD hydroquinone and transfers to FMN to form FMNH. The electron from FMNH is transferred to the domain of P450Bm3 to hydroxylase the substrate[90].

The addition of NADH or NADPH without the presence of substrate inhibits the oxidation activity of the P450Bm3[75, 81]. Experimental evidence has also shown that in the absence of substrate, the enzyme loses 70 % of its activity two minutes after addition of NADPH and after ninety minutes only 10 % of activity remained. Inactivation of the enzyme was determined to arise from a change in the reductase domain, as incubation of the haem domain with NADPH does not hamper the activity of the enzyme[91-93].

1.5 Key Residues in P450Bm3

Similar to the some of the mammalian P450s, P450Bm3 crystallises in an open conformation (PDB 1BU7)[94]. In this precatalytic conformation, the substrate is not close enough to the haem centre and therefore, there is no accurate structural data of a catalytically relevant form of the enzyme[86]. However, the available crystal structure does enable some of the key requirement of fatty acid oxidation to be elucidated. Based on the oxidation of fatty acids by P450Bm3, Fulco et al. presumed the presence of a hydrophilic region near the haem centre, and this hypothesis was supported by the crystal structure of the enzyme in the presence of palmitoleic acid[82, 95].

The carboxyl group of palmitoleic acid interacts with Arg47 and Tyr51, two polar residues in the entrance of the active site (Figure 1. 14). The mutation introduced at these two positions[96, 97], decreases the affinity of the enzyme for fatty acids. A double mutation of R47A/Y51F showed only one-third activity of the WT enzyme towards oxidation of fatty acids. Hence, Arg47 and Tyr51 are known as gatekeepers of P450Bm3[98]. Arg47 does not bond to the substrates and Tyr51 harness the substrate by forming a hydrogen bond to the fatty acid substrates[99, 100] (Figure 1. 14).

The selectivity of P450Bm3 for sub-terminal positions of the substrate can be partly attributed to the Phe87 residue. This phenylalanine is close to the haem centre and in the absence of substrate settles perpendicular to the haem[106 90] (Figure 1. 14). Upon substrate binding, the Phe87 residue rotates 90° and is placed between the haem and tail of the substrate and help to orient the aliphatic chain hydroxylation, which leads to sub-terminal hydroxylation[104]. It was found that the flexibility of the substrate assists the enzyme in increasing the activity towards its sub-terminal tail, which is closer to the haem moiety. Therefore, Phe87 may be more effective at catalysing hydroxylation at the sub-terminal position, but it is not the only driving force for regioselectivity[86]. Mutagenesis of Phe87 to smaller amino acids made the access channel larger and enabled the enzyme to oxidise bulkier substrates, e.g. naphthalene and indole[86]. F87V and F87A are examples of Phe87 mutations which are commonly employed as drug-metabolising and dealkylation variants of P450Bm3[86].

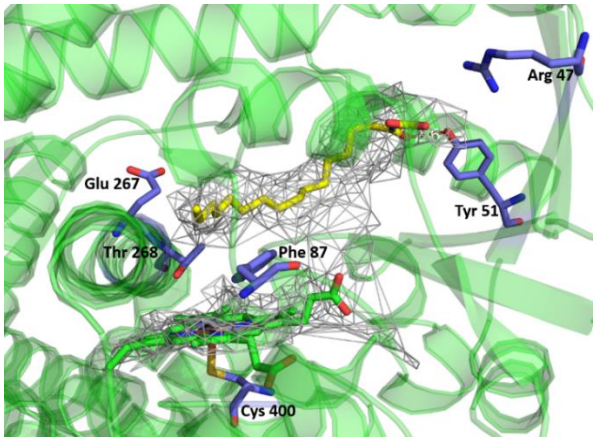

Figure 1. 14 Location of key residues in WT P450Bm3 in the presence of the N-palmitoyl glycine (yellow). The mesh area shows the active site of the enzyme (PDB: 1JPZ)[101].

An acid-alcohol pair is conserved in most P450s, which facilitates oxygen activation. In many P450s, these acid-alcohol pair are aspartic acid (Asp)-threonine (Thr) or glutamic acid (Glu)-Thr. The alcohol residue has an essential role by stabilising the water molecules close to the coordinated dioxygen via hydrogen bonding[102]. In P450Bm3, the glutamic acid and threonine residues are at positions 267 and 268 respectively[107]. The mutation of glutamic acid to glutamine decreased the activity of the WT enzyme to only 5 % with palmitic acid as the substrate[103]. The side chain of Glu267 is hydrogen bonded to a water molecule in the active site of the substrate-free crystal structures, and mutations to non-polar residues would disrupt proton delivery.

The polar nature of Thr268 enables this highly conserved residue to also contribute to proton delivery, activation of dioxygen and subsequently the stabilisation of the oxy-ferrous or ferric-hydroperoxy intermediates[104, 105]. The T268A mutation had an adverse effect on the oxidation of palmitic, arachidonic and lauric acids[119,106], which showed the significance of the threonine side-chain for hydrogen bonding to the water molecule near the active site in the WT enzyme [106]. The crystal structure of the enzyme in the presence of N-palmitoyl glycine (NPG) provided

evidence that the water molecule is stabilised by the Thr268 residue[107]. However, De Voss et al. have shown the T268A mutant is functional with myristic acid, which may indicate that specific substrates can circumvent this requirement[108]. Recently the introduction of a glutamic acid mutation at the Thr268 position converted P450Bm3 into an H_2O_2-dependent variant (see 1.7 Hydrogen peroxide dependent variants)[104].

1.6 Mutagenesis and biocatalytic applications of P450Bm3

Enzymatic reactions have emerged as promising alternatives to chemical oxidation in organic synthesis. These biocatalytic enzyme reactions occur under mild conditions[109-111] and in contrast to the chemical catalysts, are environmentally benign. P450 enzymes have been of interest because of their ability to selectively hydroxylate unreactive C-H bonds at ambient pressure and temperature[111]. Moreover, enzymes can be generated in a soluble form using *Escherichia coli* and readily purified in high yields[112-114].

The high catalytic activity of P450Bm3 has made it the most utilised enzyme of this superfamily for biocatalysis[115-117]. The highest k_{cat} (285 s^{-1}) was reported for the oxidation of arachidonic acid with WT P450Bm3[96]. However, the WT enzyme is more selective for its natural substrates, given that the key residues around the active site hamper the entrance of non-native substrates. Enzyme engineering, by introducing direct and random mutations, has increased the substrate range of P450Bm3[83, 118-121]. For example, no activity was observed for P450Bm3 towards the oxidation of alkanes before Farinas et al. reported an evolved variant of Bm3, which enabled the oxidation of octane[118].

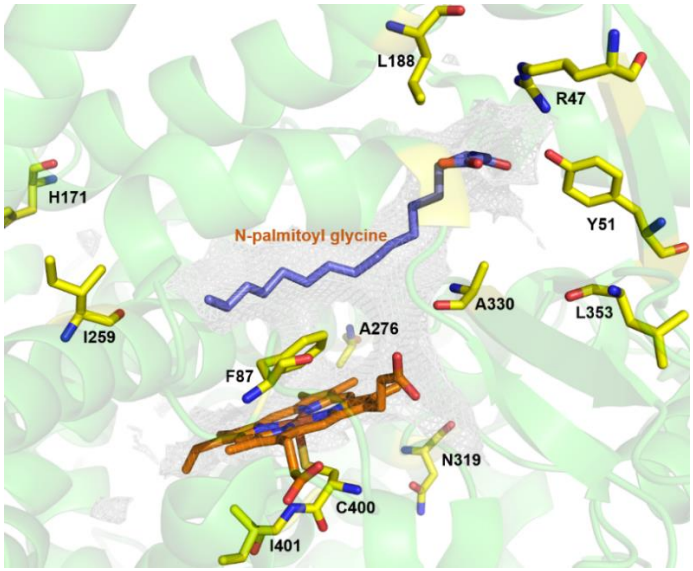

Figure 1. 15 Crystal structure of WT P450Bm3 in the presence of the N-palmitoyl glycine (blue). Shown are residues (yellow) around the active site (grey mesh) (PDB: 1JPZ)[101].

Mutation of key residues, such as Arg47 and Tyr51, also changed the preference of the enzyme towards different substrates. The R47L/Y51F variant has been used to catalyse the oxidation of more hydrophobic substrates like polycyclic aromatic hydrocarbons[122]. Isoleucine at position 401(I401P) is beneath the haem in the active site (Figure 1. 15), and it has shown that mutation of Ile401 to Pro changes the conformation of the enzyme and places it in an active state. The I401P and I401M mutations were proposed to make P450Bm3 more capable of binding hydrophobic substrates and as a consequence, the oxidation rate increased[101, 119].

The KT2 (A191T/N239H/I259V/A276T/L353I) variant has also been reported to increase the oxidation rate of P450Bm3 because of a more catalytically active conformation (Figure 1. 16)[123, 124]. KT2 was developed by random mutation; and it is of note that the mutations are not in the active site. In the WT enzyme, there are two salt bridges (Lys224-Asp251 and Asp212-Arg255) which link the I and G helices. The mutations in KT2 disrupt these bridges, leading to breakage of several hydrogen bonds in the structure and a conformational change[124]. The iron in the haem centre is pulled towards the cysteine ligand; additionally, the distal water

ligand is no longer hydrogen bonded to Ala264 which better assists the triggering of the catalytic cycle. The alteration in conformation and enzyme structure make KT2, like I401P, a catalytically ready variant (Figure 1. 16)[124]. Other variants of P450Bm3 contain mutations in and around the active site enable it to become a biocatalyst for the oxidation of arenes[92], steroids[125-128], terpenoids[129, 130] alkanes[92, 131, 132] and other substrates.

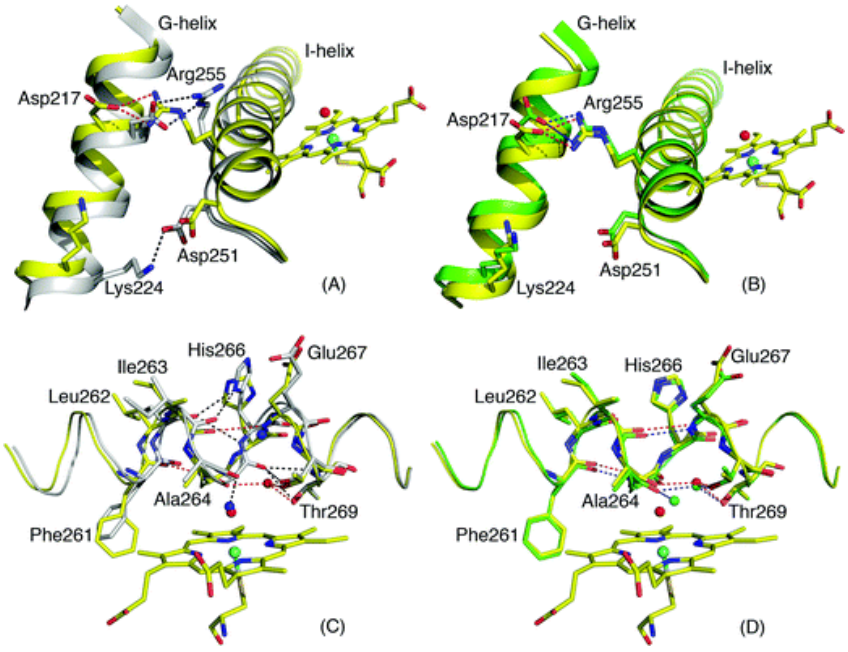

Figure 1. 16 Crystal structure overlays of substrate-free (SF) KT2 (yellow, with waters as red spheres and hydrogen bonds as red dashed lines), SF WT (grey, waters as dark blue spheres and hydrogen bonds in black) and NPG-bound WT (green, waters as green spheres and hydrogen bonds in blue). A) the Lys224-Asp251 bridge is broken in KT2: B) SF KT2 adopts the same catalytically active conformation of NPG-bound WT. C) The structure of the active site within SF WT differs from the NPG-bound WT. D) The overlay of the active site of NPG-bound WT and SF KT2, showing closely matched structures (PDB 3PSX). This figure is from "Structure, electronic properties and catalytic behaviour of an activity-enhancing CYP102A1 (P450BM3) variant" by Whitehouse et al.[124].

1.7 Hydrogen peroxide dependent variants

Cytochrome P450 enzymes are monooxygenases because they used molecular oxygen in the presence of NADH or NADPH to produce the active oxidant Compound I. In 1994, Matsunaga et al. first reported that CYP152B1 from *Sphingomonas paucimobilis* (P450SPα) oxidises fatty acids using H_2O_2[133] and the first crystal structure of the related CYP152A1 (P450BSβ) from *Bacillus subtilis* was reported by Lee et al. in 2003[12]. Both P450BSβ and P450SPα lack the acid-alcohol pair of residues, which facilitate oxygen activation for the Compound I formation[134-137] (1.5 Key Residues in P450Bm3). In P450BSβ, instead of the acid-alcohol residues, the interaction between the carboxylic group of the substrate and guanidine group of Arg242 (Figure 1. 17) assists the activation of the enzyme by formation of Compound I in the presence of the H_2O_2 (Figure 1. 18)[138].

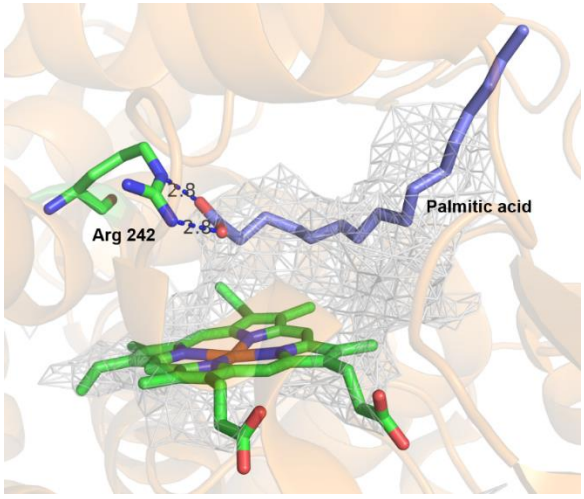

Figure 1. 17 The palmitic acid-bound P450BSβ shows the interaction (red dashed line) between Arg242 (green) and carboxylic group of the palmitic acid (blue) in the active site (grey mesh) (PDB: 1IZO)[138].

The subsequent crystal structure of P450SPα by Fujishiro et al. confirmed the importance of the carboxylic group in the substrate and its interaction with the guanidine group of Arg241 for

activation of the enzyme[139]. A recent study by Onada et al. reported the oxidation of non-native substrates of P450SPα and P450BSβ by employing short chain length n-alkyl carboxylic acids as decoy molecules[140]. The carboxylic group of the decoys binds to the glutamic acid in Arg242 (P450BSβ) or Arg241 (P450SPα), in the presence of H_2O_2, allowing the formation of Compound I and this enables the oxidation of non-native substrates (Figure 1. 18). Shoji et al. reported that the mutation of Ala245 to glutamic acid placed a carboxylate group close to the haem moiety and increased the formation of Compound I for non-native substrates and hence allowed their oxidation[141]. The location of Ala245 corresponds to the alcohol Thr268 in P450Bm3. Therefore introducing a single mutation of T268E in P450Bm3 provide a carboxylate group at position 268 and Arg241, which is essential for the formation of Compound I (Figure 1. 18), and allows P450Bm3 to be driven by hydrogen peroxide[141]. Therefore, instead of following molecular oxygen-driven the catalytic cycle of normal P450s with activation of Compound I, the H_2O_2 dependent P450Bm3 hydroxylates substrates via the H_2O_2 shunt pathway (Figure 1. 18). Considering the high expense in using NADPH, converting P450Bm3 to a H_2O_2 dependent variant benefits the industrial application of the enzyme.

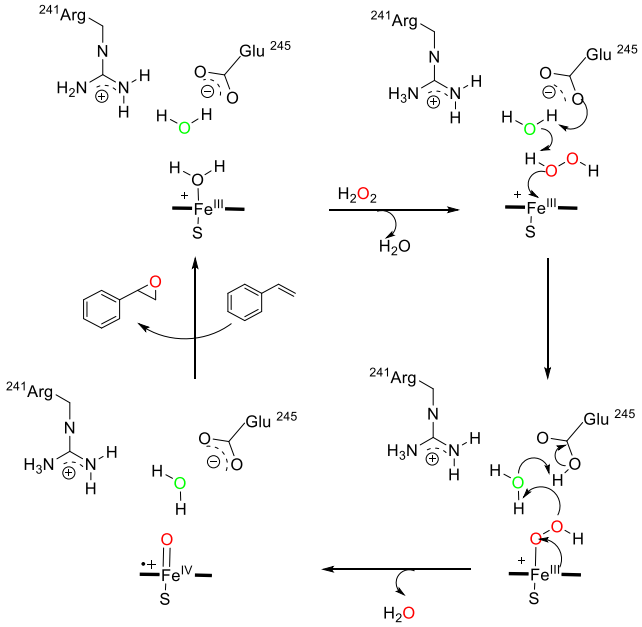

Figure 1. 18 The peroxide-driven catalytic cycle of P450 peroxygenases, such as P450SPα.

1.8 Decoy molecules

Enzyme engineering has been carried out on P450Bm3 to enable the oxidation of an extensive range of non-native substrates (1.6 Mutagenesis and biocatalytic applications of P450Bm3). Decoy molecules have also been employed to exploit the activity of P450Bm3 further. Kawakami et al. in 2011 first reported the application of decoy molecules in the oxidation of gaseous alkanes by P450Bm3[142]. Given fatty acids with 12-15 atom-long chains are the optimal substrates for P450Bm3, polyfluorinated fatty acids (PFCs) were initially chosen as decoy molecules for P450Bm3. The carboxylic group in PFCs (Figure 1. 19) will be tethered by Arg47 and Tyr51 (Figure 1. 20) enabling the enzyme to transfer into a more catalytically ready conformation[143-146]. However the strong C-F bonds, cannot be oxidised by P450Bm3[147] Compared to natural substrates, decoy molecules are designed to have a shorter length chain, leaving a cavity in the active site and therefore non-native substrates have access to space above the haem iron. The most commonly employed PFCs with P450Bm3 are polyfluorinated fatty acids with 8 to 10 chain length (PFC 8-10), and their dissociation constants have been reported K_d = 1900, 980 and 290 μM, respectively. The shorter PFCs have a lower resemblance to natural substrates, therefore their binding affinity for the active site of P450Bm3 decreases and makes them less effective decoy molecules[147, 148]. Using decoy molecules enables hydroxylation of a variety of substrates by WT P450Bm3. However, the catalytic activity is often lower than with the natural substrates, since these decoy molecules do not fully interact with the active site.

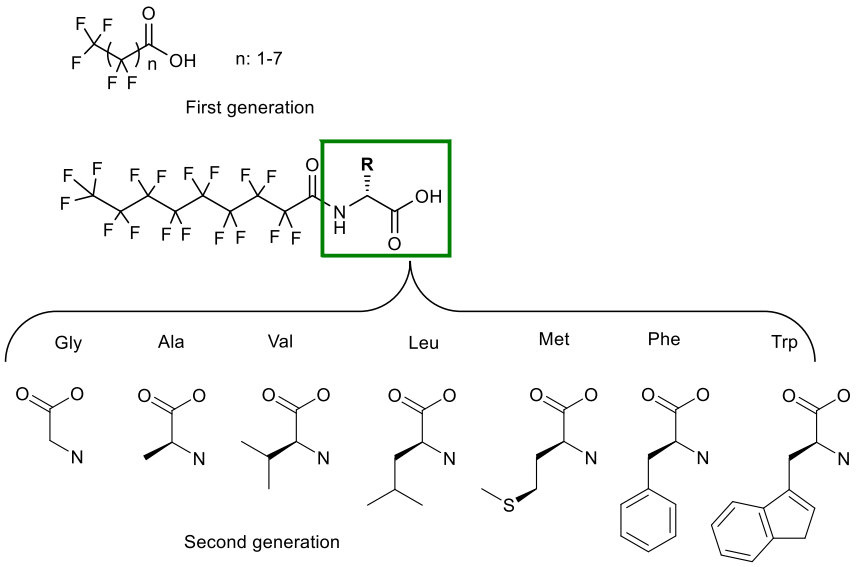

Figure 1. 19 Structures of decoy substrates designed for P450Bm3. At the top, the first generation decoy molecules are shown, and the bottom shows the second generation decoy molecules, which employ an amino acid head in place of the normal fatty acid carboxylate head (green box).

It was reported that WT P450Bm3 shows higher oxidation activity for N-palmitoyl glycine than palmitic acid because of the lower dissociation constant of the former[148]. The Gln73 and Ala74 residues form hydrogen bonds to the carboxylate group of N-palmitoyl glycine and increase the binding affinity[107]. This finding led to the proposal of "second generation" decoy molecules; these include an amino acid head, which would enhance activity more than the first generation[148] (Figure 1. 19). These amino acid-based decoys were observed to bind more tightly to WT P450Bm3 and to increase the oxidation rate of gaseous alkanes[148] (Figure 1. 20).

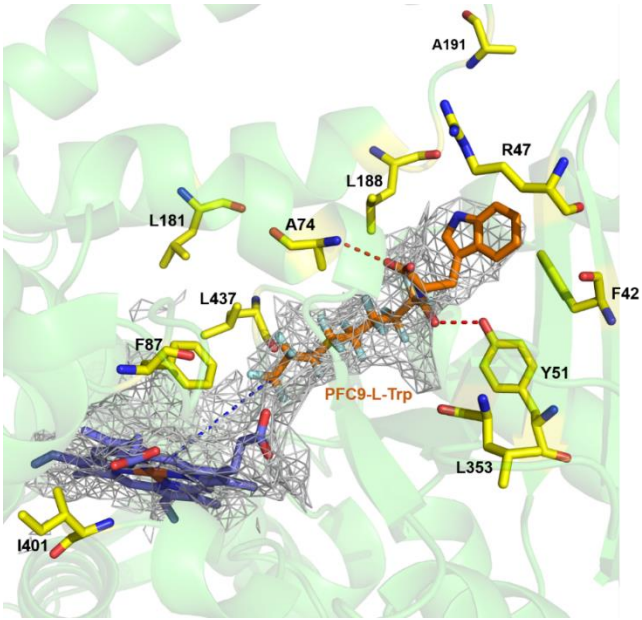

Figure 1. 20 The crystal structure of P450Bm3 with a bound PFC-9-L-Trp decoy molecule (orange). The key and hydrophobic residues (yellow) around the active site (grey mesh) are shown (PDB: 3WSP).

1.9. Immobilisation of P450Bm3

1.9.1 Zeolitic imidazolate frameworks (ZIFs)

P450 enzymes are potential biocatalyst for oxidation reactions, but one problem with the application of P450Bm3 and other enzymes in chemical synthesis is their low stability towards strong oxidative conditions. Furthermore, because of the high solubility of free enzymes in aqueous media, separation of the enzyme from the final product is difficult. Enzyme immobilisation is one approach that could address these issues and would enable the creation of a reusable heterogeneous biocatalyst. Immobilisation would also enable applications of the enzyme under more extreme reaction conditions, such as high pH and temperature as well as in the presence of an organic co-solvent[149-151].

The first example of enzyme immobilisation was reported by Nelson and Griffin in 1916 using-physical adsorption of invertase (β-D-fructofuranosidase) on charcoal[152]. The first industrial application of immobilised enzymes was reported by Tanabe Seiyaku in 1969, where an aminoacylase was physically adsorbed on DEAE-Sephadex media[153].

Immobilisation methods are classified into four categories: 1) crosslinking; 2) enzyme entrapment; (encapsulation) 3) physical adsorption; and 4) covalent binding to a presynthesised support[154-158] (Figure 1. 21). The efficiency and efficacy of enzyme immobilisation depend on the desired application, the properties of the support and the nature of the enzyme[158]. Various supports have been reported for the covalent binding of the enzyme, such as nano-porous silica, sepharose, alumina and metal-organic frameworks (MOFs)[149, 150, 159, 160].

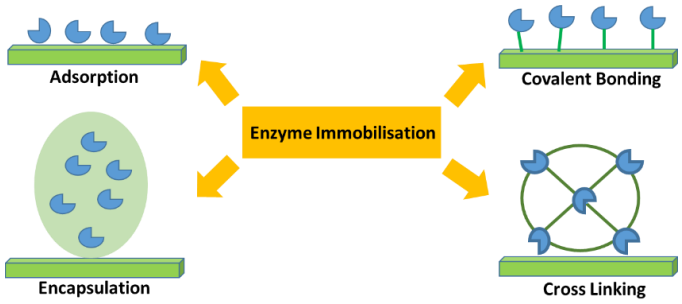

Figure 1. 21 Different methods of immobilisation include: adsorption, covalent bonding, cross-linking and encapsulation.

MOFs are emerging carriers for enzyme immobilisation[157, 161]. These porous crystals are constructed from metal ions and organic ligands in a regular lattice. The various combinations of ligands and metal ions can provide an extensive range of MOFs with useful properties, such as high porosity and large surface area[156, 162, 163]. MOFs also offer high thermal (250 ° to 500 °C) and chemical stability. Zeolitic imidazolate frameworks (ZIFs) are the first example of MOFs with useful chemical stability[164-166]. ZIFs are a subclass of MOFs constructed from tetrahedral metal ions linked to imidazole ligands with similar tetrahedral topology to

zeolites[167]. The chemical environment of a MOF is tuneable, and careful choice of the organic ligand with a proper functional group can allow strong interaction between MOF and the desired enzyme[168].

The functionality and morphology of MOFs can be modified[169-175]. For example, in isoreticular structures, longer ligands are utilised to increase void space and thus increase the porosity of the resulting MOF materials[166]. Studies by Farha et al. demonstrated that replacing the phenyl groups in ligands with less bulky alkyne ones can further increase the surface areas and porosity of the crystals[176] (Figure 1. 22).

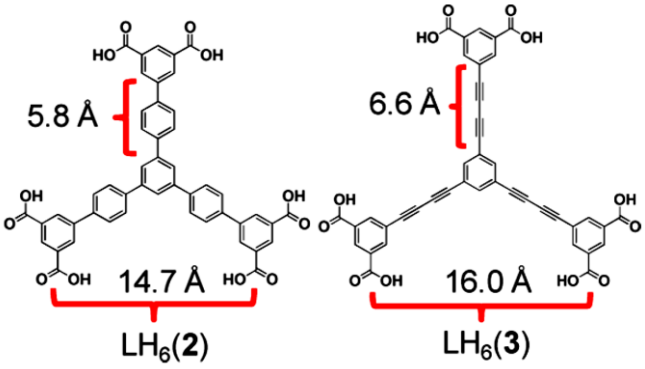

Figure 1. 22 Ligands designed for MOF formation. Replacing the phenyl linkers with alkynes was found to increase the area and porosity of crystals. This figure is from "Metal–organic framework materials with ultrahigh surface areas: is the sky the limit?" by Farha et al.[176].

These unique features of MOFs make them favourable for a wide range of applications including drug delivery[177], gas storage, and separation[178-180], catalysis[181] and energy conversion[182]. The application of MOFs as a support for enzyme immobilisation has been studied extensively. Balkus et al. reported the first example of enzyme immobilisation using MOFs in 2016. The Microperoxidase-11 (M-11) enzyme, was able to surface adsorbed onto a copper(II)-dicarboxylate MOF [161]. MOFs have been employed in four different general classes

of enzyme immobilisation strategies: 1) diffusion of the enzyme into the pores; 2) surface attachment; 3) covalent binding to the surface; and 4) *in situ* encapsulation[175, 183].

The high porosity of MOFs provides an opportunity for diffusion of enzymes with a smaller size than the pores. The earliest enzyme diffusion into the cavity pores was reported for MP-11 immobilisation in (Tb-mesoMOF) ([Tb16(tatb)16], tatb = triazine-1,3,5-tribenzoate). The size of MP-11 is about 3.3 × 1.7 × 1.1 nm[184], and diffuses in 3.9 and 4.7 (diameter) cages in Tb-mesoMOF. The immobilised MP-11 on Tb-mesoMOF showed higher activity than the free enzyme[185].

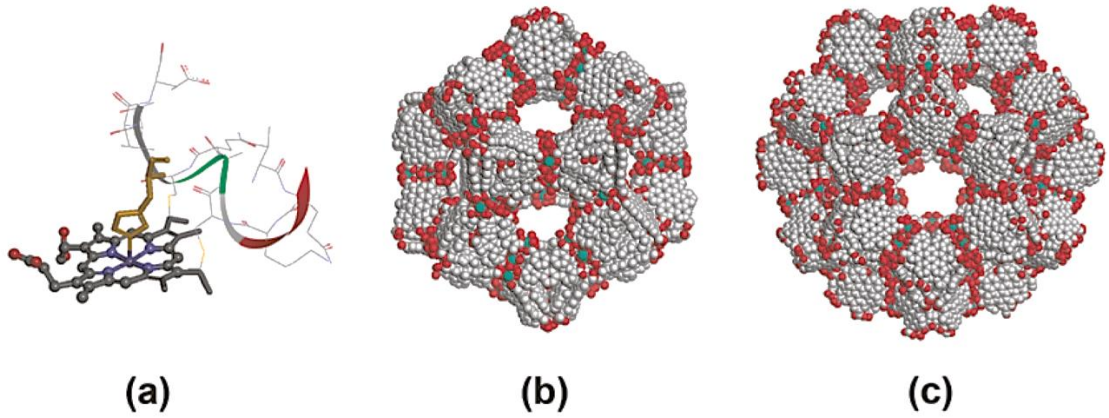

Figure 1. 23 The smaller size of the MP-11 than the cages in Tb-meso MOF, enable its diffusion. a) The crystal structure of MP-11 (PDB: 1OCD); and different cage sizes in Tb-meso MOF b) 3.9 nm diameter and c) 4.7 nm diameter cages. This figure is from "Immobilisation of MP-11 into a Mesoporous Metal–Organic Framework, MP-11@mesoMOF: A New Platform for Enzymatic Catalysis" by Lykourinou et al.[185].

Another example is the diffusion of cutinase (3 nm length) in NU-1000, which has 3.1 nm hexagonal channels and 1.5 nm edge length triangular channels[186]. Although the high porosity of MOFs allows the diffusion of proteins, sometimes the target is larger than the pore size. In these cases, alternative approaches are required for immobilisation. One of the simple

alternatives of immobilisation is to attach the protein to the surface of the MOF through weak interactions, such as hydrogen bonding or hydrophobic interactions. For this purpose, the MOF crystals can be synthesised in advance[183]. In 2006, Balkus et al. reported the first example of surface immobilisation of the enzyme on MOFs. The authors immobilised M-11 on a Cu-MOF $[Cu(OOC\text{-}C_6H_4\text{-}C_6H_4\text{-}COO)^{1/2}\ C_6H_{12}N_2]_n$. In their procedure, the pre-synthesised Cu-MOF was mixed with M-11 for physical attachment; no modification was required[161]. The immobilised M-11 showed a 65 % conversion of the substrate to product[161]. Liu et al. immobilised *Bacillus subtilis* lipase (BSL2) on HKUST-1 using a similar method ($[Cu_3(btc)_2]$, btc: 1,3,5-benzenetricarboxylate). The performance of the enzyme/MOF composites increased 17-fold[187] compared to the free enzyme. Similar to surface attachment methods, covalent binding strategies require the support materials to be synthesised in advance. However, they must be designed or post-synthetically modified to enable covalent bonding to the enzyme in a specific manner. The chemical bond formed between the amine groups of the enzyme and carboxylate groups of the MOF (or vice versa) results in a further increase in the robustness and recyclability of the enzyme/MOF compared to non-covalent surface adsorption. The pioneering work highlighting covalent binding was reported by Park et al. in 2011 for the immobilisation of *Candida antarctica* Lipase B (CAL-B) on 1D-MOF ([(Et2NH2)(In(pda)2)], pda: 1,4-phenylenediacetate), 2D-MOF ([Zn(bpydc)], bpydc: 2,2′-bipyridine 5,5′-dicarboxylate), and IRMOF-3 ($[Zn_4O(NH_2\text{-}bdc)_3]$) NH2-bdc: 2-amino-1,4-benzene dicarboxylic acid. The immobilised enzyme showed higher activity than free CAL-B while its enantioselectivity was maintained. CAL-B on IRMOF-3 showed the highest performance with a 1000-fold increase compared to the free enzyme[188].

Recently, the potential for *in situ* encapsulation of an enzyme within a framework has attracted much interest[189]. In this approach, the MOF crystals are directly synthesised around the protein, which bypasses the pore size limitation discussed above. For *in situ* encapsulation, the targeted

MOF should be synthesised at ambient temperature (or lower) to avoid deactivation of the enzyme. Embedding the enzyme into the MOF crystals provides a protective layer around the enzyme and prevents leaching of the enzyme back into solution. The first encapsulation was reported for cytochrome c (Cyt c)@ZIF-8 by Lyu et al.[189]. The small pore size of ZIF-8 (3.4 Å) prevents the diffusion of enzymes into its pores but *in situ* encapsulation overcomes this bottleneck by growing the MOF framework around the enzyme. By the addition of a solution of Cyt c and polyvinylpyrrolidone (PVP) to a methanol solution of 2-methylimidazole and zinc nitrate hexahydrate, the ZIF-8 crystal grew around Cyt c. Enzyme immobilisation often leads to loss of activity, but within ZIF-8, the performance of Cyt c@ZIF-8 improved 10-fold compared to the free enzyme. Additionally, the substrate affinity of Cyt c@ZIF-8 was increased, which may be attributed to the conformational changes of the enzyme in a methanol solution. Alternatively, the microenvironment of ZIF-8 may have improved its substrate affinity through a set of interactions in the MOF interior[189].

ZIFs have been of much interest because of their high thermal and chemical stability, high porosity, low cytotoxicity, tuneable surface and ease of synthesis under mild conditions[165, 190-192]. The first ZIF-8 synthesis was reported in dimethylformamide (DMF) by Chen et al.[193]. Different methods have been reported for synthesising ZIFs, namely; sonochemical protocols [194], microwave-assisted solvothermal method[195], mechanochemical grinding[196], solvothermal[165, 197] and hydrothermal methods[198, 199]. Furthermore, the molar ratio between the ligand and Zn^{2+} ions can change the resulting crystal size of ZIF-8. For example, the average crystal size of ZIF-8 decreased upon increasing the ratio of 2-methylimidazole (HMIM) to Zn (Figure 1. 24)[199].

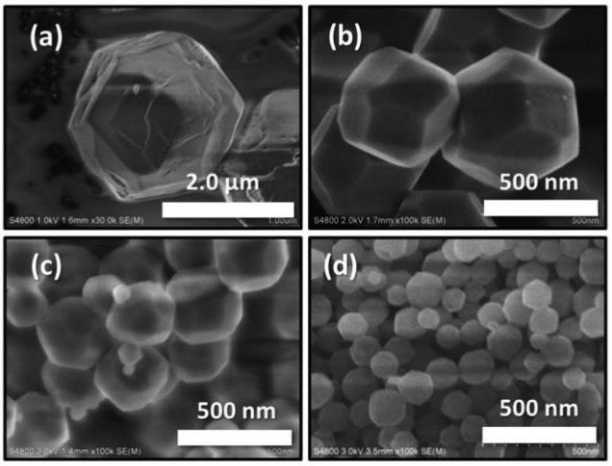

Figure 1. 24 The scanning electron microscopy of ZIF-8 crystals shows the effect of the different molar ratio of HMIM to Zn. The molar ratios are: (a) 40, (b) 60, (c) 80, and (d) 100. This figure is from "Formation of high crystalline ZIF-8 in an aqueous solution" by Kida et al.[199].

Cui et al. studied show different ratios of Zn:L (1:1 to 1:20) affected the morphology[200]. Lai et al. showed that changing the solvent from DMF to water decreased the micropore volume from 0.663 to 0.32 cm^3 g^{-1} [165, 198, 199]. A study by Polyzoidis et al. demonstrated how the reaction conditions affected the microscopic and macroscopic morphology of ZIF-8[201]. In this study, a longer reaction time (aging) gave rise to larger crystals, with well-shaped rhombic dodecahedral crystals being formed at lower concentrations of reactants. This was rationalised by an increase in concentration, leading to an increase in the number of collisions, resulting in non-uniform crystals[201]. ZIF-8 crystals are very stable in alkaline solutions[165]. However, studies from Wang et al. showed that ZIF-8 was decomposed in acidic media[202]. Such properties make ZIFs ideal candidates in drug delivery since at lower pH in the body the crystals will decompose, and the encapsulated drug will be released[202-204].

ZIFs are excellent candidates for *in situ* encapsulation of an enzyme. They have high chemical and thermal stability, in addition to which, they form in aqueous media under mild temperature and pH conditions[189]. When the activity of immobilised horseradish peroxidase (HRP) in ZIF-8 was investigated by immersing in boiling water for one hour, the free enzyme lost all its activity while HRP@ZIF-8 remained 88 % of its activity. This high stability was explained by the small pore size of ZIF-8 which fitted tightly around the enzyme. This study compared encapsulation of HRP in different pore sized of SiO_2 crystals, and it was observed that different pore sizes showed a different level of activity[205]. The smaller pore size in SiO_2, the higher activity maintained by HRP. For example, HRP@SiO_2 with 7 nm pore showed 65 % activity, while this value for 100 nm sized pores in SiO_2 was only 13 %[205]. Liang et al. synthesised ZIF-8 at a 1:4 molecular ratio of Zn to ligands for encapsulation of bovine serum albumin (BSA) and showed that by increasing the concentration of BSA the formation rate of the BSA/ZIF-8 biocomposite was enhanced, while its crystallinity decreased[205].

Additionally, it was shown that the presence and concentration of the protein affect the formation of ZIF-8 and may require a higher ratio of ligand to zinc[205-207]. A study by Pitzalis et al. showed that by decreasing the pH of the synthetic solution, the loading of the enzyme increases[208]. They also reported that the highest surface area for ZIF-8 was obtained at pH 10.2, and at pH 9.4, the surface area decreased[208].

Other types of ZIFs have been successfully employed for encapsulation. Shieh et al. reported the encapsulation of catalase within a ZIF-90 framework. One of the good examples of immobilisation is its application in the textile industry. Catalases and proteases are both employed in the textile industry. Proteases cleave the peptide bonds of the catalase; therefore, their coexistence in solution is prohibited. To protect catalase in the presence of the proteases, the catalase was encapsulated in ZIF-90 crystals. In a typical synthesis for the biocomposite,

an aqueous solution of zinc nitrate, Zn $(NO_3)_2$, was added to an aqueous solution of imidazolate-2-carboxaldehyde (HICA), catalase, and PVP as the stabilising agent. The smaller pore size of ZIF-90 than catalase prevents the leaching of the encapsulated enzyme and protecting it against protease. Overall the high chemical stability of ZIF-90 combined with its synthesis in water and size control makes it favourable support for in-situ encapsulation[209-211].

1.9.2 Bacterial compartments

Compartmentalisation is a strategy where cells use protein compartments to store nutrients and control metabolism[212, 213]. The protein-based compartments have been employed in various technologies, for example imaging probes[214], delivery systems[215] and nanoreactors[216]. For example, icosahedral viruses have been employed in the encapsulation of chemotherapeutic agents, allowing for a controlled released of medicine[217]. The encapsulation of biomolecular cargo can be performed by interior modification of protein for electrostatic, hydrophobic and hydrogen bonding interaction between cargo and protein[218-220]. Cowpea Chlorotic Mottle virus (CCMV) has been used for encapsulation by adjusting the pH. The virus solution dissociates at pH 7.5 into 90 dimers and forms capsids at pH 5.0. Cargo can be added to the CCMV at pH 7.5, and subsequent lowering of the pH to 5.0 promotes capsid formation (Figure 1. 25). Since CCMV has an interior positive charge, it favours negatively charged cargo molecules[218, 221-223].

Bacterial micro compartments (BMCs) are a family of organelles formed by 4-7 individual shell proteins, with approximately 4000 subunits yielding an icosahedral geometry with an 80-400 nm diameter[224 225]. The first study showing the possibilities of BMCs for cellular inclusion was in 1961 when dense polyhedron-shaped carboxysomes were discovered by electron microscopy inside cyanobacteria and subsequently in chemoautotrophs bacteria[226-228].

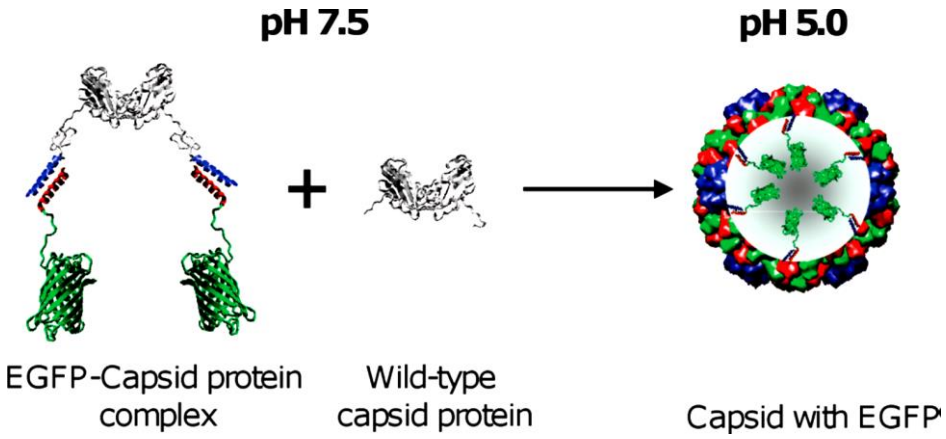

Figure 1. 25 Schematic encapsulation of enhanced green fluorescent protein (EGFP) in CCMV virus. The tagged EGFP is mixed with capsid at pH 7.5 and dialyzed to pH 5.0. This figure is from "Controlled Encapsulation of Multiple Proteins in Virus Capsids" by Minten et al.[218].

The efficient growth of a group of microorganisms under inorganic carbon-limiting conditions was attributed to the encapsulation of Rubisco (RuBisCO) and carbonic anhydrase in the carboxysome. This assisted the microbe to grow by allowing it to fix carbon dioxide via a carbon concentrating-mechanism[229, 230]. It also was suggested that the carboxysomal shell prevents oxygen from reaching the enzyme inside. As RuBisCO is a bifunctional enzyme that catalyses fixation of O_2[231, 232] and blocking an increase in oxygen concentration enhances the activity of the enzyme[233]. Subsequently, the structure of these carboxysomes was studied to gain insight into the mechanism of outer shell formation. Electron microscopy of the carboxysome showed polyhedral bodies with an average diameter of 100 nm in an icosahedral structure with 5-, 3- and 2-fold symmetry axes (Figure 1. 26 a)[234].

The crystal structure of the carboxysome showed that the shell is formed by the assembly of smaller unit proteins. In *Halothiobacillus neapolitanus*, the genes responsible for carboxysome function are encoded in the Cso operon. These small shell proteins are named carboxysome **s**hell 1 (CsoS1) and are encoded on the bacterial chromosome in order: Csos1C, Csos1A, and

Csos1B. These proteins possess 80 % sequence similarity. CsoS1A is a cyclic hexameric building block, consisting of six monomeric subunits with a central pore (Figure 1. 26 b) [235].

a b

Figure 1. 26 a) The polyhedral bodies formed by carboxysome, which possesses icosahedral symmetry, b) Representation of the hexamer structure of CsoS1A. Figure a is from "Structure of *Halothiobacillus neapolitanus* carboxysomes by cryo-electron tomography" by Schmid et al.[234]. Figure b is from "Structural analysis of CsoS1A and the protein shell of the *Halothiobacillus neapolitanus* carboxysome" by Tsai et al.[236].

A large carboxysome with a diameter of 1,100 Å has 4,500 shell subunits (triangulation number[1], T= ~75), whereas a small carboxysome shell with a diameter of ~850 Å contains ~3,500 shell subunits (T= ~60)[237]. For many years the only known BMCs were carboxysomes, until 1994, when it was found that *Salmonella enterica* could form polyhedral organelles involved in coenzyme B_{12}-dependent 1,2-propanediol degradation[238]. By packaging the B12-dependent diol dehydratase and other enzymes responsible for diol degradation in a protein shell, the cells could be protected from propionaldehyde, which is a toxic intermediate of diol degradation[239]. Further studies showed that the BMC domains could be found in enteric bacteria like *Escherichia coli*. Also, 189 BMC genes have been identified so far in the

[1] triangulation numbe (T): The number of facets per triangular face of an icosahedron

*Acidobacteria, Actinobacteria, Planctomycetes, Fusobacteria, Firmicute*s and almost all groups of the *Proteobacteria*[237].

Encapsulins are a novel class of BMCs that have been recently characterised[240]. Encapsulins were discovered as high molecular weight aggregates in by *Brevibacterium linens* in 1994[241, 242]. They have a smaller diameter than other BMCs, (25-32 nm), and are known as nano compartment proteins[242-246]. In contrast to viruses like CCMV, which are pH dependent and can be reversibly disassembled, reversely at different pH, encapsulins are highly stable. This makes encapsulin an attractive target for packaging proteins to stabilise them at higher temperatures and extreme pH[247, 248]. In contrast to BMCs that form from multiple homologous proteins, encapsulins are comprised of a single protein[249, 250], that can be employed to package the cargo protein inside. The cargo protein requires a peptide tag, identical to the native cargo encapsulin, on the C terminus region[240]. This peptide tag acts as an anchor, enabling the interaction of non-native cargo proteins with the encapsulin. Two architectures have been reported for encapsulins so far. The first group includes *Thermotoga maritima (T. maritima)*[240], *Rhodococcus erythropolis*[248] and *Mycobacterium tuberculosis*[244]. These have a triangulation number =1 (T= 1) and consist of 60 identical subunits with a 20-24 nm diameter. *Pyrococcus furious*[250] and *Myxococcus xanthus (M. xanthus)*[250] from the second group, which have a triangulation number of three (T= 3), and contained 180 identical subunits with a larger diameter (30-32 nm)[251].

Due to their properties and being able to internalize various cargo proteins by simply introducing a targeting sequence at the C-terminal, encapsulins are an attractive platform for different applications[215, 252].

Thesis objectives

Various strategies to improve the oxidation activity of P450Bm3 will be studied in this thesis. To exploit the activity of P450Bm3 in the oxidation of the non-natural substrate, different mutuant forms will be investigated. To improve the oxidation activity of P450Bm3, the rate accelerating variants (RLYFIP, KT2 and R19) will be studied, and their regio- and stereoselectivity will be compared with WT P450Bm3 (chapter 3). The effect of decoy molecules in combination with different variants will be evaluated (chapter 4). The mutation of phenylalanine in the active site, within the GVQ variant, will be studied to check how it alters the activity and selectivity of P450Bm3 (chapter 5). The effect of altering substrate and decoy molecule size on the oxidation activity of P450Bm3 variants will also be discussed (chapter 5). A potential role for P450Bm3 variants in flavour and fragrance industries will be examined in the selective biocatalytic oxidation of isophorone to (*R*)-4-hydroxyisophorone (chapter 6). The mutation of threonine 268, which is involved in dioxygen activation, will be investigated to study the changes in the catalytic cycle of P450Bm3. The epoxidation, hydroxylation and sulfoxidation activity of this haem domain which uses H_2O_2 will be compared with P450Bm3 holoenzymes. It also will be examined to assess if decoy molecules are effective in improving the activity of this variant (chapter 7). To improve the thermal and chemical stability of the P450Bm3, its immobilisation in zeolitic imidazolate frameworks (ZIF-8 and ZIF-90), as well as bacterial nanocompartment encapsulin, will be studied (chapter 8).

Chapter 2

Experimental

Experimental data for chapter 8 are provided in this chapter. Experimental details for the published papers are included in these chapters, either in the main paper or supplementary information.

General

General reagents and organics were purchased from Sigma-Aldrich, Tokyo Chemical Industry (TCI), Chem-Supply or Fluorochem. Isopropyl-β-D-thiogalactopyranoside (IPTG), antibiotics and buffer components were obtained from Astral Scientific (Australia).

UV-Vis spectroscopy assays were performed on an Agilent Cary 60 spectrophotometer and were recorded at 30 ± 0.5 ºC. Gas Chromatography-Mass Spectrometry (GC-MS) was carried out on a Shimadzu GC-2010 with GC–MS-QP2010S detector with a DB-5 MS fused silica column (30 m × 0.25 mm × 0.25 μm). Gas Chromatography (GC) was carried on a Shimadzu Nexus GC-2030 with FID detector and a DB-Wax column (30 m × 0.25 mm × 0.25 μm). The methods of GC and GC-MS methods are provided in Table 2. 1.

Table 2. 1 GC-MS and GC operating conditions

GC-MS	Method
Helium flow rate 1.3 ml min^{-1}	
Injector temperature: 250 °C	
Interfacer temperature: 280 °C	
styrene	60 °C (hold 3 min), 10 °C min^{-1} to 200 °C (hold 5 min)
isophorone	80 °C (hold 3 min), 10 °C min^{-1} to 200 °C (hold 5 min)
GC	
Helium flow rate 3.5 ml min^{-1}	
Injector temperature: 250 °C	
Interfacer temperature: 250 °C	
styrene	60 °C (hold 3 min), 6 °C min^{-1} to 120 °C (hold 2 min), 25 °C min^{-1} to 220 °C (hold 2 min)
isophorone	100 °C (hold 3 min), 8 °C min^{-1} to 180 °C (hold 6 min.), 25 °C min^{-1} to 220 °C (hold 2 min.)

2.1 Protein expression and purification

The plasmid pT7 containing the gene encoding the P450Bm3 haem domain Thr268Glu mutant (Bm3TE) was transformed into *E. coli* BL21 (DE3) competent cells and grown on an LB plate in the presence of ampicillin (100 μg ml^{-1}). A single colony was added to 500 mL of LB[2] media containing trace elements solution ($CaCl_2$, $ZnSO_4.7H_2O$, $MnSO_4.H_2O$, Na_2-EDTA, $FeCl_3.6H_2O$, $CuSO_4.5H_2O$, and $CoCl_2.6H_2O$) and ampicillin, was incubated at 37 °C, 110 g. After 14 hours incubation, the temperature was lowered to 18 °C followed by the addition of 0.02 % v/v benzyl alcohol and 2 % v/v ethanol after 30 min. IPTG (100 μM) was added to induce protein expression. Cells were harvested after 24 hours by centrifugation (5000 *g*, 10 min, 4 °C) and resuspended in Tris buffer (50 mM, pH 7.4, containing 1 mM DTT). The cells were lysed by sonication on ice for 30 min (20 s on, 40 s off) and cell debris was removed by centrifugation (40000 *g*, 20 min, 4 °C). The supernatant was loaded onto a DEAE Sepharose column (XK50, 200 mm × 40 mm; GE Healthcare) and eluted using a linear salt gradient (100-400 mM KCl in Tris buffer). The red coloured fractions which contain the P450 enzyme were

[2] LB: Yeast extract (5 g), Tryptone (10 g), NaCl (10 g)

combined and concentrated by ultrafiltration (1900 *g*, 4 °C) using 10 kDa membranes (Vivacell 100, Sartorius). Concentrated protein was desalted using a Sephadex G-25 medium grain column (250 mm × 40 mm; GE Healthcare). This was concentrated by ultrafiltration as described above to approximately 10 ml before being loaded onto a Source-Q ion-exchange column (XK26, 80 mm × 30 mm, GE Healthcare). The proteins were purified on an AKTA purifier (GE Healthcare) and eluted using a linear salt gradient (100 - 400 mM KCl in Tris buffer). Fractions with A_{418}/A_{280} > 0.5 were collected and concentrated. Afterwards, an equivalent volume of 80 % glycerol was added to protein and filter sterilised before it was stored at -20 °C.

2.2 Spin state shift

Bm3TE was diluted to ~ 3 μM with Tris buffer (50 mM, pH 7.4). An aliquot of the 2-methylimidazole (HMIM) (0.5 μL from 160 mM stock solution in ethanol) was added to 500 μL of the enzyme solution, and the spectrum was recorded from 700 nm to 250 nm. Further aliquots of the substrate were added until the enzyme solution was saturated with the substrate.

2.3 Encapsulation of Bm3TE@ZIF-8

Bm3TE (1 ml) in Milli-Q H_2O was added to 500 μl of an aqueous solution of 2-methylimidazole (HMIM, 640 mM) and mixed with 500 μl of an aqueous solution of zinc acetate dihydrate ($Zn(CH_3CO_2)_2.2H_2O$, 40mM). The molar ratio of HMIM:Zn was held at 16:1. The solution was aged at room temperature under the static condition for 24 h. The resultant white crystalline powder was collected by centrifugation (7000 *g*, 5 min) and then washed, sonicated and centrifuged (×3) to remove loosely adsorbed enzyme.

2.4 Encapsulation of Bm3TE@ZIF-90

Bm3TE (1 ml) in Milli-Q H_2O was added to 500 µl of an aqueous solution of 2-imidazole carboxaldehyde (HICA, dissolved at elevated temperature, 160 mM) and mixed with 500 µl of an aqueous solution of zinc nitrate hexahydrate ($Zn(NO_3)_2 \cdot 6H_2O$, 40 mM). The molar ratio of HICA:Zn was held at 4:1. The solution was left at room temperature under static conditions for 4 h. The precipitate was collected by centrifugation (7000 *g*, 5 min) and then washed, sonicated and centrifuged (×3) to remove any loosely adsorbed enzyme.

2.5 Pre-synthesised ZIF-8 crystals

Zinc nitrate hexahydrate ($Zn(NO_2)_3 \cdot 6H_2O$, 58.8 mg, 0.197 mmol) was dissolved in methanol (4 ml). In a separate vial 2-methylimidazole (HMIM, 64.8 mg, 0.787 mmol) was dissolved in methanol (4 ml). Both solutions were sonicated until the solids dissolved. The $(Zn(NO_2)_3 \cdot 6H_2O$ solution was added to the solution of HMIM, and the mixture was left at room temperature to age under static conditions for 24 hrs. The resultant white suspension was centrifuged (7000 *g*, 5 min) and washed with methanol (5×10 ml) then dried yielding a white crystalline powder[253].

2.6 Pre-synthesised ZIF-90 crystals

Zinc nitrate ($Zn(NO_3)_2$, 37.125 mg) was dissolved in water (2 ml) and added to 2 ml of a solution of 2-imidazole carboxaldehyde (HICA, 40.0 mg) in MilliQ H_2O/glycerol (9:1-1:1). (For PVP studies, 5.0 mg PVP (0.2 wt %,) was added to the solution). The reaction mixture was left at room temperature, and the precipitated products were collected by centrifugation (7000 *g*, 5 min) and washed[254].

2.7 Powder X-ray diffraction

Powder X-ray diffraction (PXRD) data were collected on a Bruker D8 Advance or D4 Endeavor X-ray powder diffractometer. The details of the PXRD are provided in Table 2. 2. The data obtained from the D4 instrument were converted by PowDLL Converter and expressed as the Cu source radiations.

Table 2. 2 PXRD D8 and D4 operation conditions.

X-ray powder diffractometer	Diffraction method	Source of radiation	Kα radiation (Å)	2 θ (°)
D8	capillary (0.5 mm) loaded	Cu anode	1.5418	2-52
D4	flat plate	Co anode	1.78897	5-32

2.8 Scanning electron microscopy (SEM)

SEM images were collected using a Philips XL30 Field Emission Scanning Electron Microscope (FESEM) at Adelaide Microscopy. Samples were dry loaded onto adhesive tabs on aluminium stubs and coated with a 5 nm carbon coating. N_2 (UHP grade) adsorption isotherm measurements were performed on a 3Flex physisorption analyser. The temperature was maintained at 77 K via a helium cryostat[253].

2.9 Fluorescein isothiocyanate-tagged Bm3TE

Fluorescein isothiocyanate (FITC, 0.5 mg) and Bm3TE were dissolved in carbonate-bicarbonate aqueous buffer solution (4 mL, 0.1 M, pH 9.2) and left for twelve hours in the dark at 4 °C under gentle stirring. The fluorescein-tagged Bm3TE, FITC-Bm3TE, was recovered by passing the reaction mixture through an Illustra NAP-25 column (GE Healthcare Life Sciences, NSW, Australia). The protein solution was concentrated through a 10 kDa membrane by

centrifugation at 4 °C (4000 *g* for 20 min), followed by solvent-exchange with MilliQ H_2O twice to ensure the complete removal of buffer salts in the solution. The concentrated tagged protein solution was passed again through a NAP-25 column to ensure the complete removal of unreacted FITC molecules[255].

2.10 Confocal laser scanning microscopy (CLSM)

The presence and spatial location of the fluorophore-tagged proteins in (or on) the MOFs composites was determined using CLSM (Olympus FV3000 Confocal Laser Scanning Microscope, OLYMPUS). The fluorescein-tagged proteins were excited at 488 nm, and the fluorescence signal was collected in a window from 495 to 545 nm[256].

2.11 Activity assays

The peroxygenase turnover assays for the Bm3TE variant was run in 500 µl Tris buffer (pH 7.4, 50 mM) at room temperature containing 3 µM enzyme and 5 mM of the substrate. The reaction was started by the addition of 60 mM H_2O_2 and quenched after 5 min by the addition of 400 µl ethyl acetate.

The NADPH monooxygenase turnover assays for Bm3R19 was run in 500 µl Tris buffer (pH 7.4, 50 mM), containing ~200 nM enzyme (Bm3R19 variant was generated as detailed in Chapter 7). 1 mM of the substrate and ~ 320 µM NADPH was added. The reaction was mixed by inversion and left overnight to ensure it ran to completion.

After the NADPH consumption or H_2O_2 assays were completed, 495 µL of the reaction mixture was mixed with 5 µL of an internal standard solution (p-cresol, 20 mM stock solution in DMSO). The mixture was extracted with 400 µL of ethyl acetate, and the organic extracts were used directly for GC-MS or GC analysis. Products were initially identified by GC-coelution

experiments and matching the GC-MS spectra to those of the products. Metabolites were calibrated against authentic standards using the assumption that isomeric products would give comparable responses, e.g., phenylacetaldehyde and styrene oxide were presumed to give the same detector response.

2.12 Encapsulation of Bm3R19 in Mx and Tm encapsulins

Plasmids of pCDFDuet (Novagen, Merkmillipore) containing the gene encoding the cargo plasmid (Bm3TmTP or Bm3MxTP) and pBAD with the encapsulin (TmEnc or MxEnc) genes were transformed together into *E. coli* BL21 (DE3) competent cells, for co-expression, and grown on an LB plate in the presence of ampicillin (100 μg ml^{-1}) and streptomycin (50 μg ml^{-1}). A single colony was added to 5 mL of LB media containing ampicillin and incubated at 37 °C, 110 *g* overnight. 500 μl of the overnight culture was added to 50 ml LB and incubated at 37 °C, 110 g. After 4 hours the temperature was lowered to 18 °C followed by the addition of 0.02 % v/v benzyl alcohol and 2 % v/v ethanol after another 30 min IPTG (100 μM) was added to induce cargo protein expression. Cells were harvested after 3 hours by centrifugation (5000 *g*, 7 min, 4 °C). The cell pellet was resuspended in 100 ml fresh LB containing streptomycin (50 μg ml^{-1}) and induced with 0.2 % arabinose followed by overnight incubation at 20 °C, 80 g. The overnight growth was centrifuged at 4600 *g* for 7 min to harvest the cell pellet. The pellet was resuspended in 30 ml Tris buffer (20 mM, pH 8) and sonicated on ice for 10-15 min (20 s on, 20 s off, Branson Ultrasonics Sonifier B-30, microtip, 3.2 mm). The cell lysate centrifuged at 18000 *g* for 12 min at 4 °C. The supernatant was collected, and 500 mM NaCl was added. Addition of 10 % PEG 8000 turned the solution cloudy, after a gentle mixing the solution was left on ice and centrifuged at 38000 *g* for 12 min at 4 °C after 40 min. The pellet was centrifuged again at 38000 *g* for 5 min at 4 °C, and residual supernatant was removed using a pipette. As a final wash, 5 ml Tris (20 mM, pH: 8) was added and then centrifuged at 38000

g for 5 min. The pellet was resuspended in ~13 ml cold Tris buffer (20 mM, pH 8) and filtered through 0.2 μm syringe filter. The filtered protein (3 ml) was loaded to HiPrep 16/60 Sepharcyl S-500 HR column (GE Healthcare) in Tris buffer (20 mM, pH 8) on AKTA purifier (GE Healthcare) and eluted with 1 ml min^{-1} Tris (20 mM, pH 8). The encapsulin containing fractions were collected and concentrated by ultrafiltration (1900 g, 4 °C) using 10 kDa membranes (Vivacell 100, Sartorius), then loaded to HiTrap Q FF anion exchange eluted using a linear salt gradient (0 - 1 M NaCl in Tris buffer)[252].

2.13 Sodium dodecyl sulfate polyacrylamide gel electrophoresis (SDS-PAGE)

SDS-PAGE was run using 10 % Tris-Glycine gel, staining with Coomassie Blue and ran under Tris-Glycine-SDS buffer. Colour Prestained Protein Standard, Broad Range 11 – 245 kDa (NEB) was used as a ladder for SDS-PAGE. The Gel matrixes are provided in Table 2. 3

Table 2. 3 Gel matrix for SDS-PAGE

	Separating Gel (10 %)	Stacking Gel
H_2O	3.8 ml	3.6 ml
1 M Tris pH 9	7.8 ml	-
1 M Tris pH 7	-	625 μl
10 % SDS	200 μl	50 μl
Acrylamide	4.8 ml	800 μl
10 % APS*	200 μl	50 μl
TEMED**	20 μl	5 μl

* APS: Ammonium persulfate
** TEMED: Tetramethylethylenediamine

Chapter 3

Increasing the activity and efficiency of stereoselective oxidations by using decoy molecules in combination with rate-enhancing variants of P450Bm3

Citation:

Munday, S. D.; Dezvarei, S.; Bell, S. G., ChemCatChem 2016, 8 (17), 2789-2796.

Statement of Authorship

Title of Paper	Increasing the Activity and Efficiency of Stereoselective Oxidations by using Decoy Molecules in Combination with Rate-Enhancing Variants of P450Bm3.
Publication Status	☑ Published ☐ Accepted for Publication ☐ Submitted for Publication ☐ Unpublished and Unsubmitted work written in manuscript style
Publication Details	Munday, S. D.; Dezvarei, S.; Bell, S. G., Increasing the Activity and Efficiency of Stereoselective Oxidations by using Decoy Molecules in Combination with Rate-Enhancing Variants of P450Bm3. ChemCatChem 2016, 8 (17), 2789-2796.

Principal Author

Name of Principal Author (Candidate)	Samuel D Munday
Contribution to the Paper	Preparation of the enzyme, turnovers of substrates with substrtaes with KT2 and WT variants, data analysis and discussion, manuscript preparation.
Overall percentage (%)	50
Certification:	This paper reports on original research I conducted during the period of my Higher Degree by Research candidature and is not subject to any obligations or contractual agreements with a third party that would constrain its inclusion in this thesis. I am the primary author of this paper.
Signature	Date 22/03/2019

Co-Author Contributions

By signing the Statement of Authorship, each author certifies that:

i. the candidate's stated contribution to the publication is accurate (as detailed above);

ii. permission is granted for the candidate in include the publication in the thesis; and

iii. the sum of all co-author contributions is equal to 100% less the candidate's stated contribution.

Name of Co-Author	Shaghayegh Dezvarei
Contribution to the Paper	Preparation of the enzyme, turnovers of substrates with substrates with R19 and RLYFIP variants, data analysis and discussion, manuscript preparation.
Overall percentage (%)	40
Signature	Date 08/04/19

Name of Co-Author	Stephen G. Bell
Contribution to the Paper	Experimental design, supervision, manuscript preparation.
Signature	Date 8/04/2019

ChemPubSoc Europe
DOI: 10.1002/cctc.201600551
CHEMCATCHEM Full Papers

Increasing the Activity and Efficiency of Stereoselective Oxidations by using Decoy Molecules in Combination with Rate-Enhancing Variants of P450Bm3

Samuel D. Munday, Shaghayegh Dezvarei, and Stephen G. Bell*[a]

The use of rate-accelerating variants of P450Bm3 coupled with decoy molecules is described, resulting in improved catalytic activity for hydroxylation and epoxidation reactions. Prochiral substrates were investigated to ascertain the effect of the mutant enzymes and the decoy molecules on the regio- and enantioselectivity of the oxidations. For the alkyl and alkene substituted benzene substrates tested, large improvements in the product formation activity over the wild-type enzyme were obtained. The product formation rates for the substrates tested ranged from 660 to 2210 nmol(nmol P450)$^{-1}$ min^{-1} for variants containing the R47L and Y51F mutations. Although the regioselectivity was not significantly altered in most of the turnovers, some adjustment in the enantioselectivity was observed with smaller substrates. The addition of decoy molecules often resulted in improved enantioselectivity and counteracted reductions arising from the rate-accelerating mutants.

Introduction

Cytochrome P450s (CYPs) are heme-dependent enzymes that are able to insert a single oxygen atom from molecular dioxygen into a carbon–hydrogen bond to give the corresponding alcohol or oxidise an alkene to yield an epoxide.[1] Nature has evolved many of these enzymes so that these reactions occur with total regio- and stereoselectivity.[2] The selective hydroxylation of unactivated C–H bonds by chemical methods is energy-intensive, non-selective and generates unwanted side products and toxic wastes. Biocatalytic asymmetric epoxidations are also of great interest. These CYP-mediated oxidation reactions have the potential to provide efficient biocatalysts for stereoselective oxidations to form alcohols and epoxides.[3]

CYP102A1 (P450Bm3) from *Bacillus megaterium* is a self-sufficient enzyme in which the electron transfer reductase domain is fused to the heme domain.[3b] It is soluble, easy to produce and requires only a substrate, NADPH and oxygen to operate. Its active state is a dimer that is capable of hydroxylating fatty acid substrates, at sub-terminal positions, with unusually high activity.[4] The fusion protein nature and high activity of P450Bm3 overcome two of the major hurdles to the use of these enzymes in synthesis.[3b,5] Wild-type (WT) P450Bm3 oxidises the majority of unnatural substrates at very slow rates, if at all. However, it has been used as a template for the design of biocatalysts through protein engineering.[3a,b,6] These studies have resulted in variants that are capable of selective oxidation reactions and recently even non-physiological functions such as cyclopropanation, amination and aziridination have been engineered into this enzyme.[6f,7]

P450Bm3 variants, such as I401P and KT2 (A191T/N239H/I259V/A276T/L353I) have been identified, which enhance the activity for unnatural substrate oxidation but maintain the product regioselectivity of the WT enzyme.[6a,8] The substrate-free forms of these generic accelerator mutants have been shown to have conformations that are similar to the fatty acid bound form of the enzyme (PDB: 1JPZ).[9] This is especially true in important regions such as the I helix, which is involved in the mechanism of oxygen binding and cleavage to generate the reactive intermediate.[6a,8a] In the crystal structure of the substrate-free form of the KT2 (PDB: 3PSX) and I401P (PDB: 3HF2) variants, the heme–axial water interactions were weakened. Kinetic studies also showed that the rate of the first electron transfer step for these variants in the absence of substrate were comparable to that when the substrate is bound. Therefore, it has been proposed that KT2 and I401P have catalytically ready conformations, such that substrate-induced changes to the structure play a less significant role in promoting the electron transfer steps, resulting in its ability to oxidise non-natural substrates at elevated rates.

Other variants include the R47L/Y51F (RLYF) mutant of P450Bm3, which has been shown to promote the oxidation of a range of unnatural substrates.[6a,10] It has been hypothesised that the RLYF couple allows better recognition and entry of more hydrophobic substrates. Mutations at these sites are known to reduce the affinity for the fatty acid substrate. However, this pair of amino acids is not conserved in many other members of the CYP102A subfamily, which bind and hydroxylate fatty acids.[11] The RLYF couple has been added to rate-accelerating P450Bm3 variants and has been found to further enhance their activity.[6a,8a,b] For example, the variant R19 (R47L/Y51F/H171L/Q307H/N319Y) has the RLYF couple to the KSK19

[a] S. D. Munday, S. Dezvarei, Dr. S. G. Bell
Department of Chemistry
University of Adelaide
SA, 5005(Australia)
E-mail: Stephen.bell@adelaide.edu.au

Supporting information and the ORCID identification number(s) for the author(s) of this article can be found under http://dx.doi.org/10.1002/cctc.201600551.

ChemPubSoc Europe

CHEMCATCHEM Full Papers

variant (minus the F87A mutation).[12] The RLYFIP (R47L/Y51F/I401P) variant contains the I401P mutant, which is on the proximal side of the heme and is known to be an effective rate-accelerating variant for several substrates.[8a,b]

In an alternative approach to improve the activity of P450 enzymes, chemically inert perfluorocarboxylic acids (PFCs) have been used as decoy molecules.[13] These greatly promote the oxidation of unnatural substrates such as benzenes, xylenes and short chain alkanes. The inert decoy fills part of the enzyme's active site causing conformational changes in the enzyme and constraining substrates to bind closer to the heme.[14] The structure of a PFC9-L-Trp-bound WT (PDB: 3WSP) showed that the decoy molecule (the *N*-perfluoroacyl amino acid, PFC9-L-Trp) filled the access channel but left enough space close to the heme to bind a substrate. These enzyme–substrate interactions in the vicinity of the heme remain relatively unaffected, allowing the reaction to proceed with the same selectivity of product formation.

It has been shown that incorporating the use of the decoy molecules, perfluoroctanoic (PFC8), perfluorononanoic (PFC9) and perfluorodecanoic (PFC10) acids, with WT and KT2 P450Bm3 significantly improves the rates of product formation for cyclohexane and several benzene-derived substrates. Importantly, the turnover with KT2 was more active and the product profiles of the oxygenated substrates remained predominantly unchanged.[15] The mechanisms by which decoy molecules and the rate-accelerating variants show enhanced unnatural substrate activity are different but work in concert to facilitate the oxidation of organic molecules. Here, we investigate the effect of the rate-accelerating variants and decoy molecules on the stereoselectivity of alcohol and epoxide formation by utilising substrates that are known to be oxidised to products that contain a stereocentre.

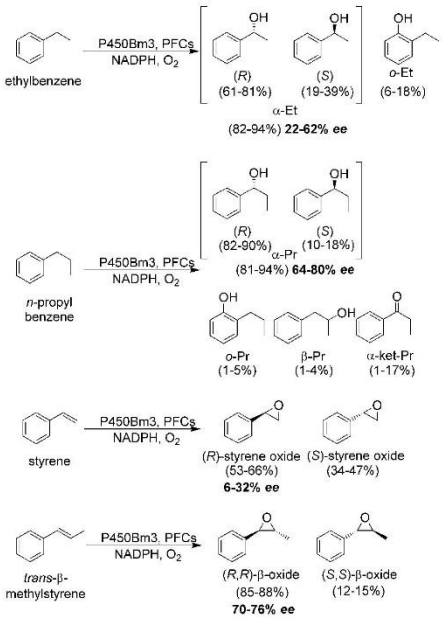

Scheme 1. Product distributions for the catalysed oxidation of ethylbenzene, *n*-propylbenzene, styrene and *trans*-β-methylstyrene in the presence and absence of decoy molecules. The products from ethylbenzene: 1-phenylethanol (α-Et) and 2-ethylphenol (*o*)-Et; from *n*-propylbenzene: 1-phenyl-1-propanol (α-Pr), 1-phenyl-2-propanol (β-Pr), 2-propylphenol (*o*)-Pr and propiophenone (α-ket-Pr); from styrene: styrene oxide; and from *trans*-β-methylstyrene: 1-phenylpropylene oxide (β-oxide). The values in italics represent the ratio of the (*R*)- and (*S*)-enantiomers of 1-phenylethanol, 1-phenyl-1-propanol and styrene oxide. For 1-phenylpropylene oxide, the values in italics represent the ratio of the (*R*,*R*) and (*S*,*S*) enantiomers of 1-phenylpropylene oxide. The values in bold are the enantiomeric excess (*ee*).

Results

Ethylbenzene and *n*-propylbenzene

Although they do not resemble the fatty acid substrates, ethylbenzene and *n*-propylbenzene are known to be oxidised by WT and KT2 P450Bm3 with high selectivity (Scheme 1).[6a,16] They are hydroxylated at the benzylic (or α) C–H bonds with *o*-hydroxylation resulting as a minor product for each (Scheme 1). In addition, WT P450Bm3 is known to be relatively stereoselective in its oxidation of *n*-propylbenzene, producing (*R*)-1-phenyl-1-propanol in excess over the (*S*) enantiomer (reported as an enantiomeric excess of 90%).[16a] Ethylbenzene and *n*-propylbenzene were both oxidised by WT and KT2 P450Bm3 in the presence and the absence of PFC decoy molecules (Figure 1, Table S1 in the Supporting Information). *n*-Propylbenzene was turned over with a product formation rate (PFR) of 368 nmol(nmol P450)$^{-1}$ min^{-1} (henceforth given as min^{-1}).[6a,16b] The WT/PFC9 combination increased the PFR four-fold over the WT reaction as a result of an increase in the rate of NADPH consumption as well as coupling efficiency (defined as the percentage of NADPH reducing equivalents used in the productive oxidation of the substrate). KT2, being in a catalytically ready conformation, oxidised *n*-propylbenzene three times faster than WT (Figure 1, Table S1). The combination of this enzyme and PFC10 was the optimum of those tested, being almost double that of KT2 (Figure 1). Overall, the combination of PFC10 with KT2 improved the rate of oxidation of *n*-propylbenzene 5.5-fold over the WT enzyme (Figure 1, Table S1).

The oxidation of ethylbenzene by the WT enzyme was significantly slower than *n*-propylbenzene (3.8 min^{-1}). Incorporating PFC9 into the reaction improved the rate 215-fold by augmentation of both the NADPH consumption rate and the coupling efficiency (Figure 1, Table S1). KT2 oxidised ethylbenzene faster than the WT enzyme and when used in combination with PFC9 the product formation rate was 350-fold greater than the WT enzyme alone (Figure 1). For both alkylbenzenes, the faster NADPH oxidation rate of KT2 was the key contributor to increased PFRs, as the coupling efficiency of the best WT and KT2 decoy molecule combinations were similar (Figure 1, Table S1).

ChemPubSoc Europe
CHEMCATCHEM Full Papers

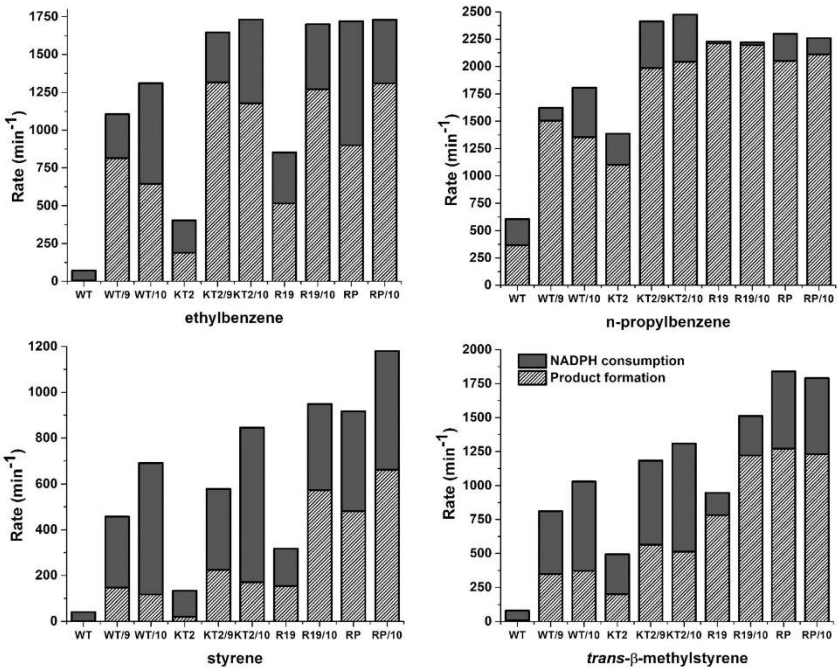

Figure 1. NADPH activity (black filled) and PFR (lined) of WT P450Bm3 and the rate-accelerating variants; KT2, R19 and RLYFIP (RP) with ethylbenzene, *n*-propylbenzene, styrene and *trans*-β-methylstyrene in the presence and absence of decoy molecules. The coupling efficiency is the ratio of the PFR to NADPH activity (Table S1).

The oxidation products were identified by GC-MS co-elution experiments with authentic standards where available. WT and KT2 P450Bm3 in the presence and absence of decoys primarily oxidised ethylbenzene and *n*-propylbenzene at the benzylic (α) position to give 1-phenyl-1-ethanol (α-Et, 83–92%,) and 1-phenyl-1-propanol (α-Pr, 91–94%) as the major products (Scheme 1, Figure 2, Table S2 in the Supporting Information). Minor products for both substrates were observed as a result of *o*-hydroxylation on the aromatic ring and for *n*-propylbenzene from hydroxylation of the β-position of the alkyl chain (2–4%, Scheme 1, Table S2). No hydroxylation of the terminal alkyl carbon was observed for either substrate nor was any desaturation product identified for ethylbenzene, which has been observed for some P450Bm3 variants.[16b] There was also the presence of a small amount of a ketone over-oxidation product of α-Pr in the *n*-propylbenzene turnovers (α-ket-Pr, 1–2%). Oxidation of either substrate at the α-position to give the hydroxylated product introduces a chiral centre (Scheme 1).

The chiral benzylic hydroxylation products were assigned by co-elution experiments by using a chiral GC column. WT and KT2 P450Bm3 were mostly selective for the (*R*)-enantiomer in the absence and presence of decoys (α-ET, 48% *ee* and α-Pr 74% *ee*). *n*-Propylbenzene was also oxidised predominantly to the (*R*)-enantiomer of α-Pr and the enantiomeric excess (*ee*) was greater than those of the equivalent ethylbenzene turnovers (Figure 2, Figure S1, Figure S2, Table S2).

WT oxidation of ethylbenzene was more enantioselective than KT2. The greatest enantiomeric excess of (*R*)-α-Et formed with WT P450Bm3 was 62% compared with 34% with KT2 (both using PFC10, Figure S1). WT and KT2 both displayed similar selectivity for (*R*)-α-Pr but the PFC9 and PFC10 decoys resulted in slightly more selective combinations for both (Figure 2, Figure S1, Table S2). The maximum enantiomeric excess of the (*R*)-α-Pr formed was 80% for WT and 72% for KT2 when decoy molecules were used (Table S2). These results agree with previous studies, which also observed the (*R*)-isomer being produced in large excess by WT P450Bm3 (Figure 2, Table S2).[16a]

Styrene and *trans*-β-methylstyrene

Styrene has previously been reported to be a poor substrate for WT P450Bm3 but other variants epoxidise this substrate to give styrene oxide as the major product. Mutations at the Ala82 and Thr438 residues have been shown to be effective in encouraging styrene oxidation.[17] The P450Bm3 variant A82F/T438F, which contains a more restricted active site, oxidised styrene to give the (*R*)-enantiomer of the epoxide in an

ChemPubSoc Europe
CHEMCATCHEM Full Papers

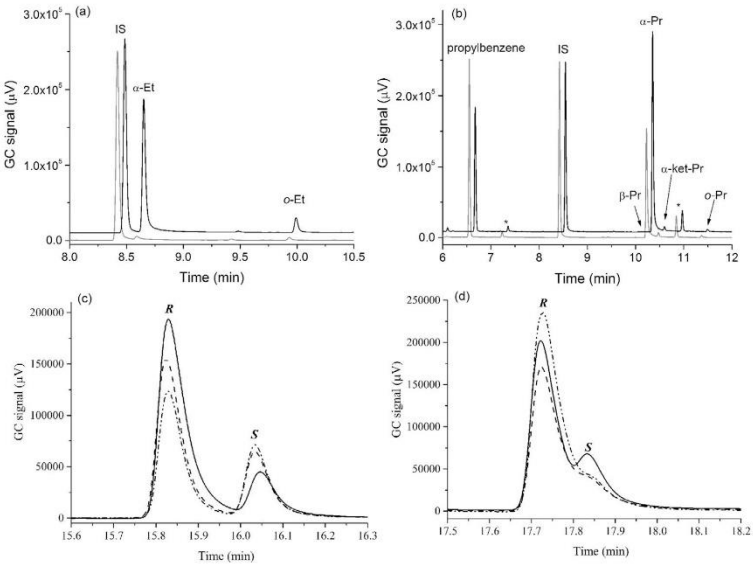

Figure 2. GC-MS analyses of (a) WT (grey) and WT/PFC9 (black) with ethylbenzene; (b) WT and WT/PFC9 with *n*-propylbenzene; (c) chiral GC analysis of the 1-phenylethanol product in the turnovers with RLYF/PFC10 (solid) R19/PFC10 (dash) and R19 (dash/dot) and (d) chiral GC analysis of the 1-phenyl-1-propanol product in the turnovers with KT2 (black) KT2/PFC10 (dash) and RLYFIP/PFC10 (dash/dot). The internal standard is labelled when shown (IS) as are impurities (*).

enantiomeric excess of 64%. *trans*-β-Methylstyrene has also been tested as a substrate with the KT2 variant and was oxidised at the double bond to give the epoxide mostly as the (*R*)-isomer (reported *ee*: 88%).[18]

The KT2 combinations oxidised both substrates with higher activities than the equivalent WT reaction in every circumstance. Overall, both styrene substrates were oxidised at slower rates than their alkylbenzene counterparts (Figure 1, Table S1). The addition of PFC9 generated the most efficient coupled reactions and PFC10 induced the highest NADPH activity but a lower coupling efficiency.

The inclusion of PFC9 in the WT-catalysed oxidation of styrene resulted in a 73-fold increase in PFR whereas PFC10 improved the rate 91-fold owing to the superior NADPH consumption rate (Figure 1, Table S1). The best improvement with a decoy and the KT2 variant was obtained by using PFC9, which increased the PFR by almost 12-fold over KT2 alone. The overall improvement of styrene oxidation was 140-fold when using KT2/PFC9 over WT (Figure 1, Table S1).

trans-β-Methylstyrene was oxidised at faster rates than styrene for all the combinations. For the WT enzyme/decoy molecule combinations, the greatest improvement was observed with PFC10 (41-fold increase in PFR) owing to a smaller reduction in coupling efficiency, compared with PFC9 combined with the fastest NADPH activity. For KT2, PFC9 was the optimum sized decoy, resulting in an almost 3-fold improvement in the PFR over KT2 alone. The coupling efficiency of the KT2/PFC9 turnover was 18% greater than the KT2/PFC10 system and was the most active combination for this substrate. The KT2/PFC9 system improved the oxidation activity of *trans*-β-methylstyrene 61-fold over the WT enzyme alone (Figure 1, Table S1).

The WT- and KT2-catalysed oxidation of both substrates was highly regioselective, with a major single product arising from both (Scheme 1, Figure 3, Table S2). Both were epoxidised at the double bond to yield styrene oxide (phenyloxirane) and 1-phenylpropylene oxide (β-oxide), respectively. Small amounts (~1%) of a second product arose in styrene turnovers, which from co-elution experiments was assigned as phenylacetaldehyde.[19] Small peaks (<1% of total product), which co-eluted phenylacetone and propiophenone, were observed in the P450Bm3-catalysed oxidation of *trans*-β-methylstyrene. No variation in the regioselectivity was observed for any of the enzyme/decoy combinations.

Styrene oxide, which contains a single stereocentre, was mostly generated as the (*R*)-stereoisomer with the enantiomeric excess ranging from 14–32% (Figure 3, Figure S1, Table S2). WT P450Bm3 epoxidation was more stereoselective than KT2 (18% vs. 14% *ee*) and the inclusion of decoys improved the enantiomeric excess of the (*R*)-isomer of both (up to 32% *ee*, Table S2). Epoxidation of *trans*-β-methylstyrene introduced two stereocentres. Both WT and KT2 were highly selective for the (*R*,*R*) isomer over the (*S*,*S*) and this oxidation was more stereoselective (≥70% *ee*) compared with that of styrene (Figure 3, Figure S1, Table S2). The results were in general agreement with those previously reported with KT2.[18] Unlike the oxidation of styrene, there was little variation in stereoselectivity between the WT and KT2 enzymes, nor did introducing

ChemPubSoc Europe
CHEMCATCHEM Full Papers

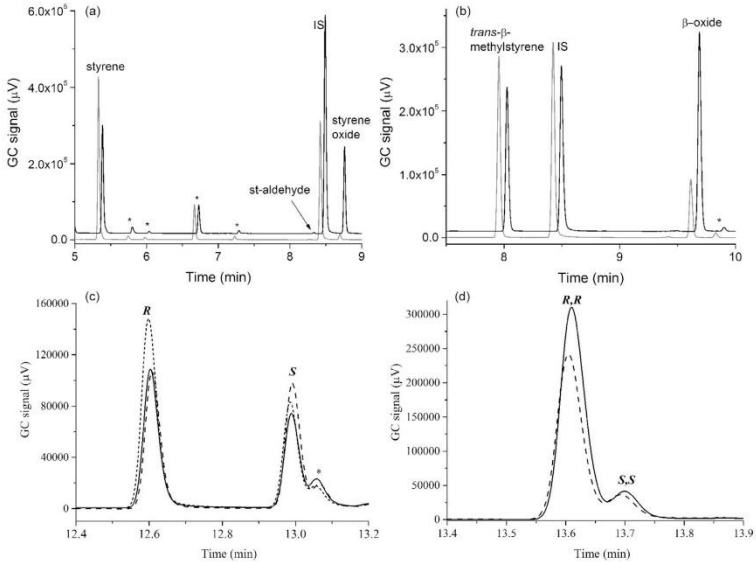

Figure 3. GC analyses of (a) WT with styrene (grey) and WT/PFC9 with styrene (black), (b) GC-MS analyses of WT and WT/PFC9 with *trans*-β-methylstyrene, (c) chiral GC analysis of the styrene oxide product in the turnovers with KT2 (black) KT2/PFC10 (dotted) and RLYFIP (dash) and (d) chiral GC analysis of the 1-phenylpropylene oxide product in the turnovers with KT2/PFC10 (dashed) and R19/PFC10 (black). The internal standard is labelled when shown (IS) as are impurities (*).

decoys significantly alter the enantiomeric excess (Figure 3 d, Table S2).

Rate-accelerating variants incorporating the R47L/Y51F couple

The above results show that the activity of P450Bm3 can be enhanced by adding fatty acid based decoy molecules to the WT enzyme and rate-accelerating variant KT2. We wanted to assess if decoy molecules could be used to enhance the oxidation of unnatural products when combined with highly active rate-enhancing variants that contain mutations at the R47 and Y51 residues. The arginine and tyrosine are known to interact with the acidic group of the fatty acids.[20] This pair of mutations would be expected to promote the oxidation of non-natural substrates but could potentially lower the affinity for the fatty acid decoy molecules. For all four substrates, the activity of product formation decreased in the order RLYFIP > R19 > KT2 > WT (Figure 1, Table S1). In all instances, both the NADPH oxidation activity and the coupling efficiency was greater for the variants containing the R47L/Y51F couple. The RLYFIP variant was better than R19 predominantly because of an increased NADPH oxidation rate even though its coupling efficiency was often lower (Figure 1, Table S1). The turnovers of *n*-propylbenzene and *trans*-β-methylstyrene with R19 and RLYFIP alone were better than the optimal KT2/PFC decoy molecule combinations (Figure 1, Table S1).

The oxidation of the smaller ethylbenzene and styrene substrates were both enhanced by adding PFC10 to the R19 and RLYFIP turnovers. In the case of ethylbenzene this was due to an increase in the coupling efficiency but the overall activity of product formation was similar to that observed with the KT2/PFC9 combination. With styrene there was an increase in both the NADPH oxidation activity and coupling efficiency when PFC10 was used as a decoy molecule (Figure 1, Table S1). There was significant improvement over the most active KT2 turnover with the rate enhancement of the RLYFIP/PFC10 combination being 410-fold more active than the WT enzyme alone (Figure 1, Table S1). The addition of the decoy molecule PFC10 to the turnover of *n*-propylbenzene with R19 or RLYFIP did not result in a significant increase in the product formation activity, which was already high (Figure 1, Table S1). Similarly, there was no increase in activity with *trans*-β-methylstyrene with the RLYFIP/PFC10 combination. However, the addition of PFC10 to R19 did enhance *trans*-β-methylstyrene oxidation mainly through an increase in the rate of NADPH oxidation (Figure 1). The epoxidation activities were enhanced over the KT2 combinations and the improvements over the WT enzyme alone for the R19 and RLYFIP mutants when using PFC10 as a decoy were both greater than 130-fold.

These combinations resulted in the highest product formation rates for the different substrates ranging from 661 min^{-1} for styrene, 1270 min^{-1} for *trans*-β-methylstyrene to 2210 min^{-1} for *n*-propylbenzene (Figure 1, Table S1).

ChemPubSoc Europe

CHEMCATCHEM Full Papers

The regioselectivities of styrene and *trans*-β-methylstyrene oxidation were unchanged compared with the WT and KT2 turnovers with epoxidation being the sole major product (>98%). The same was true for *n*-propylbenzene oxidation with 1-phenyl-1-propanol being the major product. Further oxidation to the α-ketone occurred in the R19 and RLYFIP turnovers, however, the selectivity for the α-position was ≥98% (Table S2). The regioselectivity of oxidation of ethylbenzene by R19 (82% α-Et) was similar to KT2 in that both were less selective than the WT (Table S2) in generating 1-phenylethanol as the major product. By contrast, the RLYFIP variant was marginally more selective producing 91% of 1-phenylethanol. In both instances, the addition of the PFC10 decoy molecule moderately increased the selectivity for the major product (Table S2).

The trends in enantioselectivity were more complex for the R19 and RLYFIP variants. The enantioselectivity for *trans*-β-methylstyrene oxidation was virtually unchanged across all of the variants and decoy molecule combinations although it was marginally lower for the turnovers with RLYFIP (70% vs. 75% *ee*, Table S2). The enantioselectivity of the 1-phenyl-1-propanol product in the R19 and RLYFIP turnovers was similar to the KT2 combinations although slightly lower than those of the WT (68–70% vs. 74–80% *ee*, Table S2). We note that the higher levels of the ketone further oxidation product may affect the results by favouring the oxidation of one enantiomer of the alcohol over the other. Larger changes were observed with the smaller substrates. With ethylbenzene, the preference for the *R*-enantiomer product with R19 (27% *ee*) was similar to KT2 (22% *ee*) whereas that of RLYFIP (51% *ee*) was more like the WT enzyme (48% *ee*) in having a larger enantiomeric excess (Table S2). The enantioselectivity of styrene oxide formation was lower for R19 (25% *ee*) whereas RLYFIP formed an almost equal mixture of both enantiomers (6% *ee*, Figure 3c, Table S2). Importantly, for both ethylbenzene and styrene turnovers the decoy molecule PFC10 increased the enantioselectivity of the turnover in line with what was observed for the WT and KT2 turnovers. This resulted in an improved *ee* of 62% for ethylbenzene hydroxylation by RLYFIP/PFC10 and 31% for styrene oxide formation by R19/PFC10 (Table S2).

Discussion

Overall, the rates of product formation of the four prochiral substrates were significantly increased by using decoy molecules and a generic rate-accelerator variant. Using a combination of both methods resulted in the optimal biocatalyst in terms of product formation activity (PFR). The product formation rates for the rate-accelerating mutants were higher compared with their WT equivalents owing to a combination of superior coupling efficiency and NADPH activity. This presumably arises in part from them being in a "catalytically ready" conformation. The inclusion of the perfluorinated fatty acid decoy molecules also increased the product formation rates. The decoy molecules are proposed to act in a similar fashion to the rate-accelerating mutants by placing the enzyme in a more substrate-bound like conformation, which enables more efficient oxidation. The decoy molecules can also help exclude water molecules from the active site, which could improve the coupling efficiency. For the substrates with lower activities, addition of the decoy molecule PFC10 resulted in improvements in variants containing the R47L/Y51F couple. This suggests that the decoy molecules can still effectively bind to these variants and facilitate substrate oxidation. It is also important in that this could be an effective method for improving the activity of related CYP102 family enzymes not all of which contain this pair of residues.

The turnovers of the substrates with the shorter side chains, ethylbenzene and styrene, were inferior to those of *n*-propylbenzene and *trans*-β-methylstyrene, respectively. This arose from a combination of lower NADPH oxidation rates and coupling efficiencies. The oxidation activities of the planar alkene substituted benzenes were also reduced compared with the alkylbenzene equivalents. The lower activity of the alkenes was predominantly due to lower coupling efficiency. Carbon–hydrogen bond hydroxylation is more energetically challenging than expoxidation, suggesting that these planar substrates must be bound in a less favourable location in the active site compared with the alkylbenzenes.

n-Propylbenzene oxidation proceeded with the highest activity, suggesting this substrate was well positioned in the active site for efficient C–H bond abstraction. As a consequence, the improvements observed with this substrate on addition of decoy molecules were reduced compared with the other substrates. The oxidation of *n*-propylbenzene is superior to ethylbenzene, toluene and *n*-butylbenzene, suggesting the three-carbon alkyl group is of the optimal size and fit for binding in the active site of P450Bm3.[6a,8c,16b] The majority of the alkyl benzene oxidation occurred at the benzylic or α-position, which contain the most reactive C–H bonds in the molecule. This contrasts with the oxidation of toluene and anisole, which occurs predominantly at the *ortho* C–H bond on the aromatic ring. Although the oxidation of the more rigid styrenes was less active than their alkylbenzene equivalents, both resulted in the formation of a major single product arising from epoxidation of the double bond. In addition to being more active and tightly coupled, the oxidation of *n*-propylbenzene and *trans*-β-methylstyrene were more stereoselective than those of ethylbenzene and styrene. The longer alkyl or vinyl side chain must modify the binding orientation to place one face of the molecule significantly closer than the other and in a more favourable position for efficient oxidation. Alternatively, the smaller substrates may be more mobile in the active site and bind in multiple orientations, which results in the decrease in stereoselectivity and coupling efficiency. It is of note that mutating the Thr438 residue to Phe, which would decrease the size of the active site, improves the enantioselectivity of P450Bm3 styrene oxidation to give (*R*)-styrene oxide at 64% *ee*.[17]

As observed previously, the regioselectivity of the oxidation reactions were predominantly unchanged. The largest deviation in the regioselectivity was observed with ethylbenzene where oxidation at the benzylic C–H bond (as opposed to the *ortho* aromatic site) varied from 82–94%. This implies that the substrates must be positioned in similar orientations in the

ChemPubSoc Europe

CHEMCATCHEM Full Papers

enzyme active site in the presence of the decoy molecules. Changes were observed in the stereoselectivity of oxidation on using the rate-accelerating mutants and the addition of the decoy molecules. The decoy molecules caused some turnovers to be slightly more stereoselective while the rate-accelerating variants sometimes decreased the enantioselectivity. However, the variation in the enantioselectivity for each product was generally small with the smaller substrates, ethylbenzene and styrene, showing greater changes. With *trans*-β-methylstyrene no substantial changes were observed in the enantioselectivity across the turnovers. Taken together, these observations on the relative amounts of each enantiomer show that while the generic rate-accelerator mutants and the decoy molecules do not seem to alter the binding orientation of the substrate enough to modify the regioselectivity of the reactions, they can induce changes in the enantioselectivity. This must arise from a shift in the location of the molecule in the active site relative to the reactive iron–oxygen species. Chiral decoy molecules, which have been tested with P450 peroxygenase enzymes, may have the potential to be used for generating larger changes in the enantioselectivity of the products.[21]

Conclusions

The improved activity and efficiency shows that the decoy molecule combined with rate-accelerator variants have the potential to improve the productivity of regio- and stereoselective biocatalysis reactions. In some instances, the enantiomeric excess was improved by the use of the decoy molecule and this could therefore be used as a strategy to improve the stereoselectivity of C–H bond oxidations or alkene epoxidations. The combination of a rate-accelerating mutant and a decoy molecule could also be used in conjunction with other active site mutations, which are known to reverse the enantioselectivity of certain reactions.

Experimental Section

General

Production and purification of full-length P450Bm3 variants for in vitro use was carried out as described previously.[6a,8a] General reagents and organics were from Sigma–Aldrich, TCI, Acros or VWR. Buffer components, NADPH, and isopropyl-β-D-thiogalactopyranoside (IPTG) were from Astral Scientific and Biovectra, (Scimar, Australia). UV/Vis spectroscopy was performed with Varian Cary 5000 or Agilent Cary 60 spectrophotometers. Gas chromatography mass spectrometry (GC-MS) analyses were carried out with a Shimadzu GC-17A instrument coupled to a QP5050A MS detector using a DB-5 MS fused silica column (30 m×0.25 mm, 0.25 μm) and helium as the carrier gas. GC and chiral chromatography were performed with a Shimadzu Tracera GC coupled to a barrier discharge ionization detector (BID) detector using a RT-BDEXse chiral silica column (Restek: 30 m×0.32 mm×0.25 μm) or a Supelcowax column (30 m×0.32 mm×0.25 μm) and helium as the carrier gas. Retention times and methods are given in the Supporting Information (Table S2).

Activity assays

NADPH turnovers were run in oxygenated Tris buffer (1200 μL, 50 mM), pH 7.4 at 30 °C, containing enzyme (0.2 μM) and bovine liver catalase (120 μg). Assays were held at 30 °C for 1 min prior to the addition of the decoy molecule (100 μM) and the substrate (1 mM substrate from a 100 mM stock in DMSO). Finally, NADPH was added, from a 20 mg mL^{-1} stock solution, to a final concentration of approximately 320 μM (equivalent to 2 AU). A period of 10 seconds was allowed to elapse after NADPH addition before the absorbance decay at 340 nm was measured. The reactions were allowed to run until all the NADPH was consumed. The NADPH turnover rate was derived by using $\varepsilon_{340}=6.22$ mM^{-1} cm^{-1}.

Product analysis

After the NADPH consumption assays were completed, 990 μL of the reaction mixture was mixed with 10 μL of an internal standard solution (*trans*-4-phenyl-3-buten-2-one or *p*-cresol, 20 mM stock solution in DMSO). The mixture was extracted with 400 μL of ethyl acetate and the organic extracts were used directly for GC-MS or GC analysis. Products were identified by co-elution with authentic product standards or matching the GC-MS mass spectra to those expected for the standards (see the Supporting Information). Products were calibrated against standards by using the assumption that isomeric products would give comparable responses, for example, 1-phenylethanol (α-Et) and 2-ethylphenol ((*o*)-Et) were presumed to give the same detector response.

Acknowledgements

S.G.B. acknowledges the ARC for a Future Fellowship (FT140100355). The authors also thank the University of Adelaide for an M. Phil Scholarship (for S.D.M.) and an International Postgraduate Award (for S.D.). The authors thank Prof. Luet-Lok Wong (University of Oxford, UK) for the constructs of the P450Bm3 variants.

Keywords: asymmetric catalysis · C–H bond oxidation · cytochrome P450 monooxygenases · enzyme catalysis · epoxidation

[1] a) P. R. Ortiz de Montellano, *Chem. Rev.* **2010**, *110*, 932–948; b) P. R. O. de Montellano, *Cytochrome P450: Structure, Mechanism and Biochemistry, 3rd ed.*, Plenum, New York, **2005**; c) A. Sigel, H. Sigel, R. Sigel, *The Ubiquitous Roles of Cytochrome P450 Proteins*, Wiley, Weinheim, **2007**; d) F. P. Guengerich, *Chem. Res. Toxicol.* **2001**, *14*, 611–650.

[2] a) D. B. Hawkes, K. E. Slessor, P. V. Bernhardt, J. J. De Voss, *ChemBioChem* **2010**, *11*, 1107–1114; b) I. C. Gunsalus, B. N. Ganguli, M. Katagiri, J. C. Tsibris, P. Debrunner, H. Frauenfelder, *Science* **1968**, *160*, 438–439.

[3] a) S. G. Bell, N. Hoskins, C. J. C. Whitehouse, L. L. Wong, in *Metal Ions in Life Sciences* (Eds.: A. Sigel, H. Sigel, R. K. Sigel), *The Ubiquitous Roles of Cytochrome P450 Proteins Metal Ions in Life Sciences* (Eds.: A. Sigel, H. Sigel, R. K. Sigel), John Wiley & Sons, Ltd, Chichester, UK, **2007**, pp. 437–476; b) C. J. Whitehouse, S. G. Bell, L. L. Wong, *Chem. Soc. Rev.* **2012**, *41*, 1218–1260; c) G. D. Roiban, M. T. Reetz, *Chem. Commun.* **2015**, *51*, 2208–2224; d) R. Fasan, *ACS Catal.* **2012**, *2*, 647–666.

[4] S. S. Boddupalli, R. W. Estabrook, J. A. Peterson, *J. Biol. Chem.* **1990**, *265*, 4233–4239.

[5] P. K. Chowdhary, M. Alemseghed, D. C. Haines, *Arch. Biochem. Biophys.* **2007**, *468*, 32–43.

[6] a) C. J. Whitehouse, S. G. Bell, H. G. Tufton, R. J. Kenny, L. C. Ogilvie, L. L. Wong, *Chem. Commun.* **2008**, 966–968; b) A. Seifert, S. Vomund, K.

Grohmann, S. Kriening, V. B. Urlacher, S. Laschat, J. Pleiss, *ChemBioChem* **2009**, *10*, 853–861; c) J. A. McIntosh, P. S. Coelho, C. C. Farwell, Z. J. Wang, J. C. Lewis, T. R. Brown, F. H. Arnold, *Angew. Chem. Int. Ed.* **2013**, *52*, 9309–9312; *Angew. Chem.* **2013**, *125*, 9479–9482; d) S. Kille, F. E. Zilly, J. P. Acevedo, M. T. Reetz, *Nat. Chem.* **2011**, *3*, 738–743; e) G. Di Nardo, G. Gilardi, *Int. J. Mol. Sci.* **2012**, *13*, 15901–15924; f) P. S. Coelho, E. M. Brustad, A. Kannan, F. H. Arnold, *Science* **2013**, *339*, 307–310; g) N. H. Tran, D. Nguyen, S. Dwaraknath, S. Mahadevan, G. Chavez, A. Nguyen, T. Dao, S. Mullen, T. A. Nguyen, L. E. Cheruzel, *J. Am. Chem. Soc.* **2013**, *135*, 14484–14487.

[7] a) C. C. Farwell, R. K. Zhang, J. A. McIntosh, T. K. Hyster, F. H. Arnold, *ACS Cent. Sci.* **2015**, *1*, 89–93; b) T. K. Hyster, C. C. Farwell, A. R. Buller, J. A. McIntosh, F. H. Arnold, *J. Am. Chem. Soc.* **2014**, *136*, 15505–15508; c) R. Singh, M. Bordeaux, R. Fasan, *ACS Catal.* **2014**, *4*, 546–552; d) R. Singh, J. N. Kolev, P. A. Sutera, R. Fasan, *ACS Catal.* **2015**, *5*, 1685–1691.

[8] a) C. J. C. Whitehouse, S. G. Bell, W. Yang, J. A. Yorke, C. F. Blanford, A. J. Strong, E. J. Morse, M. Bartlam, Z. Rao, L. L. Wong, *ChemBioChem* **2009**, *10*, 1654–1656; b) C. J. C. Whitehouse, W. Yang, J. A. Yorke, B. C. Rowlatt, A. J. F. Strong, C. F. Blanford, S. G. Bell, M. Bartlam, L.-L. Wong, Z. Rao, *ChemBioChem* **2010**, *11*, 2549–2556; c) C. J. Whitehouse, W. Yang, J. A. Yorke, H. G. Tufton, L. C. Ogilvie, S. G. Bell, W. Zhou, M. Bartlam, Z. Rao, L. L. Wong, *Dalton Trans.* **2011**, *40*, 10383–10396.

[9] D. C. Haines, D. R. Tomchick, M. Machius, J. A. Peterson, *Biochemistry* **2001**, *40*, 13456–13465.

[10] A. B. Carmichael, L. L. Wong, *Eur. J. Biochem.* **2001**, *268*, 3117–3125.

[11] S. D. Munday, N. K. Maddigan, R. J. Young, S. G. Bell, *Biochim. Biophys. Acta* **2016**, *1860*, 1149–1162.

[12] C. J. C. Whitehouse, D. Phil Thesis, University of Oxford (UK), **2009**.

[13] a) Z. Cong, O. Shoji, C. Kasai, N. Kawakami, H. Sugimoto, Y. Shiro, Y. Watanabe, *ACS Catal.* **2015**, *5*, 150–156; b) O. Shoji, T. Kunimatsu, N. Kawakami, Y. Watanabe, *Angew. Chem. Int. Ed.* **2013**, *52*, 6606–6610; *Angew. Chem.* **2013**, *125*, 6738–6742.

[14] a) O. Shoji, T. Fujishiro, H. Nakajima, M. Kim, S. Nagano, Y. Shiro, Y. Watanabe, *Angew. Chem. Int. Ed.* **2007**, *46*, 3656–3659; *Angew. Chem.* **2007**, *119*, 3730–3733; b) N. Kawakami, O. Shoji, Y. Watanabe, *Angew. Chem. Int. Ed.* **2011**, *50*, 5315–5318; *Angew. Chem.* **2011**, *123*, 5427–5430; c) F. E. Zilly, J. P. Acevedo, W. Augustyniak, A. Deege, U. W. Hausig, M. T. Reetz, *Angew. Chem. Int. Ed.* **2011**, *50*, 2720–2724; *Angew. Chem.* **2011**, *123*, 2772–2776.

[15] S. D. Munday, O. Shoji, Y. Watanabe, L. L. Wong, S. G. Bell, *Chem. Commun.* **2016**, *52*, 1036–1039.

[16] a) Q. S. Li, J. Ogawa, R. D. Schmid, S. Shimizu, *FEBS Lett.* **2001**, *508*, 249–252; b) C. J. Whitehouse, S. G. Bell, L. L. Wong, *Chem. Eur. J.* **2008**, *14*, 10905–10908.

[17] W. C. Huang, P. M. Cullis, E. L. Raven, G. C. Roberts, *Metallomics* **2011**, *3*, 410–416.

[18] C. A. Denard, M. J. Bartlett, Y. Wang, L. Lu, J. F. Hartwig, H. Zhao, *ACS Catal.* **2015**, *5*, 3817–3822.

[19] a) J. A. Fruetel, J. R. Collins, D. L. Camper, G. H. Loew, P. R. O. Demontellano, *J. Am. Chem. Soc.* **1992**, *114*, 6987–6993; b) D. P. Nickerson, C. F. Harford-Cross, S. R. Fulcher, L. L. Wong, *FEBS Lett.* **1997**, *405*, 153–156.

[20] a) C. F. Oliver, S. Modi, W. U. Primrose, L. Y. Lian, G. C. Roberts, *Biochem. J.* **1997**, *327*, 537–544; b) H. Li, T. L. Poulos, *Nat. Struct. Biol.* **1997**, *4*, 140–146.

[21] T. Fujishiro, O. Shoji, N. Kawakami, T. Watanabe, H. Sugimoto, Y. Shiro, Y. Watanabe, *Chem. Asian J.* **2012**, *7*, 2286–2293.

[22] a) R. Agudo, G. D. Roiban, R. Lonsdale, A. Ilie, M. T. Reetz, *J. Org. Chem.* **2015**, *80*, 950–956; b) G. D. Roiban, R. Agudo, A. Ilie, R. Lonsdale, M. T. Reetz, *Chem. Commun.* **2014**, *50*, 14310–14313.

Received: May 7, 2016
Published online on August 5, 2016

Heterogeneous & Homogeneous & Bio- & Nano-
CHEMCATCHEM
CATALYSIS

Supporting Information

Increasing the Activity and Efficiency of Stereoselective Oxidations by using Decoy Molecules in Combination with Rate-Enhancing Variants of P450Bm3

Samuel D. Munday, Shaghayegh Dezvarei, and Stephen G. Bell*[a]

cctc_201600551_sm_miscellaneous_information.pdf

Increasing the activity and efficiency of stereoselective oxidations using decoy molecules in combination with rate enhancing variants of P450Bm3

Samuel D. Munday, Shaghayegh Dezvarei and Stephen G. Bell*

SUPPLEMENTARY MATERIAL

Tables

Table S 1: In vitro oxidation activity data for wild-type and KT2 P450Bm3 with and without PFCs of ethylbenzene, propylbenzene, styrene and trans–β-methylstyrene. (30ºC, [P450Bm3] = 0.2 µM; [PFC] = 100 µM; [Substrate] = 1 mM, PFC and substrate stocks in DMSO. Data are means of at least three experiments. N = NADPH consumption rate, PFR = product formation rate (each in nmol.min^{-1} (nmol-P450)$^{-1}$). C = coupling efficiency (%).

	WT	WT PFC8	WT PFC9	WT PFC10	KT2	KT2 PFC8	KT2 PFC9	KT2 PFC10	R19	R19 PFC10	RLYFIP	RLYFIP PFC10
						ethylbenzene						
N	71 ± 4	441 ± 1	1106 ± 19	1311 ± 13	404 ± 6	993 ± 9	1646 ± 12	1730 ± 12	852 ± 11	1700 ± 30	1720 ± 40	1730 ± 20
C	5.3 ± 1.5	57 ± 1	74 ± 2	49 ± 2	47 ± 2	74 ± 1	80 ± 3	68 ± 3	60 ± 1	74 ± 1	53 ± 3	76 ± 1
PFR	3.8 ± 1.2	250 ± 3	814 ± 33	645 ± 33	189 ± 2	737 ± 7	1317 ± 53	1177 ± 58	514 ± 6	1270 ± 20	900 ± 45	1310 ± 30
						n-propylbenzene						
N	607 ± 14	1164 ± 25	1622 ± 20	1807 ± 20	1386 ± 24	2050 ± 20	2412± 35	2475 ± 31	2230 ± 110	2220 ± 90	2300 ± 20	2260 ± 15
C	61 ± 1	86 ± 1	93 ± 5	75 ± 5	79 ± 1	84 ± 6	82 ± 9	82 ± 7	99 ± 8	99 ± 6	94 ± 4	88 ± 2
PFR	368 ± 2	1002 ± 26	1504 ± 78	1353 ± 74	1101 ± 26	1716 ± 135	1987 ± 184	2042 ± 179	2210 ± 70	2210 ± 200	2140 ± 80	2030 ± 60
						styrene						
N	41 ± 1	214 ± 4	457 ± 11	691 ± 7	133 ± 4	359 ± 4	579 ± 9	846 ± 12	317 ± 8	949 ± 15	917 ± 16	1180 ± 80
C	4.0 ± 0.6	27 ± 2	32 ± 1	17 ± 1	14.7 ± 0.4	35 ± 2	39 ± 1	20.1 ± 0.4	48 ± 5	60 ± 2	52 ± 4	56 ± 3
PFR	1.6 ± 0.2	58 ± 4	146 ± 4	117 ± 7	20 ± 1	124 ± 6	225 ± 8	170 ± 3	154 ± 17	572 ± 14	481 ± 29	661 ± 69
						***trans*-β-methylstyrene**						
N	80 ± 5	298 ± 10	810 ± 10	1029 ± 15	494 ± 12	825 ± 9	1182 ± 21	1309 ± 23	947 ± 85	1510 ± 10	1840 ± 40	1790 ± 80
C	11.5 ± 0.7	36 ± 1	43 ± 1	36 ± 1	40 ± 1	37 ± 2	48 ± 2	30 ± 2	83 ± 9	81 ± 4	68 ± 5	70 ± 4
PFR	9 ± 1	108 ± 3	349 ± 13	372 ± 16	200 ± 6	303 ± 16	565 ± 30	513 ± 30	782 ± 40	1220 ± 60	1270 ± 65	1230 ± 20

2

Table S2: Product distributions arising from the turnovers of wild-type and KT2 P450Bm3 with and without decoy molecules for ethylbenzene, n-propylbenzene, styrene and *trans*-β-methylstyrene. The products from ethylbenzene: 1-phenylethanol (α-Et), 2-ethylphenol and (*o*)-Et; from n-propylbenzene: 1-phenyl-1-propanol (α-Pr), 1-phenyl-2-propanol (β-Pr), 2-propylphenol (*o*)-Pr and propiophenone (α-ket-Pr); from styrene: styrene oxide; and from *trans*-β-methylstyrene: 1- phenylpropylene oxide (β-oxide). Values are reported as a mean of at least three experiments. The values in italics represent the enantiomeric excess (*ee*) of the *(R)*-enantiomer of 1-phenylethanol, 1-phenyl-1-propanol and styrene oxide. For 1-phenylpropylene oxide, the values in italics represent the enantiomeric excess of the (*R,R*) enantiomer.

	WT	WT PFC8	WT PFC9	WT PFC10	KT2	KT2 PFC8	KT2 PFC9	KT2 PFC10	R19	R19 PFC10	RLYFIP	RLYFIP PFC10
ethylbenzene												
α-Et	>90	89	90	92	83	90	91	92	82	87	91	94
ee (*R*)	*48*	*50*	*56*	*62*	*22*	*22*	*28*	*34*	*27*	*40*	*51*	*62*
o-Et	<10	11	10	8	17	10	9	8	18	12	9	6
propylbenzene												
α-Pr	91	93	94	93	93	92	91	92	82	81	83	83
ee (*R*)	*74*	*78*	*80*	*80*	*62*	*68*	*72*	*72*	*69*	*69*	*68*	*70*
β-Pr	4	3	3	2	2	3	3	3	~1	~1	~1	~1
o-Pr	3	3	2	4	4	4	5	4	~1	~1	~1	~1
α-ket-Pr	2	1	1	1	1	1	1	1	16	17	15	15
styrene												
styrene oxide	>98	>98	>98	>98	>98	>98	>98	>98	>98	>98	>98	>98
ee (*R*)	*18*	*30*	*32*	*32*	*14*	*28*	*30*	*30*	*25*	*31*	*6*	*15*
***trans*-β-methylstyrene**												
β-oxide	>98	>98	>98	>98	>98	>98	>98	>98	>98	>98	>98	>98
ee (*R,R*)	*<75*	*75*	*75*	*75*	*70*	*75*	*75*	*75*	*73*	*75*	*70*	*70*

3

The GC and chiral GC RTs the substrates and products. [a] *trans*-β-methylstyrene, [b] RT of the (*R*,*R*) isomer. [c] RT of the (*S*,*S*) isomer.

Substrate/product	m/z	GC RT (min)	GC-MS RT (min)	GC wax RT (min)	Chiral GC (*R*) (min)	Chiral GC (*S*) (min)
ethylbenzene	106.1	4.2	3.3	1.5		
α-Et	122.1	8.4	6.9	9.0	15.8	16.0
o-Et	122.1	9.9	8.2	12.0		
n-propylbenzene	120.1	6.6	4.9	1.8		
α-Pr	136.1	10.3	8.5	9.95	17.7	17.8
α-ket-Pr	134.1	10.4	8.7	7.65		
β-Pr	136.1	10.0	8.2	9.2		
o-Pr	136.1	11.4	9.6	-		
styrene	104.1	5.3	3.8	2.05		
styrene oxide	120.1	8.7	6.95	6.0	12.6	13.0
phenylacetaldehyde	120.1	8.4	6.55	-		
trans-β-MS[a]	118.1	7.9	6.2	3.2		
β-oxide	134.1	9.6	7.9	6.2	13.6[b]	13.7[c]
α-ket-Pr	134.1	10.4	8.7	7.65		
phenylacetone	134.0	9.8	8.2	7.75		

GC-MS method: Injector 250 °C Interface 280 °C; the oven temperature was held at 60 °C for 3 minutes and then increased at 10 °C min^{-1} to 140 °C where it was held for 5 minutes then increased at 25 °C min^{-1} to 220 °C and held for 1 minute (total 20.0 min).

GC method (wax column): Injector 250 °C Interface 270 °C; the oven temperature was held at 100 °C for 3 minutes and then increased at 8 °C min^{-1} to 220 °C where it was held for 2 minutes (total 20.0 min).

Chiral GC method : Injector 230 °C Interface 230 °C; the oven temperature was held at 60 °C for 3 minutes and then increased at 5 °C min^{-1} to 140 °C where it was held for 5 minutes then increased at 20 °C min^{-1} to 200 °C and held for 2 minutes (total 30.0 min).

4

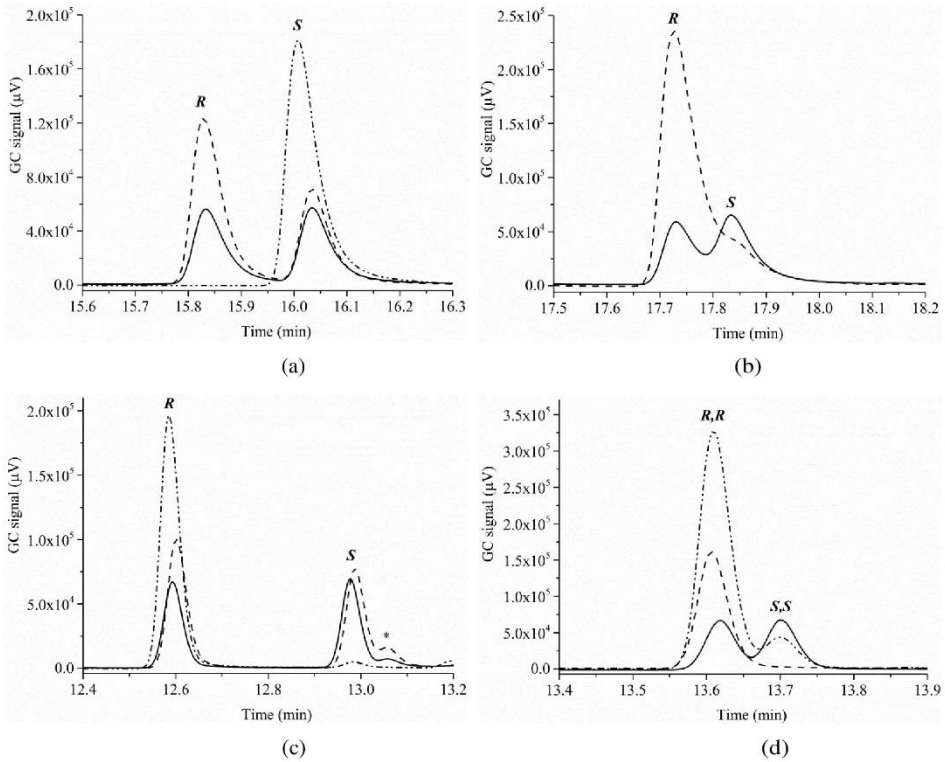

Figure S1: Chiral GC analyses of (a) ethylbenzene turnover (dashed line) a racemic mixture of 1-phenylethanol (solid) and (*S*)-1-phenylethanol (dash-dot); (b) propylbenzene turnover (dashed line) and racemic mixture of 1-phenyl-1-propanol; (c) styrene turnover (dashed line) with racemic mixture of styrene oxide (solid) and (*R*)-styrene oxide (dash-dot) and (d) *trans*-β-methylstyrene turnover (dash-dot), a racemic mixture of *trans*-1-phenylpropylene oxide (solid) and (R,R)-*trans*-1-phenylpropylene oxide (dash/dot).

5

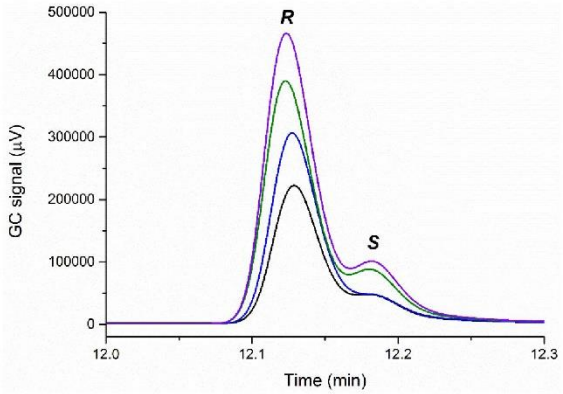

Figure S2. Chiral GC analyses of the 1-phenyl-1-propanol product form in the propylbenzene turnovers with WT (black), WT/PFC9 (blue), KT2 (green) and KT2/PFC9 (magenta). The WT enzyme has been reported to form an excess (90% ee) of the *R* enantiomer [1] which was used to identify this form. Note the method used here was slightly different that that used to determine the ee as the separation was better given method.

6

GC-MS data
ethylbenzene

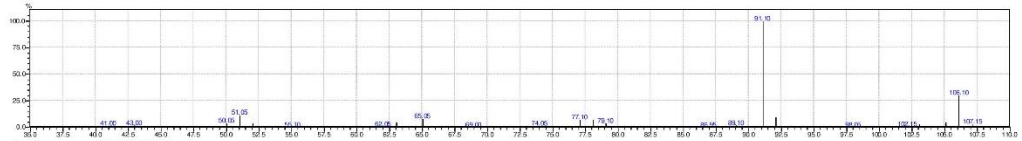

ethylbenzene GCMS 3.3 min

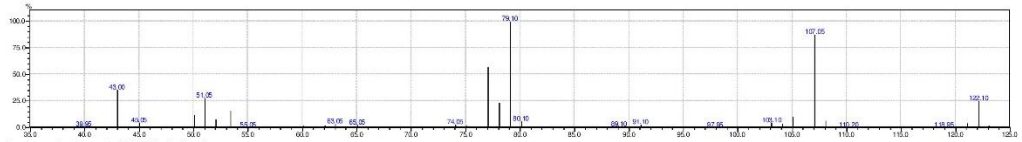

1-phenylethanol GCMS 6.9 min

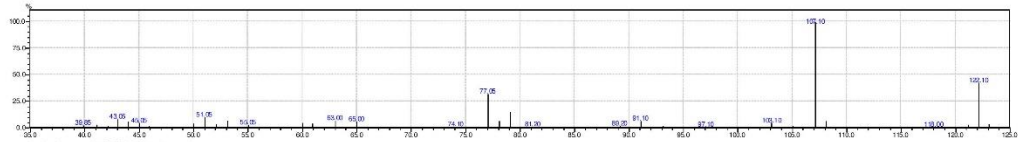

2-ethylphenol GCMS 8.2 min

7

Propylbenzene

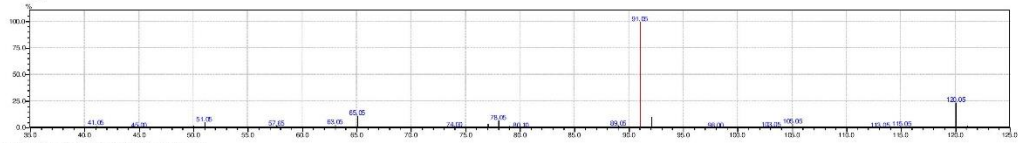

propylbenzene GCMS 4.9 min

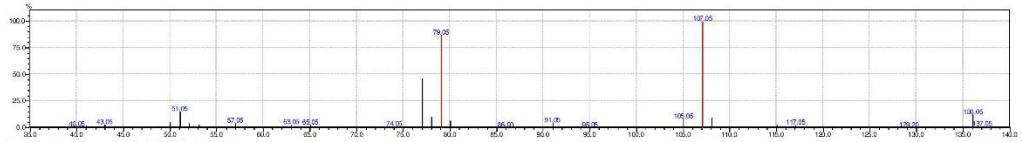

1-phenyl-1-propanol GCMS 8.5 min

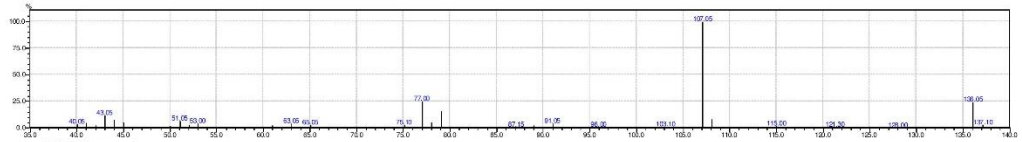

ortho GCMS 9.6 min

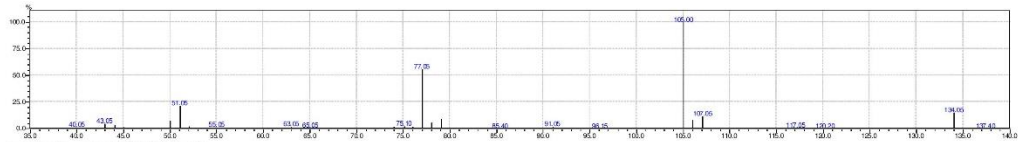

propiophenone GCMS 8.7 min

8

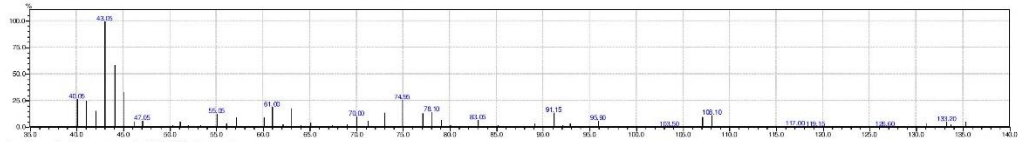

1-phenyl-2-propanol GCMS 8.2 min

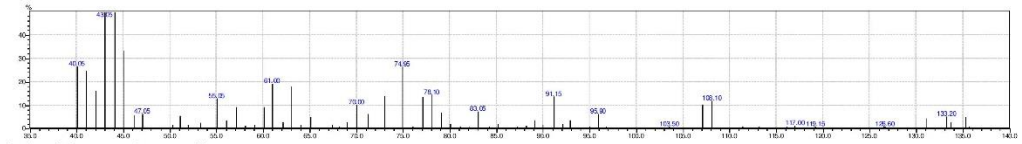

1-phenyl-2-propanol zoomed in

9

Styrene

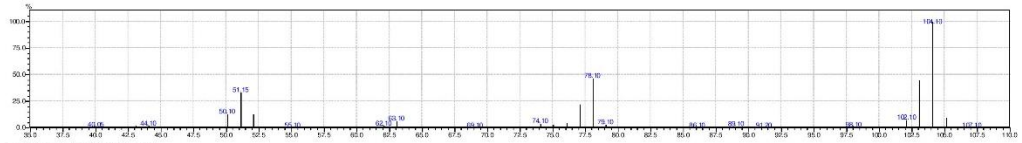

styrene GCMS 3.8 min

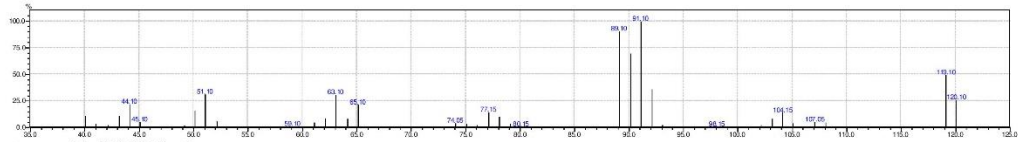

styrene oxide GCMS 7.1 min

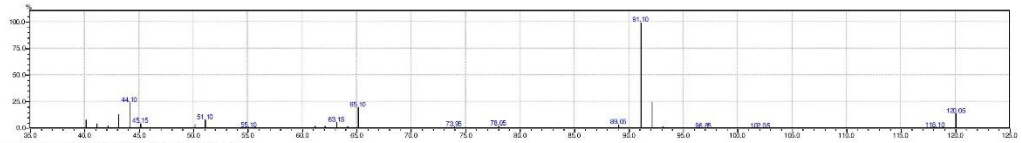

phenylacetaldehyde GCMS 6.7 min

10

***trans*-beta-methylstyrene**

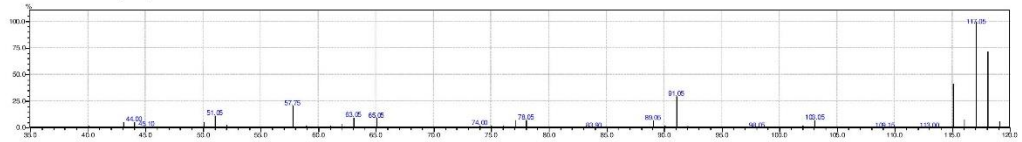

trans-beta-methylstyrene GCMS 6.2 min

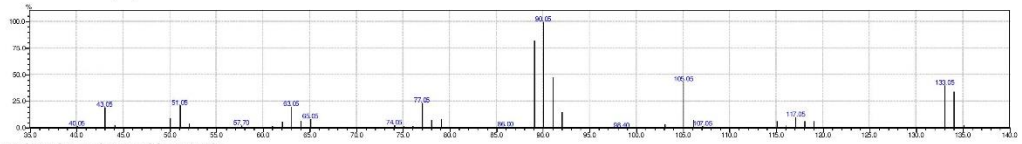

1-phenylpropylene oxide 7.9 min

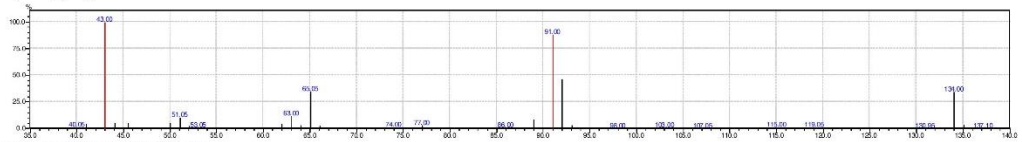

phenylacetone GCMS 8.2 min

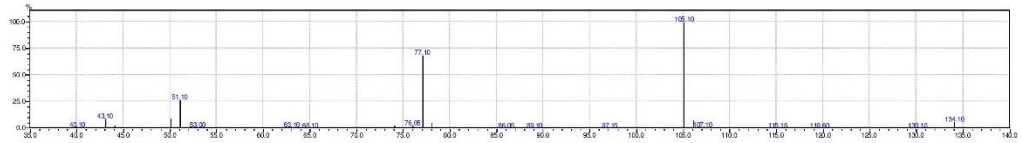

propiophenone GCMS 8.7 min

11

References

[1] Q.S. Li, J. Ogawa, R.D. Schmid, S. Shimizu, Residue size at position 87 of cytochrome P450 BM-3 determines its stereoselectivity in propylbenzene and 3-chlorostyrene oxidation, FEBS Lett., 508 (2001) 249-252.

12

Chapter 4

Examination of selectivity in the oxidation of ortho-and meta-disubstituted benzenes by CYP102A1 (P450 Bm3) variants

Citation:

Munday, S. D.; Dezvarei, S.; Lau, I. C. K.; Bell, S. G., ChemCatChem 2017, 9 (13), 2512-2522.

Statement of Authorship

Title of Paper	Examination of Selectivity in the Oxidation of ortho-and meta-Disubstituted Benzenes by CYP102A1 (P450 Bm3) Variants
Publication Status	☑ Published ☐ Accepted for Publication ☐ Submitted for Publication ☐ Unpublished and Unsubmitted work written in manuscript style
Publication Details	Munday, S. D.; Dezvarei, S.; Lau, I. C. K.; Bell, S. G., Examination of Selectivity in the Oxidation of ortho-and meta-Disubstituted Benzenes by CYP102A1 (P450 Bm3) Variants. ChemCatChem 2017, 9 (13), 2512-2522.

Principal Author

Name of Principal Author (Candidate)	Samuel D Munday
Contribution to the Paper	Preparation of the enzyme, turnovers of substrates with substrates, product formation, data analysis and discussion, manuscript preparation.
Overall percentage (%)	60
Certification:	This paper reports on original research I conducted during the period of my Higher Degree by Research candidature and is not subject to any obligations or contractual agreements with a third party that would constrain its inclusion in this thesis. I am the primary author of this paper.
Signature	Date 22/03/2019

Co-Author Contributions

By signing the Statement of Authorship, each author certifies that:

i. the candidate's stated contribution to the publication is accurate (as detailed above);

ii. permission is granted for the candidate in include the publication in the thesis; and

iii. the sum of all co-author contributions is equal to 100% less the candidate's stated contribution.

Name of Co-Author	Shaghyegh Dezvarei
Contribution to the Paper	Preparation of the enzyme, turnovers of substrates with substrates, product formation, data analysis and discussion, manuscript preparation.
Overall percentage (%)	25
Signature	Date 08/04/19

Name of Co-Author	Ian C. Lau
Contribution to the Paper	Product formation, analysis.
Signature	Date 23/03/19

Name of Co-Author	Stephen G. Bell		
Contribution to the Paper	Experimental design, supervision, manuscript preparation.		
Signature		Date	8/04/2019

ChemPubSoc Europe
DOI: 10.1002/cctc.201700116
CHEMCATCHEM Full Papers

Examination of Selectivity in the Oxidation of *ortho*- and *meta*-Disubstituted Benzenes by CYP102A1 (P450 Bm3) Variants

Samuel D. Munday, Shaghayegh Dezvarei, Ian C.-K. Lau, and Stephen G. Bell*[a]

Cytochrome P450 CYP102A1 (P450 Bm3) variants were used to investigate the products arising from the P450 catalysed oxidation of a range of disubstituted benzenes. The variants used all generated increased levels of metabolites compared to the wild-type enzyme. With *ortho*-halotoluenes up to six different metabolites could be identified whereas the oxidation of 2-methoxytoluene generated only two aromatic oxidation products. Addition of an ethyl group markedly shifted the selectivity for oxidation to the more reactive benzylic position. Epoxidation of an alkene was also preferred to aromatic oxidation in 2-methylstyrene. Significant minor products arising from the migration of one substituent to a different position on the benzene ring were formed during certain P450-catalysed substrate turnovers. For example, 2-bromo-6-methylphenol was formed from the turnover of 2-bromotoluene and the dearomatisation product 6-ethyl-6-methylcyclohex-2,4-dienone was generated from the oxidation of 2-ethyltoluene. The RLYF/A330P variant altered the product distribution enabling the generation of certain metabolites in higher quantities. Using this variant produced 4-methyl-2-ethylphenol from 3-ethyltoluene with $\geq$90% selectivity and with a biocatalytic activity suitable for scale-up of the reaction.

Introduction

Cytochrome P450 (CYP) monooxygenases catalyse the oxidation of a wide variety of substrates using atmospheric dioxygen. Their archetypal reaction type is the conversion of an unreactive carbon–hydrogen bond in aliphatic and aromatic molecules to an alcohol using a reactive iron–oxo radical cation, compound I intermediate.[1] This ability to oxidise a broad array of organic substrates enables CYP enzymes to have roles in many metabolic pathways.[2] Xenobiotic detoxification and metabolite production are two of the major roles P450s perform within organisms.[3] One of the major roadblocks in the study of many membrane-bound P450 enzymes is that they can often be difficult to produce and have low activities, making in-depth studies of them more complex. As such, bacterial P450 enzymes have often been used to examine the structure, function and mechanism of this class of enzymes.[1a,b,4]

P450 Bm3 (CYP102A1), a fatty acid hydroxylase, from *Bacillus megaterium*, has been widely researched because of its high catalytic activity and its ease of production and use.[5] It is a catalytically self-sufficient enzyme in which the P450 heme domain is fused to a reductase domain meaning it only requires NADPH and oxygen to oxidise its substrate.[6] Many variants with enhanced activity towards non-natural substrates and improved product selectivity have been generated.[5,7] As a result, variants with the ability to promote terminal and stereoselective alcohol hydroxylation, phenol formation, and epoxidation have been reported.[8] More recently forms that can catalyse reactions that are not normally supported by P450 enzymes such as cyclopropanation and amination have been designed.[9] In addition CYP102A1 and a number of evolved variants have been shown to act on certain pharmaceuticals producing similar metabolites to mammalian P450s.[10] Changes to oxidation profiles can be brought about by minor alterations in substrate structure, or by mutagenesis of the enzyme.[8b,11] Therefore CYP102A1 can be used to investigate the behaviour of CYP enzymes in the oxidative metabolism and degradation of certain compounds.

P450-catalysed oxidations of drug molecules and substrates which contain substituted benzene, toluene and related aromatic moieties can often generate multiple metabolites.[11a,12] These can include products arising from rearrangement reactions.[13] In earlier work, it was established that CYP102A1 and its variants would preferentially oxidise most alkylbenzenes at the benzylic position to generate an alcohol ($\approx$99% for wild type with propylbenzene) a similar outcome to that observed with mammalian P450s.[8b,14] With toluene, *o*-hydroxylation was the preferred outcome, ($\approx$97% selectivity), which is different to the product distribution of microsomal enzymes.[14] Subsequent work showed that *o*-hydroxylation was also favoured for a range of other monosubstituted benzenes including chlorobenzene and anisole (Figure S1, Supporting Information).[15] The reactions with *o*-, *m*- and *p*-xylene are more complex and these are oxidised by variants of CYP102A1 to generate multiple products (Figure S2). *p*-Xylene has been reported to be oxi-

[a] S. D. Munday, S. Dezvarei, I. C.-K. Lau, Dr. S. G. Bell
Department of Chemistry
University of Adelaide
Adelaide. SA, 5005 (Australia)
E-mail: Stephen.bell@adelaide.edu.au
Supporting information and the ORCID identification number(s) for the author(s) of this article can be found under https://doi.org/10.1002/cctc.201700116.

ChemPubSoc Europe

CHEMCATCHEM Full Papers

dised at the benzylic methyl group[16] but other researchers have shown that 2,5-dimethylphenol was the major product.[17] The product profile resulting from *m*-xylene oxidation consisted of 2,4-dimethylphenol as the major product (87%) with 2,6-dimethylphenol (11%) and benzylic oxidation (2%) occurring in lower amounts (Figure S2).[11a] The product distribution obtained from the oxidation of *o*-xylene was more diverse and consisted of benzylic oxidation (47%), 2,3-dimethylphenol (27%) and 3,4-dimethylphenol (10%) formation (Figure S2).[11a] In addition, two products arising from the shift of a methyl group were also obtained and identified, such as 2,6-dimethylphenol (8%), and 6,6-dimethylcyclohexa-2,4-dienone (8%). This latter metabolite resulted from dearomatisation of the benzene ring.[11a]

These studies determining the product distributions of CYP102A1 oxidation of substituted benzenes can be used to complement xenobiotic metabolism with isolated mammalian P450 enzymes or microsomes. For example, the oxidation of alkyl-substituted benzenes and styrenes by mammalian enzymes tend to favour oxidation on the substituent whereas methoxy-substituted benzenes generate phenols as the major products.[18] Methyl and other substituents have been reported to migrate in a similar manner to hydrogen in the NIH shift mechanism during the oxidation of substituted benzenes by mammalian P450s and model systems.[19] However, the reactions with microsomes or eukaryotic P450s tend to be significantly less efficient generating low levels of product over longer periods of time, which can hinder the identification of minor metabolites.

In the CYP102A1 turnovers, the partition between aromatic and benzylic hydroxylation is thought to be primarily governed by the orientation of the substrate with C–H bond reactivity playing an important but secondary role. In the singly substituted benzene substrates such as toluene and anisole, the substituents must be orientated away from the heme iron enabling aromatic oxidation.[14,15,17b] For substituted aromatics with ethyl and longer alkyl chains, such as *n*-propylbenzene, the side chains must be more closely held over the heme iron giving metabolites arising from benzylic oxidation.[14,20] The balance between the different pathways in P450-catalysed oxidation appears to be delicately poised.[11a,12,16] For example *o*-xylene and *m*-xylene show significant differences in the relative amount of aromatic versus benzylic oxidation products, and deuteration of the methyl groups of *o*-xylene led to an increase in phenolic hydroxylation by microsomal P450s.[21]

Mutant variants of CYP102A1 can improve the activity of the enzyme for alkylbenzenes and also alter the product distribution towards or away from benzylic hydroxylation.[8b,14] Variants of CYP102A1 that contain the R47L and Y51F mutations (RLYF) at the entrance of the substrate access channel have been shown to facilitate the entry of small hydrophobic molecules.[8a,14] Other rate-accelerating variants have been developed, and these improve the activity of the enzyme for non-natural substrates but on the whole maintain the product selectivity of the wild type (WT) enzyme.[11b,14,22] Among these variants are the rate accelerators RLYF/I401P (R47L/Y51F/I410P), KT2 (A191T/N239H/I259V/A276T/L353I) as well as R19 (R47L/Y51F/H171L/Q307H/N319Y).[11b,14,17b,20,22] The RLYF/I401P variant contains the I401P mutant which is on the C-terminal side of the distal cysteine ligand whereas the other mutations in the KT2 and R19 variants are remote from the active site and located throughout the heme domain of the enzyme (Figure 1).[11b,22a]

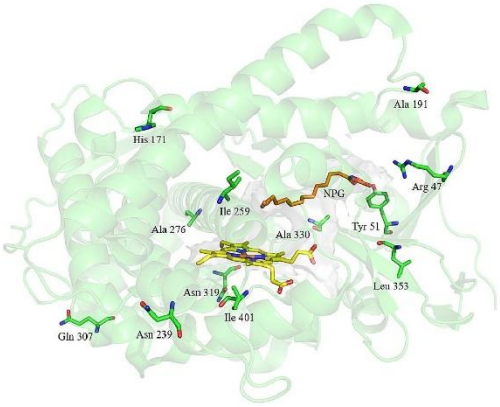

Figure 1. Location of the residues that have been mutated in the different CYP102A1 variants (KT2, R19, RLYF/I401P and RLYF/A330P) used in this study. The residues are shown on the structure of the substrate-bound (NPG: *N*-palmitoylglycine) WT CYP102A1 (PDB: 1JPZ).

The crystal structures of the KT2 variant and I401P mutant, which shares characteristics in common with RLYF/I401P, have been solved (PDB: 3PSX and PDB: 3HF2, respectively).[11b,22b] These reveal that both have altered conformations, which in certain aspects more closely resemble the substrate-bound WT enzyme (PDB: 1JPZ)[23] than substrate-free CYP102A1 (PDB: 1BU7).[24] These rate-accelerating variants are hypothesised to be in "catalytically ready" conformations minimising substrate gating and enabling more efficient substrate oxidation.[11b,22] The R19 variant has also been demonstrated to accelerate the oxidation of non-physiological substrate but its structure is yet to be solved.[14,20]

The RLYF/A330P mutant, in which the A330P mutation is in the active site, does not retain the ability to oxidise fatty acids.[11b] The structure of the A330P mutant has been solved (PDB: 3M4V) and it shows the Pro329 residue is reoriented into the substrate access channel, generating a smaller active site (Figure 1).[11b] This results in distinctive product distributions relative to the WT enzyme and the rate accelerating variants described above. The RLYF/A330P variant can therefore oxidise non-natural substrates with high activity and altered product distributions.[11b]

In this paper, we consider the in vitro oxidation of *m*- and *o*-substituted benzene substrates which have different substituents on the aromatic ring. These were tested with WT CYP102A1 and four different variants (KT2, RLYF/I401P, R19 and RLYF/A330P). Our intention was to investigate how altering the substituent modified the substrate–enzyme interactions and

ChemPubSoc Europe

CHEMCATCHEM Full Papers

therefore the activity and product distribution. This would enable an assessment of the extent to which CYP102A1 can be used to generate individual or multiple oxygenated metabolites of these compounds and if there were any rearrangement products that arise from the mechanism of aromatic oxidation.[1f,19e,25]

Results

The four CYP102A1 variants, KT2, R19, RLYF/I401P and RLYF/A330P, and the WT enzyme were tested with disubstituted benzene substrates as well as with toluene and anisole as controls (Figure 2). For all the substrates tested, the generic accel-

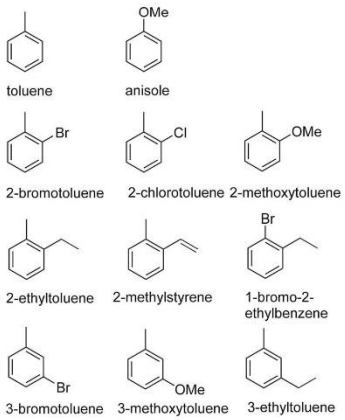

Figure 2. Substrates tested for their in vitro activity with WT CYP102A1 and its variants.

erator variants enhanced the product formation activity of the turnover by increasing the NADPH consumption rate and the coupling efficiency (Table 1). KT2 was the slowest variant and those containing the RLYF couple improved the activity by a significantly greater degree (Table 1). The improvement in product formation activity over the WT enzyme ranged from 110-fold for 2-chlorotoluene to greater than 1000-fold for 3-bromotoluene. The acceleration of product formation activity ranged from 240 to 1600 nmol (nmol P450) $^{-1}$ min^{-1} (henceforth abbreviated to min^{-1}), for each substrate (Table 1). In all but one case the greatest improvement over the WT enzyme was induced by RLYF/I401P. For example, with WT CYP102A1 no product formation activity was observed with 3-bromo- and 3-methoxytoluene but product formation rates of 920 and 499 min^{-1} were observed with the RLYF/I401P variant.

The product formation activities of the doubly substituted benzenes were greater than those of toluene and anisole, and the *ortho*-substituted substrates were converted at higher activities than their *meta*-substituted equivalents (Table 1). The highest product formation rates were observed with 2-ethyltoluene. The substrate preference of the RLYF/A330P variant was different from the other mutants tested, and the highest activities were obtained with 2-bromo- and 2-chlorotoluene (Table 1).

Table 1. In vitro oxidation activity and selectivity of P450 Bm3 variants and decoy molecules with toluene, anisole and *ortho*- and *meta*-substituted benzene derivatives.[a]

	WT	KT2	R19	RLYF/IP	RLYF/AP
Toluene					
N[b]	22±0.9	137±4	118±6	819±4	251±5
C[c]	1.6±0.5	10±3	32±3	38±1	44±1
PFR[d]	0.3±0.1	7±2	38±4	308±9	111±4
Anisole					
N[b]	122±2	189±2	464±10	1175±16	121±2
C[c]	1.4±0.1	7±1	36±3	36±2	24±0.4
PFR[d]	2.0±0.1	14±2	166±14	424±33	29±0.3
2-Bromotoluene					
N[b]	61±6	265±9	1487±22	1810±7	2320±12
C[c]	2.3±0.5	46±1	39±1	54±2	42±1
PFR[d]	1.5±0.4	123±7	574±19	984±39	987±28
2-Chlorotoluene					
N[b]	80±11	245±2	1030±24	1690±11	1990±25
C[c]	11±5	39±1	42±1	61±4	47±3
PFR[d]	9±3	96±3	435±15	1025±70	935±55
2-Methoxytoluene					
N[b]	50±3	57±1	159±6	1090±11	606±9
C[c]	6.2±0.5	31±2	28±1	63±1	52±2
PFR[d]	3.1±0.3	18±1	44±1	689±11	315±12
2-Ethyltoluene					
N[b]	52±4	219±9	1320±12	1640±11	1250±12
C[c]	13±5	77±1	83±1	98±1	81±1
PFR[d]	7±3	169±8	1100±18	1600±23	315±12
1-Bromo-2-ethylbenzene					
N[b]	56±1	572±2	1370±12	2150±4	1765±71
C[c]	7±1	41±1	43±3	35±2	42±1
PFR[d]	3.8±0.5	237±7	599±45	840±35	737±47
2-Methylstyrene					
N[b]	53±3	179±12	313±7	754±23	325±21
C[c]	0.7±0.1	16±.	24±1	32±2	5±0.3
PFR[d]	0.3±0.03	28±4	75±5	240±5	17±0.5
3-Bromotoluene					
N[b]	91±13	593±12	2020±34	1970±16	911±11
C[c]	n.d.	30[e]	44±1	47±3	32±4
PFR[d]	n.d.	170[e]	879±21	920±65	296±34
3-Methoxytoluene					
N[b]	27±11	135±2	547±14	872±16	710±15
C[c]	n.d.	38±1	59±3	57±2	63±1
PFR[d]	n.d.	52±2	321±8	499±23	444±13
3-Ethyltoluene					
N[b]	112±5	572±2	1320±55	1850±62	1480±34
C[c]	6±0.2	44±1	50±1	56±0.6	44±1
PFR[d]	6.6±0.01	250±5	656±35	1030±43	652±16

[a] All data are reported as the means of at least three experiments unless otherwise indicated. n.d.: no levels of product formation were observed. [b] N = NADPH turnover rate (nmol (nmol P450)$^{-1}$ min^{-1}). [c] C = coupling efficiency (%). [d] PFR = Product formation rate (nmol (nmol P450)$^{-1}$ min^{-1}). [e] determined from a single experiment.

Most products were identified by GC co-elution experiments with authentic standards. If these were not available, analysis by NMR spectroscopy or mass spectra (MS) were used (Supporting Information). The product distributions for toluene and anisole oxidation by each variant were similar to those observed with WT. In all cases, the predominant position of hydroxylation was *ortho* to the substituent with a small amount of *para*-hydroxylation observed (Figure S1, Supporting Informa-

ChemPubSoc Europe
CHEMCATCHEM Full Papers

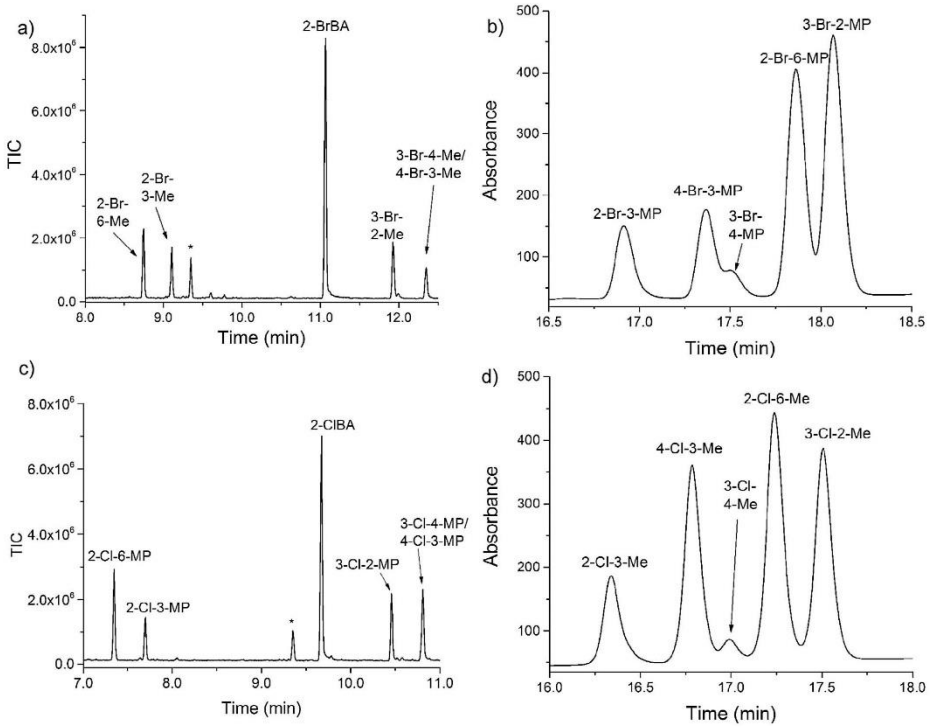

Figure 3. GC–MS and HPLC analyses of *o*-substituted toluenes: (a) GC–MS chromatogram of RLYF/I401P + 2-Br; (b) HPLC chromatogram of RLYF/A330P + 2-Br (retention time, RT, of 2-BrBA: 8.8 min, not shown); (c) GC–MS chromatogram of RLYF/I401P + 2-Cl; (d) HPLC chromatogram of RLYF/A330P + 2-Cl (RT of 2-ClBA: 13.6 min, not shown).

tion).[14,15,20,26] All the variants, except R19, oxidised toluene at the benzylic position to a small extent. R19 reduced the selectivity of anisole oxidation at the *para* position. No demethylation of anisole was detected in any instance. The major metabolite arising from toluene oxidation by mammalian systems is benzyl alcohol, and aromatic oxidation is preferred to demethylation in anisole metabolism with the *para*-phenol as the major product.[18c,e]

Both 2-chloro- and 2-bromotoluene were oxidised into six metabolites by each variant (Figure 3 and Scheme 1). With GC–MS experiments, it was not possible to distinguish between 4-halo-3-methylphenol and 3-halo-4-methylphenol (X = bromo or chloro in 4-X-3-MP and 3-X-4-MP), therefore, HPLC was used to determine the relative proportion of these products (Figure 3). The product distribution was relatively consistent between both substrates and most variants. However, as expected, the RLYF/A330P variant generated different relative amounts of each product (Scheme 1). For all variants other than RLYF/A330P, the major products were the benzyl alcohols (2-BrBA and 2-ClBA, Scheme 1). A mixture of other products resulted from hydroxylation at each position around the benzene ring. For the rate-accelerating variants, the 3-halo-2-methylphenol (3-X-2-MP) product was formed in the second highest quantity followed by 2-halo-6-methylphenol (2-X-6-MP) and 4-halo-3-methylphenol (4-X-3-MP, Scheme 1). The RLYF/A330P variant was less selective for benzyl alcohol formation and 2-Cl-6-MP and 3-Br-2MP were the major products (Scheme 1). The 2-X-6-MP product must arise from a shift of the methyl or halide substituent. Unlike the case of the turnover of *o*-xylene, no dearomatisation product that arose by the shift of a halide to the methyl-bound carbon or vice versa could be detected. However, the total proportion of rearrangement products with the halotoluenes was similar to those formed with *o*-xylene. Additionally, there was no evidence of dehalogenation of either substrate which has been shown to occur in the oxidation of perhalogenated benzenes by P450s.[27]

Replacing the halogen atom with the larger methoxy substituent in 2-methoxytoluene resulted in the formation of only two products in similar quantities (Scheme 1 and Figure S3). Both were phenols with one metabolite 2-methoxy-3-methylphenol (2-MeO-3-MP) identified by GC–MS coelution experiments after synthesis of the standard (see Experimental Section). The other was 4-methoxy-3-methylphenol (4-MeO-3-MP, Scheme 1 and Supporting Information). The generic accelera-

ChemPubSoc Europe
CHEMCATCHEM Full Papers

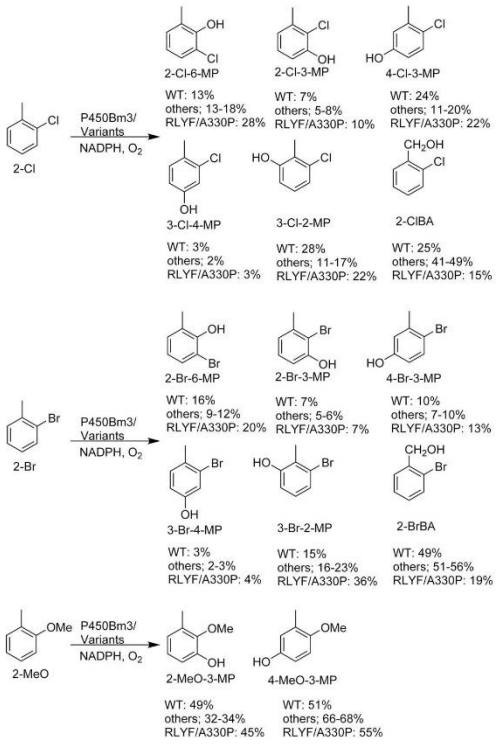

Scheme 1. Product distribution arising from the oxidation of 2-chlorotoluene (2-Cl), 2-bromotoluene (2-Br) and 2-methoxytoluene (2-MeO) by the CYP102A1 variants (RLYF/A330P, WT: wild type CYP102A1, others: the generic accelerators KT2, RlYF/I401P and R19). MP: methylphenol, BA: benzyl alcohol.

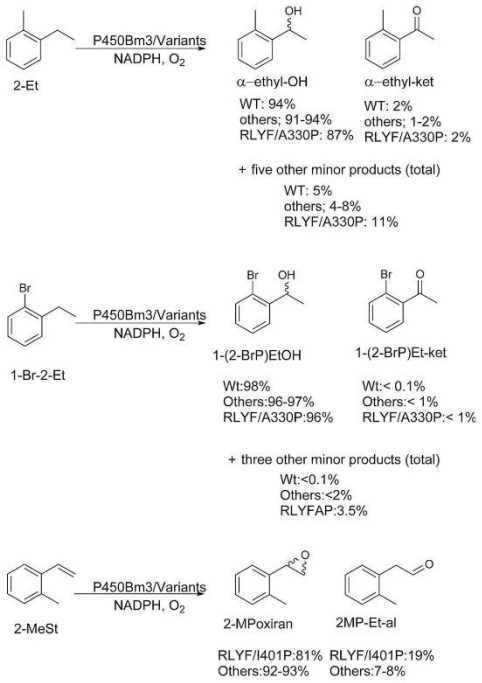

Scheme 2. Product distribution arising from the oxidation of 2-ethyltoluene (2-Et), 1-bromo-2-ethylbenzene (1-Br-2-Et) and 2-methylstyrene (2-MeSt) by the CYP102A1 variants. See Scheme 1 for labels. For 2-MeSt, the WT and RLYF/A330P enzymes are grouped with the others and RLYF/I401P is given separately.

tors in RLYF/I401P, KT2 and R19 favoured the formation of 4-MeO-3-MP, with a maximum of 68% observed using RLYF/I401P and R19 (Scheme 1).

Modification of the *ortho* substituent to an ethyl moiety introduced a more reactive benzylic methanediyl site at the α-position. The major product of 2-ethyltoluene oxidation across all variants was consequently shifted towards oxidation at this position generating 1-(2-methylphenyl)ethanol (1-(2-MePh)EtOH or α-ethyl-OH, Scheme 2). Further oxidation of this alcohol to give the ketone (2-Meacetph, α-ethyl-ket, 1–2%) was also observed. 2-Ethyltoluene was oxidised into five other minor products (total $<12\%$) as a result of either aromatic or benzylic oxidation (Figure S4). These were produced in small quantities and no authentic standards were available so their full characterisation was not possible (Figure S5). The mass spectra fragmentation patterns observed for each metabolite (see Supporting Information) indicated that three were phenolic products and another the benzyl alcohol (2-ethylbenzyl alcohol, retention time: 9.8 min). The fifth had a significantly shorter retention time (7.0 min) and different MS fragmentation pattern than the others (Supporting Information). *o*-Xylene oxidation by CYP102A1 yields a dearomatisation product (6,6-DMCHD) with a short retention time (Figure S2).[11a] This metabolite has a distinctive MS spectrum compared to those arising from phenol formation or benzylic methyl hydroxylation. Therefore, this product was assigned as 6-ethyl-6-methylcyclohexa-2,4-dienone (6-E-6-MCHD, Scheme 2, Supporting Information). The oxidation of 1-bromo-2-ethylbenzene was also highly selective for benzylic oxidation generating 1-(2-bromophenyl)ethanol (Scheme 2, Figure S6 and Figure S7). The selectivity for the major product was similar to that of 2-ethyltoluene, and fewer minor products were observed (Figure S6). These were assigned as arising from further oxidation to the ketone and phenol production (Scheme 2).

Changing the ethyl group to an alkene resulted in epoxidation as the most abundant reaction in the 2-methylstyrene conversions (Figure S7 and Experimental Section). A significant amount of an aldehyde rearrangement side product was the only other product observed (Scheme 2). More of the aldehyde product was observed in the turnover of the styrene by the RLYF/I401P compared to those from the other variants.

Chiral analysis of the 1-(2-methylphenyl)ethanol, 1-(2-bromophenyl)ethanol and 2-methylstyrene oxide products arising

ChemPubSoc Europe

CHEMCATCHEM Full Papers

from the turnovers of 2-ethyltoluene, 1-bromo-2-ethylbenzene and 2-methylstyrene was undertaken (Figure S8–S10). All the enzyme-catalysed turnovers showed little enantioselectivity with the WT, KT2 and R19 variants, and the maximum enantiomeric excess (*ee*) observed was 18% (Table S1). The RLYF/I401P variant increased the enantioselectivity of all the turnovers as did the RLYF/A330P, however, the maximum *ee* observed was 44% (Table S1 and Figure S8–10).

Three substrates with *meta*-arranged substituents were analysed (3-bromotoluene, 3-methoxytoluene and 3-methyltoluene).[11a] 3-Bromotoluene was oxidised to four products (Scheme 3 and Figure S11), with the major metabolite with all the variants being 4-bromo-2-methylphenol (4-Br-2-MP, Scheme 3). 2-Bromo-6-methylphenol (2-Br-6-MP), 2-bromo-4-methylphenol (2-Br-4-MP) and 3-bromobenzyl alcohol (3-BrBA) were formed as minor products (Scheme 3 and Figure S12). Similar to *m*-xylene and 3-bromotoluene, the major metabolite from 3-methoxytoluene oxidation also arose from hydroxylation *ortho* to the methyl group, giving 4-methoxy-2-methylphenol (4-MeO-2-MP, Scheme 3). Minor products included 2-methoxy-4-methylphenol (2-MeO-4-MP), 2-methoxy-6-methylphenol (2-MeO-6-MP) and 2-methoxy-5-methylphenol (2-MeO-5-MP) (Scheme 3 and Supporting Information).

The oxidation of 3-ethyltoluene by most variants generated a mixture of two major products (Scheme 3 and Figure S13). In agreement with the introduction of the more reactive ethyl group in *ortho*-substituted benzenes, one of these was identified as 1-(3-methylphenyl)ethanol (1-(3-MP)EtOH; NMR spectrum in the Supporting Information). The RLYF/A330P variant oxidised this substrate more selectively generating 92% of the second unidentified product (Figure S14). This metabolite was isolated using this variant and characterised as 4-methyl-2-ethylphenol (4-Me-2-EtP) by matching the NMR data with that reported in the literature (Supporting Information).[28] The enantioselectivity of the 1-(3-MP)EtOH product was determined, and in most instances a small preference for one enantiomer was observed. The highest selectivity was in the RLYF/I401P turnover which showed an *ee* of 46% (Table S1 and Figure S15).

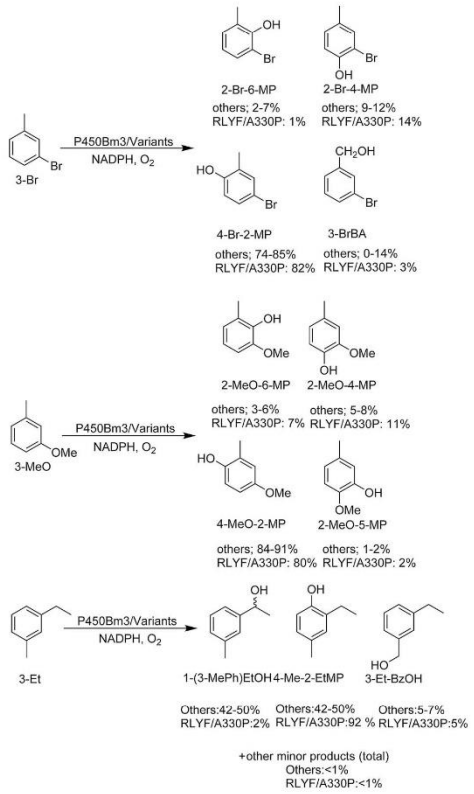

Scheme 3. Product distribution arising from the oxidation of 3-bromotoluene (3-Br), 3-methoxytoluene (3-Br) and 3-ethyltoluene (3-Et) by the CYP102A1 variants. No product was observed after the turnover with the WT enzyme with 3-Br or 3-MeO. The WT CYP102A1 data is included with others for 3-Et.

Discussion

The product formation rates were higher for the disubstituted benzenes than for the monosubstituted toluene and anisole. The epoxidation of 2-methylstyrene occurred at a lower activity compared to the hydroxylation of the other substrates, which agrees with previous results comparing the oxidation of styrenes and alkylbenzenes with CYP102A1 variants.[20] The more rigid planar nature of the vinyl substituent may orientate the molecule in a less favourable location for oxidation as reflected by the lower coupling efficiencies observed despite the higher reactivity of alkenes versus alkyl groups. The coupling efficiency and the product formation rates were improved for variants containing the RLYF mutations. This can be attributed to the improved uptake of small hydrophobic substrates into the active site compared to KT2 and WT CYP102A1. In addition, there may be less water in the active site of the RLYF variants. All of the RLYF/I401P, R19 and KT2 variants acted as generic accelerators, which improved the activity while leaving the product distribution relatively unchanged. RLYF/I401P altered the enantioselectivity of hydroxylation and epoxidation suggesting the orientation of the substrate in the active site has been changed in this variant. Owing to the presence of an active-site mutation, RLYF/A330P altered the selectivity of the substrate oxidation reactions. The most dramatic example of this was the selective formation of 4-methyl-2-ethylphenol from 3-ethyltoluene.

Substituents of different size, reactivity and electronic properties, as well as the relative positions of these groups, had an effect on the product profiles observed. The oxidation of the majority of the toluenes and anisoles by all the variants showed clear preferences for hydroxylation at the C–H bond next to a methyl or methoxy group. This implied that a methyl or methoxy group was sequestered in the active site such that

ChemPubSoc Europe
CHEMCATCHEM Full Papers

the adjacent aromatic C–H bond was best poised for oxidation by the enzyme.

The product distributions arising from the turnover of 2-chlorotoluene and 2-bromotoluene were similar as were the product formation activities and coupling efficiencies, both of which were higher than that of *o*-xylene. The major metabolite generated with each of these substrates is the benzyl alcohol (except with the RLYF/A330P variant). This suggests that the orientation of these substrates in the active site would be expected to be analogous to that of *o*-xylene with one substituent sequestered in the active site such that the adjacent one is oxidised. The selectivity and improved coupling efficiency indicated that the chloro or bromo substituents may be preferably sequestered positioning the methyl group for benzylic oxidation. Hydroxylation also occurred at each position around the aromatic ring generating a wide range of metabolites in good yield suggesting the substrate is mobile or that multiple binding orientations are possible.

The rationalisation for the formation of the observed products appears to be satisfied by the aromatic epoxidation mechanism and the products which are in line with the ring-opened intermediates that are stabilised by resonance effects (Scheme S1–3). The σ-cation complex mechanism could also be occurring and all the products observed could be generated by this pathway.[1g] In contrast to the *o*-xylene turnovers, there was no evidence of any product resulting from the shift of either substituent to the adjacent carbon bonded to the second substituent. The halide or methyl group could undergo a 1,2-shift with the adjacent hydrogen to give 2-Cl-6-MP and 2-Br-6-MP (Scheme S1) in a similar fashion to the migration of H in the NIH shift mechanism of arenes. The RLYF/A330P variant could be used to boost the amount of products which arise from substituent migrations. Several examples of halide or methyl group migration have been reported during the oxidation of halobenzenes and xylenes.[19c–e, 29] The 2-X-6-MP products could arise from the epoxide intermediate on either side of the halide or methyl group or from the epoxide between the two substituents (Scheme 4). Other epoxidations could ring-open to form the identical resonance-stabilised intermediate, which could provide routes to 2-X-6-MP formation. However, in this case, the ring opens to form an intermediate that is stabilised by induction only and so may not be preferred

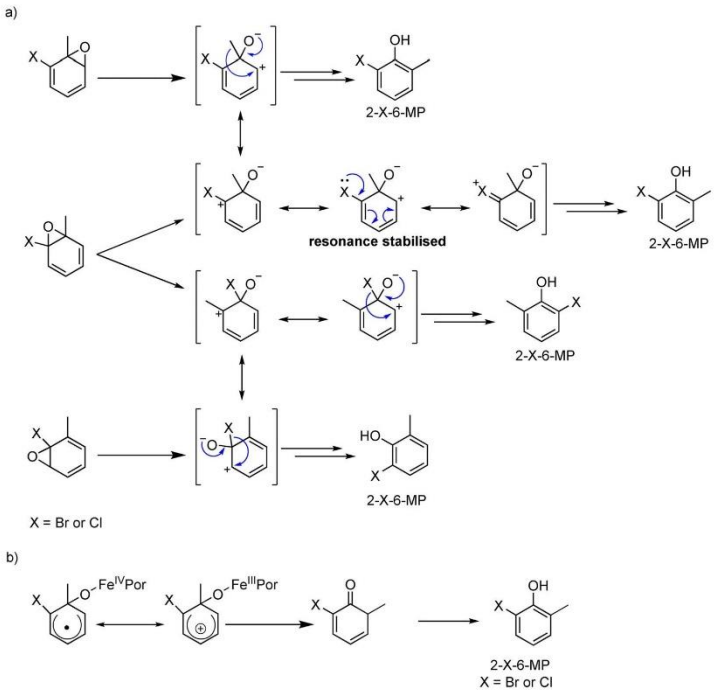

Scheme 4. a) Potential pathways for 2-X-6-MP formation through the ring opening of an epoxide intermediate and shift of the methyl group. Ring opening of the epoxide which resides between the two substituents results in two zwitterionic intermediates. One of these intermediates is stabilised relative to the other by resonance owing to the delocalisation of the lone pair of the bromo or chloro substituent (Scheme 4). The positive charge can reside on the electronegative halogen, providing the stabilisation. This pathway is not stabilised by induction but the resonance effect may provide a more significant impact on product formation and so this pathway, which requires the shift of the methyl group rather than the halogen, may be more likely. b) One potential route to 2-X-6-MP through the alternative sigma bonded cation complex mechanism of Shaik.

ChemPubSoc Europe

CHEMCATCHEM Full Papers

(Scheme 4). Determining exactly which substituent is shifted to give products such as 2-X-6-MP was not possible from these experiments.

The oxidation of 2-methoxytoluene by the CYP102A1 variants showed significant differences to that of the other *ortho*-substituted substrates. There was no oxidative demethylation or benzyl alcohol formation observed, which suggested that sequestration of the methyl substituent does not result in an attack at the *ortho* methoxy group or vice versa. In addition no phenol oxidation product *ortho* to the methyl group was formed. We cannot rule out that the positioning of this substrate in the active site is significantly different compared to that of 2-ethyltoluene, *o*-xylene and the halogenated toluenes. The two phenol products that were observed, 2-MeO-3-MP and 4-MeO-3-MP, could arise from the pathways of aromatic oxidation, which pass through ring-opened intermediates that are resonance-stabilised by the delocalised negative charge introduced by the methoxy group (Scheme S2). The major product arose from hydroxylation *para* to the methoxy group, which is analogous to the selectivity of anisole oxidation by xenobiotic oxidising P450s.

The dominant products of 2-ethyltoluene and 1-bromo-2-ethylbenzene oxidation arose from benzylic hydroxylation of the ethyl group. The coupling efficiency for the 2-ethyltoluene substrate was high across each variant, indicating that the substrate is well positioned for oxidation. The methyl group of 2-ethylbenzene may be sequestered in the active site such that the benzylic position in the ethyl group is placed best for hydroxylation. The coupling efficiency of 2-ethyltoluene oxidation was significantly higher than those of 1-bromo-2-ethylbenzene and 2-methylstyrene indicating a more favourable substrate binding orientation in the CYP102A1 active site. Intriguingly 3-ethyltoluene resulted in a mixture of two major products including 4-methyl-2-ethylphenol. This indicates that the *meta*-substituted substrate must be positioned in the active site in different orientations than the *ortho*-substituted equivalent.

One of the minor products of the 2-ethyltoluene was assigned as the dearomatisation product 6-E-6-MCHD. It has been shown that the epoxide, which results in the formation of the dearomatisation products, could be expanded to generate the oxepin, in this case, 2-E-7-MOx (Figure S5). Oxepin formation has been previously detected by a bacterial P450-catalysed oxidation of *tert*-butylbenzene, but we found no evidence for the oxepin in this work. None was reported in the oxidation of *o*-xylene.[11a,30] The stability of the oxepin has been shown to vary depending on the solvent and other conditions.[30] The different stereochemistry of methyl and ethyl versus the *tert*-butyl substituents may also alter the stability of the different products and intermediates. Whether the methyl or ethyl group, or a mixture of both, shift remains to be determined.

In the turnovers of 3-bromotoluene and 3-methoxytoluene, all the variants were highly selective for the formation of 4-Br-2-MP and 4-MeO-2-MP, respectively. In both, the hydroxyl group is installed *ortho* to the methyl substituent (Scheme S3). The formation of 2-MeO-5-MP requires the shift of the methoxy group to place it *para* to the methyl group and no equivalent shift occurred in the 3-bromotoluene or 3-ethyltoluene turnovers. 3-BrBA was generated in small quantities with 3-bromotoluene. The shift of a methoxy substituent in the turnover of 3-methoxytoluene to generate 2-methoxy-5-methylphenol was also not observed for 2-methoxytoluene. The selectivity of the turnovers with the *meta*-substituted toluenes for the major product was greater than their *ortho* counterparts. All of this implies that the orientations of significantly different substituted benzene substrates in the enzyme active site are not the same but that molecules of similar size and shape give rise to products that are hydroxylated at the same relative position.

Compared to mammalian enzymes, CYP102A1 oxidation of toluene-based substrates gives rise to lower benzylic oxidation with increased hydroxylation *ortho* to the methyl group. In general, for both bacterial and mammalian enzyme, styrene epoxidation and benzylic oxidation of ethyl substituents bestows the major products. Importantly, methyl and halogen migrations have both been reported previously with mammalian P450s and have now been shown to occur with CYP102A1. The more open nature and larger size of the active site of the mammalian enzymes presumably favours oxidation at more reactive sites of the substrate. The narrower active site of CYP102A1 enables the alkylbenzene molecules to be orientated to allow oxidation at less reactive C–H bonds. The most striking example is the oxidation of 3-ethyltoluene to 4-methyl-2-ethylphenol by the RLYFAP mutant despite the presence of an ethyl group in the substrate.

Conclusions

Increasing the number of substituents and their properties, as well as modifying their relative positions, has a significant impact on the regioselectivity of CYP102A1-catalysed oxidation of substituted benzenes. The variants used all generated increased levels of product compared to the WT enzyme, and those containing the RLYF mutations were the most successful at improving the product formation activity (500 to 1600 min^{-1}). This resulted in the generation of the metabolites in significantly higher yields allowing facile characterisation. RLYF/A330P provided different product distributions to the other enzymes, the most striking example is the switch in selectivity with 3-ethyltoluene to generate a single major product, 4-methyl-2-ethylbenzene at high activity, >650 min^{-1}, despite the presence of the more reactive benzylic C–H bonds. In addition, the major product from the 2-chlorotoluene oxidation by this mutant involves a shift of one of the substituents to generate 2-chloro-6-methylphenol. The presence of an *ortho*-ethyl substituent markedly improved the selectivity for oxidation at the reactive benzylic methylene. Epoxidation of alkenes was also preferred though the activity of this reaction was lower. The electron-donating methoxy group had a significant impact on the selectivity of oxidation. The *ortho*-substituted halotoluenes generated many products including a significant proportion from the migration of one or more substituents. The results presented here provide an insight as to how CYP102A1 variants may be used to generate metabolites of

ChemPubSoc Europe

CHEMCATCHEM Full Papers

xenobiotic detoxification. The substituent shifts in the CYP102A1 oxidations are an important observation. The design and testing of a wider range of substrates in which the relative position, size and electronic properties of the substituents are varied would assist in P450 mechanism interrogation.

Experimental Section

General

Reagents and organic substrates were from Sigma–Aldrich, TCI, Fluorochem, VWR or Enamine. Buffer components, NADPH and isopropyl-β-D-thiogalactopyranoside (IPTG) were from Astral Scientific, Australia. UV/Vis spectra and spectroscopic activity assays were recorded at 30±0.5 °C on an Agilent CARY-60 or Varian CARY-5000 spectrophotometer. Gas ghromatography-mass spectrometry (GC–MS) data were collected on a Shimadzu GC-17A using a QP5050A GC–MS detector and a DB-5 MS fused silica column (30 m × 0.25 mm, 0.25 μm). The injector and interface were maintained at 250 °C and 280 °C, respectively. GC and chiral analysis were performed with a Shimadzu Tracera GC coupled to a barrier discharge ionisation detector (BID) detector using a Supelcowax column (30 m × 0.32 mm, 0.25 μm) or RT-BDEXse chiral silica column (Restek: 30 m *x* 0.32 mm, 0.25 μm), respectively. In all instances helium was used as the carrier gas.

Cloning, expression and purification

Plasmids (pET28 based; Merck Millipore) containing the relevant CYP102A1 gene were transformed into *Escherichia coli* strain BL21(DE3) and the transformed cells were cultured in 2×YT medium at 37 °C with 30 μg mL^{-1} kanamycin.[14] When the OD_{600} of the culture reached 0.6–0.8 the temperature was reduced to 20 °C, 0.5 mM IPTG, 3 mL L^{-1} of trace elements solution was added (trace elements solution per litre; 0.74 g $CaCl_2{\cdot}H_2O$, 0.18 g $ZnSO_4{\cdot}7H_2O$, 0.132 g $MnSO_4{\cdot}4H_2O$, 20.1 g Na_2EDTA, 16.7 g $FeCl_3{\cdot}6H_2O$, 0.10 g $CuSO_4{\cdot}5H_2O$, 0.25 g $CoCl_2{\cdot}6H_2O$). After further growth for 18 h at 20 °C, cells were harvested by centrifugation, resuspended in 40 mM potassium phosphate, pH 7.4, 1 mM in dithiothreitol (buffer P) and lysed by sonication on ice (40 cycles of 20 s with a minute between each cycle). The crude extracts were then centrifuged at 37 000 *g* for 25 min at 4 °C to remove the cell debris. The supernatant was loaded onto a GE-Healthcare DEAE fast-flow Sepharose column (200×50 mm) pre-equilibrated with buffer P from which the protein was eluted using a linear gradient of 80–400 mM ammonium sulfate in buffer P. The red P450 containing fractions were collected and concentrated by ultrafiltration, desalted using a Sephadex G-25 column pre-equilibrated with buffer P, and re-concentrated by ultrafiltration. The solution was centrifuged at 7000 g for 10 min at 4 °C before FPLC anion-exchange purification on an GE-Healthcare Source 15Q column (120×26 mm) using a linear gradient of 0–30% 16 *x* phosphate buffer. Fractions containing P450 were collected, concentrated by ultrafiltration and filter sterilised before storing at −20 °C in 50% (*v*/*v*) glycerol. Glycerol and salts were removed from proteins immediately prior to experiments using a GE Healthcare 5 mL PD-10 desalting column pre-equilibrated with 50 mM Tris buffer, pH 7.4.

NADPH turnover rate determinations

NADPH turnovers were run in 1200 μL of 50 mM oxygenated Tris, pH 7.4 at 30 °C, containing 0.2 μM enzyme and 125 μg bovine liver catalase. Assays were held at 30 °C for 1 min prior to NADPH addition as a 20 mg mL^{-1} stock to a final concentration of ≈320 μM (equivalent to 2 AU). A period of ten seconds was allowed to elapse after NADPH addition before the absorbance decay at 340 nm was measured. Finally 1 mM substrate was added as a 100 mM stock solution in DMSO or EtOH. The NADPH consumption rate was derived using $\varepsilon_{340}=6.22$ mM^{-1} cm^{-1}. All data are reported as the mean of at least three experiments.

Product analysis

If authentic product standards were available, they were utilised for identification purposes by HPLC and GC coelution experiments and analysis of the MS fragmentation pattern. The epoxide product of 2-methylstyrene was generated by adding the substrate (5 mmol) to a solution of mCPBA (3.4 mg, 10 mmol) in acetonitrile (1 mL) and this mixture was used for coelution experiments. 2-Methoxy-3-methylphenol was synthesised by following a literature procedure; 2-methoxytoluene (125 mg, 1 mmol) was added to a solution of hydrogen peroxide (30%, 2 mL) in glacial acetic acid (10 mL). The reaction was monitored by GC–MS after adding the mixture (1 mL aliquots) into water and extraction into ethyl acetate.[31] 1-(2-Methylphenyl)ethanol was synthesised by dropwise addition of sodium borohydride (20 mg, 0.5 mmol) in water (5 mL) to a stirring solution of 2′-methylacetophenone (67 mg, 0.5 mmol) in acetonitrile (5 mL). The reactions were monitored by GC–MS.

After the NADPH consumption assays or whole-cell incubations had finished 990 μL of the reaction mixture was mixed with 10 μL of an internal standard solution (*p*-cresol or *trans*-4-phenyl-3-buten-2-one, 20 mM stock solution). The mixture was extracted with 400 μL of ethyl acetate and the organic extracts were used directly for GC–MS analysis. The oven temperature was held at 80 °C for 3 min and then increased at 7 °C min^{-1} up to 220 °C were it was held for 3 min. Metabolite yields were calculated using calibration of authentic samples and by making the assumption that isomeric mono-oxygenated products would give comparable responses (Table S2). Samples containing a range of concentrations of the chosen product including internal standard in 50 mM Tris, pH 7.4 were extracted as above. The integrated peak areas were expressed as ratios of the internal standard peak area and plotted against product concentration.

On requirement of HPLC analysis the organic solvent was removed under a stream of nitrogen before resuspending in acetonitrile/water. HPLC was performed using an Agilent 1260 Infinity pump equipped with an Agilent Eclipse Plus C18 column (250 mm × 4.6 mm, 5 μm), an autoinjector and UV detector. A gradient, 20–95%, of acetonitrile (with trifluoroacetic acid, 0.1%) in water (TFA, 0.1%) applied at 1 mL min^{-1} was used. Samples were identified through coelution experiments. The GC and HPLC retention times of the substrate and products are given in the supporting information.

Whole-cell oxidations and product characterisation

For whole-cell oxidation turnovers the required CYP102A1 gene was produced as described above in 200 mL of media. The cell pellet was harvested and resuspended in 200 mL of *E. coli* minimal media (EMM; K_2HPO_4, 7 g, KH_2PO_4, 3 g, Na_3citrate, 0.5 g, $(NH_4)_2SO_4$, 1 g, $MgSO_4$, 0.1 g, 20% glucose, 20 mL and glycerol, 1% *v*/*v* per litre), each in a 2 L baffled flask.[32] Substrate (a 1 mM aliquot) was added to each flask and shaken (180 rpm, 30 °C). Three further additions of substrate (1 mM) were made every 2 h before leaving

ChemPubSoc Europe

CHEMCATCHEM Full Papers

the cultures to shake overnight. During the incubation 1 mL of culture was removed for GC-MS analysis to monitor the reaction.

The supernatant was extracted in ethyl acetate (3×100 mL), washed with brine (100 mL) and dried with magnesium sulfate, the organic extracts were combined, the solvent was removed, first by vacuum distillation and then under a stream of nitrogen. The products were purified by using silica gel chromatography using a hexane/ethyl acetate stepwise gradient ranging from 4:1 to 3:2 hexane to ethyl acetate using 5% increases every 50 mL. The composition of the fractions was assessed by thin-layer chromatography and GC–MS and those containing single products (≥95%) were combined for characterisation. The solvent was removed under reduced pressure and the purified product was dissolved in $CDCl_3$ for characterisation by NMR spectroscopy and GC–MS. NMR spectra were acquired on a Varian Unity-plus spectrometer operating at 500 MHz for ^1H and 126 MHz for ^{13}C. A combination of ^1H, ^{13}C, COSY and HSQC experiments was used to determine the structures of the products.

Acknowledgements

S.G.B. acknowledges the ARC for a Future Fellowship (FT140100355). The authors also thank the University of Adelaide for M. Phil Scholarships (for S.D.M. and I.C.K.L) and an International Postgraduate Award (for S.D.). The authors thank Prof. Luet-Lok Wong (University of Oxford, UK) for the gene constructs of the CYP102A1 variants.

Conflict of interest

The authors declare no conflict of interest.

Keywords: arenes · biocatalysis · enzyme catalysis · mutagenesis · oxidation

[1] a) P. R. Ortiz de Montellano, *Chem. Rev.* **2010**, *110*, 932–948; b) T. L. Poulos, *Chem. Rev.* **2014**, *114*, 3919–3962; c) A. Sigel, H. Sigel, R. Sigel, *The Ubiquitous Roles of Cytochrome P450 Proteins*, John Wiley & Sons, Weinheim, **2007**, p; d) J. Rittle, M. T. Green, *Science* **2010**, *330*, 933–937; e) M. Asaka, H. Fujii, *J. Am. Chem. Soc.* **2016**, *138*, 8048–8051; f) J. W. Daly, D. M. Jerina, B. Witkop, *Experientia* **1972**, *28*, 1129–1149; g) S. P. de Visser, S. Shaik, *J. Am. Chem. Soc.* **2003**, *125*, 7413–7424; h) S. Shaik, D. Kumar, S. P. de Visser, A. Altun, W. Thiel, *Chem. Rev.* **2005**, *105*, 2279–2328; i) S. Shaik, S. Cohen, Y. Wang, H. Chen, D. Kumar, W. Thiel, *Chem. Rev.* **2010**, *110*, 949–1017.

[2] P. R. Ortiz de Montellano in *Cytochrome P450: Structure, Mechanism, and Biochemistry Vol.*, Springer International Publishing, Switzerland, **2015**.

[3] F. P. Guengerich in *The Ubiquitous Roles of Cytpchrome P450 Proteins* Vol. 3, (Eds.: A. Sigel, H. Sigel, R. Sigel), Wiley-VCH, Weinheim, **2007**, pp. 561–589.

[4] a) C. M. Krest, E. L. Onderko, T. H. Yosca, J. C. Calixto, R. F. Karp, J. Livada, J. Rittle, M. T. Green, *J. Biol. Chem.* **2013**, *288*, 17074–17081; b) T. H. Yosca, J. Rittle, C. M. Krest, E. L. Onderko, A. Silakov, J. C. Calixto, R. K. Behan, M. T. Green, *Science* **2013**, *342*, 825–829.

[5] C. J. Whitehouse, S. G. Bell, L. L. Wong, *Chem. Soc. Rev.* **2012**, *41*, 1218–1260.

[6] a) L. O. Narhi, A. J. Fulco, *J. Biol. Chem.* **1987**, *262*, 6683–6690; b) R. T. Ruettinger, L. P. Wen, A. J. Fulco, *J. Biol. Chem.* **1989**, *264*, 10987–10995.

[7] a) S. Kille, F. E. Zilly, J. P. Acevedo, M. T. Reetz, *Nat. Chem.* **2011**, *3*, 738–743; b) V. B. Urlacher, S. G. Bell, L. L. Wong in *The Bacterial Cytochrome P450 Monooxygenases: P450cam and P450BM-3* (Eds.: R. D. Schmid, V. B. Urlacher), Wiley, New York, **2007**, pp. 99–122; c) R. Fasan, *ACS Catal.* **2012**, *2*, 647–666; d) G. D. Roiban, M. T. Reetz, *Chem. Commun.* **2015**, *51*, 2208–2224; e) S. G. Bell, N. Hoskins, C. J. C. Whitehouse, L. L. Wong in *Design and Engineering of Cytochrome P450 Systems* (Eds.: A. Sigel, H. Sigel, R. Sigel), Wiley-VCH, Weinheim, **2007**, pp. 437–476.

[8] a) A. B. Carmichael, L. L. Wong, *Eur. J. Biochem.* **2001**, *268*, 3117–3125; b) Q. S. Li, J. Ogawa, R. D. Schmid, S. Shimizu, *FEBS Lett.* **2001**, *508*, 249–252; c) Q. S. Li, J. Ogawa, R. D. Schmid, S. Shimizu, *Appl. Environ. Microbiol.* **2001**, *67*, 5735–5739; d) M. W. Peters, P. Meinhold, A. Glieder, F. H. Arnold, *J. Am. Chem. Soc.* **2003**, *125*, 13442–13450; e) R. J. Sowden, S. Yasmin, N. H. Rees, S. G. Bell, L. L. Wong, *Org. Biomol. Chem.* **2005**, *3*, 57–64; f) W. T. Sulistyaningdyah, J. Ogawa, Q. S. Li, R. Shinkyo, T. Sakaki, K. Inouye, R. D. Schmid, S. Shimizu, *Biotechnol. Lett.* **2004**, *26*, 1857–1860.

[9] a) P. S. Coelho, E. M. Brustad, A. Kannan, F. H. Arnold, *Science* **2013**, *339*, 307–310; b) C. C. Farwell, R. K. Zhang, J. A. McIntosh, T. K. Hyster, F. H. Arnold, *ACS Cent. Sci.* **2015**, *1*, 89–93; c) T. K. Hyster, C. C. Farwell, A. R. Buller, J. A. McIntosh, F. H. Arnold, *J. Am. Chem. Soc.* **2014**, *136*, 15505–15508; d) R. Singh, M. Bordeaux, R. Fasan, *ACS Catal.* **2014**, *4*, 546–552.

[10] a) C. R. Otey, G. Bandara, J. Lalonde, K. Takahashi, F. H. Arnold, *Biotechnol. Bioeng.* **2006**, *93*, 494–499; b) B. M. van Vugt-Lussenburg, M. C. Damsten, D. M. Maasdijk, N. P. Vermeulen, J. N. Commandeur, *Biochem. Biophys. Res. Commun.* **2006**, *346*, 810–818; c) D. H. Kim, K. H. Kim, D. H. Kim, K. H. Liu, H. C. Jung, J. G. Pan, C. H. Yun, *Drug Metab. Dispos.* **2008**, *36*, 2166–2170; d) G. Di Nardo, G. Gilardi, *Int. J. Mol. Sci.* **2012**, *13*, 15901–15924; e) K. H. Kim, J. Y. Kang, D. H. Kim, S. H. Park, D. Kim, K. D. Park, Y. J. Lee, H. C. Jung, J. G. Pan, T. Ahn, C. H. Yun, *Drug Metab. Dispos.* **2011**, *39*, 140–150; f) S. H. Park, D. H. Kim, D. Kim, H. C. Jung, J. G. Pan, T. Ahn, C. H. Yun, *Drug Metab. Dispos.* **2010**, *38*, 732–739; g) A. M. Sawayama, M. M. Chen, P. Kulanthaivel, M. S. Kuo, H. Hemmerle, F. H. Arnold, *Chem. Eur. J.* **2009**, *15*, 11723–11729; h) E. Stjernschantz, B. M. van Vugt-Lussenburg, A. Bonifacio, S. B. de Beer, G. van der Zwan, C. Gooijer, J. N. Commandeur, N. P. Vermeulen, C. Oostenbrink, *Proteins* **2008**, *71*, 336–352; i) B. M. van Vugt-Lussenburg, E. Stjernschantz, J. Lastdrager, C. Oostenbrink, N. P. Vermeulen, J. N. Commandeur, *J. Med. Chem.* **2007**, *50*, 455–461; j) R. Weis, M. Winkler, M. Schittmayer, S. Kambourakis, M. Vink, J. R. Rozzell, A. Glieder, *Adv. Synth. Catal.* **2009**, *351*, 2140–2146; k) X. Ren, J. A. Yorke, E. Taylor, T. Zhang, W. Zhou, L. L. Wong, *Chem. Eur. J.* **2015**, *21*, 15039–15047; l) G. Di Nardo, A. Fantuzzi, A. Sideri, P. Panicco, C. Sassone, C. Giunta, G. Gilardi, *J Biol. Inorg. Chem.* **2007**, *12*, 313–323.

[11] a) C. J. Whitehouse, N. H. Rees, S. G. Bell, L. L. Wong, *Chem. Eur. J.* **2011**, *17*, 6862–6868; b) C. J. Whitehouse, W. Yang, J. A. Yorke, B. C. Rowlatt, A. J. Strong, C. F. Blanford, S. G. Bell, M. Bartlam, L. L. Wong, Z. Rao, *ChemBioChem* **2010**, *11*, 2549–2556.

[12] C. J. Whitehouse, S. G. Bell, L. L. Wong, *Chem. Eur. J.* **2008**, *14*, 10905–10908.

[13] P. R. Ortiz de Montellano, S. D. Nelson, *Arch. Biochem. Biophys.* **2011**, *507*, 95–110.

[14] C. J. Whitehouse, S. G. Bell, H. G. Tufton, R. J. Kenny, L. C. Ogilvie, L. L. Wong, *Chem. Commun.* **2008**, 966–968.

[15] A. Dennig, N. Lulsdorf, H. Liu, U. Schwaneberg, *Angew. Chem. Int. Ed.* **2013**, *52*, 8459–8462; *Angew. Chem.* **2013**, *125*, 8617–8620.

[16] D. A. Rock, A. E. Boitano, J. L. Wahlstrom, D. A. Rock, J. P. Jones, *Bioorg. Chem.* **2002**, *30*, 107–118.

[17] a) A. Dennig, J. Marienhagen, A. J. Ruff, L. Guddat, U. Schwaneberg, *ChemCatChem* **2012**, *4*, 771–773; b) S. D. Munday, O. Shoji, Y. Watanabe, L. L. Wong, S. G. Bell, *Chem. Commun.* **2016**, *52*, 1036–1039.

[18] a) C. Sams, G. D. Loizou, J. Cocker, M. S. Lennard, *Toxicol. Lett.* **2004**, *147*, 253–260; b) M. A. Wenker, S. Kezic, A. C. Monster, F. A. De Wolff, *Xenobiotica* **2001**, *31*, 61–72; c) W. Tassaneeyakul, D. J. Birkett, J. W. Edwards, M. E. Veronese, W. Tassaneeyakul, R. H. Tukey, J. O. Miners, *J. Pharmacol. Exp. Ther.* **1996**, *276*, 101–108; d) M. Fay, C. Eisenmann, S. Diwan, C. de Rosa, *Toxicol. Ind. Health* **1998**, *14*, 571–781; e) J. Daly, *Biochem. Pharmacol.* **1970**, *19*, 2979–2993; f) P. E. Weller, N. Narasimhan, J. A. Buben, R. P. Hanzlik, *Drug Metab. Dispos.* **1988**, *16*, 232–237.

[19] a) H. Sakurai, M. Kito, *Chem. Pharm. Bull.* **1977**, *25*, 2330–2335; b) W. Dunges, *Nature* **1973**, *243*, 60–61; c) J. Koerts, A. E. Soffers, J. Vervoort, A. De Jager, I. M. Rietjens, *Chem. Res. Toxicol.* **1998**, *11*, 503–512; d) J. J. Bogaards, B. van Ommen, C. R. Wolf, P. J. van Bladeren, *Toxicol. Appl. Pharmacol.* **1995**, *132*, 44–52; e) D. M. Jerina, N. Kaubisch, J. W. Daly, *Proc. Natl. Acad. Sci. USA* **1971**, *68*, 2545–2548.

ChemPubSoc Europe

CHEMCATCHEM Full Papers

[20] S. D. Munday, S. Dezvarei, S. G. Bell, *ChemCatChem* **2016**, *8*, 2789 – 2796.
[21] R. P. Hanzlik, K. H. J. Ling, *J. Am. Chem. Soc.* **1993**, *115*, 9363 – 9370.
[22] a) C. J. Whitehouse, S. G. Bell, W. Yang, J. A. Yorke, C. F. Blanford, A. J. Strong, E. J. Morse, M. Bartlam, Z. Rao, L. L. Wong, *ChemBioChem* **2009**, *10*, 1654 – 1656; b) C. J. Whitehouse, W. Yang, J. A. Yorke, H. G. Tufton, L. C. Ogilvie, S. G. Bell, W. Zhou, M. Bartlam, Z. Rao, L. L. Wong, *Dalton Trans.* **2011**, *40*, 10383 – 10396.
[23] D. C. Haines, D. R. Tomchick, M. Machius, J. A. Peterson, *Biochemistry* **2001**, *40*, 13456 – 13465.
[24] I. F. Sevrioukova, H. Li, H. Zhang, J. A. Peterson, T. L. Poulos, *Proc. Natl. Acad. Sci. USA* **1999**, *96*, 1863 – 1868.
[25] K. R. Korzekwa, D. C. Swinney, W. F. Trager, *Biochemistry* **1989**, *28*, 9019 – 9027.
[26] O. Shoji, T. Kunimatsu, N. Kawakami, Y. Watanabe, *Angew. Chem. Int. Ed.* **2013**, *52*, 6606 – 6610; *Angew. Chem.* **2013**, *125*, 6738 – 6742.
[27] J. C. Hackett, T. T. Sanan, C. M. Hadad, *Biochemistry* **2007**, *46*, 5924 – 5940.
[28] A. Fischer, G. N. Henderson, *Can. J. Chem.* **1981**, *59*, 2314 – 2327.
[29] C. den Besten, M. Ellenbroek, M. A. van der Ree, I. M. Rietjens, P. J. van Bladeren, *Chem.-Biol. Interact.* **1992**, *84*, 259 – 275.
[30] J. E. Stok, S. Chow, E. H. Krenske, C. Farfan Soto, C. Matyas, R. A. Poirier, C. M. Williams, J. J. De Voss, *Chem. Eur. J.* **2016**, *22*, 4408 – 4412.
[31] H. Orita, M. Shimizu, T. Hayakawa, K. Takehira, *Bull. Chem. Soc. Jap.* **1989**, *62*, 1652 – 1657.
[32] S. G. Bell, C. F. Harford-Cross, L.-L. Wong, *Protein Eng.* **2001**, *14*, 797 – 802.

Manuscript received: January 17, 2017
Revised manuscript received: February 28, 2017
Accepted manuscript online: March 5, 2017
Version of record online: June 1, 2017

Heterogeneous & Homogeneous & Bio- & Nano-
CHEMCATCHEM
CATALYSIS

Supporting Information

Examination of Selectivity in the Oxidation of *ortho*- and *meta*-Disubstituted Benzenes by CYP102A1 (P450 Bm3) Variants

Samuel D. Munday, Shaghayegh Dezvarei, Ian C.-K. Lau, and Stephen G. Bell*[a]

cctc_201700116_sm_miscellaneous_information.pdf

The m/z values, GC-MS and HPLC retention times (RT) of substrates and products (abbreviations MP – methyphenol, BA – benzyl alcohol, EtP – ethylphenol, MeOP – methoxyphenol, Phac – phenacetaldehyde, MePh – methylphenyl, acetph – acetophenone).

Substrate/Product	m/z (AMU)	GC-MS RT (min)	HPLC RT (min)
toluene	92	2.1	
2-MP	108	7.1	
4-MP	108	7.2	
2-MBA	108	6.5	
anisole	108	4.3	
2-MeOP	124	7.5	
4-MeOP	124	9.4	
2-bromotoluene	172	6.6	
2-Br-6-MP	188	8.7	17.8
2-Br-3-MP	188	9.1	16.9
2-BrBA	188	11.0	8.8
3-Br-2-MP	188	11.9	18.1
3-Br-4-MP	188	12.3	17.4
4-Br-3-MP	188	12.3	17.5
2-chlorotoluene	128	5.0	
2-Cl-6-MP	144	7.3	17.2
2-Cl-3-MP	144	7.7	16.3
2-ClBA	144	9.7	13.6
3-Cl-2-MP	144	10.5	17.5
3-Cl-4-MP	144	10.8	17.0
4-Cl-3-MP	144	10.8	16.6
2-methylanisole	122	6.1	
2-MeO-3-MP	138	8.4	
4-MeO-3-MP	138	11.2	
3-bromotoluene	172	6.6	
2-Br-6-MP	188	8.7	
2-Br-4-MP	188	9.0	
3-BrBA	188	11.7	
4-Br-2-MP	188	12.0	
3-methylanisole	122	6.3	
2-MeO-6-MP	138	9.0	
2-MeO-5-MP	138	9.2	
2-MeO-4-MP	138	9.3	
4-MeO-2-MP	138	10.9	
5-MeO-2-MP	138	10.9	not observed as a product.

1

Substrate/Product	m/z (AMU)	GC-MS RT (min)	GC Chiral RT (min)
2-ethyltoluene	120	5.5	
1-(2-MePh)EtOH (α-ethyl-OH)	136	9.1	19.1, 19.7
2-Meacetph (α-ethyl-ket)	134	8.3	
6-E-6-MCHD	136	7.0	
EMP_a	136	9.2	
2-Et-BA	136	9.8	
EMP_b	136	10.0	
EMP_c	136	10.7	
3-ethyltoluene	120	5.1	
1-(3-MePh)EtOH	136	8.6	17.9, 18.2
3-EtBA	136	9.7	
2-Et-4-MP	136	9.8	
2-methylstyrene	118	5.7	
2-MePhac	134	8.4	
2-MS-epox	134	8.7	15.6, 16.0
1-bromo-2-ethylbenzene	185	7.8	
Br-Et-P_a	201	10.0	
Br-Et-P_b	201	10.4	
2-Br-acetph	199	10.6	
1-(2-BrPh)EtOH	201	11.1	18.4, 19.5
Br-Et-P_c	201	12.9	

2

Table S1 Chiral analysis of the P450 turnovers of 3-ethyltoluene, 1-bromo-2-ethylbenzene, 2-ethyltoluene and 2-methylstyrene.

3-ethyltoluene

Variants / RT	17.8	18.2
R19	55	45
RLYFIP	73	27
KT2	50	50
WT	57	43
RLYFAP	26	74

1-bromo-2-ethylbenzene

variants / RT	18.5	19.5
R19	55	45
RLYFIP	67	33
KT2	55	45
WT	58	42
RLYFAP	72	28

2-ethyltoluene

variants / RT	19.1	19.7
R19	43	57
RLYFIP	55	45
KT2	45	55

2-methylstyrene

variants / RT	15.6	16.0
R19	54	46
RLYFIP	57	43
KT2	52	48
WT	50.5	49.5
RLYFAP	28	72

3

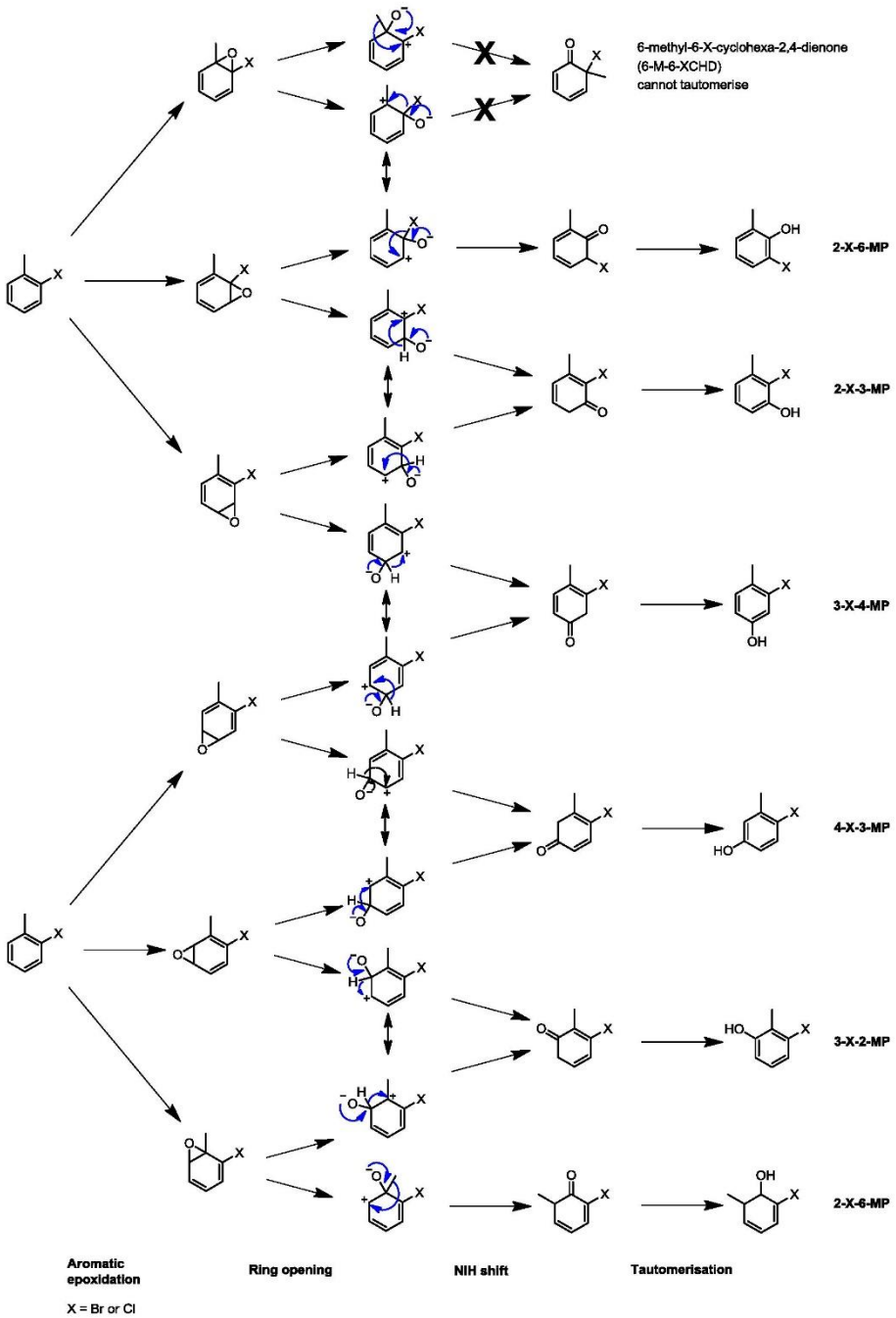

Scheme S1 Aromatic hydroxylation pathways in the oxidation of 2-bromotoluene and 2-chlorotoluene. Pathways that do not lead to an observed product have been indicated with an X.

4

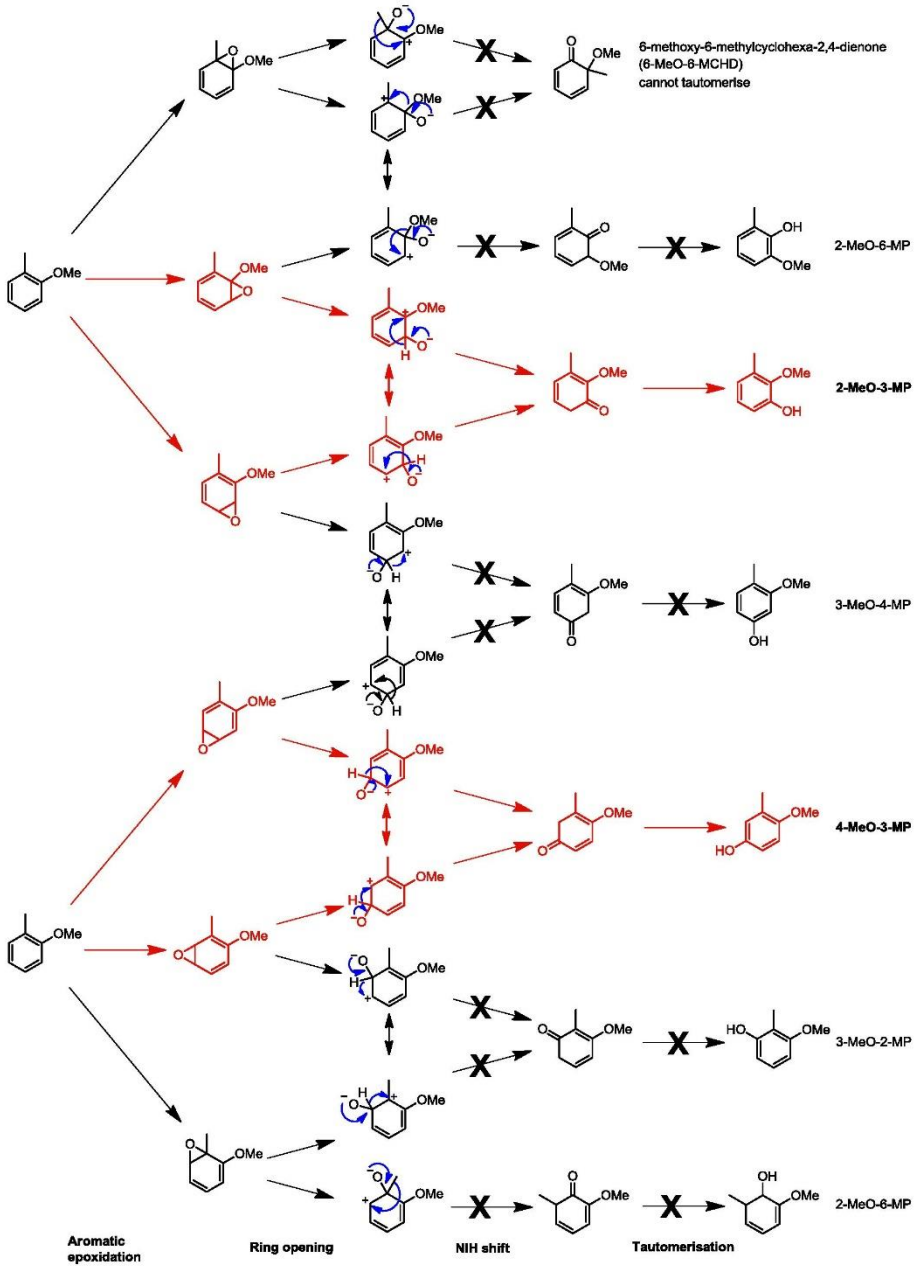

Scheme S2 Aromatic hydroxylation pathways in the oxidation of 2-methylanisole. Products that were observed and the pathways that lead to these are highlighted in red. Pathways that do not lead to an observed product have been indicated with an X.

5

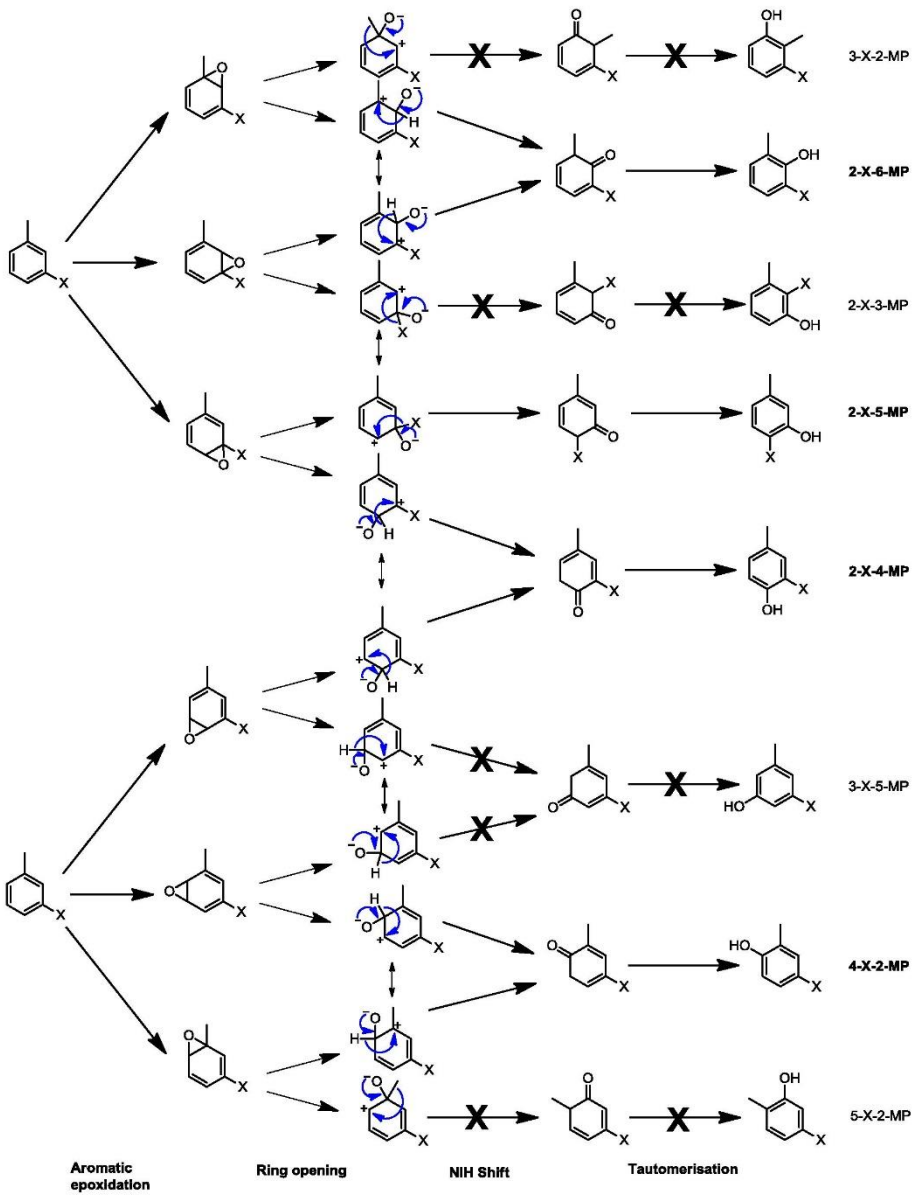

Scheme S3 Aromatic hydroxylation pathways in the oxidation of *meta*-substituted toluenes. Pathways that do not lead to an observed product have been indicated with an X.

6

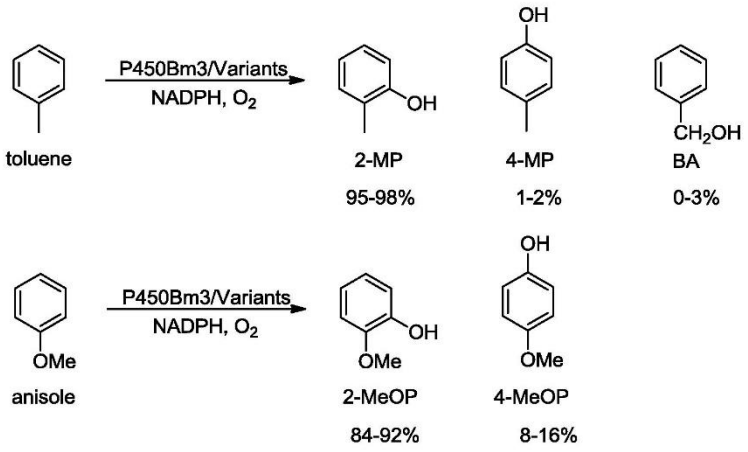

Fig. S1 Product distribution of toluene and anisole oxidation by the CYP102A1 variants.

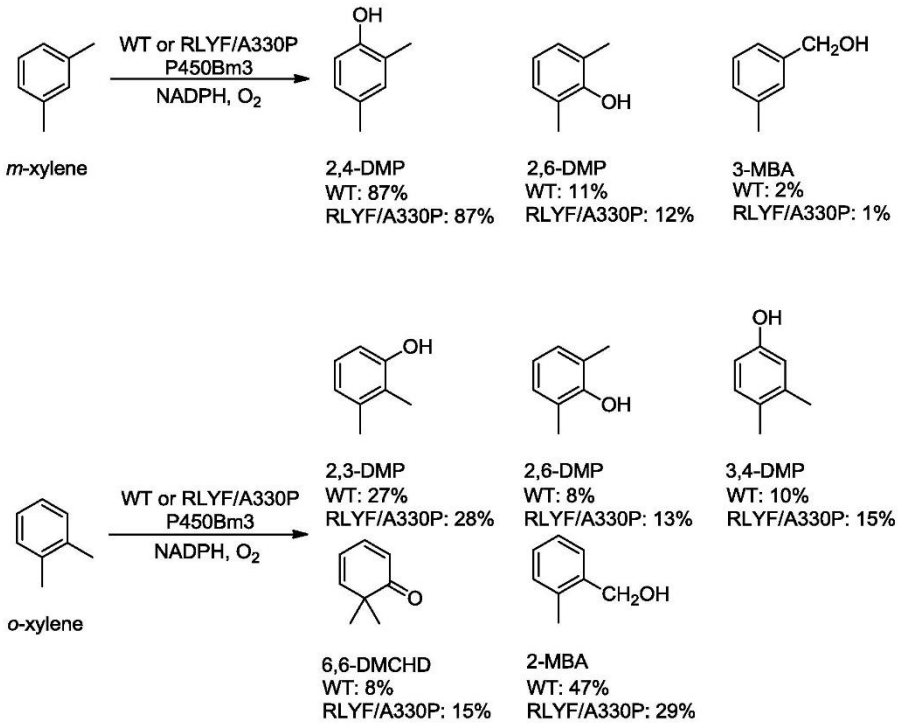

Fig. S2 Product distribution of *o*-xylene and *m*-xylene oxidation by the CYP102A1 variants.

7

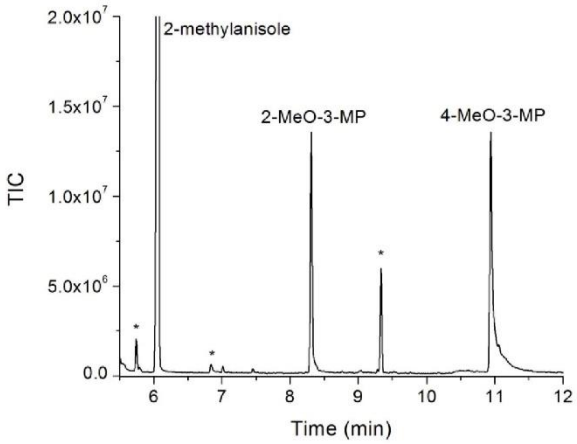

Fig. S3 GC-MS chromatogram of the turnover of 2-methylanisole by RLYF/I401P. The products are labelled as are impurities (*). 4-MeO-3-MP was identified by GC-MS coelution experiments with an authentic product standard. 2-MeO-3-MP was identified by coelution experiments with the synthesised product using a literature method.

8

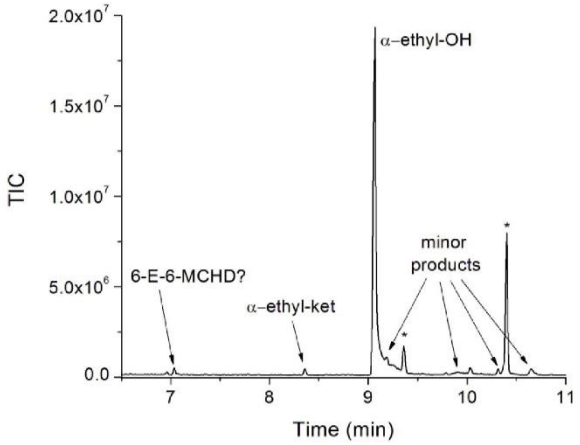

Fig. S4 GC-MS chromatogram of the turnover of 2-ethyltoluene by RLYF/I401P. The assigned major products are labelled as are impurities (*).The RT of minor hydroxylated products are: 7.0 9.2, 9.8, 10.4 and 10.7 min (see Fig. S3). The product 2-Meacetph (α-ethyl-ket) was identified by GC-MS coelution experiments with an authentic standard. This standard was reduced with $NaBH_4$ to produce the 1-(2-MePh)EtOH (α-ethyl-OH) coeluted with the main product from the turnover. The minor products were assigned as phenols, 6-E-6-MCHD and the methylbenzylic alcohol by analysing their retention times and MS fragmentation patterns (See figure S3 and the MS section in the supporting information).

9

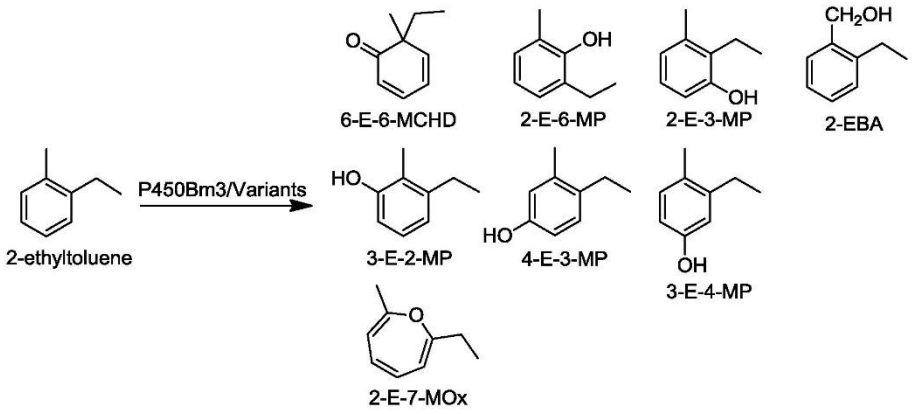

Fig. S5 The potential minor products arising from the oxidation of 2-ethyltoluene. The major product of 2-ethyltoluene oxidation was 1-(2-methylphenyl)ethanol (α-ethyl-OH, RT 9.1 min, 87-94% of all the product generated). Further oxidation of this alcohol to give the ketone (α-ethyl-ket, RT 8.3 min, 1-2%) was also observed. 2-Ethyltoluene was oxidised into five other minor products (total <12%) as a result of either aromatic or aliphatic oxidation. Using expected differences in the fragmentation patterns in the MS spectra of benzylic alcohols and phenols and comparison with the *o*-xylene turnover products inferred that a phenol with a shorter retention time (9.2 min) may be 2-ethyl-3-methylphenol (2-E-3-MP) or 2-ethyl-6-methylphenol (2-E-6-MP). Later eluting products (RT: 10.0 Min and 10.7 min) could be 3-ethyl-2-methylphenol (3-E-2-MP), 3-ethyl-4-methylphenol (3-E-4-MP) or 4-ethyl-3-methylphenol (4-E-3-MP). No evidence for the oxepin product could be found.

10

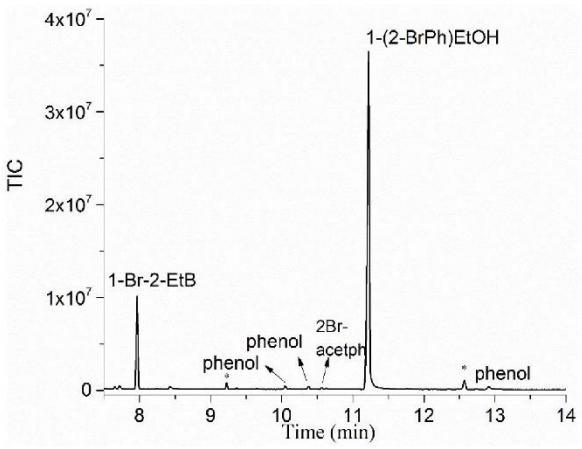

Fig. S6 GC-MS chromatogram of the turnover of 2-bromo-1-ethylbenzene by KT2 The products are labelled as are impurities (*). The 2-bromoacetophenone and 1-(2-bromophenyl)ethanols were characterised by their MS fragmentation patterns. The minor products were characterised as phenols by the MS fragmentation pattern.

11

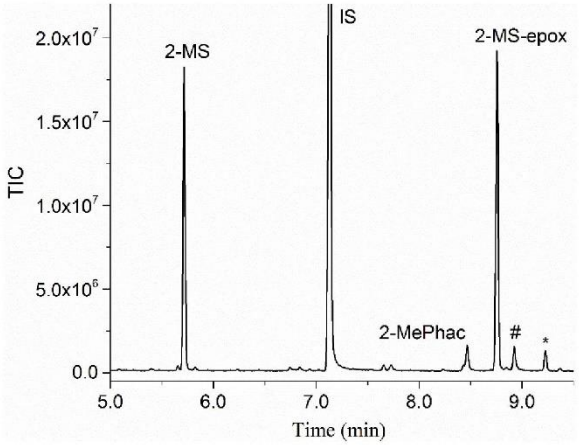

Fig. S7 GC-MS chromatogram of the turnover of 2-methylstyrene by KT2. The products are labelled as are impurities (*). A peak (#) was assigned as a 1-(2-methylphenyl)ethanol impurity which was formed due the presence of small amounts of 2-ethyltolune in the starting material. The epoxide was assigned by coelution of the turnover with the product from the reaction of 2-methylstyrene and *m*-chloroperbenzoic acid (mCPBA). The aldehyde had a distinctive MS fragmentation pattern.

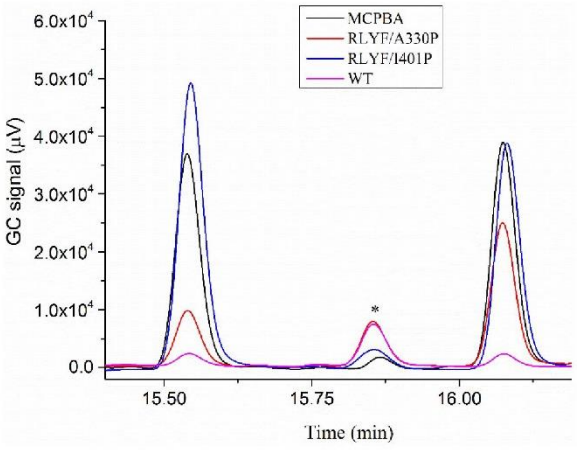

Fig. S8 Chiral GC chromatogram of the turnover of 2-methylstyrene by *m*-chloroperbenzoic acid (MCPBA) and the WT, RLYF/I401P (RLYFIP) and RLYF/A330P (RLYFAP) variants of CYP102A1. Impurities or minor product are labelled (*). The two enantiomers have retention times of 15.6 and 16.2 min.

13

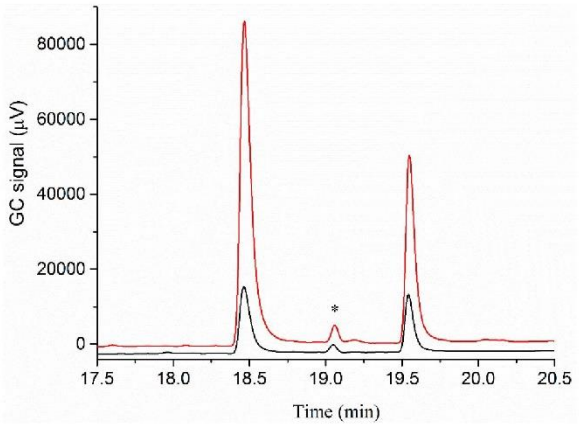

Fig. S9 Chiral GC chromatogram of the turnover of 1-bromo-2-ethylbenzene by the WT (black) and RLYF/I401P (RLYFIP; red) variants of CYP102A1. Impurities or minor product are labelled (*). The two enantiomers have retention times of 18.5 and 19.6 min.

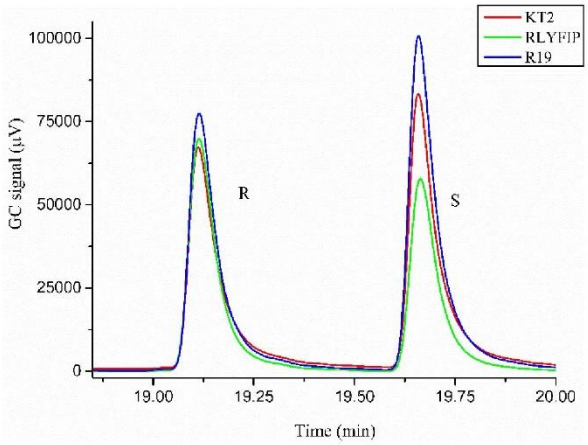

Fig. S10 Chiral GC chromatogram of the turnover of 2-ethyltoluene by KT2, RLYF/I401P (RLYFIP) and R19 variants of CYP102A1. The two enantiomers have retention times of 19.1 and 19.7 min.

15

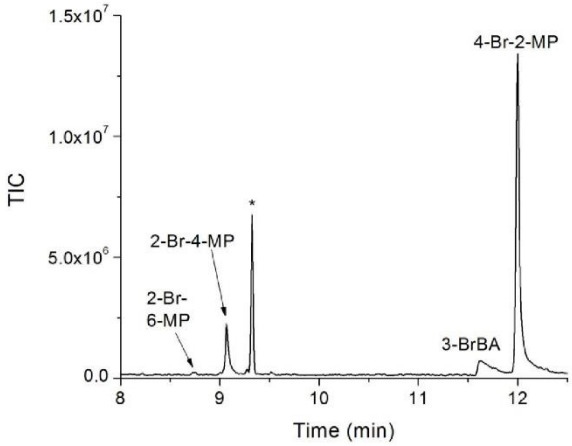

Fig. S11 GC-MS chromatogram of the turnover of 3-bromotoluene by RLYF/I401P. The products are labelled as are impurities (*). All the products were assigned by GC-MS coelution experiments with authentic product standards.

16

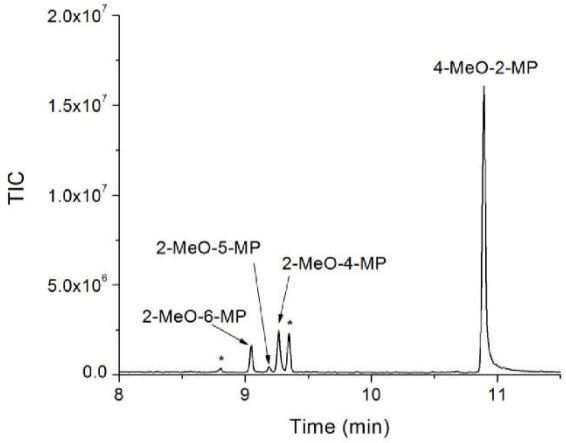

Fig. S12 GC-MS chromatogram of the turnover of 3-methylanisole by RLYF/I401P. The products are labelled as are impurities (*). The products were assigned by coalition with authentic samples. The rearrangement product (2-MeO-5-MP) was confirmed by analysing 2-methyl-5-methoxyphenol which has a significantly different retention time and MS fragmentation pattern (see MS data). GC-MS analysis showed no cross contamination of 3-methylanisole with 4-methylanisole which could generate 2-MeO-5-MP.

17

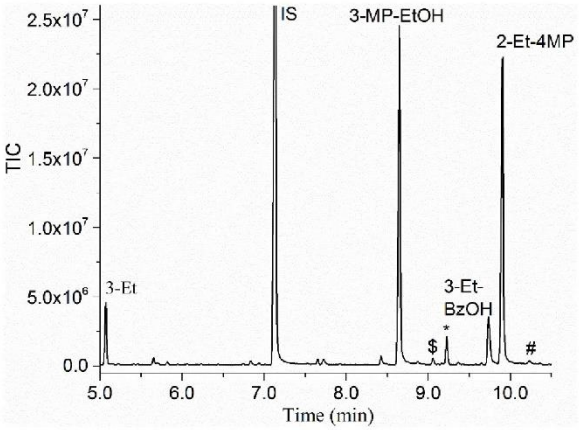

Fig. S13 GC-MS chromatogram of the turnover of 3ethyltoluene byKT2. The two major products were isolated from a larger scale whole-cell turnover and characterised by NMR. The products are labelled as are impurities (*). The peak at RT 9.05 min ($) was assigned as a phenol product and a peak (#) at RT 10.25 min could be assigned as a further oxidation product (m/z = 152.1) by their MS fragmentation patterns.

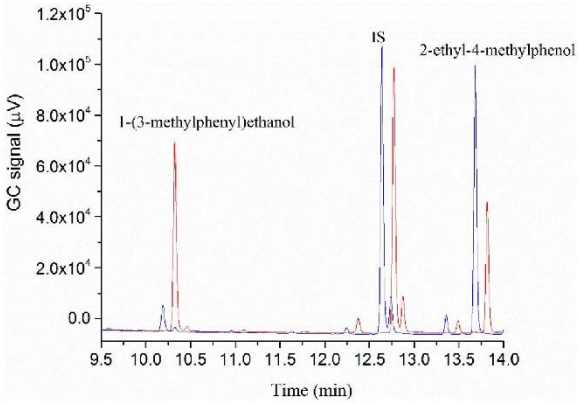

Fig. S14 GC chromatogram of the turnover of 3-ethyltoluene by RLYF/I401P (red) and RLYF/A330P (blue). The two major products are labelled as is the internal standard. The traces have been offset along the x-axis for clarity.

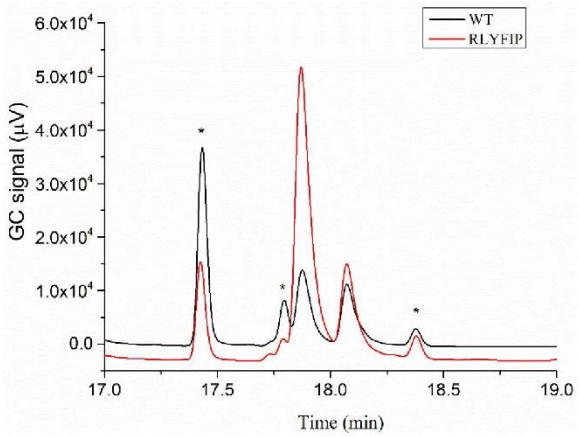

Fig. S15 Chiral GC chromatogram of the turnover of 3-ethyltoluene by the WT and RLYF/I401P (RLYFIP) variants of CYP102A1. Impurities or minor product are labelled (*). The two enantiomers have retention times of 17.9 and 18.2 min.

MS data

2-chlorotoluene

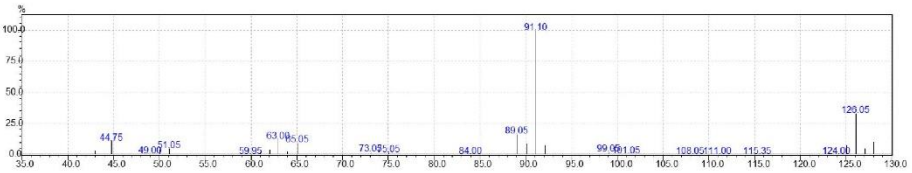

2-Cl

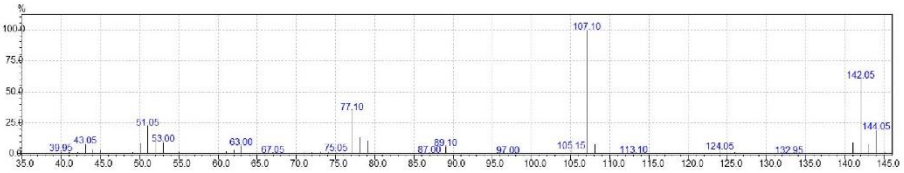

2-Cl-3-MP

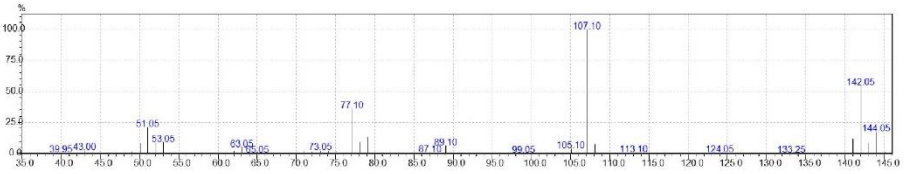

2-Cl-6-MP

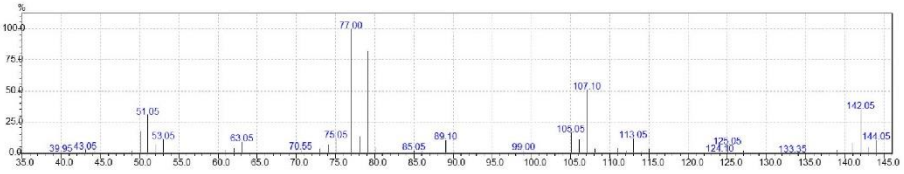

2-Cl-BA

20

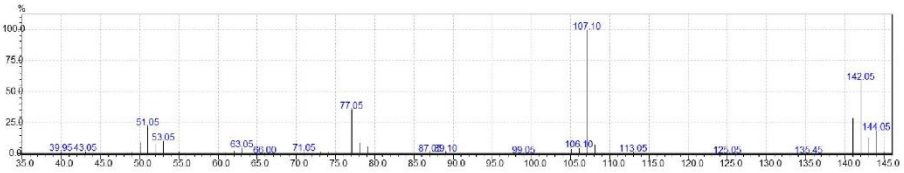

3-Cl-2-MP

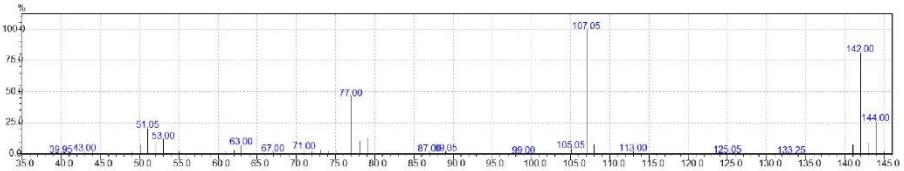

3-Cl-4-MP (and 4-Cl-3MP)

21

2-bromotoluene

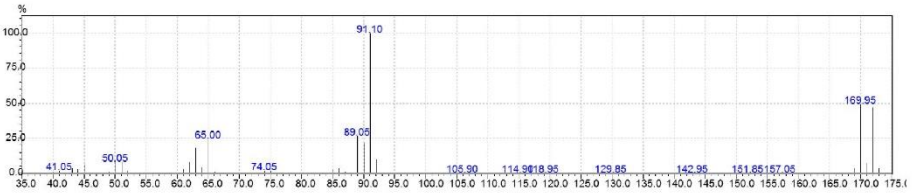

2-Br

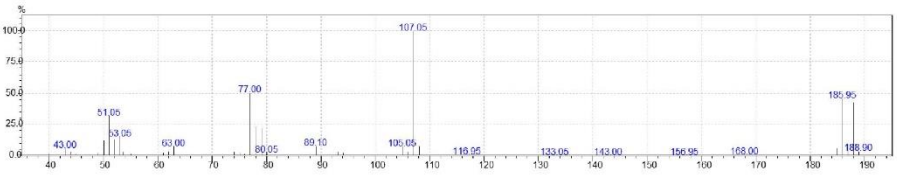

2-Br-3-MP

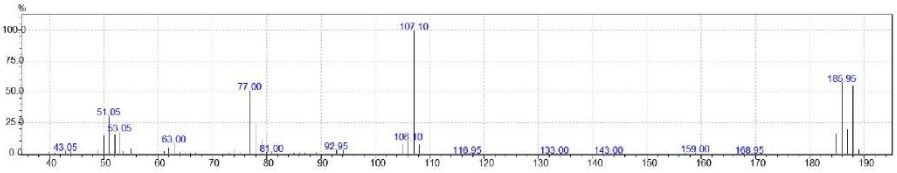

2-Br-6-MP

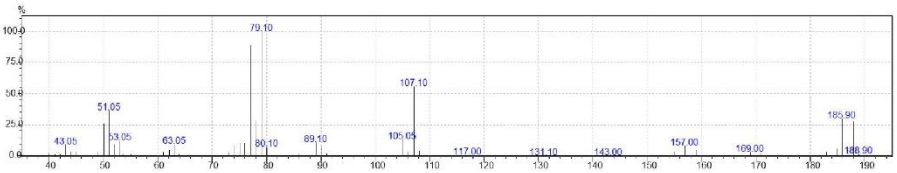

2-BrBA

22

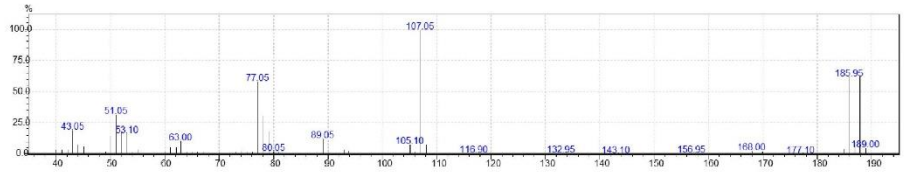

3-Br-2-MP

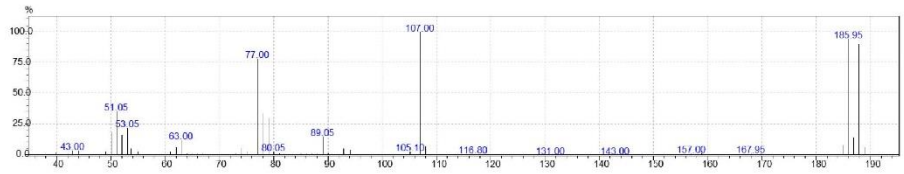

3-Br-4MP (and 4-Br-3MP)

23

2-methylanisole

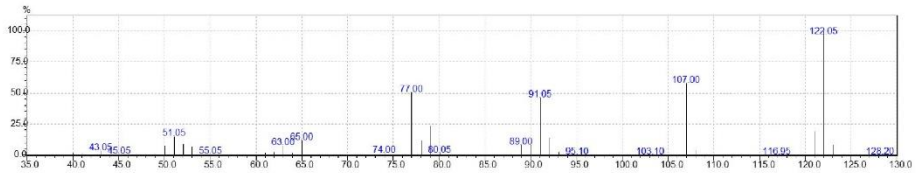

2-MeO

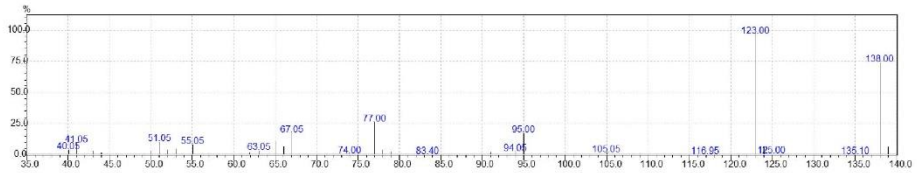

2-MeO-3-MP

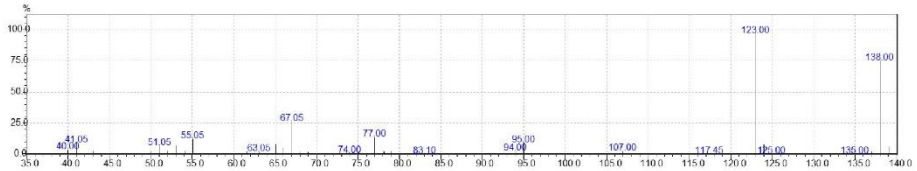

4-MeO-3-MP

2-ethyltoluene

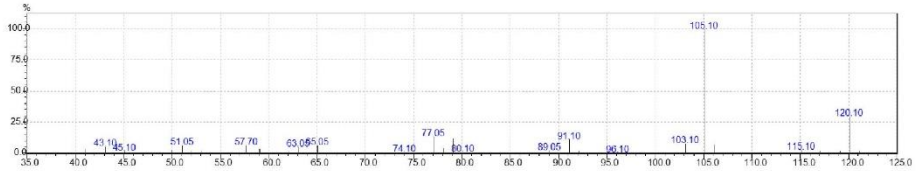

2-Et

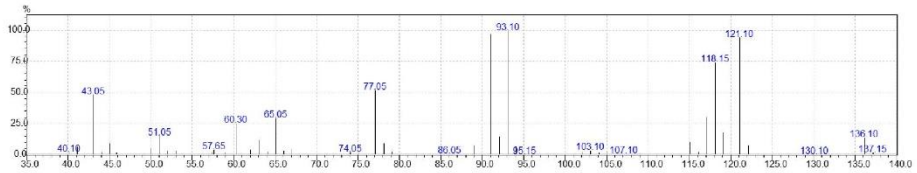

1-(2-MePh)EtOH (α-ethyl-OH)

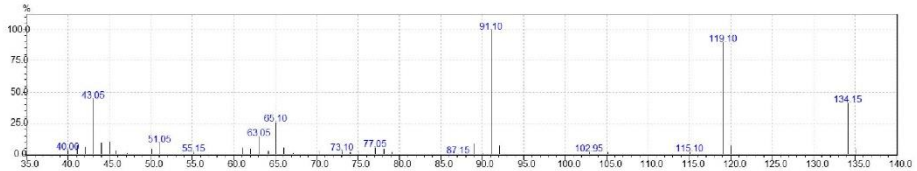

2-Meacetph (α-ethyl-ket)

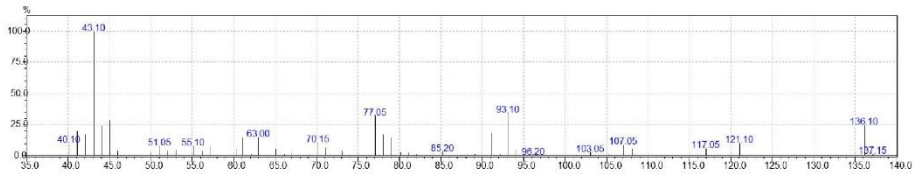

2-Et 7.0 min (6-E-6-MCHD)

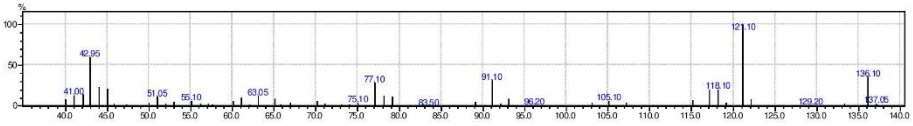

EMP_b 10.0 min

25

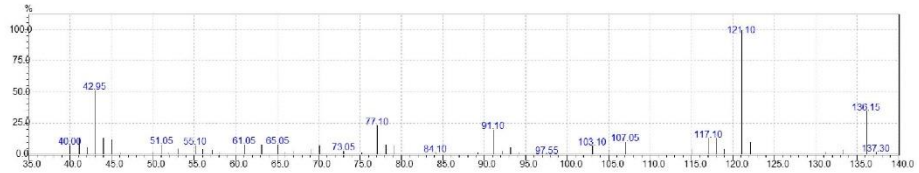

EMP_c 10.7 min

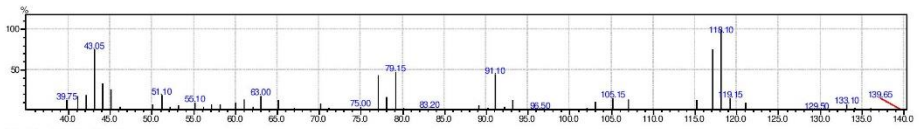

2-Et-BA 9.8 min

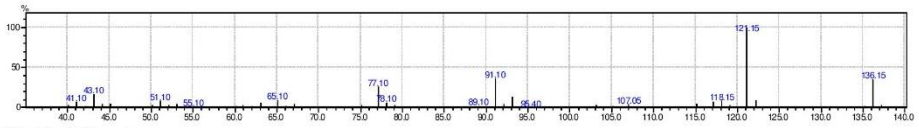

EMP_a 9.2 min

3-bromotoluene

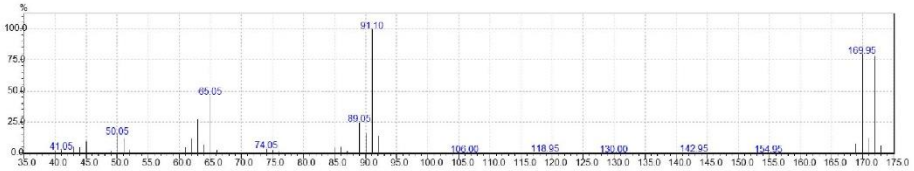

3-Br

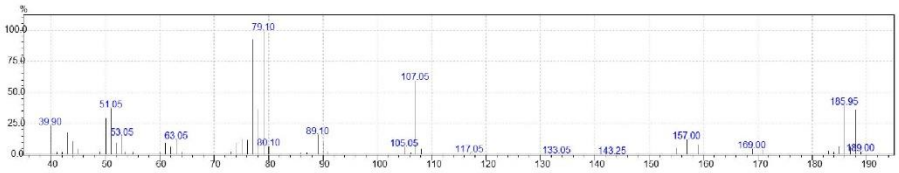

3-BrBA

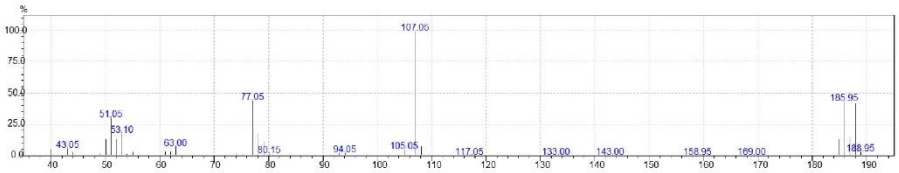

2-Br-4-MP

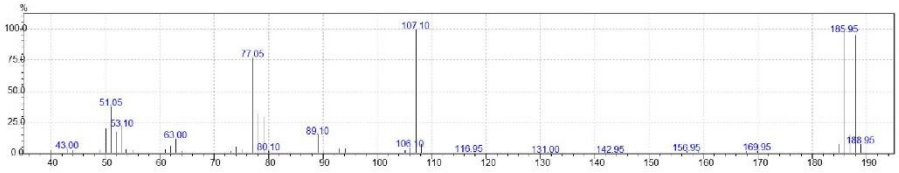

4-Br-2-MP

Note 2-Br-6-MP is also a product from 2-Br turnover.

27

3-methylanisole

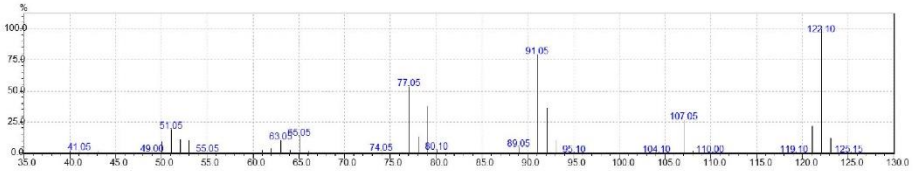

3-MeO

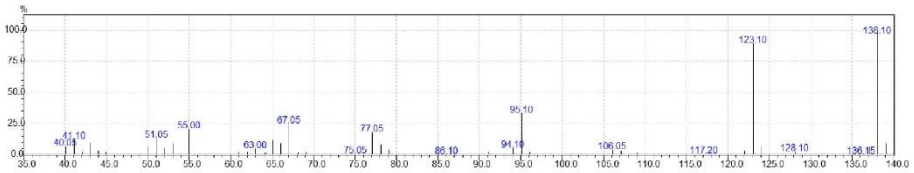

2-MeO-6-MP

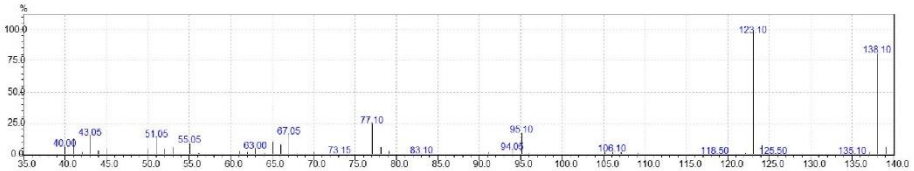

2-MeO-4-MP

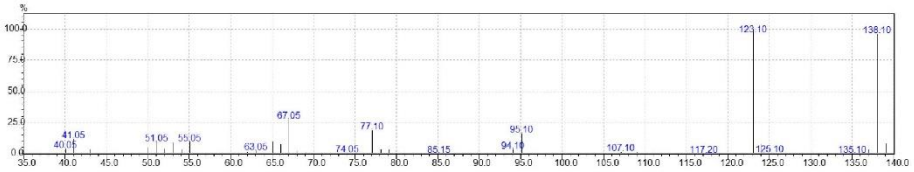

4-MeO-2-MP

28

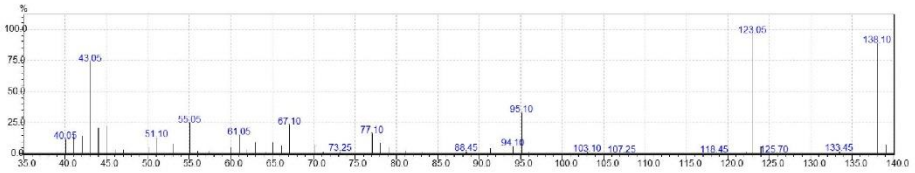

2-MeO-5-MP

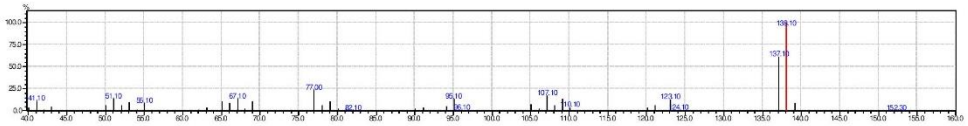

5-MeO-2-MP (5-methoxy 2-methylphenol standard – not observed as a product)

29

1-bromo-2-ethylbenzene

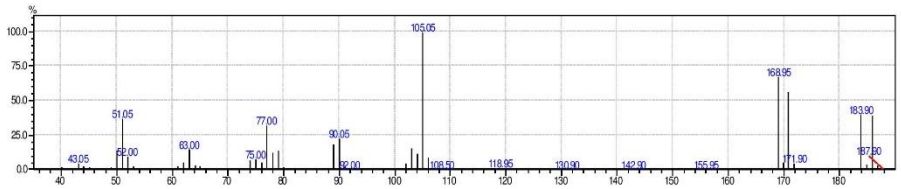

1-Br-2-Etbz sub: 7.86

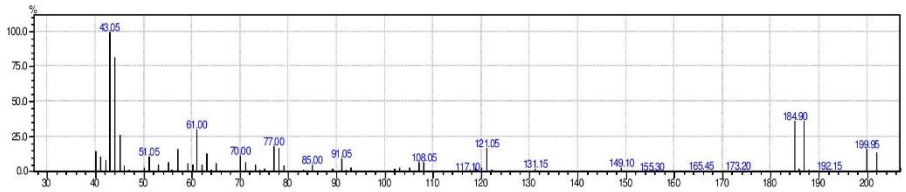

1-Br-2-Etbz RT: 10.0 phenol

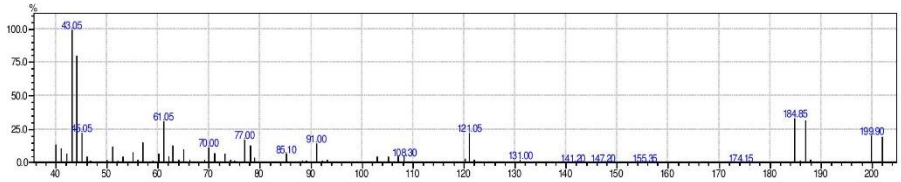

1-Br-2-Etbz RT: 10.35 phenol

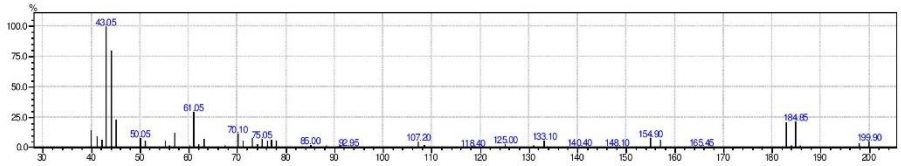

2-Br-acetph RT: 10.6

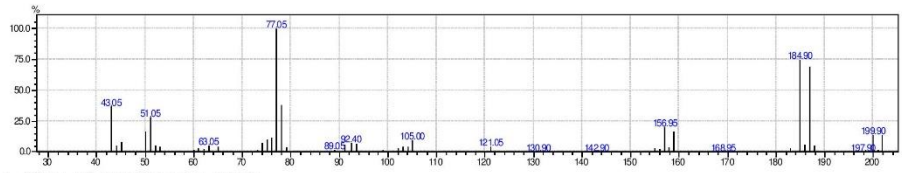

1-(2-BrPh)EtOH RT: 11.2

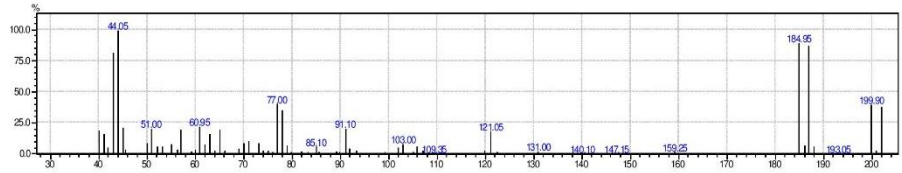

1-Br-2-Etbz RT: 12.2 phenol

31

3-ethyltoluene

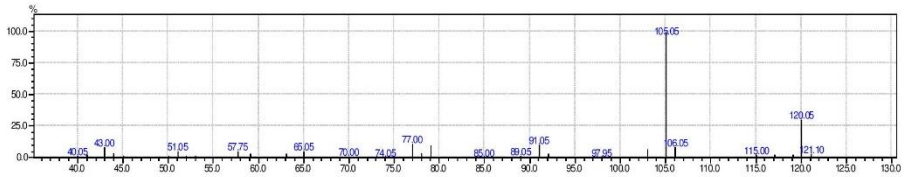

3Et 5.0

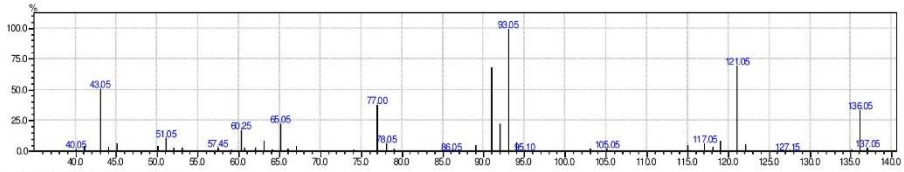

1-(3-MPh)EtOH RT: 8.6

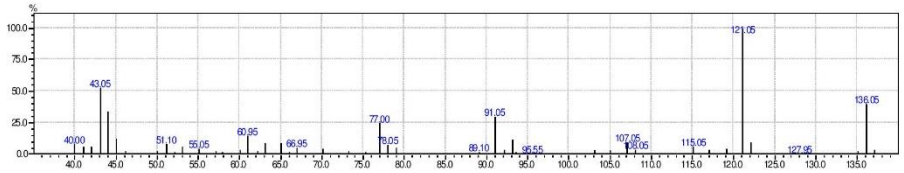

3Et RT: 9.05 phenol

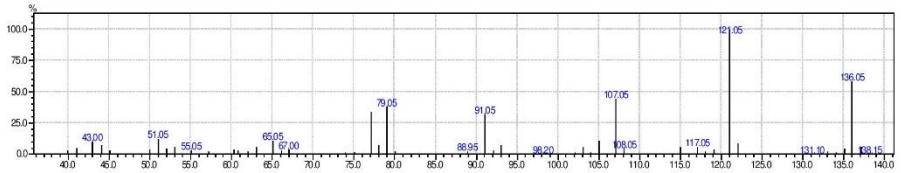

3Et RT: 9.7 3EtBz-OH

32

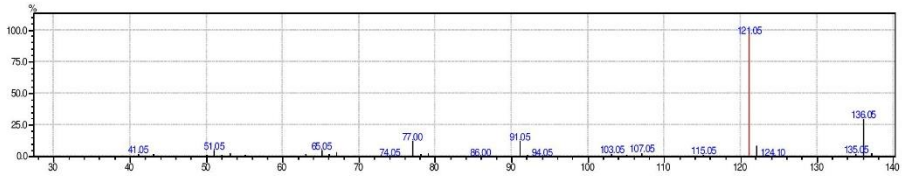

2-Et-4-MP RT: 9.88

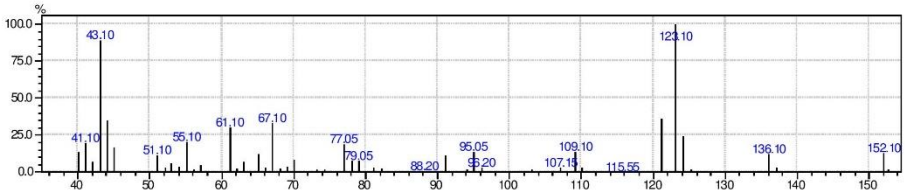

3Et RT: 10.25 – further oxidation product. Peak at 152 need to expand MS

33

2-methylstyrene

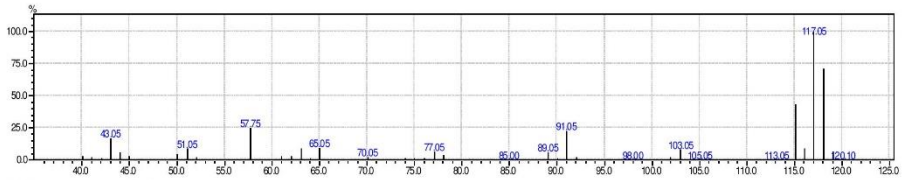

2Mestyrene-5.6

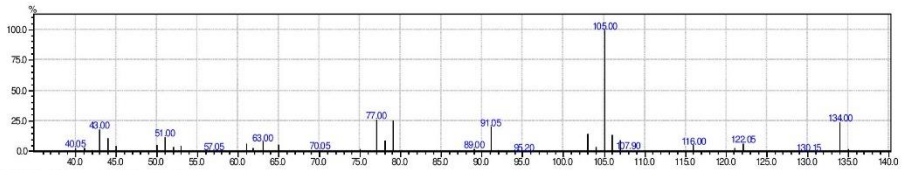

2-MePhac RT: 8.46

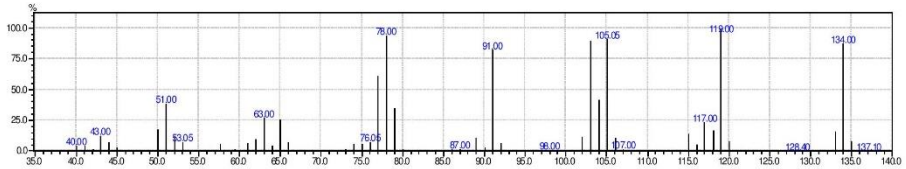

2-MS-epox RT: 8.73

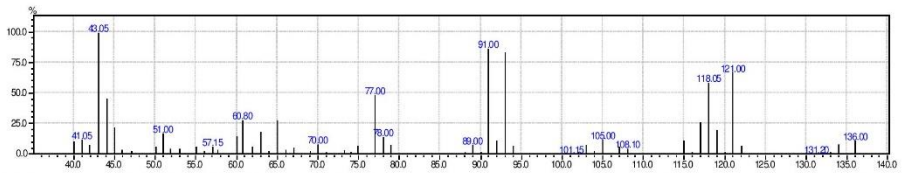

2Mestyrene RT: 8.9 This is α-ethyl-OH a minor product from 2-ethyltoluene impurity which was found in the sample.

34

NMR Data

1-(3-methylphenyl)ethanol

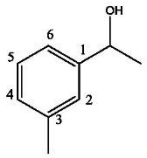

^{1}H NMR (500 MHz, $CDCl_3$): δ 7.23 (dd, *J* = 7.4 Hz and 7.5 Hz 1H), 7.20 (s, 1H), 7.16 (d, *J* = 7.5 Hz, 1H) 7.09 (d, *J* = 7.4 Hz, 1H), 4.86 (q, *J* = 6.5 Hz, 1H), 2.87 (s, 3H) 1.49 (d, *J* = 6.5 Hz, 3H)

^{13}C NMR (126 MHz, $CDCl_3$): δ 148.42, 140.82, 131.07, 130.88, 128.75, 125.07, 73.12, 27.7, 24.11

35

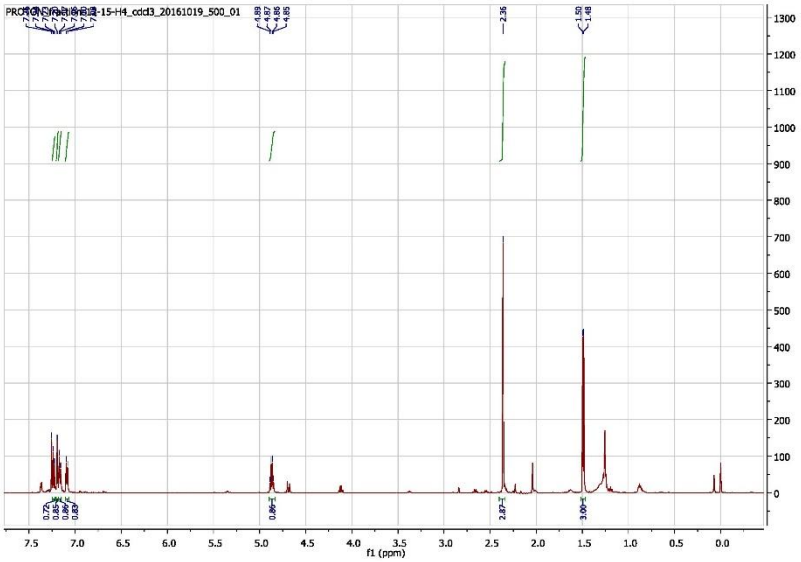

^{1}H NMR of 1-(3-methylphenyl)ethanol

36

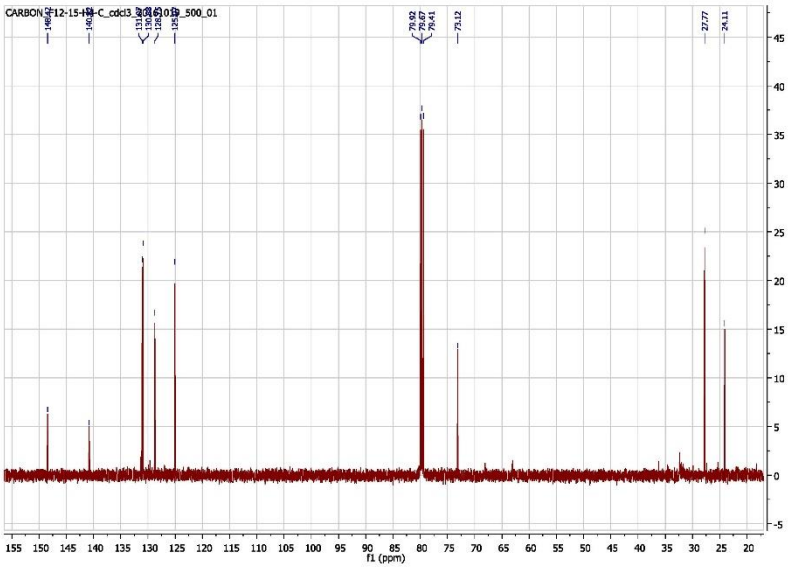

^{13}C NMR of 1-(3-methylphenyl)ethanol

37

4-methyl-2-ethylphenol

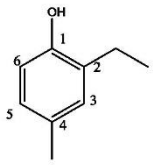

^{1}H NMR (500 MHz, $CDCl_3$): δ 6.96 (s, 1H), 6.90 (d, *J* = 8.1 Hz 1H), 6.69 (d, *J* = 8.1 Hz, 1H) 2.54 (q, 2H *J* = 7.6 Hz, 2H), 2.22 (s, 3H), 1.19 (t, *J* = 7.6 Hz, 3H).

38

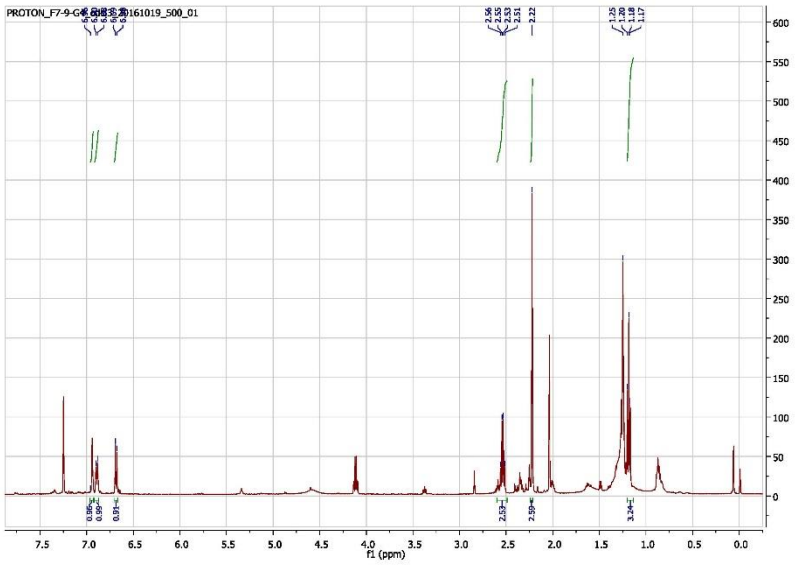

^{1}H NMR of 4-methyl-2-ethylphenol

39

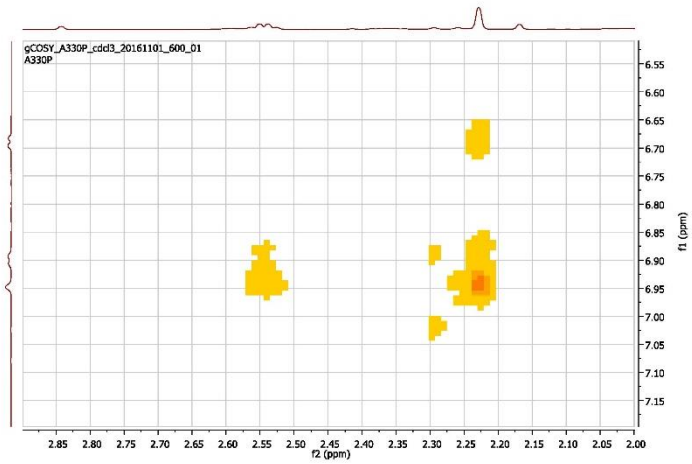

Part of the ^{1}H COSY NMR of 4-methyl-2-ethylphenol. The CH_3 and CH_2 from the Ethyl substituent both correlate with singlet aromatic proton but the Me correlates with a doublet and singlet aromatic peaks confirming the location of the phenol.

40

Chapter 5

Stereoselective hydroxylation of isophorone by variants of the cytochromes P450 CYP102A1 and CYP101A1

Citation:

Dezvarei, S.; Lee, J. H. Z.; Bell, S. G., Enzyme Microb Technol 2018, 111, 29-37.

Statement of Authorship

Title of Paper	Stereoselective hydroxylation of isophorone by variants of the cytochromes P450 CYP102A1 and CYP101A1
Publication Status	☑ Published ☐ Accepted for Publication ☐ Submitted for Publication ☐ Unpublished and Unsubmitted work written in manuscript style
Publication Details	Dezvarei, S.; Lee, J. H. Z.; Bell, S. G., Stereoselective hydroxylation of isophorone by variants of the cytochromes P450 CYP102A1 and CYP101A1. Enzyme Microb Technol 2018, 111, 29-37.

Principal Author

Name of Principal Author (Candidate)	Shaghayegh Dezvarei
Contribution to the Paper	Preparation of CYP102A1, whole cell and NADPH turnovers of isophorone by CYP102A1, synthesizing the products, products characterisation, analysis of substrates and products, manuscript preparation.
Overall percentage (%)	50
Certification:	This paper reports on original research I conducted during the period of my Higher Degree by Research candidature and is not subject to any obligations or contractual agreements with a third party that would constrain its inclusion in this thesis. I am the primary author of this paper.
Signature	Date 08/09/19

Co-Author Contributions

By signing the Statement of Authorship, each author certifies that:

i. the candidate's stated contribution to the publication is accurate (as detailed above);

ii. permission is granted for the candidate in include the publication in the thesis; and

iii. the sum of all co-author contributions is equal to 100% less the candidate's stated contribution.

Name of Co-Author	Joel Lee
Contribution to the Paper	Preparation of CYP101A1, whole cell and NADPH turnovers of isophorone by CYP101A1 , characterisation of the products, analysis of the products, manuscript preparation.
Signature	Date 4/4/2019

Name of Co-Author	Stephen G. Bell
Contribution to the Paper	Experimental design, supervision, manuscript preparation.
Signature	Date 8/4/2019

Please cut and paste additional co-author panels here as required.

Enzyme and Microbial Technology 111 (2018) 29–37

Contents lists available at ScienceDirect

Enzyme and Microbial Technology

journal homepage: www.elsevier.com/locate/enzmictec

Stereoselective hydroxylation of isophorone by variants of the cytochromes P450 CYP102A1 and CYP101A1

Shaghayegh Dezvarei[1], Joel H.Z. Lee[1], Stephen G. Bell*

Department of Chemistry, School of Physical Sciences, University of Adelaide, Adelaide, 5005, Australia

ARTICLE INFO

Keywords:
Cytochrome P450
Isophorone
Hydroxylation
Stereoselective
Regioselective

ABSTRACT

The stereoselective oxidation of hydrocarbons is an area of research where enzyme biocatalysis can make a substantial impact. The cyclic ketone isophorone was stereoselectively hydroxylated (≥95%) by wild-type CYP102A1 to form (*R*)-4-hydroxyisophorone, an important chiral synthon and flavour and fragrance compound. CYP102A1 variants were also selective for 4-hydroxyisophorone formation and the product formation rate increased over the wild-type enzyme by up to 285-fold, with the best mutants being R47L/Y51F/I401P and A74G/F87V/L188Q. The latter variant, which contained mutations in the distal substrate binding pocket, was marginally less selective. Combining perfluorodecanoic acid decoy molecules with the rate accelerating variant R47L/Y51F/I401P engendered further improvement with the purified enzymes. However when the decoy molecules were used with A74G/F87V/L188Q the amount of product generated by the enzyme was reduced. Addition of decoy molecules to whole-cell turnovers did not improve the productivity of these CYP102A1 systems. WT CYP101A1 formed significant levels of 7-hydroxyisophorone as a minor product alongside 4-hydroxyisophorone. However the F87W/Y96F/L244A/V247L CYP101A1 mutant was ≥98% selective for (*R*)-4-hydroxyisophorone. A comparison of the two enzyme systems using whole-cell oxidation reactions showed that the best CYP101A1 variant was able to generate more product. We also characterised that the further oxidation metabolite 4-ketoisophorone was produced and then subsequently reduced to levodione by an endogenous *Escherichia coli* ene reductase.

1. Introduction

Cytochromes P450 (P450s)[2] are a family of enzymes that carry out oxidative transformations including hydroxylations, epoxidations, heteroatom oxidations and dealkylations as well as other more complex reactions [1–3]. Most P450s catalyse the oxidation of their substrate via a high-valent iron-oxo radical cation intermediate which inserts an oxygen atom into unactivated carbon-hydrogen bonds using a radical rebound mechanism [4,5]. The key steps of the catalytic cycle are substrate binding, electron transfer and dioxygen binding followed by the activation of the oxygen by delivery of a second electron. These electrons are sourced from a nicotinamide cofactor (NADH or NADPH) and delivered via electron transfer partners as required [6–8]. These enzymes offer advantages over traditional methods of synthesis, in that the process of carbon-hydrogen bond hydroxylation occurs with high regio- and stereoselectivity in a single step under ambient conditions. The combination of all of these factors result in P450s being attractive enzymes for biocatalytic applications which could be used to complement traditional synthetic chemistry [9–11].

$P450_{cam}$ (CYP101A1) is a bacterial P450 that catalyses the stereospecific hydroxylation of (1*R*)-camphor to 5-exo-hydroxycamphor [9,12]. It uses a Class I electron transfer system, comprising of the FAD dependent, putidaredoxin reductase (PdR) and the [2Fe-2S] ferredoxin, putidaredoxin (Pdx) to obtain electrons from NADH [13,14]. The development of active site mutants which catalyse the oxidation of alternative substrates highlighted the biocatalytic potential of CYP101A1 and this family of enzymes in general [9,15–19]. For example, a number of active-site mutations introduced into CYP101A1 at phenylalanine 87, tyrosine 96, leucine 244 and valine 247, were found to improve its selectivity toward other monoterpenes, including *S*-limonene and (+)-α-pinene, enabling a route to the production of compounds for the flavour and fragrance industries [20,21]. The enzyme

* Corresponding author.
E-mail address: stephen.bell@adelaide.edu.au (S.G. Bell).
[1] These authors contributed equally to this work.
[2] *Abbreviations*: P450, cytochrome P450; P450cam, CYP101A1 from *Pseudomonas putida*; P450BM3, CYP102A1 from Bacillus megaterium; Pdx, [2Fe-2S] ferredoxin from *Pseudomonas putida*; PdR, flavin dependant ferredoxin reductase from *Pseudomonas putida*; EMM, E. coli minimal media; PFC, perfluorocarboxcylic acid, IPTG, Isopropyl β-D-1-thiogalactopyranoside; TLC, Thin layer chromatography, NADH, reduced nicotinamide adenine dinucleotide; NADPH, reduced nicotinamide adenine dinucleotide phosphate; DMSO, dimethyl sulfoxide.

https://doi.org/10.1016/j.enzmictec.2018.01.002
Received 28 May 2017; Received in revised form 2 January 2018; Accepted 4 January 2018
Available online 05 January 2018

has also been altered to oxidise substrates as varied as gaseous alkanes, such as ethane, and large polycyclic aromatic hydrocarbons, including pyrene [15,17,19,20,22–26].

The cytochrome P450 CYP102A1(P450Bm3) from *Bacillus megaterium* oxidises fatty acid substrates close to the omega terminus at high activities [27,28]. It and other members of the CYP102A subfamily are unusual in that the electron transfer partner domain is fused to the heme domain [29–32]. CYP102A1 is soluble, easy to produce and the self-sufficient nature and high activity overcome two of the major hurdles to the use of P450 enzymes in synthesis. CYP102A1 has a high specificity for NADPH over NADH as the electron source [33], and it has been used as a template for the design of selective oxidation biocatalysts through rational protein engineering and directed evolution [9,17,34–37]. For example, CYP102A1 isoforms have been created which enable the cyclopropanation, amination and aziridination of various substrates [38–42]. CYP102A1 variants, which enhance the oxidation activity for unnatural substrates but do not alter the product regioselectivity, have been identified [43–46]. These include the R47L/Y51F (RLYF) mutant of CYP102A1, where the two mutations are located at the entrance of the substrate access channel, which enhanced the oxidation of hydrophobic unnatural substrates such as polyaromatic hydrocarbons [47]. Studies of other generic accelerator mutants, such as I401P and KT2 (A191T/N239H/I259V/A276T/L353I), revealed that in the absence of substrate the rate of the first electron transfer step was comparable to that when a fatty acid is bound [44,46]. Structural analysis of these variants has been used to rationalise this behaviour with the mutants having conformations which more closely resemble the fatty acid bound form of the enzyme and have longer heme-iron axial water interactions [44,46]. These more catalytically ready conformations result in substrate binding-induced changes to the structure playing a less significant role in promoting the electron transfer steps. This accounted for their ability to oxidise non-natural substrates, including alkylbenzenes and alkanes, at elevated rates. The combination of the RLYF couple with rate accelerating CYP102A1 variants has also been found to further enhance their activity [46,48]. In addition CYP102A1 variants, in which phenylalanine 87 in the enzyme active site has been mutated, have been reported to modify the substrate binding profile and product selectivity of the enzyme [36,49–52]. The GVQ variant (A74G/F87V/L188Q) of CYP102A1 has been reported to be an effective biocatalyst for a range of organic molecules including aromatic hydrocarbons, alkanes and norisoprenoids [43,53].

Chemically inert perfluorocarboxylic acid (PFC) decoy molecules have also been used to improve the activity of CYP102A1 [54]. These greatly promote the oxidation of unnatural substrates such as benzenes, xylenes and short chain alkanes by the wild-type (WT) enzyme [54–57]. They work as the shorter fluorinated fatty acid decoy molecule is used to fill part of the enzyme's active site resulting in conformational changes in the enzyme. However there is enough space in the vicinity of the heme to allow a substrate to bind and the regioselectivity of oxidation is largely unaffected [56]. We have shown that it is possible to use decoy molecules, in conjugation with the rate accelerating mutants of CYP102A1 to substantially enhance the rates of product formation for cyclohexane and benzene-derived substrates and improve the productivity of regio- and stereo-selective biocatalytic reactions [48,57].

The selective oxidation of isophorone to 4-hydroxisophorone, which is an important flavour and fragrance compound as well as a synthetic intermediate for pigments and drug molecules, is a suitable target for biocatalytic oxidation [58–61]. Recently WT CYP102A1 was shown to be capable of generating 4-hydroxyisophorone on a kilogram scale [59]. During the preparation of this manuscript a report combining CYP101A1 variants with an alcohol dehydrogenase to generate 4-ketoisophorone was published [62]. Here we report the stereoselective oxidation of isophorone by mutant forms of CYP102A1 and CYP101A1. We show that the *in vitro* oxidation activity with the CYP102A1 variants was improved using these variants and decoy molecules. Whole-cell oxidation of isophorone was used to compare the activity of the class I CYP101A1 system with the self-sufficient CYP102A1 variants. Using these systems we were also able to identify the major and minor products arising from moonoxygenase activity and those from further processing by *Escherichia coli*.

2. Materials and methods

2.1. General

General reagents and isophorone were from Sigma-Aldrich, or VWR. Buffer components, NADPH, and isopropyl-β-D-thiogalactopyranoside (IPTG) were from Astral Scientific (Australia). Production and purification of full-length CYP102A1 variants for *in vitro* use was carried out as described previously [43,57]. UV/vis spectroscopy was performed on an Agilent Cary 60 spectrophotometer. Gas chromatography mass spectrometry (GC–MS) analyses were carried out on a Shimadzu GC-17A instrument coupled to a QP5050A MS detector using a DB-5 MS fused silica column (30 m × 0.25 mm, 0.25 μm) and helium as the carrier gas. Additional GC analysis and chiral chromatography were performed on a Shimadzu Tracera GC coupled to Barrier discharge Ionisation Detector (BID) detector using a Supelcowax column (30 m × 0.32 mm × 0.25 um) and a RT®-BDEXse chiral silica column (Restek; 30 m × 0.32 mm × 0.25 um), respectively. Helium was used as the carrier gas. The detailed GC methods used are given in the Supplementary Material.

2.2. Activity assays

CYP102A1 *in vitro* NADPH turnovers were run at 30 °C in 1200 μL of 50 mM Tris, pH 7.4 at 30 °C, containing 0.2 μM enzyme and 120 μg bovine liver catalase. The buffer was saturated with oxygen gas just before use and the assays were allowed to equilibrate for 1 min prior to the addition of the decoy molecule (100 μM) if present, and isophorone (1 mM substrate from a 100 mM stock in DMSO). Finally NADPH was added, from a 20 mg mL^{-1} stock, to a final concentration of ~320 μM (equivalent to 2 AU). A period of 10 s was allowed to elapse after NADPH addition before the rate of absorbance decay at 340 nm was measured. The reactions were allowed to run until all the NADPH was consumed. The NADPH turnover rate was derived using $\varepsilon_{340} = 6.22\ mM^{-1}\ cm^{-1}$. Similar experiments in which the concentration of the added isophorone was altered (0.1–2 mM) were performed to determine the catalytic activity of the enzyme.

2.3. In vivo metabolite generation and product identification

The CYP101A1 variants were screened using a plasmid system pCWSGB++ which contained the genes for PdR, Pdx and the relevant mutant (Table S1) [16,17,19,20,22,23]. The DNA was transformed into competent DH5α *Escherichia coli* (*E. coli*) cells and a single colony was grown in 2x LB media and protein produced as previously described [16]. The cell pellet was harvested by centrifugation and resuspended in *E. coli* minimal media (EMM; K_2HPO_4, 7 g, KH_2PO_4, 3 g, Na_3citrate, 0.5 g, $(NH_4)_2SO_4$, 1 g, $MgSO_4$, 0.1 g, 20% glucose, 20 mL and glycerol, 1% v/v per litre). Isophorone was added and the cells (30 mL in a 250 mL Erlenmeyer flask) were shaken at 200 rpm and 30 °C. Aliquots of the turnover (1 mL, supernatant and cells) were taken and extracted with ethyl acetate for analysis by GC–MS.

To isolate and identify the isophorone products, for which standards were not readily available, and to compare the CYP102A1 and CYP101A1 turnovers whole-cell oxidation systems utilising the plasmid pET28 containing the CYP102A1 gene of interest or the pCWSGB++ CYP101A1 system were used. The plasmids were transformed into competent BL21(DE3) cells and grown on LB plates containing 100 μg mL^{-1} ampicillin (pCW) or 30 μg mL^{-1} kanamycin (pET28). A single colony was inoculated into 500 mL 2 x LB broth in a 2 L flask and grown at 37 °C overnight or for smaller scale growths 50 mL in a 250 mL

flask). Protein expression was induced by the addition of 60 μM IPTG (from a 0.4 M stock in H_2O), and the temperature was reduced to 20 °C and the shaker speed to 110 rpm. The growths were allowed to continue for another 16 h before the culture was harvested by centrifugation and washed with EMM. The cell pellet was resuspended in the same volume of media (EMM) and split into flasks as required. Isophorone (2 mM from a 100 mM stock in ethanol) was added to the resuspended cells (50 mL in a 250 mL flask or 200 mL in a 2 L baffled flask for large scale growths) the reactions were shaken at 150 rpm and 30 °C. A second aliquot of isophorone was added to the small scale whole-cell turnovers after 6 h and the reactions were allowed to proceed for another 14 h. For large scale turnovers two further aliquots of substrate were added after 3 and 6 h. For both large and small scale reactions an aliquot of 20x phosphate buffer (pH 7.4, 1/40th of the total reaction volume) was added to the mixture to help maintain the pH. The large scale reactions were also allowed to proceed for 20 h.

For the comparison of the CYP101A1 and CYP102A1 variants, *in vivo*, the plasmid systems were transformed into the *E. coli* strain BL21(DE3) and grown in LB with the relevant antibiotics. The cells were harvested, resuspended in EMM and the biotransformations were performed in triplicate as described above (50 mL in 250 mL flask). The biomass yield was recorded as the cell wet weight and the concentration of P450 was determined by lysing the cells (via sonication) and recording the CO difference spectrum of the supernatant [63].

2.4. Product analysis

After the *in vitro* NADPH consumption assays were completed, 990 μL of the reaction mixture was mixed with 10 μL of an internal standard solution (*p*-cresol, 20 mM stock solution in DMSO). For whole-cell turnovers 990 μL aliquots of the turnover (including cells) were taken for analysis (after addition of the same internal standard). The mixture was extracted with 400 μL of ethyl acetate and the organic extracts were used directly for GC–MS or GC analysis. Products were initially identified by matching the GC–MS mass spectra to those expected for the metabolites (see Supplementary Material). The amount formed was determined by calibrating against isophorone and 4-ketoisophorone using the assumption that the hydroxyl isomeric products would give comparable responses *e.g.* 4-hydroxyisophorone and 7-hydroxyisophorone were presumed to give a similar detector response to isophorone.

To determine the identity of the unknown product observed in the GC–MS analysis of the GVQ CYP102A1 variant (which was expected to arise from non-P450 catalysed enzyme activity) a whole-cell turnover was performed with *E. coli* containing an empty pET vector. The cells were grown as above and a 2 mM aliquot of 4-ketoisophorone was added. After 20 h all the substrate had been converted to a single product which was isolated and analysed by MS and NMR (Supplementary Material).

Chiral normal phase HPLC analysis was carried out on a Shimadzu system equipped with a DGU-20A5R degasser, 2x LC-20AR pumps, SIL-20AC HT autosampler, SPD-M20A photodiode array detector and a CT0-20AC column oven. Separation of the chiral products was carried out using a CHIRALPAK® IG column (5 μm particle size, 4.6 mm diameter × 150 mm; Daicel Chemical Industries Ltd.) equipped with a Chiralpak® IG guard column (5 μm particle size, 4.0 mm diameter × 10 mm; Daicel Chemical Industries Ltd.) operating in isocratic mode with 95% hexane and 5% isopropanol at 0.5 mL min^{-1} for 38 min. The injection volume was 5 μL and the absorbance was monitored at 254 nm. Retention times were as follows: ketoisophorone, 14.8 min; (*R*)-4-hydroxyisophorone, 26.9 min, (*S*)-4-hydroxyisophorone 29.4 min.

2.5. Isolation of isophorone oxidation products

The supernatant (200 mL) from an *in vivo* turnover of isophorone was extracted in ethyl acetate (3 × 100 mL), washed with brine (100 mL) and dried with magnesium sulphate and the organic extracts were pooled and the solvent was removed by vacuum distillation and then under a stream of nitrogen. The products were purified by silica gel chromatography using a hexane/ethyl acetate stepwise gradient ranging from 80:20 to 50:50 hexane to ethyl acetate with 2.5% increases every 100 mL. The composition of the fractions was assessed by TLC and GC–MS and those containing single products (≥95%) were combined for characterisation. The solvent was removed under reduced pressure.

The purified product was dissolved in $CDCl_3$ and the organics characterised by NMR spectroscopy and GC–MS. NMR spectra were acquired on a Varian Unity-plus spectrometer operating at 500 MHz for ^1H and 126 MHz for ^{13}C. A combination of ^1H, ^{13}C, COSY, HSQC and HMBC experiments was used to determine the structures of the products. The specific rotation was determined using an Anton-Paar MCP 100 modular circular polarimeter.

The epoxidation of isophorone and 4-ketoisophorone was undertaken using the method of Fioroni and coworkers [64]. In summary, 250 μL of an aqueous solution of 2 M NaOH was added to 1.0 mmol of substrate. The mixture was dissolved in 1.62 mL of water at 0–2 °C with stirring. After 10 min 0.15 mL of 30 wt% aqueous hydrogen peroxide was added. The product was extracted after 6 h with ethyl acetate. Using this method approximately 30% of the isophorone was oxidised to isophorone oxide while the conversion for 4-ketoisophorone epoxidation was ≥ 99%.

The reduction of 4-ketoisophorone to generate a racemic mixture of 4-hydroxyisophorone was undertaken using the method of Ishihara [65]. 4-Ketoisophorone (0.4 mmol) was reduced with sodium borohydride (0.1 mmol) in methanol at −5 to 0 °C to afford the product which was confirmed by GC coelution and MS analysis with the sample isolated from the whole-cell oxidation system which had been characterised by NMR. This sample was used for chiral HPLC analysis.

2.6. NMR data

4-hydroxyisophorone: ^1H NMR (500 MHz, $CDCl_3$) δ 5.86 (s, 1H, H2), 4.03 (s, 1H, H4), 2.41 (d, J = 16.3 Hz, 1H, H6), 2.21 (d, J = 16.3 Hz, 1H, H6), 2.06 (s, 3H, H7), 1.07 (s, 3H, H8/H9), 1.02 (s, 3H, H8/H9); ^{13}C NMR (126 MHz, $CDCl_3$): δ 202.12 (C1), 164.61 (C3), 128.64 (C2), 79.28 (C4), 51.62 (C6), 41.17 (C5), 29.57 (C8/C9), 24.24 (C8/C9), 24.01 (C7).

7-hydroxyisophorone: ^1H NMR (500 MHz, $CDCl_3$) δ 6.15 (s, 1H, H2), 4.22 (s, 2H, H7), 2.27 (s, 3H, H6), 2.14 (s, 2H, H4), 1.05 (s, 6H, H8 & H9). ^{13}C NMR (126 MHz, $CDCl_3$) δ 200.09 (C1), 162.22 (C3), 122.11 (C2), 65.03 (C7), 51.56 (C6), 40.26 (C4), 33.66 (C5), 28.23 (C8 & C9).

levodione: ^1H NMR (500 MHz, $CDCl_3$) δ 3.03 (m, 1H, H6), 2.77 (d, 1H, H5), 2.74 (d, 1H, H3), 2.52 (d, 1H, H3), 2.35 (d, 1H, H5), 1.21 (s, 3H, CH_3), 1.15 (d, 3H, CH_3) 1.12 (s, 3H, CH_3). ^{13}C NMR (126 MHz, $CDCl_3$): δ 216.73 (C1), 210.60 (C4) 55.38 (C3), 47.51 (C5), 46.85 (C2), 42.47 (C6), 29.16 (C8), 28.21 (C9), 17.21 (C7).

2.7. Substrate binding assays

UV/Vis spectroscopy was performed on an Agilent Cary 60 spectrophotometer. For substrate binding the CYP102A1 enzymes were diluted to ~1 to 2 μM in 50 mM Tris, pH 7.4. After addition of the isophorone or the PFC10 decoy molecule (as 1 μL aliquots from a 100 mM stock in DMSO or ethanol) the spectra was recorded.

3. Results

3.1. CYP102A1 catalysed oxidation of isophorone

WT CYP102A1 has been shown to be capable of selective hydroxylation of isophorone but no enzymatic turnover data was reported

[59]. We have shown that certain generic accelerator variants of this enzyme, which combine mutations outside of the distal active site pocket with the R47L and Y51F mutants at the entrance to the substrate access channel, can facilitate the oxidation of non-physiological substrates while maintaining the selectivity. These include the R19 (R47L/Y51F/H171L/Q307H/N319Y) and RP (R47L/Y51F/I401P) variants which have been shown to be effective at oxidising hydrophobic molecules such as alkylbenzenes. Decoy molecules, such as the perfluorocarboxylic (PFC) acids, perfluorononanoic acid (PFC9) and perfluorodecanoic acid (PFC10), can also be combined with CYP102A1 variants to enhance the rate of oxidation of similarly sized substrates to isophorone [48,55]. In these previous studies PFC10 resulted in the highest product formation rates due to a large increase in the turnover of the catalytic cycle whereas PFC9 generally resulted in a higher coupling efficiency of the reducing equivalents to product formation. Therefore both PFC9 and PFC10 were tested with the CYP102A1 variants to see if isophorone oxidation could be improved.

We determined the rates of NADPH oxidation and product formation and the coupling efficiency for isophorone oxidation with the purified CYP102A1 variants, in the presence and absence of the polyfluorinated carboxylic acids (Table 1). All the variants tested gave rise to a single major oxidation product using GC–MS analysis. In each turnover there were additional minor products, which from coelution experiments and analysis of the MS spectra were consistent with the further oxidation product 4-ketoisophorone and the epoxidation metabolite, isophorone oxide (Fig. 1). The oxidation of isophorone by WT CYP102A1 was slow (PFR; 0.2 nmol(nmol-CYP)$^{-1}$min^{-1}; henceforth abbreviated to min^{-1}) and generated low levels of the hydroxylated metabolite. Addition of both PFC9 and PFC10 improved the overall product yield. PFC10 increased the rate of production formation 29-fold as a result of boosting the NADPH oxidation rate and the coupling efficiency. The rate accelerating variants all increased the amount of product formation arising from isophorone oxidation. The product formation decreased in the order RLYFIP > R19 > KT2 > WT with the highest PFR being 45 min^{-1} (Table 1).

The oxidation of isophorone by all of these variants was also enhanced by adding the PFC9 and PFC10 decoy molecules. This arose due to an increase in both the NADPH oxidation activity and coupling efficiency resulting in more oxidation metabolites being formed in a shorter amount of time (Fig. 1, Table 1, Fig. S1). The product formation rate was always greater with PFC10 (Table 1). In line with previous studies the overall enhancement induced by the decoy molecules in rate accelerating variants was lower than that observed with the WT enzyme ranging from 30-fold for KT2 and 4-fold for RLYFIP. However the combined effect of the rate accelerating variants and decoy molecules produced the highest levels of isophorone oxidation. The RLYFIP variant was better than R19, both in the absence and presence of the decoy molecules (Table 1). The RLYFIP variant, which contain the RLYF couple at the entrance of the substrate access channel, was better than KT2 predominantly due to improved coupling efficiencies (Table 1). The RLYFIP and PFC10 combination resulted in the highest product formation rate for isophorone, 180 min^{-1} (Table 1).

In order to compare the effect of the decoy molecule on the kinetic parameters we determined the k_{cat} and K_m for the CYP102A1 enzyme variant in the presence and absence of PFC10. It was not possible to determine these values accurately for the WT enzyme but for each variant the addition of the decoy molecule resulted in an increase in k_{cat}

Table 1
NADPH oxidation rate (N), product formation rate (PFR) and coupling efficiency (C) for purified CYP102A1 variants with isophorone. The assays were conducted using 1 mM substrate, ~320 μM NADPH and 0.2 μM CYP enzyme in 50 mM Tris, pH 7.4. Coupling efficiency is the percentage of NADPH utilised for the formation of isophorone products. N and PFR are reported as mean ± S.D. ($n \geq 3$) and given in nmol(nmol-CYP)$^{-1}$min^{-1}. Examples of the NADH oxidation assays and the GC chromatogram of the product areas are provided in Fig. S2).

	isophorone		
	N	C	PFR
WT	57 ± 2	0.3 ± 0.1	0.2 ± 0.1
WT/PFC9	98 ± 3	3.4 ± 0.3	3.3 ± 0.2
WT/PFC10	318 ± 2	1.8 ± 0.1	5.8 ± 0.2
KT2	65 ± 1	4.4 ± 1	2.8 ± 0.7
KT2/PFC9	384 ± 2	6.0 ± 0.3	23 ± 1
KT2/PFC10	1260 ± 10	12 ± 1	150 ± 5
R19	148 ± 38	8.8 ± 0.5	13 ± 4
R19/PFC9	346 ± 8	14 ± 1	49 ± 2
R19/PFC10	497 ± 34	16 ± 1	83 ± 6
RLYFIP	425 ± 28	11 ± 1	45 ± 2
RLYFIP/PFC9	894 ± 6	16 ± 1	142 ± 4
RLYFIP/PFC10	1090 ± 30	16 ± 1	180 ± 8
GVQ	365 ± 3	16 ± 2	57 ± 5
GVQ/PFC9	1530 ± 20	2.5 ± 0.2	38 ± 3
GVQ/PFC10	1880 ± 30	1.0 ± 0.1	18 ± 1

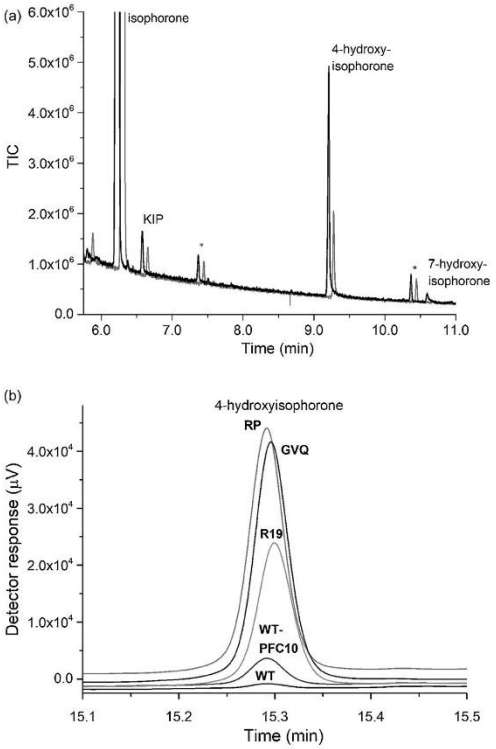

Fig. 1. (a) GC–MS analysis of the *in vitro* turnover of isophorone by the CYP102A1 variants R19 (grey) and GVQ (black). Note the chromatograms have been offset along the x-axis for clarity. Impurities are labelled (*), as are isophorone (RT 6.2 min), 4-hydroxyisophorone (RT 9.15 min) and 7-hydroxyisophorone (KIP; RT 10.6 min). A small amount of the further oxidation product 4-ketoisophorone (RT 6.6 min) was identified in both reactions. 7-Hydroxyisophorone was only observed in the GVQ turnover. (b) GC analysis (wax column) in the region of the 4-hydroxyisophorone product (RT 15.3 min) for different *in vitro* CYP102A1 turnovers. The chromatograms are labelled from those which generate the lowest amount of this product to the highest; WT, WT + PFC10, R19, GVQ and RLYFIP (RP). See Table 1 for turnover parameters.

and a decrease in K_m (KT2; k_{cat} ~20 min^{-1}; K_m > 2 mM: KT2/PFC10; k_{cat} 202 ± 6 min^{-1}, K_m 380 ± 10 μM: R19; k_{cat} 22 ± 1 min^{-1}, K_m 650 ± 40 μM: R19/PFC10; k_{cat}150 ± 30 min^{-1}, K_m 440 ± 110 μM: RLYFIP; k_{cat} 155 ± 6 min^{-1}, K_m 750 ± 30 μM and RLYFIP/PFC10; k_{cat} 330 ± 60 min^{-1}, K_m 440 ± 150 μM). The kinetic parameters were also in accord with lower improvements the decoy molecule induced with the R19 and RLYFIP variants compared to the enhancement for KT2 (Table 1, Fig. S1).

We also tested the A74G/F87 V/L188Q (GVQ) mutant with isophorone. This variant contains three mutations in the substrate access channel and active site of the enzyme. As such it alters the enzyme activity for more hydrophobic substrates and changes the selectivity of the enzyme. The oxidation of isophorone by this variant gave rise to the same major and minor products as the WT enzyme alongside an additional minor product at a later retention time (Fig. 1). The oxidation with the GVQ variant was more efficient, 57 min^{-1}, than RLYFIP and the other variants. This was predominantly due to a higher coupling efficiency (Table 1). However while the addition of the decoy molecules enhanced the NADPH oxidation rate with the GVQ mutant there was a significant reduction in the coupling efficiency and as a consequence lower levels of product formation with isophorone and this variant (Table 1).

To explore the different behaviour of the GVQ variant with the decoy molecules we determined the spin state shift of the ferric heme after addition of PFC10 to the different CYP102A1 mutants. With the WT and rate accelerating variants minimal alteration in the spin state from the low-spin to the high-spin (HS) form, as measured by UV–vis, was observed (≤15% HS). A small shift was seen with the rate accelerating variants following addition of isophorone after PFC10 (Fig. S2, 40% HS). PFC10 did induce a shift with GVQ (55% HS) indicating perturbation of the water bound to the heme-iron. Isophorone addition to GVQ resulted in a small shift (≤20% HS). This increased to 50% HS when PFC10 and isophorone were added. Overall the data shows that the fatty acid based decoy molecule is bound closer to the heme in the GVQ variant as it can displace the heme iron-bound water molecule.

3.2. Identification of the products arising from CYP102A1 oxidation of isophorone

A single major product (> 90%) was detected by GC–MS in the *in vitro* oxidation of isophorone by all CYP102A1 variants. The catalytic oxidation of isophorone by the CYP102A1 variants was performed, in the presence and the absence of decoy molecules, using a whole-cell system to generate greater quantities of this product for characterisation (Fig. S3). No material change in the levels of product formation was observed *in vivo* for either variant when decoy molecules were added. Significantly more product was generated in turnovers using the variants when compared to the WT CYP102A1 enzyme (Fig. S4). The whole-cell turnovers with the R19 and RLYFIP variants were the most selective and the overall conversion of the isophorone into product was approximately 30% after 20 h resulting in approximately 1-1.2 mM product (as determined by the amount of product formed). The turnovers were combined extracted and the product was isolated, purified (~6 mg after purification) and identified as 4-hydroxyisophorone (4-hydroxy-3,5,5-trimethyl-2-cyclohexen-1-one), by NMR and the MS fragmentation pattern (Fig. S3 and Supplementary Material). The GVQ variant was less selective generating the minor metabolites observed in the *in vitro* turnovers in greater quantities (Fig. S4). The minor products were not isolated in sufficient yield or purity, from any of the variants, for NMR characterisation. Analysis of the MS fragmentation pattern suggested that the as yet unidentified later eluting product was 7-hydroxyisophorone (see Supplementary Material). Further oxidation to 4-ketoisophorone was also observed in the GVQ turnovers as was the formation of another as yet unidentified metabolite (*vide infra*).

3.3. CYP101A1 catalysed oxidation of isophorone

While there were significant improvements in the product formation of 4-hydroxyisophorone using the CYP102A1 variants, without and when combined with the decoy molecules, the coupling efficiency was moderate (Table 1). We therefore wanted to assess if other P450 enzymes could selectively oxidise this substrate. Previously we have shown that CYP101B1 from *Novosphingobium aromaticivorans* was able to generate three products, including 4-hydroxyisophorone, but in low yield [66]. As isophorone is similar in chemical composition and size to camphor we decided to screen its oxidation with WT CYP101A1 and a selection of mutant forms (Table S1). We used a small library of CYP101A1 mutant enzyme encoding genes (fourteen including the WT enzyme), which had previously been generated and cloned into a whole-cell oxidation system with the physiological electron transfer partners, putidaredoxin (Pdx) and putidaredoxin reductase (PdR) [16]. These mutants were chosen as they previously had shown good activity and selectivity with hydrocarbon and terpenoid based substrates such as isomers of limonene and pinene, which are of a similar size to isophorone [15,19,20,67,68].

The screen was performed using the available whole-cell system to determine which variants would hydroxylate isophorone in a selective manner. WT CYP101A1 catalysed oxidation of isophorone generated two detectable products by GC–MS. The major product (89%) co-eluted with 4-hydroxyisophorone with the second having a later elution time, which was the same as that of the minor metabolite observed in the oxidation of isophorone by the CYP102A1 GVQ variant. Of the CYP101A1 mutants screened with isophorone two variants were promising in that they generated more product and were more selective for 4-hydroxyisophorone than the WT enzyme. These were F87W/Y96F/V247L and F87W/Y96F/L244A/V247L which produced 4-hydroxyisophorone at 93% and 98%, respectively (Fig. 2a). The remaining mutants tested generated lower levels of product and were in general less selective, though 4-hydroxyisophorone was the major product in all cases (Fig. 2b).

Both products were extracted from a larger scale whole-cell oxidation turnover using the F87W/Y96F/V247L mutant (Fig. S5). They were purified and isolated by silica chromatography and the major product from both enzyme turnovers was confirmed as 4-hydroxyisophorone (35 mg; Fig. S3). The second less abundant product was characterised as 7-hydroxyisophorone (12 mg; 3-hydroxymethyl-5,5-dimethyl-2-cyclohexen-1-one, Fig. S3).

3.4. Enantioselectivity of 4-hydoxyisophorone formation with CYP102A1 and CYP101A1

4-Hydroxyisophorone can be generated as two enantiomers. To analyse the enantioselectivity of the biocatalytic hydroxylations the turnovers were analysed by chiral chromatography. In all cases a single peak was observed by GC (Fig. 2b). Analysis by chiral HPLC also resulted in the observation of a single major peak from the enzyme catalysed reactions. The reduction of 4-ketoisophorone by sodium borohydride generates a racemic mixture of 4-hydroxyisophorone and this mixture was separated into two peaks by chiral HPLC but not GC (Fig. S6). The optical rotation of the purified 4-hydroxyisophorone from the whole-cell turnovers of the CYP101A1 and CYP102A1 variants was measured in methanol. The specific rotation $[\alpha]_D$ 20 = +113.2 (c = 1.00, methanol) − was found to be in agreement with that reported in the literature for the pure (*R*)-enantiomer [58,59], which is also in agreement with the results reported by Turner and coworkers [62].

3.5. Comparison of CYP102A1 and CYP101A1 systems

CYP102A1 and it variants are often the P450 of choice for biocatalytic reactions due to their self-sufficient nature, level and ease of

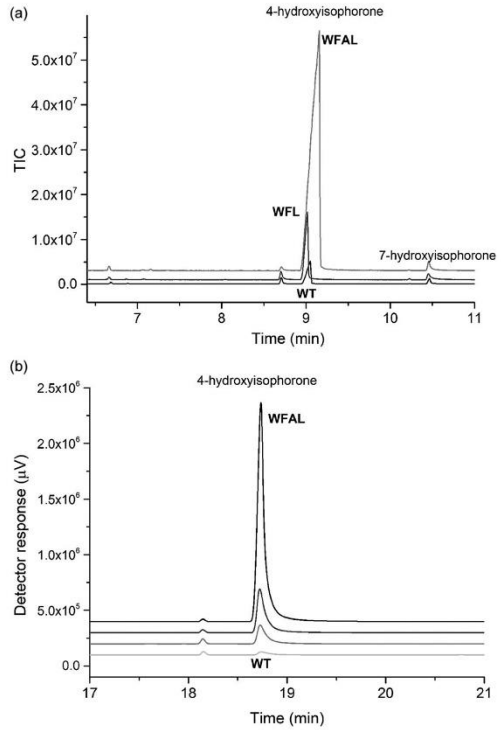

Fig. 2. (a) GC–MS analysis of the whole-cell turnovers of isophorone by WT CYP101A1 (black) and the variants WFAL (light grey) and WFL (grey). 4-Hydroxyisophorone (RT 9.0 min) and the minor product (7-hydroxyisophorone at RT 10.45 min) are labelled. Note the chromatograms have been offset along the y-axis for clarity. (b) The GC (chiral) chromatogram in the region of the 4-hydroxyisophorone product (RT 18.7 min). The amount of product generated by the different whole-cell CYP101A1 turnovers, from lowest to highest, was WT, F87W/Y96F/L244A, WFL and WFAL. Note the enantiomers of 4-hydroxyisophorone are not separated using this method.

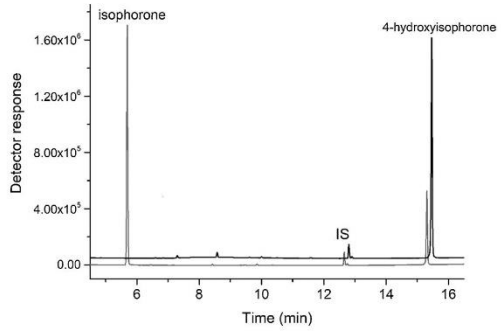

Fig. 3. GC chromatograms (wax column) of the whole-cell turnover of the CYP101A1 variant WFAL after 7 (grey) and 20 h (black). Shown are the isophorone substrate (5.8 min), internal standard (IS; 12.8 min) and 4-hydroxyisophorone product (15.3 min). The chromatograms have been slightly offset along the x- and y-axes for clarity. There was an increase in the amount of product (935 ± 10 μM to ~2.5 mM) from 7 to 20 h samples and the majority of the added substrate (4 mM) was consumed at the end of the turnover.

production and high levels of activity. The CYP101A1 system requires additional electron transfer proteins but whole-cell oxidation systems of this and other class I systems have been generated. These also have high oxidation activity [16,69,70]. The CYP101A1 variants tested here generated more product for characterisation than the CYP102A1 systems using the whole-cell oxidation system. A direct comparison between the two systems is not trivial due the disparate electron transfer systems (FMN versus iron sulfur ferredoxins, Class I versus Class III fused system), cofactor utilisation (NADH versus NADPH) and the different requirements of the plasmid systems used (pET28 versus pCWori). However we assessed if the CYP101A1 system would still give rise to increased levels of product when both systems were grown under similar conditions. The F87W/Y96F/V247L/L244A CYP101A1 system was first compared in DH5α and BL21(DE3) cells to see if this made a difference to the overall levels of product formation. In both types of cells almost all of the added substrate (4 mM) was consumed and similar levels of product (≥ 2.5 mM) were generated after a 20 h reaction suggesting the cell type is not of major significance when comparing the two systems (Fig. 3).

Next the WFAL CYP101A1 variant was compared with the RLYFIP and R19 variants of CYP102A1. The whole-cell oxidations were carried out in BL21(DE3) cells. Both systems generated similar levels of cell biomass (8–10 grammes of cell wet weight per litre of culture, Table S2). The amount of P450 detected in the CYP102A1 variants was lower than for the WT CYP102A1 system (88–183 nM) but was substantially higher than those of the CYP101A1 system (25–54 nM, Table S2). After seven hours the level of product formed with the R19 (~570 ± 100 μM) was lower than that with RLYFIP (~650 ± 100 μM) which was lower again than that of the CYP101A1 system (~935 ± 10 μM, Fig. 4a). After leaving the samples for a further 13 h the CYP101A1 system was able to convert almost all of the substrate (4 mM) to product; 2.8–4 mM of the major metabolite could be detected at the end of the reactions (Fig. 3). Despite the higher P450 expression levels the conversion in the CYP102A1 turnovers were lower and the amount of product detected was ~1200 ± 50 μM and 1200 ± 100 μM for the RLYFIP and R19 variants, respectively (Fig. 4a). Overall the whole-cell turnover of isophorone with the CYP101A1 variants seems to be better than with CYP102A1 (> 50000 total turnovers versus 11000 for the CYP102A1 variants). The GVQ CYP102A1 variant was also tested and the maximum levels of product formation were similar to those observed with the RLYFIP variant (Fig. 4b and Fig. S6). Additional oxidation products were detected during the whole-cell oxidations with CYP102A1 variants (Fig. S4 and Fig. S7). Two of these were assigned from the MS fragmentation patterns as the epoxides of isophorone and 4-ketoisophorone (Fig. 5). This was confirmed by coelution experiments with the products from the reactions of isophorone and 4-ketoisophorone with hydrogen peroxide in an alkaline solution, which generates the epoxides (Materials and Methods). The other metabolite, which was detected during the CYP102A1 turnovers, had an MS fragmentation pattern consistent with that of levodione. This is formed by reduction of the alkene double bond of 4-ketoisophorone (Fig. 5) [62]. To verify the identity of this product we ran a control reaction with 4-ketoisphorone in *E. coli* containing an empty pET vector. The 4-ketoisophorone (2 mM) was completely converted in less than 20 h into the same metabolite observed in the enzyme turnovers. This was extracted, isolated and identified by NMR as levodione (Fig. S3, Supplementary Material).

4. Discussion

Overall the formation of 4-hydroxyisophorone by CYP102A1 was significantly increased using generic rate accelerator variants and the GVQ mutant. The regio- and stereoselectivity of the hydroxylation was largely unaffected with all reactions giving rise to the (*R*)-enantiomer of 4-hydroxyisophorone as the major product. The most efficient *in vitro* turnovers contained the decoy molecule PFC10 and variants with the

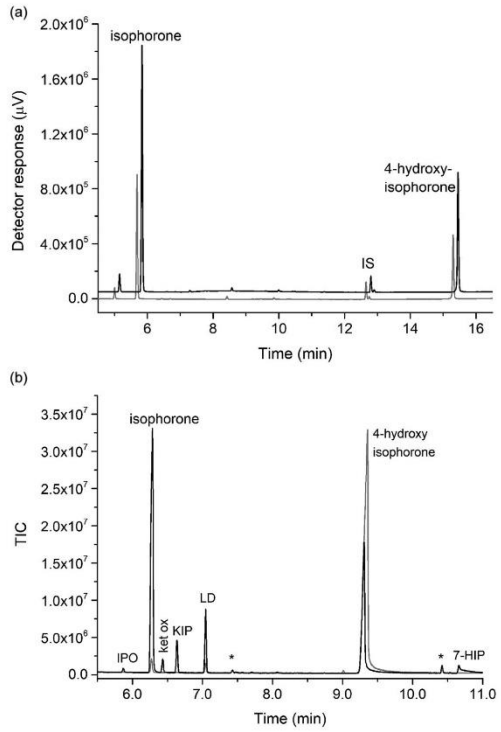

Fig. 4. (a) GC chromatograms (wax column) of the whole-cell turnover of the CYP102A1 variant RLYFIP after 7 (grey) and 20 h (black). Shown are the isophorone substrate (5.8 min), internal standard (IS; 12.8 min) and 4-hydroxyisophorone product (15.3 min). The chromatograms have been slightly offset along the x- and y-axes for clarity. Compared to the CYP101A1 WFAL whole-cell turnovers there were lower levels of product at both 7 (650 ± 100 μM) and 20 h (1100 ± 100 μM, see Fig. 3). Note that there is a significant amount of unconverted substrate after 20 h (~1.5 mM) (b) GC–MS chromatograms of the turnover of isophorone with the CYP101A1 variant WFAL (grey) and the CYP102A1 variant GVQ (black). The retention times are the same as those in Fig. 1. Additional metabolites can be seen in the GVQ turnover and include isophorone oxide (IPO; RT 5.9 min), 4-ketoisophorone epoxide (ket ox, RT 6.9 min), 4-ketoisophorone (KIP, RP 6.2 min) and levodione (LD 7.1 min). See the Supplementary Material for MS analysis of the metabolites.

R47L/Y51F couple. However compared to smaller substrates such as cyclohexane and ethylbenzene the coupling efficiency of the optimal systems was moderate. The selective nature of the turnover suggests that the substrate is held in enzyme active site with only one C − H bond close to the reactive iron-oxo cation radical intermediate but it must be far enough away to make the oxidation relatively inefficient. The larger size of isophorone may be one reason for the less efficient oxidation but smaller decoy molecules did not improve the levels of product formation and mutagenesis around the CYP102A1 active site may be required to optimise the hydroxylation further.

One important observation from this work is that the decoy molecules did not improve isophorone oxidation with the A74G/F87V/L188Q CYP102A1 variant. This may arise as mutations at these positions in the active site and access channel of the enzyme may alter the position of fatty acid binding, as evidenced by the different behaviour of the spin state of this variant upon addition of PFC10. This would result in the decoy molecules binding closer to the heme and interfering with rather than enhancing the oxidation of non-natural substrates. As such the perfluorinated decoy molecule could now be positioned between the isophorone and the heme, displacing the iron-bound water and increasing the NADPH oxidation rate but resulting in a reduced C—H bond abstraction and coupling efficiency. The addition of the decoy molecules did not improve the whole-cell oxidation activity. This may be due to reduced uptake of the perfluorinated fatty acids by the cells, though further optimisation of the relative amounts of decoy molecule and substrate in whole-cell reactions may improve this [71,72].

Isophorone is of a similar size to camphor and the WT CYP101A1 enzyme was able to oxidise isophorone but this reaction was not as selective as WT CYP102A1. The oxidation of isophorone using a library of CYP101A1 mutants, derived from previous rational protein engineering studies (Supplementary Material), revealed that certain variants catalysed the selective formation of (*R*)-hydroxyisophorone. All of these variants modified the tyrosine 96 residue which interacts with the camphor carbonyl group. The more hydrophobic active site of the F87W/Y96F/V247L and F87W/Y96F/L244A/V247L (WFAL) mutants must be able to bind isophorone to enable more efficient and selective hydroxylation. The WFAL mutant; designed by rational mutagenesis for pinene and chlorinated benzene hydroxylation, was found to be the best CYP101A1 variant for isophorone oxidation obtained by us and also by Turner and coworkers who used a library constructed using saturation mutagenesis at fourteen residues in the enzyme active site [19,20,62].

A comparison between the whole-cell oxidation activities of the best CYP101A1 and CYP102A1 variants showed that, despite lower levels of P450 production, the class I CYP101A1 system was superior over a longer period of time in shake flask conversions (385 mg L^{-1}). A direct comparison of the three component class I system versus the single component self-sufficient CYP102A1 system is difficult. The coupling efficiency and oxidation rates of the CYP102A1 system may be lower than that of the CYP101A1 variants [73]. Alternatively the concentration and rate of regeneration of cellular NADPH required by CYP102A1 may be different to that of NADH utilised by the CYP101A1 system [74–77]. The level of P450 holoprotein production of both systems in *E. coli* is known to be high but perhaps the fused CYP102A1 system is less stable under the turnover conditions used. The improvement in the CYP102A1 variants over the WT enzyme and the better whole-cell oxidation of isophorone by the CYP101A1 system should lead to refinements in the up sizing of this reaction. Recently researchers at DSM have scaled up the activity of WT CYP102A1 in a fermentor system. Using high cell densities, thirty times the amount used in our experiments, and the addition of additional NADPH enabled 4-hydroxyisophorone to be produced at 10 g L^{-1} and at space-time yields of 1.5 g L^{-1} h^{-1} [59]. Given the low activity of the WT enzyme for this reaction this level of product formation is encouraging for the use of the CYP102A1 variants reported here. Whole-cell double oxidation of 10 mM α-isophorone to 4-ketoisophorone, using twenty times the amount of cells in our experiments on a 1 mL scale, was used to obtain a 65% yield of the product [62]. While a direct comparison of these systems is challenging due to differences in scale, biomass, redox partner utilisation, cofactor regeneration and the expression systems used the amount of product obtained from each relative to the amount of cell biomass is comparable (this work 45 mg g^{-1} L^{-1}, DSM 33 mg g^{-1} L^{-1}, double oxidation 5 mg g^{-1} L^{-1}). Taken together these systems show promise for the future scale up of metabolites from isophorone oxidation using bacterial cytochrome P450 systems.

5. Conclusion

Variants of both the CYP101A1 and CYP102A1 cytochrome P450 enzymes were able to regio- and stereo-selectively hydroxylate isophorone to (*R*)-4-hydroxyisophorone. Decoy molecules were shown to improve the rate of product formation with the rate accelerating CYP102A1 variants but inhibited the performance of the A74G/F87V/L188Q variant which has mutations in the active site and substrate

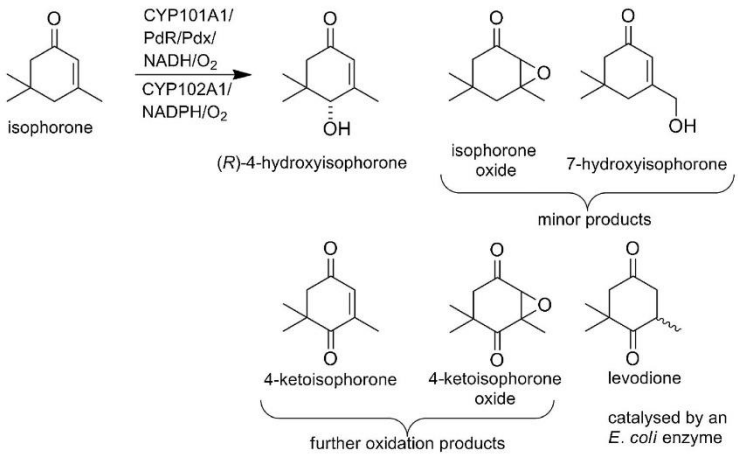

Fig. 5. The turnover of isophorone to (*R*)-4-hydroxyispophorone. The structures of the minor and further products which were generated in certain turnovers are also shown.

access channel. Whole-cell oxidation reactions with the optimal CYP101A1 variants were more productive than the best CYP102A1 mutants. The addition of decoy molecules to the whole-cell turnovers did not have a major effect on the levels of product formation. Further protein engineering of both systems could lead to more efficient systems for the oxidation of isophorone. Increasing the coupling efficiency of the CYP102A1 variants and improving the CYP101A1 whole-cell oxidation system would enhance the productivity.

Acknowledgements

S.G.B. acknowledges the Australian Research Council (ARC) for a Future Fellowship (FT140100355). The authors also acknowledge support through an Australian Government Research Training Program Scholarship (M. Phil for J.H.Z.L.) and thank the University of Adelaide International Postgraduate Award (for S.D.). The authors thank Prof. Luet-Lok Wong (University of Oxford, UK) for the gene constructs of the CYP101A1 and CYP102A1 variants.

Appendix A. Supplementary data

Supplementary data associated with this article can be found, in the online version, at https://doi.org/10.1016/j.enzmictec.2018.01.002.

References

[1] M.J. Cryle, J.E. Stok, J.J. De Voss, Reactions catalyzed by bacterial cytochromes P 450, Aust. J. Chem. 56 (8) (2003) 749–762.
[2] F.P. Guengerich, Common and uncommon cytochrome P450 reactions related to metabolism and chemical toxicity, Chem. Res. Toxicol. 14 (6) (2001) 611–650.
[3] P.R. Ortiz de Montellano, Cytochrome P450: Structure, Mechanism, and Biochemistry Cytochrome P450: Structure, Mechanism, and Biochemistry, Springer International Publishing, Switzerland, 2015.
[4] J. Rittle, M.T. Green, Cytochrome P450 compound I: capture, characterization, and CH bond activation kinetics, Science 330 (6006) (2010) 933–937.
[5] J.T. Groves, G.A. McClusky, Aliphatic hydroxylation via oxygen rebound − oxygen-Transfer catalyzed by iron, J. Am. Chem. Soc. 98 (3) (1976) 859–861.
[6] S.G. Bell, L.L. Wong, Iron: heme proteins, mono- & dioxygenases, in: M. Sono, J.H. Dawson (Eds.), Encyclopedia of Inorganic Chemistry, 2005.
[7] F. Hannemann, A. Bichet, K.M. Ewen, R. Bernhardt, Cytochrome P450 systems–biological variations of electron transport chains, Biochim. Biophys. Acta 1770 (3) (2007) 330–344.
[8] A.W. Munro, H.M. Girvan, K.J. McLean, Cytochrome P450–redox partner fusion enzymes, Biochim. Biophys. Acta 1770 (3) (2007) 345–359.
[9] V.B. Urlacher, S.G. Bell, L.L. Wong, The bacterial cytochrome P450 monooxygenases: p450cam and P450BM-3, in: R.D. Schmid, V.B. Urlacher (Eds.), Modern Biooxidation, Wiley, New York, 2007, pp. 99–122.
[10] G.D. Roiban, M.T. Reetz, Expanding the toolbox of organic chemists: directed evolution of P450 monooxygenases as catalysts in regio- and stereoselective oxidative hydroxylation, Chem. Commun. 51 (12) (2015) 2208–2224.
[11] V.B. Urlacher, M. Girhard, Cytochrome P450 monooxygenases: an update on perspectives for synthetic application, Trends Biotechnol. 30 (1) (2012) 26–36.
[12] T.L. Poulos, B.C. Finzel, A.J. Howard, High-resolution crystal structure of cytochrome P450cam, J. Mol. Biol. 195 (3) (1987) 687–700.
[13] J.A. Peterson, M.C. Lorence, B. Amarneh, Putidaredoxin reductase and putidaredoxin – cloning, sequence determination, and heterologous expression of the proteins, J. Biol. Chem. 265 (11) (1990) 6066–6073.
[14] M.J. Honeychurch, A.O. Hill, L.L. Wong, The thermodynamics and kinetics of electron transfer in the cytochrome P450cam enzyme system, FEBS Lett. 451 (3) (1999) 351–353.
[15] D.P. Nickerson, C.F. Harford-Cross, S.R. Fulcher, L.L. Wong, The catalytic activity of cytochrome P450cam towards styrene oxidation is increased by site-specific mutagenesis, FEBS Lett. 405 (2) (1997) 153–156.
[16] S.G. Bell, C.F. Harford-Cross, L.-L. Wong, Engineering the CYP101 system for in vivo oxidation of unnatural substrates, Protein Eng. 14 (10) (2001) 797–802.
[17] R.J. Sowden, S. Yasmin, N.H. Rees, S.G. Bell, L.L. Wong, Biotransformation of the sesquiterpene (+)-valencene by cytochrome P450cam and P450BM-3, Org. Biomol. Chem. 3 (1) (2005) 57–64.
[18] S.G. Bell, N. Hoskins, C.J.C. Whitehouse, L.L. Wong, Design and engineering of cytochrome P 450 systems, Met. Ions Life Sci. (2007) 437–476.
[19] F. Xu, S.G. Bell, Z. Rao, L.L. Wong, Structure-activity correlations in pentachlorobenzene oxidation by engineered cytochrome P450cam, Protein Eng. Des. Sel. 20 (10) (2007) 473–480.
[20] S.G. Bell, X. Chen, R.J. Sowden, F. Xu, J.N. Williams, L.L. Wong, Z. Rao, Molecular recognition in (+)-alpha-pinene oxidation by cytochrome P450cam, J. Am. Chem. Soc. 125 (3) (2003) 705–714.
[21] S.G. Bell, R.J. Sowden, L.-L. Wong, Engineering the haem monooxygenase cytochrome P450 for monoterpene oxidation, Chem. Commun. 7 (2001) 635–636.
[22] C.F. Harford-Cross, A.B. Carmichael, F.K. Allan, P.A. England, D.A. Rouch, L.L. Wong, Protein engineering of cytochrome p450(cam) (CYP101) for the oxidation of polycyclic aromatic hydrocarbons, Protein Eng. 13 (2) (2000) 121–128.
[23] J.P. Jones, E.J. O'Hare, L.L. Wong, Oxidation of polychlorinated benzenes by genetically engineered CYP101 (cytochrome P450(cam)), Eur. J. Biochem. 268 (5) (2001) 1460–1467.
[24] F. Xu, S.G. Bell, J. Lednik, A. Insley, Z. Rao, L.-L. Wong, The heme monooxygenase cytochrome P450cam can be engineered to oxidize ethane to ethanol, Angew. Chem. Int. Ed. Engl. 44 (26) (2005) 4029–4032.
[25] A. Eichler, L. Gricman, S. Herter, P.P. Kelly, N.J. Turner, J. Pleiss, S.L. Flitsch, Enantioselective benzylic hydroxylation catalysed by P450 monooxygenases: characterisation of a P450cam mutant library and molecular modelling, Chembiochem 17 (5) (2016) 426–432.
[26] O. Sibbesen, Z. Zhang, P.R. Ortiz de Montellano, Cytochrome P450cam substrate specificity: relationship between structure and catalytic oxidation of alkylbenzenes, Arch. Biochem. Biophys. 353 (2) (1998) 285–296.
[27] P.P. Ho, A.J. Fulco, Involvement of a single hydroxylase species in the hydroxylation of palmitate at the omega-1, omega-2 and omega-3 positions by a preparation from Bacillus megaterium, Biochim. Biophys. Acta 431 (2) (1976) 249–256.
[28] C.J. Whitehouse, S.G. Bell, L.L. Wong, P450(BM3)(CYP102A1): connecting the dots, Chem. Soc. Rev. 41 (3) (2012) 1218–1260.
[29] M. Budde, S.C. Maurer, R.D. Schmid, V.B. Urlacher, Cloning expression and characterisation of CYP102A2, a self-sufficient P450 monooxygenase from Bacillus subtilis, Appl. Microbiol. Biotechnol. 66 (2) (2004) 180–186.
[30] M. Dietrich, S. Eiben, C. Asta, T.A. Do, J. Pleiss, V.B. Urlacher, Cloning, expression and characterisation of CYP102A7, a self-sufficient P450 monooxygenase from

Bacillus licheniformis, Appl. Microbiol. Biotechnol. 79 (6) (2008) 931–940.
[31] K.Y. Choi, E. Jung, D.H. Jung, B.P. Pandey, H. Yun, H.Y. Park, R.J. Kazlauskas, B.G. Kim, Cloning, expression and characterization of CYP102D1, a self-sufficient P450 monooxygenase from streptomyces avermitilis, FEBS J. 279 (9) (2012) 1650–1662.
[32] S.D. Munday, N.K. Maddigan, R.J. Young, S.G. Bell, Characterisation of two self-sufficient CYP102 family monooxygenases from Ktedonobacter racemifer DSM44963 which have new fatty acid alcohol product profiles, Biochim. Biophys. Acta 1860 (6) (2016) 1149–1162.
[33] M.G. Joyce, I.S. Ekanem, O. Roitel, A.J. Dunford, R. Neeli, H.M. Girvan, G.J. Baker, R.A. Curtis, A.W. Munro, D. Leys, The crystal structure of the FAD/NADPH-binding domain of flavocytochrome P450 BM3, FEBS J. 279 (9) (2012) 1694–1706.
[34] P. Meinhold, M.W. Peters, A. Hartwick, A.R. Hernandez, F.H. Arnold, Engineering cytochrome P450 BM3for terminal alkane hydroxylation, Adv. Synth. Catal. 348 (6) (2006) 763–772.
[35] W.C. Huang, A.C. Westlake, J.D. Marechal, M.G. Joyce, P.C. Moody, G.C. Roberts, Filling a hole in cytochrome P450 BM3 improves substrate binding and catalytic efficiency, J. Mol. Biol. 373 (3) (2007) 633–651.
[36] S. Kille, F.E. Zilly, J.P. Acevedo, M.T. Reetz, Regio- and stereoselectivity of P450-catalysed hydroxylation of steroids controlled by laboratory evolution, Nat. Chem. 3 (9) (2011) 738–743.
[37] G. Di Nardo, G. Gilardi, Optimization of the bacterial cytochrome P450 BM3 system for the production of human drug metabolites, Int. J. Mol. Sci. 13 (12) (2012) 15901–15924.
[38] R. Singh, M. Bordeaux, R. Fasan, P450-catalyzed intramolecular C-H amination with arylsulfonyl azide substrates, ACS Catal. 4 (2) (2014) 546–552.
[39] R. Singh, J.N. Kolev, P.A. Sutera, R. Fasan, Enzymatic C(sp)-H amination: p450-Catalyzed conversion of carbonazidates into oxazolidinones, ACS Catal. 5 (3) (2015) 1685–1691.
[40] P.S. Coelho, E.M. Brustad, A. Kannan, F.H. Arnold, Olefin cyclopropanation via carbene transfer catalyzed by engineered cytochrome P450 enzymes, Science 339 (6117) (2013) 307–310.
[41] T.K. Hyster, C.C. Farwell, A.R. Buller, J.A. McIntosh, F.H. Arnold, Enzyme-controlled nitrogen-atom transfer enables regiodivergent C-H amination, J. Am. Chem. Soc. 136 (44) (2014) 15505–15508.
[42] C.C. Farwell, R.K. Zhang, J.A. McIntosh, T.K. Hyster, F.H. Arnold, Enantioselective enzyme-catalyzed aziridination enabled by active-site evolution of a cytochrome P450, ACS Cent. Sci. 1 (2) (2015) 89–93.
[43] C.J. Whitehouse, S.G. Bell, H.G. Tufton, R.J. Kenny, L.C. Ogilvie, L.L. Wong, Evolved CYP102A1 (P450(BM3)) variants oxidise a range of non-natural substrates and offer new selectivity options, Chem. Commun. 8 (2008) 966–968.
[44] C.J. Whitehouse, S.G. Bell, W. Yang, J.A. Yorke, C.F. Blanford, A.J. Strong, E.J. Morse, M. Bartlam, Z. Rao, L.L. Wong, A highly active single-mutation variant of P450(BM3) (CYP102A1), Chembiochem 10 (10) (2009) 1654–1656.
[45] C.J. Whitehouse, W. Yang, J.A. Yorke, B.C. Rowlatt, A.J. Strong, C.F. Blanford, S.G. Bell, M. Bartlam, L.L. Wong, Z. Rao, Structural basis for the properties of two single-site proline mutants of CYP102A1 (P450(BM3)), Chembiochem 11 (18) (2010) 2549–2556.
[46] C.J. Whitehouse, W. Yang, J.A. Yorke, H.G. Tufton, L.C. Ogilvie, S.G. Bell, W. Zhou, M. Bartlam, Z. Rao, L.L. Wong, Structure electronic properties and catalytic behaviour of an activity-enhancing CYP102A1 (P450(BM3)) variant, Dalton Trans. 40 (40) (2011) 10383–10396.
[47] A.B. Carmichael, L.L. Wong, Protein engineering of Bacillus megaterium CYP102. The oxidation of polycyclic aromatic hydrocarbons, Eur. J. Biochem. 268 (10) (2001) 3117–3125.
[48] S.D. Munday, S. Dezvarei, S.G. Bell, Increasing the activity and efficiency of stereoselective oxidations by using decoy molecules in combination with rate-enhancing variants of P450Bm3, ChemCatChem 8 (17) (2016) 2789–2796.
[49] Q.S. Li, J. Ogawa, R.D. Schmid, S. Shimizu, Residue size at position 87 of cytochrome P450 BM-3 determines its stereoselectivity in propylbenzene and 3-chlorostyrene oxidation, FEBS Lett. 508 (2) (2001) 249–252.
[50] Q.S. Li, J. Ogawa, R.D. Schmid, S. Shimizu, Engineering cytochrome P450 BM-3 for oxidation of polycyclic aromatic hydrocarbons, Appl. Environ. Microbiol. 67 (12) (2001) 5735–5739.
[51] G.D. Roiban, R. Agudo, A. Ilie, R. Lonsdale, M.T. Reetz, CH-activating oxidative hydroxylation of 1-tetralones and related compounds with high regio- and stereoselectivity, Chem. Commun. 50 (92) (2014) 14310–14313.
[52] A. Seifert, S. Vomund, K. Grohmann, S. Kriening, V.B. Urlacher, S. Laschat, J. Pleiss, Rational design of a minimal and highly enriched CYP102A1 mutant library with improved regio-, stereo- and chemoselectivity, Chembiochem 10 (5) (2009) 853–861.
[53] Q.S. Li, U. Schwaneberg, P. Fischer, R.D. Schmid, Directed evolution of the fatty-acid hydroxylase P450 BM-3 into an indole-hydroxylating catalyst, Chem. Eur. J. 6 (9) (2000) 1531–1536.
[54] N. Kawakami, O. Shoji, Y. Watanabe, Use of perfluorocarboxylic acids to trick cytochrome P450BM3 into initiating the hydroxylation of gaseous alkanes, Angew. Chem. Int. Ed. Engl. 50 (23) (2011) 5315–5318.
[55] O. Shoji, T. Kunimatsu, N. Kawakami, Y. Watanabe, Highly selective hydroxylation of benzene to phenol by wild-type cytochrome P450BM3 assisted by decoy molecules, Angew. Chem. Int. Ed. Engl. 52 (26) (2013) 6606–6610.
[56] Z. Cong, O. Shoji, C. Kasai, N. Kawakami, H. Sugimoto, Y. Shiro, Y. Watanabe, Activation of wild-type cytochrome P450BM3 by the next generation of decoy molecules: enhanced hydroxylation of gaseous alkanes and crystallographic evidence, ACS Catal. 5 (1) (2015) 150–156.
[57] S.D. Munday, O. Shoji, Y. Watanabe, L.L. Wong, S.G. Bell, Improved oxidation of aromatic and aliphatic hydrocarbons using rate enhancing variants of P450Bm3 in combination with decoy molecules, Chem. Commun. 52 (5) (2016) 1036–1039.
[58] M. Hennig, K. Püntener, M. Scalone, Synthesis of (R)- and (S)-4-hydroxyisophorone by ruthenium-catalyzed asymmetric transfer hydrogenation of ketoisophorone, Tetrahedron: Asymmetry 11 (9) (2000) 1849–1858.
[59] I. Kaluzna, T. Schmitges, H. Straatman, D. van Tegelen, M. Müller, M. Schürmann, D. Mink, Enabling selective and sustainable P450 oxygenation technology. production of 4-Hydroxy-ü-isophorone on kilogram scale, Org. Process Res. Dev. 20 (4) (2016) 814–819.
[60] Y. Mikami, Y. Fukunaga, M. Arita, Y. Obi, T. Kisaki, Preparation of aroma compounds by microbial transformation of isophorone with aspergillus niger, Agric. Biol. Chem. 45 (3) (1981) 791–793.
[61] Y.A. Joe, Y.M. Goo, Y.Y. Lee, Microbiological oxidation of isophorone to 4-hydroxyisophorone and chemical transformation of 4-hydroxyisophorone to 2,3,5-trimethyl-p-benzoquinone, Arch. Pharm. Res. 12 (2) (1989) 73–78.
[62] M. Tavanti, F. Parmeggiani, J.R. Gómez Castellanos, A. Mattevi, N.J. Turner, One-pot biocatalytic double oxidation of α-Isophorone for the synthesis of ketoisophorone, ChemCatChem 9 (17) (2017) 3338–3348.
[63] T. Omura, R. Sato, The carbon monoxide-binding pigment of liver microsomes. I. Evidence for its hemoprotein nature, J. Biol. Chem. 239 (1964) 2370–2378.
[64] G. Fioroni, F. Fringuelli, F. Pizzo, L. Vaccaro, Epoxidation of [small alpha],[small beta]-unsaturated ketones in water. An environmentally benign protocol, Green Chem. 5 (4) (2003) 425–428.
[65] M. Ishihara, T. Tsuneya, H. Shiota, M. Shiga, K. Nakatsu, Identification of new constituents of quince fruit flavor (Cydonia-Oblonga mill = Cydonia-Vulgaris pers), J. Org. Chem. 51 (4) (1986) 491–495.
[66] E.A. Hall, M.R. Sarkar, J.H.Z. Lee, S.D. Munday, S.G. Bell, Improving the monooxygenase activity and the regio- and stereoselectivity of terpenoid hydroxylation using ester directing groups, ACS Catal. 6 (2016) 6306–6317.
[67] P.A. England, D.A. Rouch, A.C.G. Westlake, S.G. Bell, D.P. Nickerson, M. Webberley, S.L. Flitsch, L.L. Wong, Aliphatic vs aromatic CH bond activation of phenylcyclohexane catalysed by cytochrome P450cam, Chem. Commun. 3 (1996) 357–358.
[68] S.G. Bell, D.A. Rouch, L.-L. Wong, Selective aliphatic and aromatic carbon-hydrogen bond activation catalysed by mutants of cytochrome p450cam, J. Mol. Catal. B: Enzym. 3 (6) (1997) 293–302.
[69] S.G. Bell, A. Dale, N.H. Rees, L.L. Wong, A cytochrome P450 class I electron transfer system from Novosphingobium aromaticivorans, Appl. Microbiol. Biotechnol. 86 (1) (2010) 163–175.
[70] S.G. Bell, A.B. Tan, F.O. Johnson, L.L. Wong, Selective oxidative demethylation of veratric acid to vanillic acid by CYP199A4 from *Rhodopseudomonas palustris* HaA2, Mol. Biosyst. 6 (1) (2010) 206–214.
[71] M. Schrewe, N. Ladkau, B. Bühler, A. Schmid, Direct terminal alkylamino-Functionalization via multistep biocatalysis in one recombinant whole-Cell catalyst, Adv. Synth. Catal. 355 (9) (2013) 1693–1697.
[72] S. Schneider, M.G. Wubbolts, D. Sanglard, B. Witholt, Biocatalyst engineering by assembly of fatty acid transport and oxidation activities for In vivo application of cytochrome P-450BM-3 monooxygenase, Appl. Environ. Microbiol. 64 (10) (1998) 3784–3790.
[73] J.E. Stok, E.A. Hall, I.S.J. Stone, M.C. Noble, S.H. Wong, S.G. Bell, J.J. De Voss, In vivo and in vitro hydroxylation of cineole and camphor by cytochromes P450CYP101A1, CYP101B1 and N242A CYP176A1, J. Mol. Catal. B: Enzym. 128 (2016) 52–64.
[74] S.S. Boddupalli, R.W. Estabrook, J.A. Peterson, Fatty acid monooxygenation by cytochrome P-450BM-3, J. Biol. Chem. 265 (8) (1990) 4233–4239.
[75] P.W. Roome, J.A. Peterson, The reduction of putidaredoxin reductase by reduced pyridine nucleotides, Arch. Biochem. Biophys. 266 (1) (1988) 32–40.
[76] J.L. Brumaghim, Y. Li, E. Henle, S. Linn, Effects of hydrogen peroxide upon nicotinamide nucleotide metabolism in Escherichia coli: changes in enzyme levels and nicotinamide nucleotide pools and studies of the oxidation of NAD(P)H by Fe(III), J. Biol. Chem. 278 (43) (2003) 42495–42504.
[77] R. Neeli, O. Roitel, N.S. Scrutton, A.W. Munro, Switching pyridine nucleotide specificity in P450 BM3: mechanistic analysis of the W1046H and W1046A enzymes, J. Biol. Chem. 280 (18) (2005) 17634–17644.

Supplementary Material

GC analysis methods:

GC-MS: the oven temperature was held at 80 °C for 3 minutes then increased at 10 °C min^{-1} to 200 °C and held for 5 minutes. The injector and interface temperature were 250 °C and 280 °C, respectively.

GC: the oven temperature was held at 100 °C for 3 minutes then increased at 8 °C min^{-1} to 220 °C and held for 2 minutes. The injector and detector temperature were 250 °C and 270 °C, respectively.

GC chiral: the oven temperature was held at 80 °C for 3 minutes then increased at 5 °C min^{-1} to 200 °C and held for 3 minutes. The injector and detector temperature were both 230 °C.

Table S1 CYP101A1 mutants tested for isophorone oxidation in this work alongside the WT enzyme. These variants were in the pCWSGB++ whole-cell expression system and were generated using site directed mutagenesis [1-10].

Mutant
Y96F/I395G
F87A/Y96F
F87L/Y96F
Y96F/L244A
F87W/Y96F/V247L
F87L/Y96F/V247L
F87W/Y96F/L244A
F87W/Y96F/L244A/V247L
Y96F/L244A
Y96A
Y96F
Y96F/V247L
Y96L/V247A

Table S2 The cell biomass (cell wet weight) and concentration of P450 enzyme in the whole-cell oxidation of isophorone with different CYP102A1 and CYP101A1 variants.

Enzyme	Cell biomass g/L	Concentration of P450 (nM)
CYP102A1-WT	10.5 ± 0.2	183
CYP102A1-GVQ	8.5 ± 0.2	88
CYP102A1-RLYFIP	9.5 ± 0.1	108
CYP101A1-WT	8.3 ± 0.2	25
CYP101A1-WFAL	8.6 ± 0.6	54
pET 28	8.4 ± 0.6	-

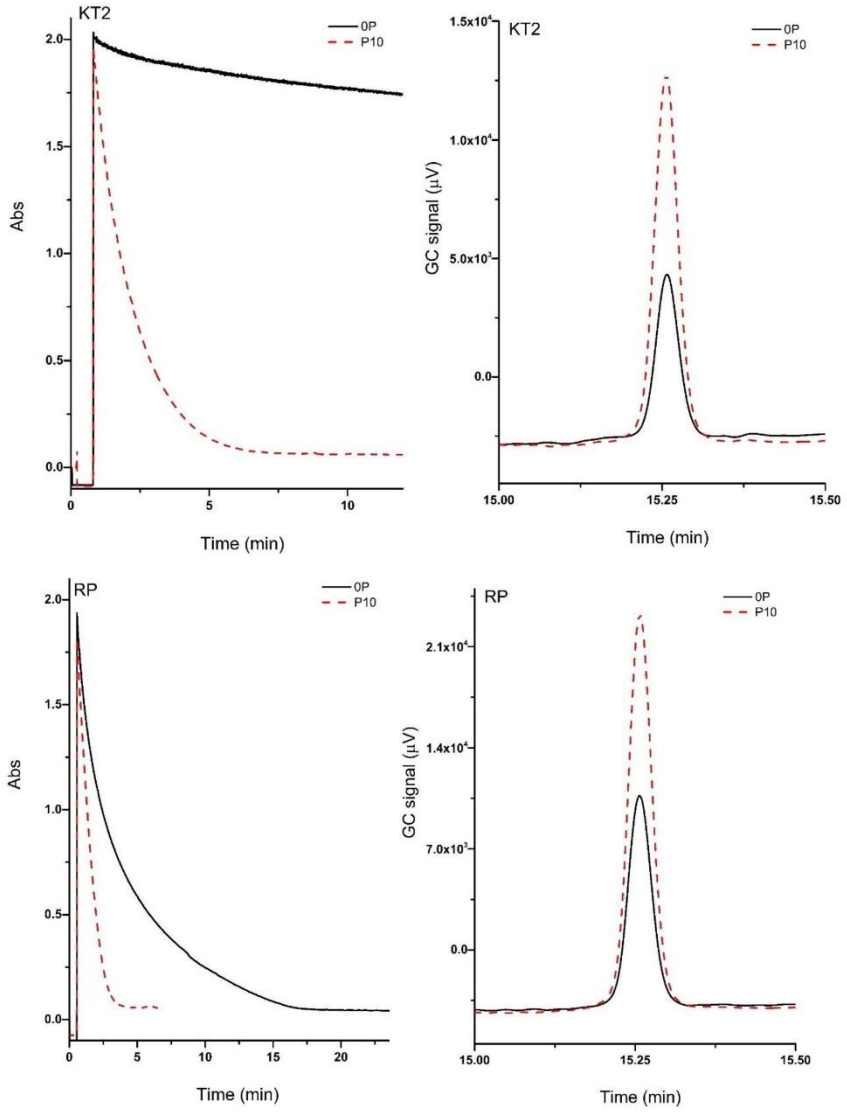

Figure S1 NADPH oxidation rates and GC analysis of the *in vitro* turnovers of the KT2 (top) and RLYFIP (bottom, labelled RP) variants in the absence of decoy molecule (black line) and in combination with PFC10 (dash red line, labelled P10). The assays show the increased rate of NADH oxidation and greater amount of product formed when using the decoy molecule resulting in the greater product formation rates.

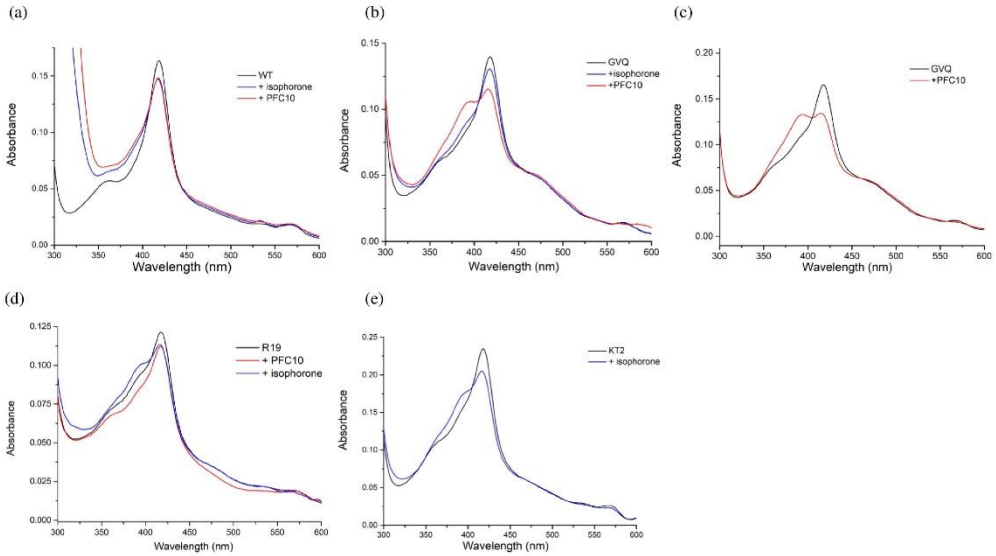

Figure S2 Analysis of the ferric spin state shift of CYP102A1 variants on addition of the substrate (isophorone) and/or the decoy molecule PFC10. (a) WT CYP102A1 with isophorone followed by addition of PFC10, (b) GVQ with isophorone followed by addition of PFC10, (c) GVQ and addition of only PFC10, (d) R19 with addition of PFC10 followed by addition of isophorone and (e) KT2 and addition of isophorone. Note the same shifts observed above were obtained if the PFC10 or isophorone substrate were added separately.

Figure S3 NMR and GC-MS data for isolated products

4-hydroxyisophorone

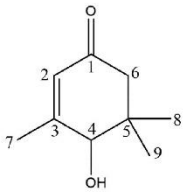

Data for 4-hydroxy-3,5,5-trimethylcyclohex-2-enone:

Yield: 0.0353g

GCMS: Mass (m/z = 154.05)

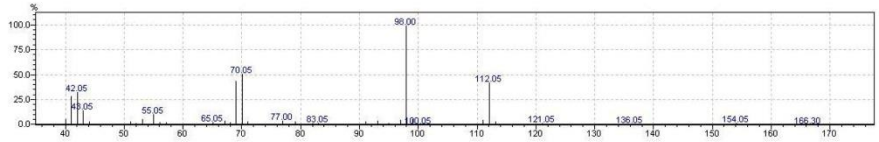

^{1}H-NMR

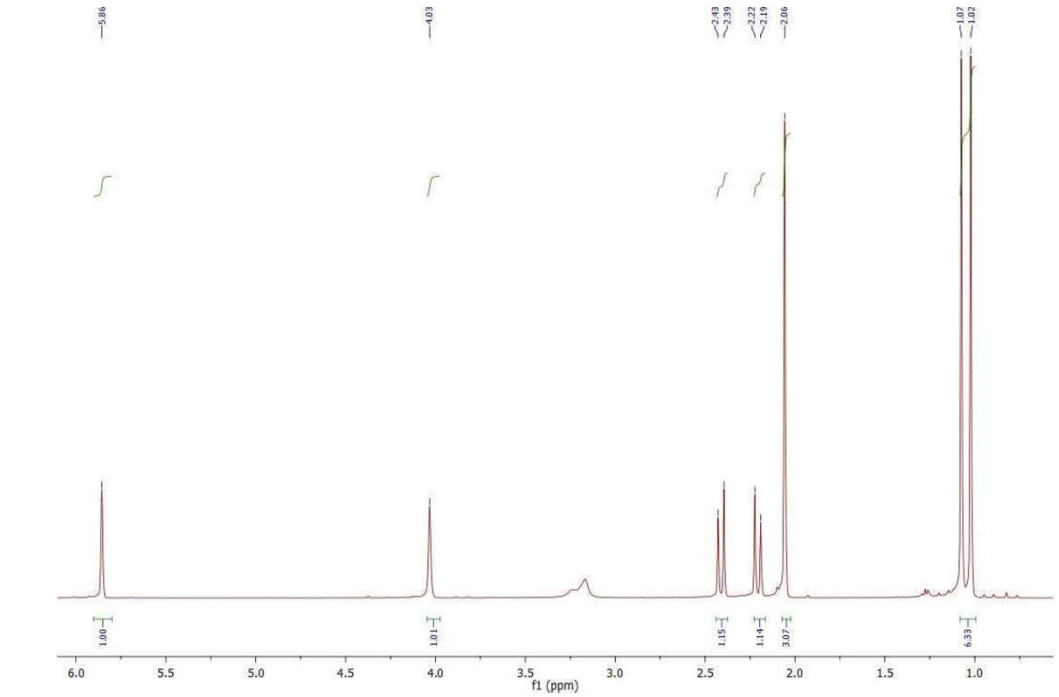

^{13}C NMR:

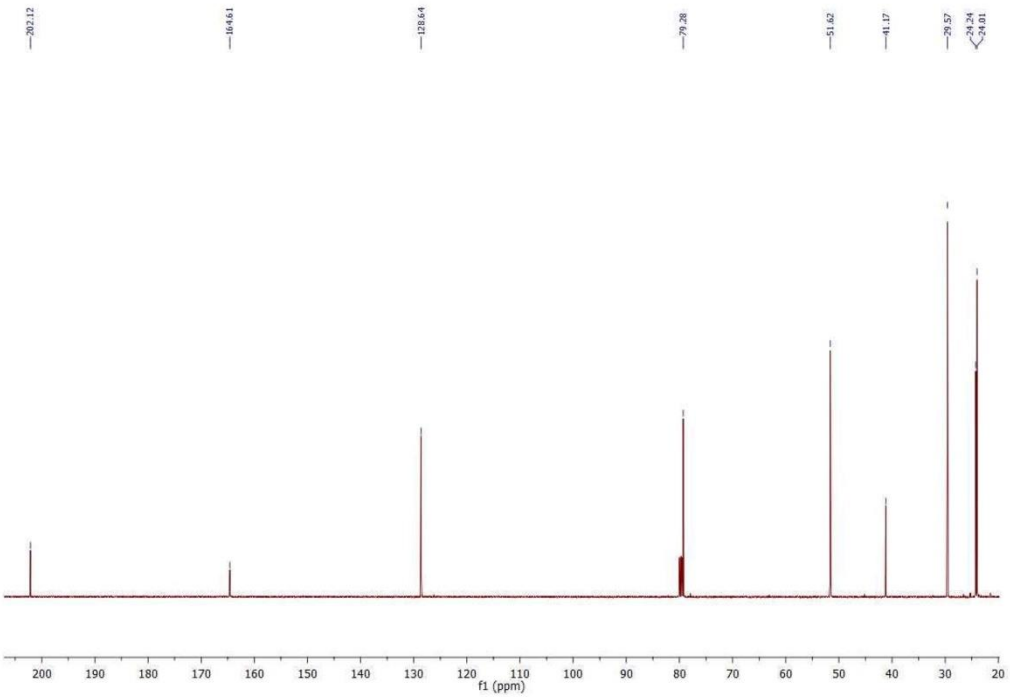

^{1}H-^{1}H COSY

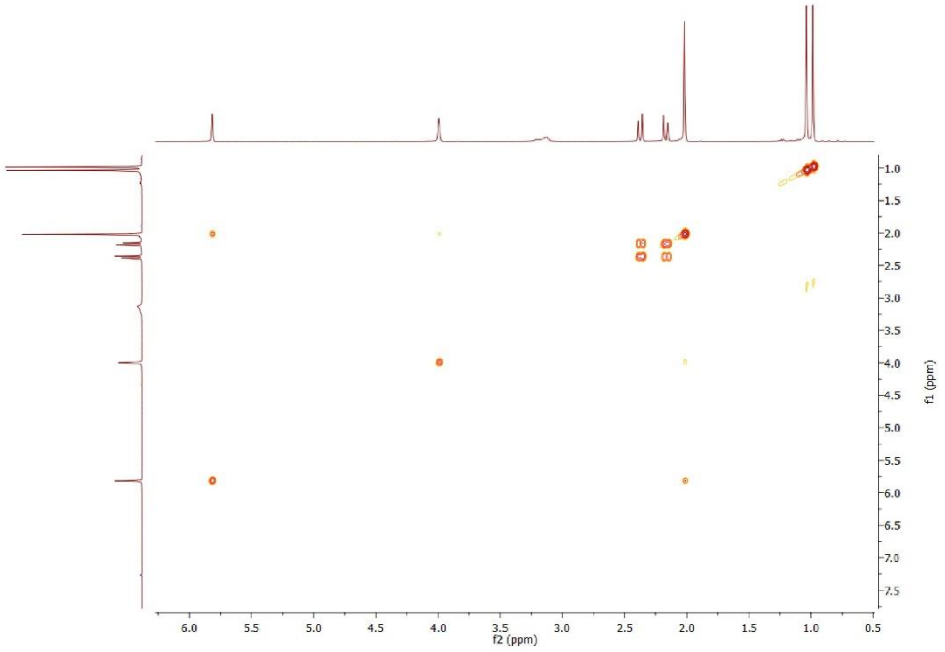

^{13}C-^{1}H HSQC

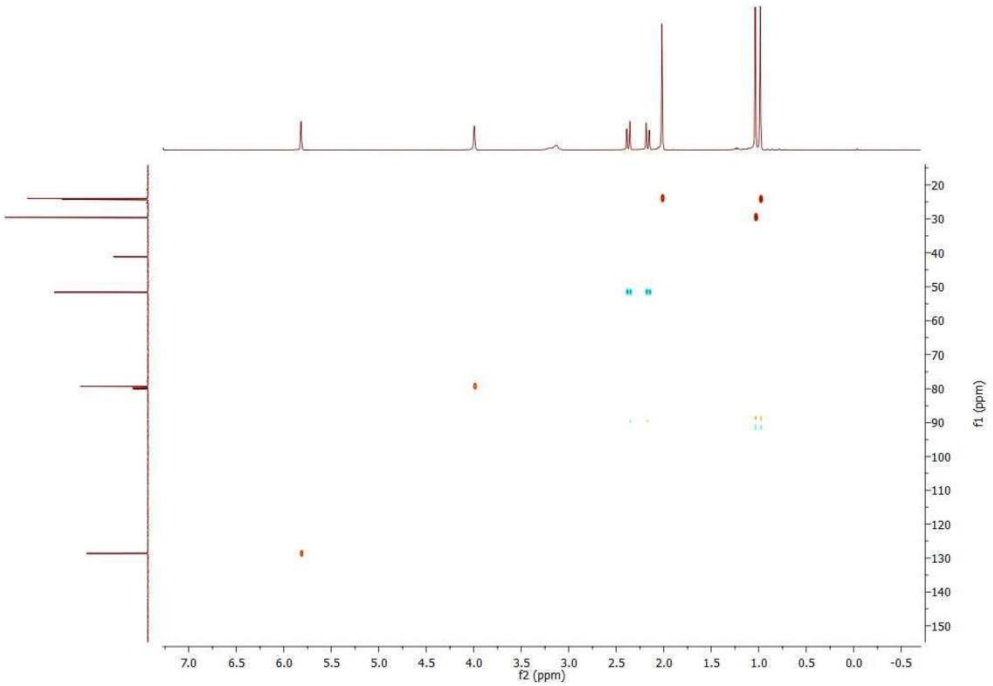

^{13}C-^{1}H HMBC

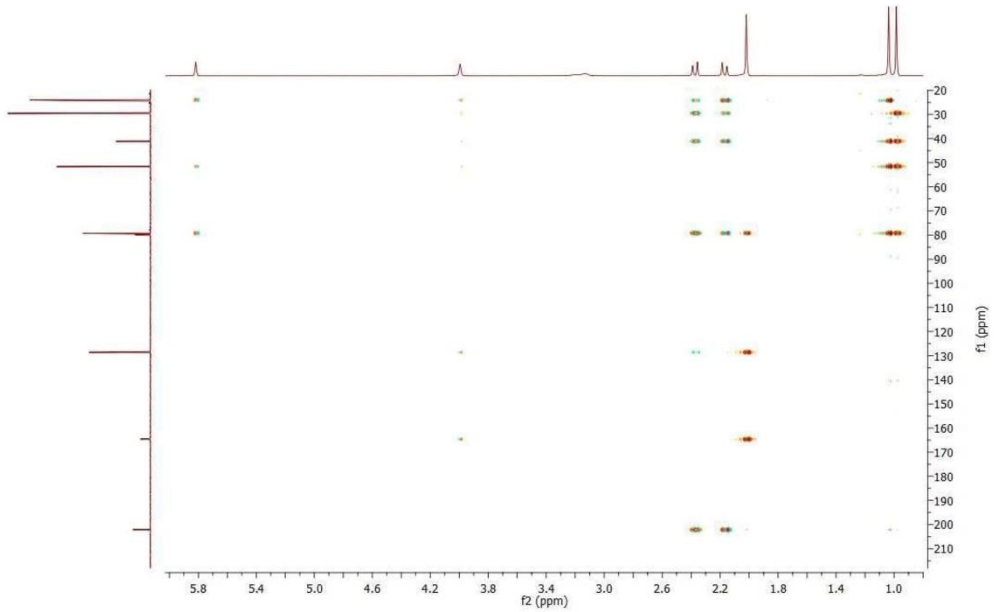

7-hydroxyisophorone (3-(hydroxymethyl)-5,5-dimethylcyclohex-2-enone)

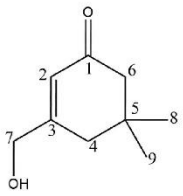

Yield: 0.0116g

GCMS: Mass (m/z = 154.05)

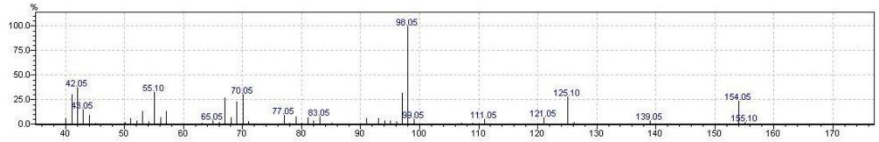

^{1}H NMR:

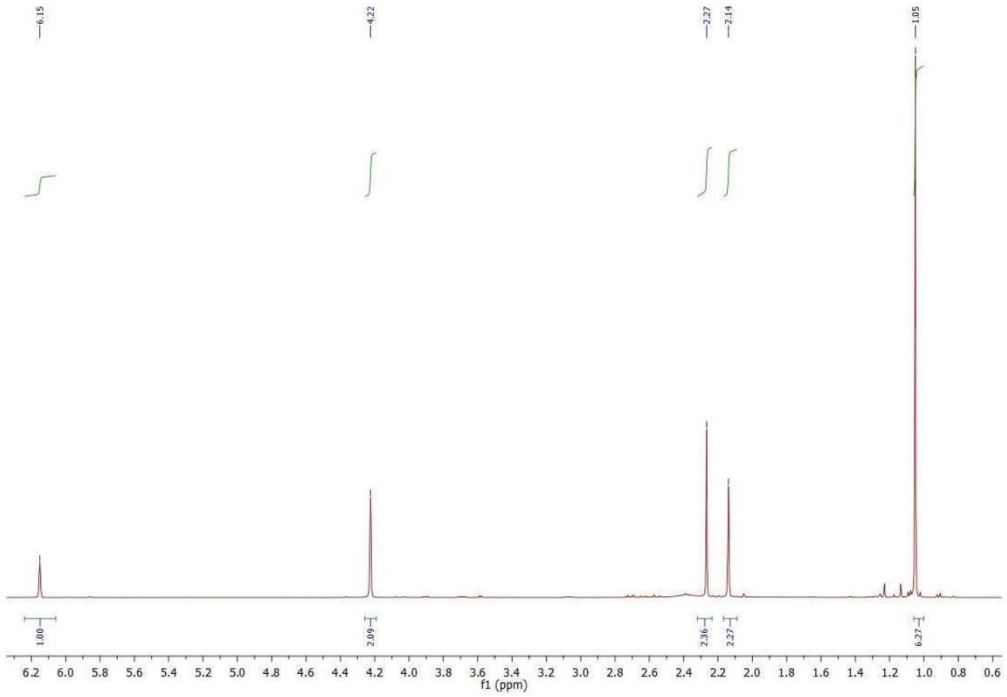

^{13}C NMR

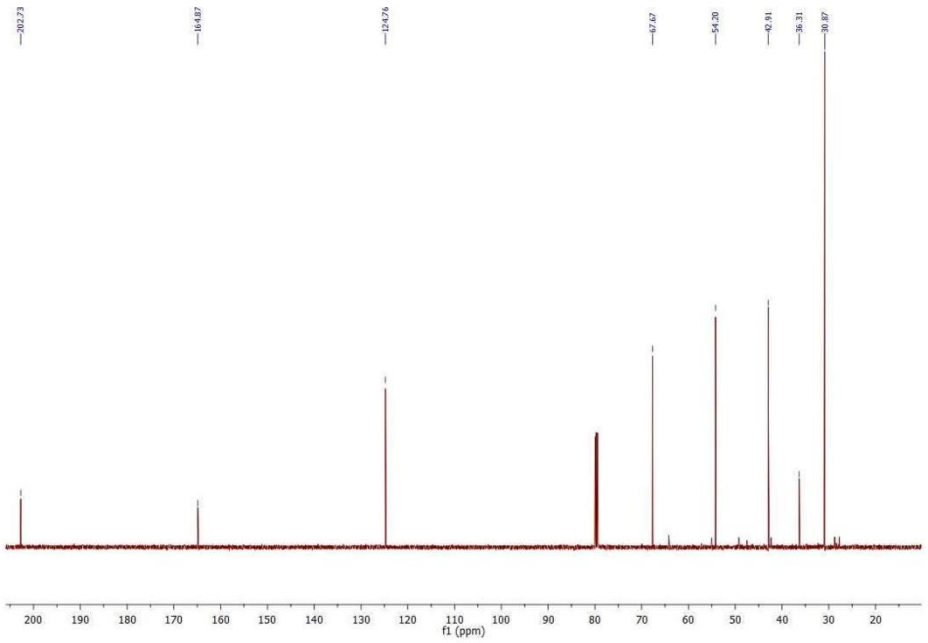

^{1}H-^{1}H COSY:

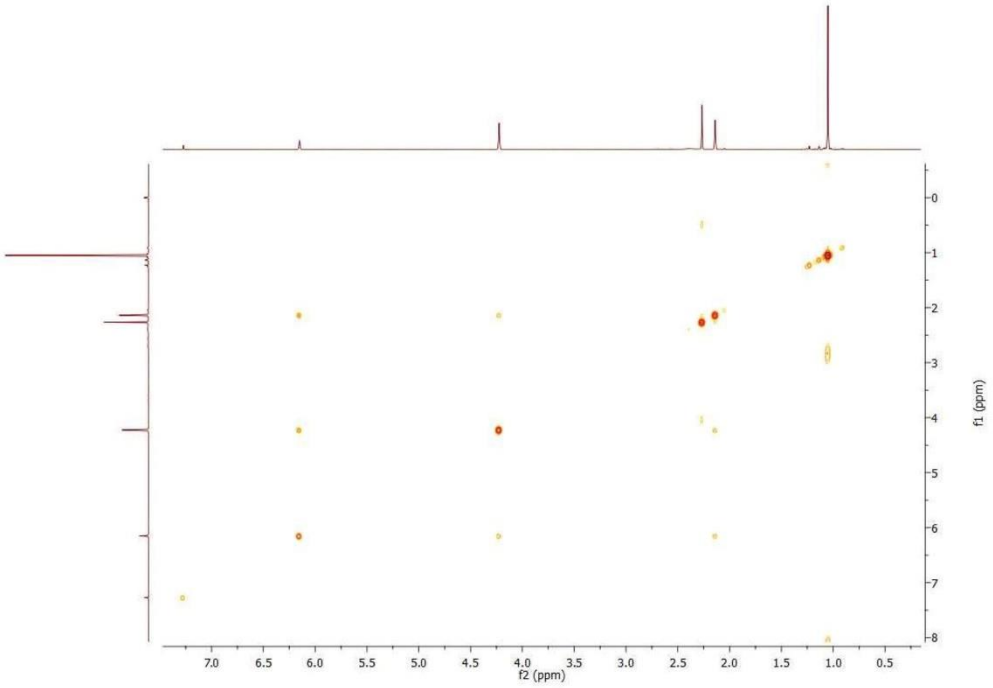

^{13}C-^{1}H- HSQC

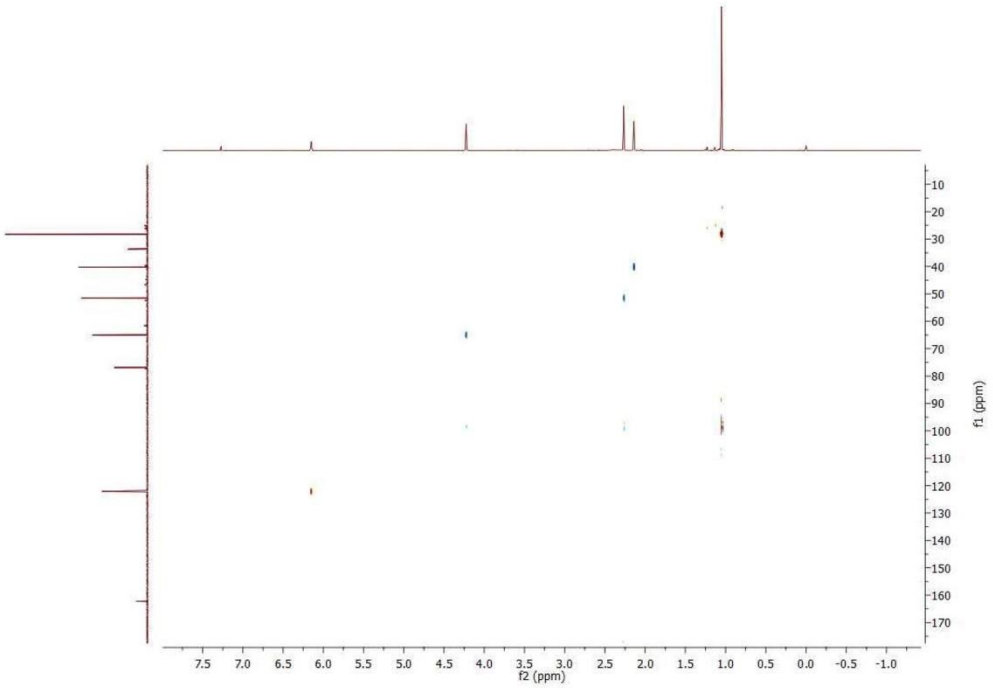

^{13}C-^{1}H HMBC

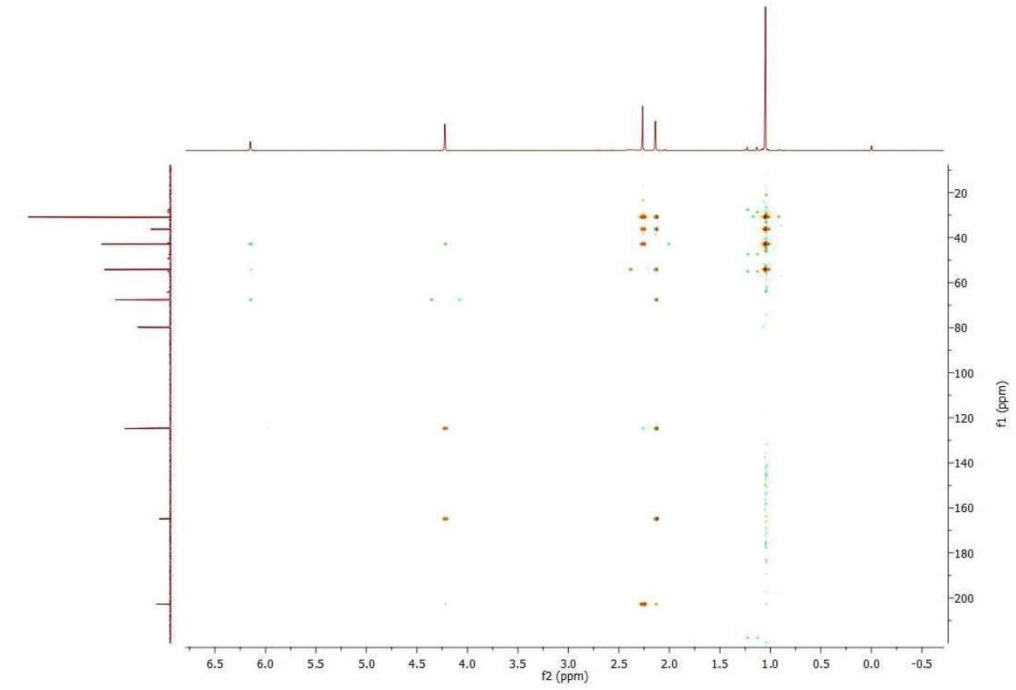

levodione 2,2,6-trimethyl-1,4-cyclohexanedione

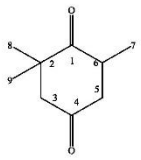

MS of Levodione RT

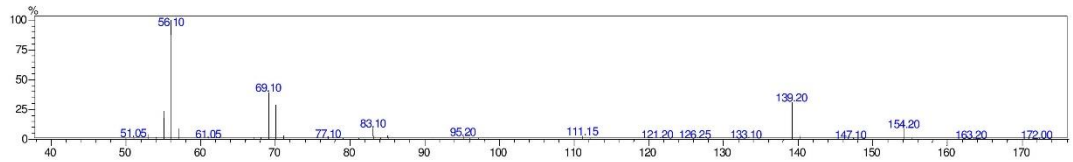

^{1}H NMR

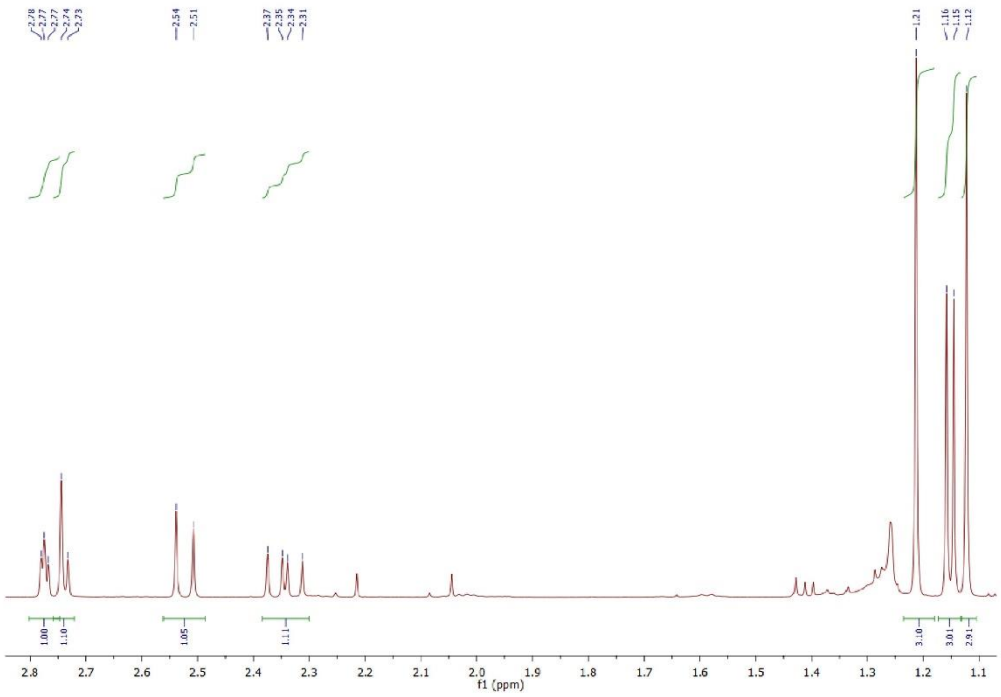

^{13}C NMR

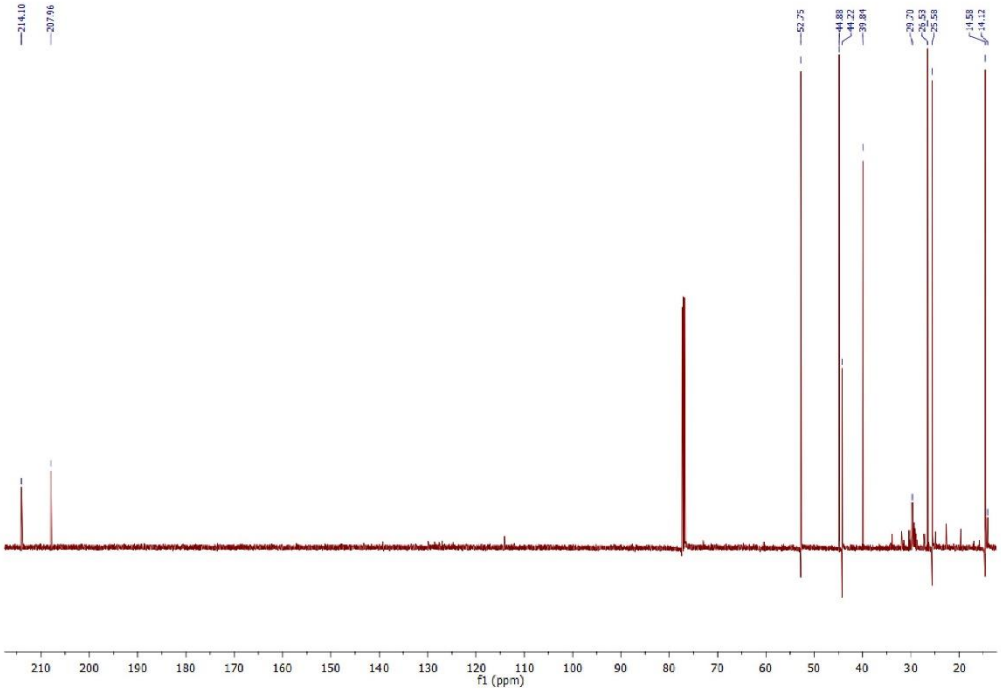

^{1}H-^{1}H COSY:

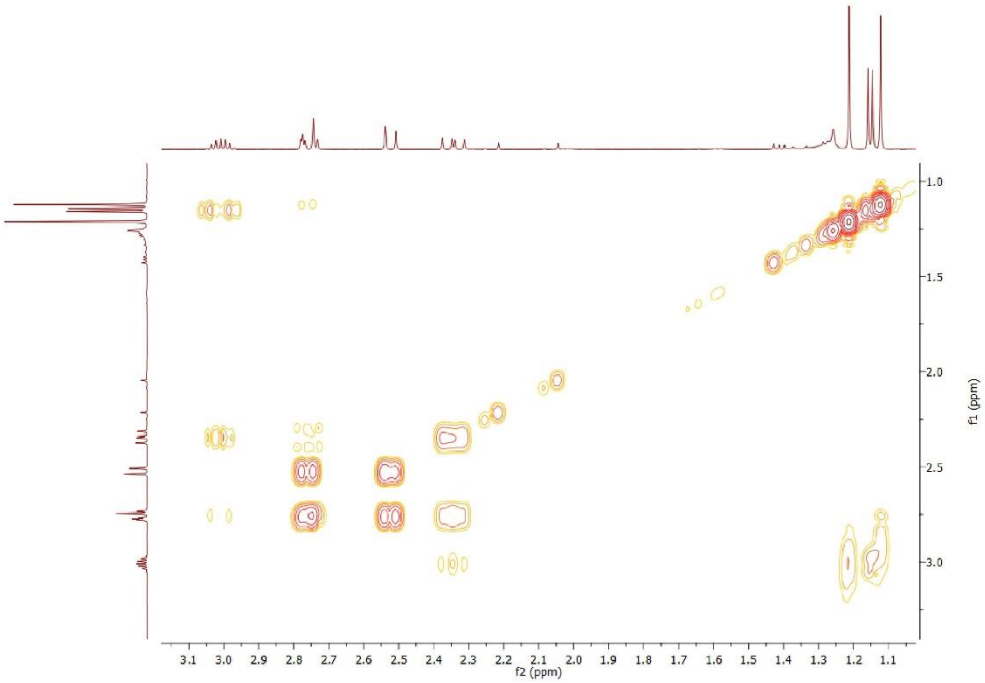

^{13}C-^{1}H HSQC

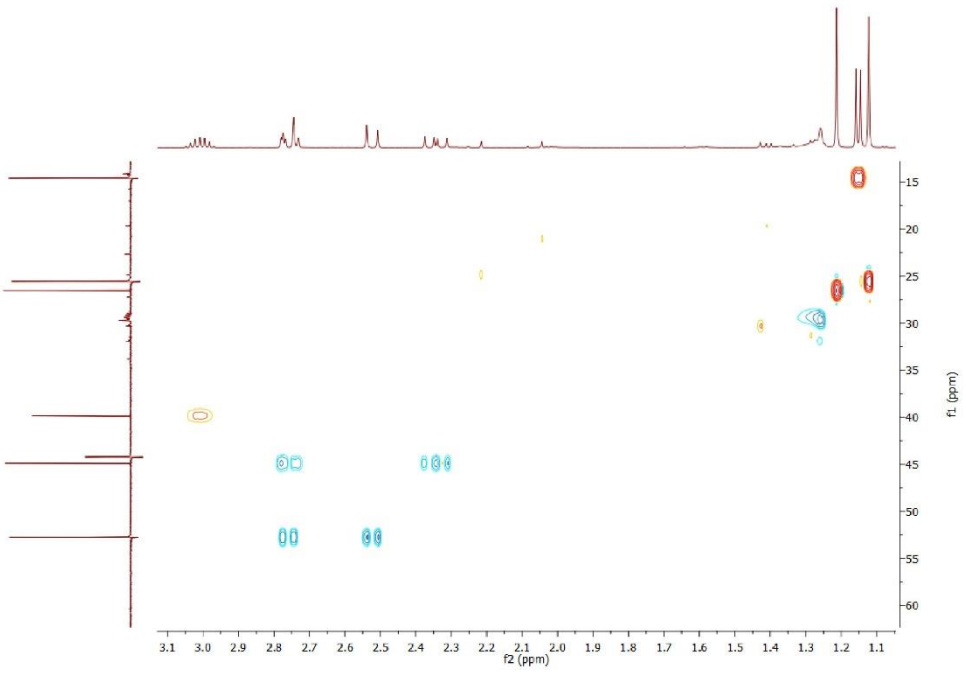

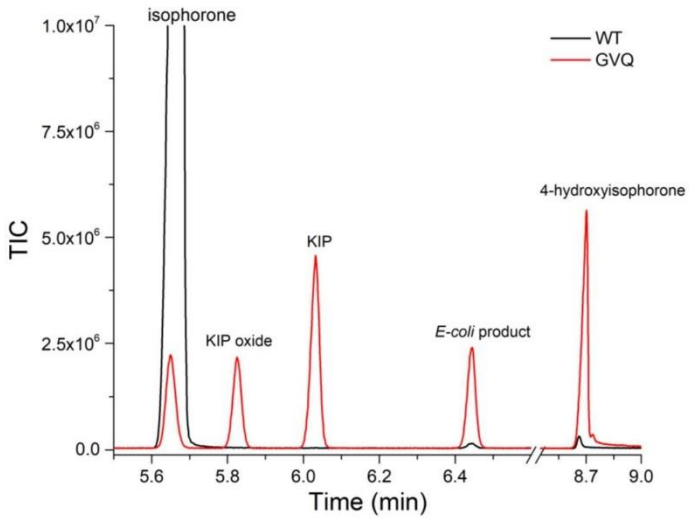

Figure S4 GC-MS analysis of the whole-cell turnover of isophorone by the WT (black) and GVQ variant (red) of CYP102A1 after 20 hours (one aliquot of 2 mM substrate was added). Products were identified as 4-hydroxyisophorone, 4-ketoisophorone (KIP), ketoisophorone oxide (KIP oxide) and the product arising from action of an *E. coli* enzyme, subsequently identified as levodione.

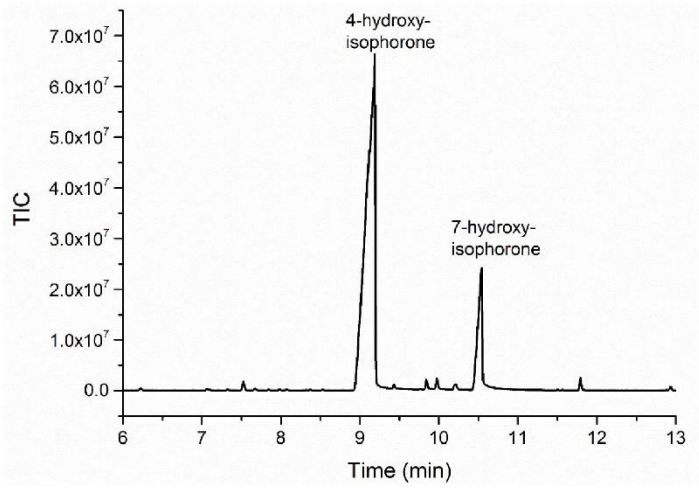

Figure S5 GC-MS analysis of the extract obtained after large scale whole-cell turnover of isophorone by the WFL mutant of CYP101A1. 4-Hydroxyisophorone (RT 9.0 min) and the minor product 7-hydroxyispohorone at RT 10.45 min were obtained.

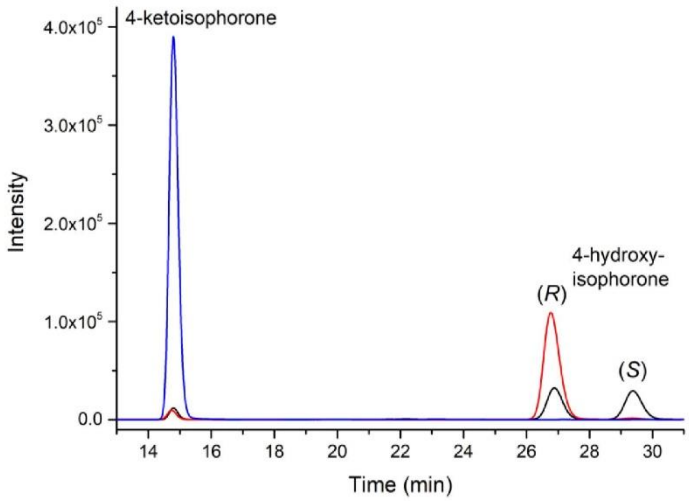

Figure S6 Chiral HPLC analysis of the 4-hydroxyisophorone product from the oxidation of isophorone by the WFAL mutant. Shown are the analyses of the product from enzyme oxidation (red), the racemic product generated by $NaBH_4$ reduction of 4-ketoisophorone (black) and a 4-ketoisophorone control (blue). The (*R*) and (*S*) enantiomers were assigned by matching the optical rotation of the isolated enzyme product to that of the pure (*R*) enantiomer. Note a single product peak was observed by GC analysis.

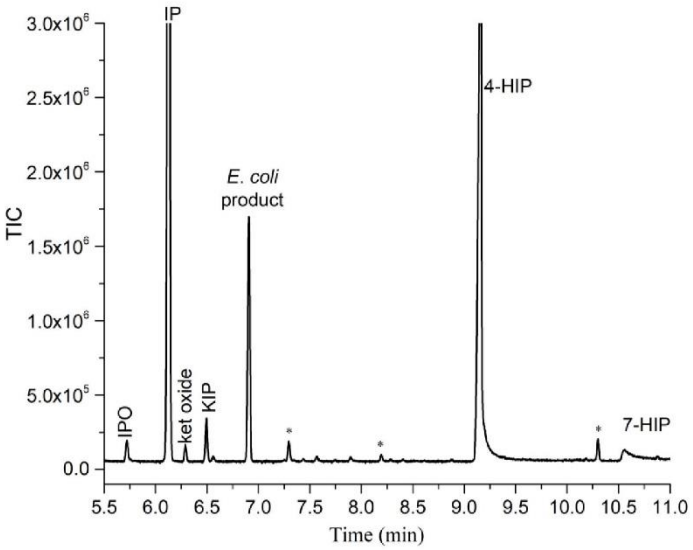

Figure S7 GC-MS analysis of the whole-cell turnover of the CYP102A1 variant GVQ after 20 hours (two aliquots of 2 mM substrate added). Labelled are the isophorone substrate (IP, RT 5.8 min), isophorone oxide (IPO, RT 5.7 min), 4-ketoisophorone oxide (ket oxide, RT 6.3 min), 4-ketoisophorone (KIP, RT 6.5 min), (*R*)-4-hydroxyisophorone (4-HIP, RT 9.15 min), 7-hydroxyisophorone (7-HIP, RT 10.5 min). The additional peak which arises during the *E. coli* whole-cell turnovers was subsequently identified as levodione arising for the probable action of an ene reductase enzyme from *E. coli* on 4-ketoisophorone.

MS data

RT 5.7 min 2, 3-epoxy-3, 5, 5-trimethyl-1-cyclohexanone (IPO)

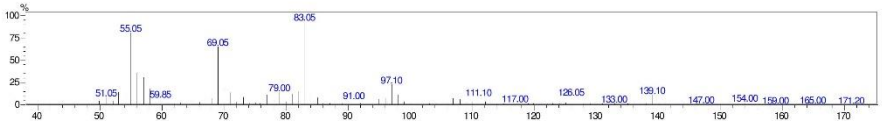

RT 6.3 min 4-isophorone ketone epoxide

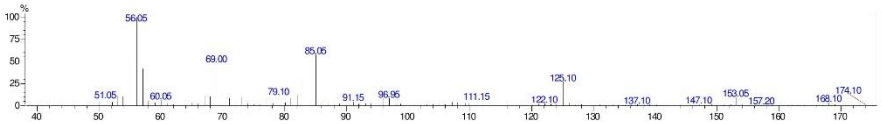

RT 6.5 min 2,6,6-trimethylcyclohex-2-ene-1,4-dione (KIP)

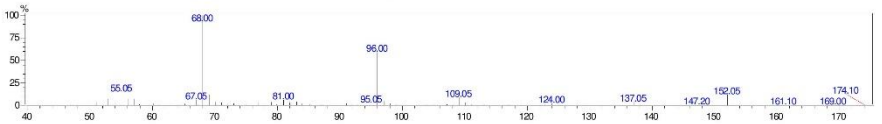

RT 6.9 min product from endogenous *E. coli* enzyme acting on 4-ketoisophorone – assigned as levodione

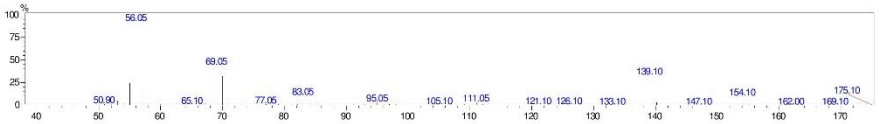

RT 9.15 min 4-hydroxy-isophorone (4-HIP)

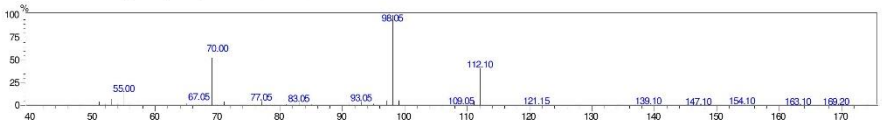

RT 10.5 min 7-hydroxy-isophorone (7-HIP)

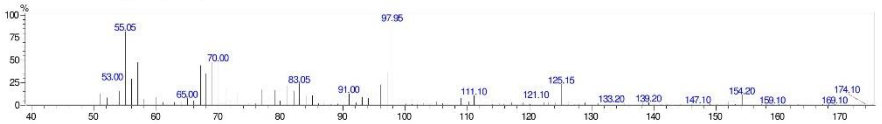

References

[1] F. Xu, S.G. Bell, J. Lednik, A. Insley, Z. Rao, L.-L. Wong, The Heme Monooxygenase Cytochrome P450cam Can Be Engineered to Oxidize Ethane to Ethanol, Angew. Chem. Int. Ed. Engl. 44(26) (2005) 4029-4032.
[2] J.P. Jones, E.J. O'Hare, L.L. Wong, Oxidation of polychlorinated benzenes by genetically engineered CYP101 (cytochrome P450(cam)), Eur. J. Biochem. 268(5) (2001) 1460-7.
[3] C.F. Harford-Cross, A.B. Carmichael, F.K. Allan, P.A. England, D.A. Rouch, L.L. Wong, Protein engineering of cytochrome p450(cam) (CYP101) for the oxidation of polycyclic aromatic hydrocarbons, Protein Eng. 13(2) (2000) 121-8.
[4] D.P. Nickerson, C.F. Harford-Cross, S.R. Fulcher, L.L. Wong, The catalytic activity of cytochrome P450cam towards styrene oxidation is increased by site-specific mutagenesis, FEBS Lett. 405(2) (1997) 153-6.
[5] P.A. England, D.A. Rouch, A.C.G. Westlake, S.G. Bell, D.P. Nickerson, M. Webberley, S.L. Flitsch, L.L. Wong, Aliphatic vs aromatic C-H bond activation of phenylcyclohexane catalysed by cytochrome P450cam, Chem. Commun. (3) (1996) 357-358.
[6] S.G. Bell, R.J. Sowden, L.-L. Wong, Engineering the haem monooxygenase cytochrome P450 for monoterpene oxidation, Chem. Commun. (7) (2001) 635-636.
[7] S.G. Bell, X. Chen, R.J. Sowden, F. Xu, J.N. Williams, L.L. Wong, Z. Rao, Molecular recognition in (+)-alpha-pinene oxidation by cytochrome P450cam, J. Am. Chem. Soc. 125(3) (2003) 705-714.
[8] S.G. Bell, C.F. Harford-Cross, L.-L. Wong, Engineering the CYP101 system for in vivo oxidation of unnatural substrates, Protein Eng. 14(10) (2001) 797-802.
[9] F. Xu, S.G. Bell, Z. Rao, L.L. Wong, Structure-activity correlations in pentachlorobenzene oxidation by engineered cytochrome P450cam, Protein Eng. Des. Sel. 20(10) (2007) 473-80.
[10] R.J. Sowden, S. Yasmin, N.H. Rees, S.G. Bell, L.L. Wong, Biotransformation of the sesquiterpene (+)-valencene by cytochrome P450cam and P450BM-3, Org. Biomol. Chem. 3(1) (2005) 57-64.

Chapter 6

Efficient hydroxylation of cycloalkanes by co-addition of decoy molecules to variants of the cytochrome P450 CYP102A1

Citation:

Dezvarei, S.; Onoda, H.; Shoji, O.; Watanabe, Y.; Bell, S. G., J Inorg Biochem 2018, 183, 137-145.

Statement of Authorship

Title of Paper	Efficient hydroxylation of cycloalkanes by co-addition of decoy molecules to variants of the cytochrome P450 CYP102A1
Publication Status	☑ Published ☐ Accepted for Publication ☐ Submitted for Publication ☐ Unpublished and Unsubmitted work written in manuscript style
Publication Details	Dezvarei, S.; Onoda, H.; Shoji, O.; Watanabe, Y.; Bell, S. G., Efficient hydroxylation of cycloalkanes by co-addition of decoy molecules to variants of the cytochrome P450 CYP102A1. *Journal of Inorganic Biochemistry* **2018,** *183*, 137-145.

Principal Author

Name of Principal Author (Candidate)	Shaghayegh Dezvarei		
Contribution to the Paper	Enzyme preparation, performing oxidation experiments of cycloalkanes to generate products, products characterisation, analysis of substrates and products, interpreted data and discussion, wrote manuscript.		
Overall percentage (%)	80		
Certification:	This paper reports on original research I conducted during the period of my Higher Degree by Research candidature and is not subject to any obligations or contractual agreements with a third party that would constrain its inclusion in this thesis. I am the primary author of this paper.		
Signature		Date	08/04/19

Co-Author Contributions

By signing the Statement of Authorship, each author certifies that:

i. the candidate's stated contribution to the publication is accurate (as detailed above);
ii. permission is granted for the candidate in include the publication in the thesis; and
iii. the sum of all co-author contributions is equal to 100% less the candidate's stated contribution.

Name of Co-Author	Hiroki Onoda		
Contribution to the Paper	Docking studies of cyclohexane and cyclooctane.		
Signature		Date	25th March 2019

Name of Co-Author	Osami Shoji		
Contribution to the Paper	Providing the second generation of decoy molecules.		
Signature		Date	28th March 2019

Name of Co-Author	Yoshihito Watanabe

Contribution to the Paper	Providing the second generation of decoy molecules.
Signature	Date: March 25, 2019

Name of Co-Author	Stephen G. Bell
Contribution to the Paper	Experimental design, supervision, manuscript preparation.
Signature	Date: 8/04/2019

Journal of Inorganic Biochemistry 183 (2018) 137–145

Contents lists available at ScienceDirect

Journal of Inorganic Biochemistry

journal homepage: www.elsevier.com/locate/jinorgbio

Efficient hydroxylation of cycloalkanes by co-addition of decoy molecules to variants of the cytochrome P450 CYP102A1

Shaghayegh Dezvarei[a], Hiroki Onoda[b], Osami Shoji[b], Yoshihito Watanabe[c], Stephen G. Bell[a,*]

[a] Department of Chemistry, University of Adelaide, Adelaide 5005, Australia
[b] Department of Chemistry, Graduate School of Science, Nagoya University, Furo-cho, Chikusa-ku, Nagoya 464-8602, Japan
[c] Research Center for Materials Science, Nagoya University, Furo-cho, Chikusa-ku, Nagoya, 464-8602, Japan

ARTICLE INFO

Keywords:
Monooxygenase
Cytochrome P450
Cycloalkanes
Hydroxylation
Heme proteins

ABSTRACT

The wild-type cytochrome P450 (CYP) monooxygenase enzyme CYP102A1 (P450Bm3) has low activity for cycloalkane oxidation. The oxidation of these substrates by variants of this enzyme in combination with perfluorinated decoy molecules (PFCs) was investigated to improve productivity. The use of rate accelerating variants, which have mutations located outside of the substrate binding pocket as well as an active site variant of CYP102A1 (A74G/F87V/L188Q) all enhanced cycloalkane oxidation (C5 to C10). The addition of the decoy molecules to the wild-type and the rate accelerating mutants of CYP102A1 boosted the substrate oxidation rates even further. However, the levels of cycloalkanol product decreased with the larger alkanes when the decoy molecules were used with the variant A74G/F87V/L188Q, which contained mutations within the substrate binding pocket. For the majority of the enzymes and PFC decoy molecule combinations the highest levels of oxidation were obtained with cyclooctane. When larger second generation decoy molecules, based on modified amino acids were utilised there was a significant improvement in the oxidation of the smaller cycloalkanes by the wild-type enzyme and one other variant. This resulted in significant improvements in biocatalytic oxidation of cyclopentane and cyclohexane. However, the use of these optimised decoy molecules did not significantly improve cycloalkane oxidation over the fluorinated fatty acid derivatives when combined with the best rate accelerating variant, R47L/Y51F/I401P. Overall our approach enabled the cycloalkanes to be oxidised 300- to 8000-fold more efficiently than the wild-type enzyme at product formation rates in excess of 500 and up to 1700 nmol·nmol-CYP^{-1}·min^{-1}.

1. Introduction

Cyclic alcohols are important building blocks for the production of valuable industrial chemicals such as cyclohexanol which is used in the production of Nylon-6,6 [1,2]. The direct oxidation of cycloalkanes as a primary step for preparing the corresponding alcohols is therefore of significant interest [1]. The high stability of saturated C—H bonds in alkanes makes these compounds unreactive and they require forcing conditions such as high temperature and pressure, or a reactive oxidant in order to proceed [3,4]. Various organic and inorganic methods have been used to facilitate the oxidation of cycloalkanes [5–7]; nevertheless these reactions remain challenging. The catalysts used in these chemical methods can be expensive, cannot be recovered or reused or proceed with low selectivity and the reactions often undergo further undesired oxidation. In addition these catalysts are often toxic and have an adverse impact on the environment [8].

Enzymatic approaches for C—H hydroxylation have emerged as an alternative method for alkane and cycloalkane oxidation [8–13]. Efficient enzyme biocatalysis for these processes would benefit industry and the environment as they occur under mild conditions in aqueous media. Taking advantage of enzymes as biocatalysts could overcome many of the hurdles of chemocatalysts, namely the expense, poor selectivity and environmental toxicity [13,14]. The cytochrome P450 heme monooxygenases (CYPs) are often Nature's enzyme of choice when selective oxidation of a complex substrate is required. They catalyse the hydroxylation of unreactive C—H bonds at ambient temperature and pressure using a reactive compound I iron-oxo species [15–24].

The CYP102A1 enzyme (P450Bm3) has often been employed as a biocatalyst to catalyse hydroxylation reactions [25–29]. This enzyme was discovered in the 1970s by Fulco, it was the third enzyme isolated from *Bacillus megaterium* and as such was named Bm3 [30,31]. CYP102A1 is one of the most utilised P450 enzyme systems due to its high activity, solubility and self-sufficient nature. The electron

* Corresponding author.
E-mail address: stephen.bell@adelaide.edu.au (S.G. Bell).

https://doi.org/10.1016/j.jinorgbio.2018.03.001
Received 20 December 2017; Received in revised form 1 March 2018; Accepted 1 March 2018
Available online 04 March 2018

transferring reductase domain is fused to the heme domain and it only needs the cofactor nicotinamide adenine dinucleotide phosphate (NADPH) and dioxygen to function [29]. Fatty acids of carbon chain length 12–15 are good substrates for this enzyme and hydroxylation of the acids occurred at subterminal position (ω-1 to ω-3) [29,31]. Cycloalkanes are not the natural substrates of CYP102A1 therefore the enzyme must be modified to find conditions under which their hydroxylation will occur. Enzyme engineering by altering the amino acid sequences has been used to exploit this enzyme for alkane oxidation [25–27]. Two broad approaches have been utilised to adapt CYP102A1. The first makes changes in the substrate binding pocket (rational mutagenesis) [29,32,33] and the second involves directed evolution or random mutagenesis with a suitable screening method [28,34–36].

Another approach which has been applied to enhance CYP102A1 biocatalysis is the use of decoy molecules [37]. These are inert dummy substrates which promote the catalytic activity of the enzyme [38]. Perfluorocarboxylic acids (PFCs) have been used with CYP102A1 with promising results for small alkanes, including cyclohexane, and benzene [39]. The binding of the PFCs, which resemble the natural fatty acid substrates, initiates conformational changes in the heme domain enhancing substrate hydroxylation. The PFCs leave enough space in the substrate binding pocket for an additional molecule to bind. The decoys also appear to compel the substrates to bind more closely to the heme centre and facilitate the exclusion of water molecules. This is reflected in a lower proportion of the reducing equivalents being channelled into uncoupling pathways and resulted in higher levels of hydroxylation [39]. The use of decoy molecules can be combined with mutated variants to oxidise unnatural substrates with high catalytic productivity [39–41]. Second generation decoy molecules based on PFC modified L-amino acids (e.g. PFC9-L-Ala; *N*-perfluorononanoyl-L-alanine) have recently been synthesised to further enhance the activity of small molecules, such as propane. These bind to CYP102A1 with higher affinity than the PFCs. A crystal structure of the *N*-perfluorononanoyl-L-tryptophan (PFC9-L-Trp) bound CYP102A1 heme domain has been obtained which revealed the conformational changes that are induced within the enzyme (Fig. 1) [42].

Here we use decoy molecules in combination with the wild-type (WT) enzyme and four engineered variants of CYP102A1 for the hydroxylation of differently sized cycloalkanes. Three of the variants employed KT2 (A191T/N239H/I259V/A276T/L353I), R19 (R47L/Y51F/H171L/Q307H/N319Y) and RP (R47L/Y51F/I401P) are rate accelerating forms of the enzyme, generated by random or rational mutagenesis or a combination of both [43,44]. These have higher activity with non-natural substrates, including alkanes, but maintain the selectivity of the WT enzyme [39–41]. The substrate free forms of the KT2 and I401P mutants have structural conformations which more closely resemble the fatty acid bound form of the enzyme. This, in combination with a longer heme-iron axial water length, results in substrate induced conformational changes playing a less significant role in promoting the catalytic cycle and enables the enhanced oxidation of non-natural substrates [43,44]. The arginine 47 and tyrosine 51 residues, which have been altered in the R19 and RP variants, form hydrophilic interactions with fatty acid substrates and the changes render the active site more hydrophobic [28]. The combination of this pair of mutations with the rate accelerating mutation found in the R19 and RP variants have been shown to favour the hydroxylation of hydrophobic substrates [39–41]. This has been shown to enhance the oxidation of hydrophobic substrates but could reduce the effectiveness of the acid derived decoy molecules [28,43]. The fourth variant GVQ (A74G/F87V/L188Q) was obtained from site saturation mutagenesis of three residues located in the active site or substrate access channel of CYP102A1 [25,45,46]. This variant increased the activity of the enzyme for hydrophobic substrates but can change the selectivity of oxidation as the modifications are in the active site of the enzyme [25,47]. By using both first and second generation decoy molecules with smaller and larger cycloalkanes than cyclohexane we set out to gain a better understanding of the relationship between the size and shape of the decoy molecule and substrate to the performance of the enzyme catalysed oxidations.

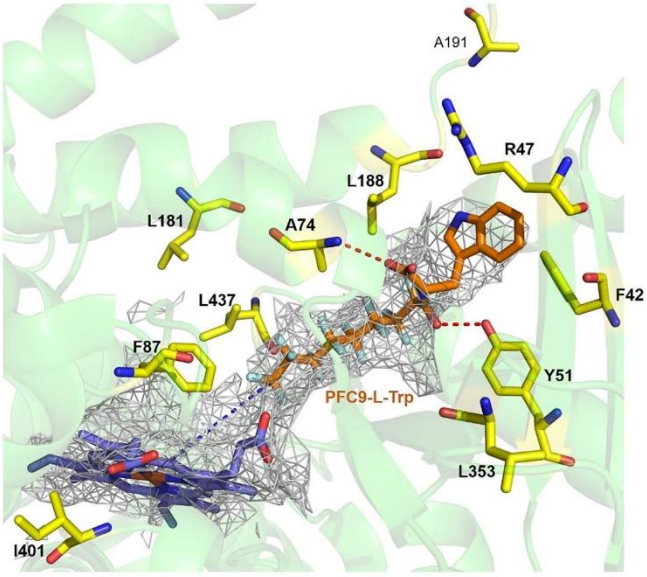

Fig. 1. The crystal structure of CYP102A1 with PFC9-L-Trp decoy molecule (PDB: 3WSP), the access channel (grey wireframe) and hydrophobic or mutated residues (yellow) are shown. The hydrogen bond between PFC9-L-Trp/Y51 and PFC9-L-Trp/A74 (dashed line) and the distance between PFC9-L-Trp and heme domain (dashed line) have been indicated.

2. Experimental

2.1. General

General reagents, organics and the PFC decoy molecules were obtained from Sigma-Aldrich, TCI, Fluorochem, Acros or VWR. The second generation decoy molecules, derived from amino acids were synthesised as described previously [42]. Buffer components, and isopropyl-β-D-thiogalactopyranoside (IPTG) were from Astral Scientific (Australia). The CYP102A1 enzyme and mutants were prepared as described previously (Supplementary information) [28]. UV/Vis spectroscopy was performed on an Agilent Cary 60 spectrophotometer. Gas chromatography was carried out on a Shimadzu Tracera GC coupled to Barrier discharge Ionization Detector (BID) detector using a Supelcowax column (30 m × 0.32 mm × 0.25 μm) and helium as the carrier gas. For cyclopentane and cyclohexane the oven temperature was held at 60 °C for 3 min then increased at 5 °C min^{-1} to 120 °C and maintained for 2 min then increased at 25 °C min^{-1} to 220 °C. For cyclooctane and cyclodecane the oven temperature began at 100 °C for 3 min then increased at 8 °C min^{-1} to 220 °C and held at this temperature for a further 2 min. The injector and detector temperature were 250 °C and 270 °C, respectively. Gas Chromatography-Mass Spectrometry (GC–MS) data were collected on a Shimadzu GC-2010 coupled to a GC–MS-QP2010S detector. Both were equipped with a DB-5 MS fused silica column (30 m × 0.25 mm, 0.25 μm). The injector and interface were maintained at a constant temperature of 250 °C and 280 °C. The oven temperature was held at 60 °C for 1 min and then increased at 10 °C min^{-1} up to 200 °C and it was maintained for 5 min. The product GC–MS/GC retention times were as follows: cyclopentanol, 1.8/5.7 min; cyclohexanol 3.3/7.8 min; cyclooctanol 7.3/8.3 min and cyclodecanol 10.9/10.8 min.

2.2. Substrate turnover assays

NADPH turnover assays (final volume 1200 μL) were performed at 30 °C in Tris buffer (pH 7.4, 50 mM). The buffer was oxygenated before the addition of the other components, including 0.2 μM enzyme and 120 μg bovine liver catalase. Assays were sustained at 30 °C for 1 min prior to the addition of the decoy molecule (100 μM) and the substrate (1 mM) followed by NADPH (from a 20 mg mL^{-1} stock, to a final concentration of ~320 μM; equivalent to 2 AU). A period of 10 s was allowed to elapse after cofactor addition before quantitating the NADPH oxidation rate by monitoring the decrease in the absorbance at 340 nm. The reactions were allowed to run until all the reducing equivalents were consumed. The NADPH turnover rate was derived using $\varepsilon 340 = 6.22\ mM^{-1}\ cm^{-1}$.

2.3. Extraction and GC analysis

Before extraction 200 μM of a *p*-cresol internal standard (10 μL of a 20 mM stock solution) was added, to 990 μL of the turnover. This mixture was then extracted with 400 μL ethyl acetate and the layers separated via centrifugation at 12000*g* for 3 min. The extract was analysed by GC and a calibration curve was obtained in order to quantify the amount of product in each reaction. All the products were identified by coelution with authentic standards and MS analysis. The fatty acids turnovers were extracted, derivatised and analysed by GC–MS as described previously [48].

2.4. Substrate docking experiments

The X-ray crystal structures of the PFC9-L-Trp bound and substrate free forms of the heme domain of WT CYP102A1 (PDB: 3WSP and 1BU7, respectively) were used as the initial template. Compound I was modelled from the heme and the oxygen atom of the axial ligand was placed 1.65 Å above the Fe atom by Maestro [49]. The protons of histidine residues were estimated by Proteins Preparation Wizard of Maestro. The structures of ligands for docking simulation were finalised using AutoDockTools [50]. The docking site was defined as the whole protein for the initial search of the ligand binding site, or as 20 Å × 20 Å × 20 Å from substrate binding pocket for other studies. The docking simulations were performed by AutoDock Vina [51]. After each simulation, hydrogen atoms of the cycloalkane ligands were added, and the distances between ligand atoms and those of Compound I were analysed by Maestro. The model of the GVQ (A74G/F87V/L188Q) mutant was prepared by mutation of the WT structure (PDB: 1BU7) using PyMol Mutagenesis Wizard based on the M11 (R47L/E64G/F81I/F87V/E143G/L188Q/Y198C/E267V/H285Y/G415S; PDB: 5E9Z) [52] and PM (R47L/F87V/L188Q/E267V/F81I; PDB: 4ZF6) mutant crystal structures [53].

3. Results and discussion

3.1. Cycloalkane oxidation by CYP102A1 variants

The heme domain in CYP102A1 is a funnel shaped shaft surrounded by hydrophobic residues, including Phe-42, Phe-87, Leu-181 and Leu-437, and is suited to the oxidation of medium to long chain fatty acids (Fig. 1). The WT enzyme was able to oxidise all the tested cycloalkane substrates, cyclopentane through to cyclodecane (Fig. 2 and Table 1). In all instances a single product arising from hydroxylation was observed (Scheme 1). However, the amount of product and the rate it was generated at was very low with the maximum activity observed for cyclooctane oxidation; 2.9 ± 0.7 nmol·nmol-CYP^{-1}·min^{-1} (henceforth abbreviated to min^{-1}). All four of the CYP102A1 variants tested resulted in increased levels of oxidation product across the cycloalkanes. For all the cycloalkanes the RP variant resulted in the highest product formation rate. The trends in the remaining mutants did show variation depending on the substrate (Table 1). For example, the GVQ variant, which should increase the size of the substrate binding pocket was an improved biocatalyst for cyclodecane oxidation compared to R19 and KT2 (Table 1). However, the R19 mutant was better at oxidising both cyclooctane and cyclohexane than GVQ (Table 1).

The size of the cycloalkane substrate had a significant effect on the rate of product formation. The highest turnover rate, up to 1050 min^{-1}, observed for all the variants, including GVQ, was with cyclooctane (Table 1). The maximum activity for both cyclohexane and cyclodecane being 411 and 283 min^{-1}, respectively. The product formation rate with the smallest substrate cyclopentane was significantly slower, with the highest observed being 62 min^{-1}. Overall; by using a selection of CYP102A1 variants we were able to improve the product formation rates of cycloalkane oxidation from 160-fold for cyclodecane to 1500-fold for cyclohexane (Table 1). We also tested cyclododecane with our variants in the presence and absence of decoy molecules but little or no oxidation metabolites were observed (data not shown). The rate accelerating variants all enhanced the oxidation of the hydrophobic cycloalkane over the WT enzyme. This presumably arises due to a combination of the conformation changes that these mutations have been shown to induce and increased hydrophobicity of the substrate access channel. The R19 and RP variants, which contain the Arg47Leu and Tyr51Phe mutations, located at the entrance to the substrate access channel to allow easier access of hydrophobic substrates, were the most active variants (Table 1).

3.2. The effect of PFC decoy molecules on cycloalkane oxidation

Next we assessed if cycloalkane oxidation could be improved using PFC based decoy molecules (PFC8, PFC9 and PFC10; perfluoroctanoic acid, perfluornonanoic acid and perfluordecanoic acid) [37,39]. The addition of PFCs enhanced the productive turnover of the WT enzyme with all four cycloalkanes (Fig. 2 and Table 1). In agreement with previous results, the greatest increases in the product formation rate for

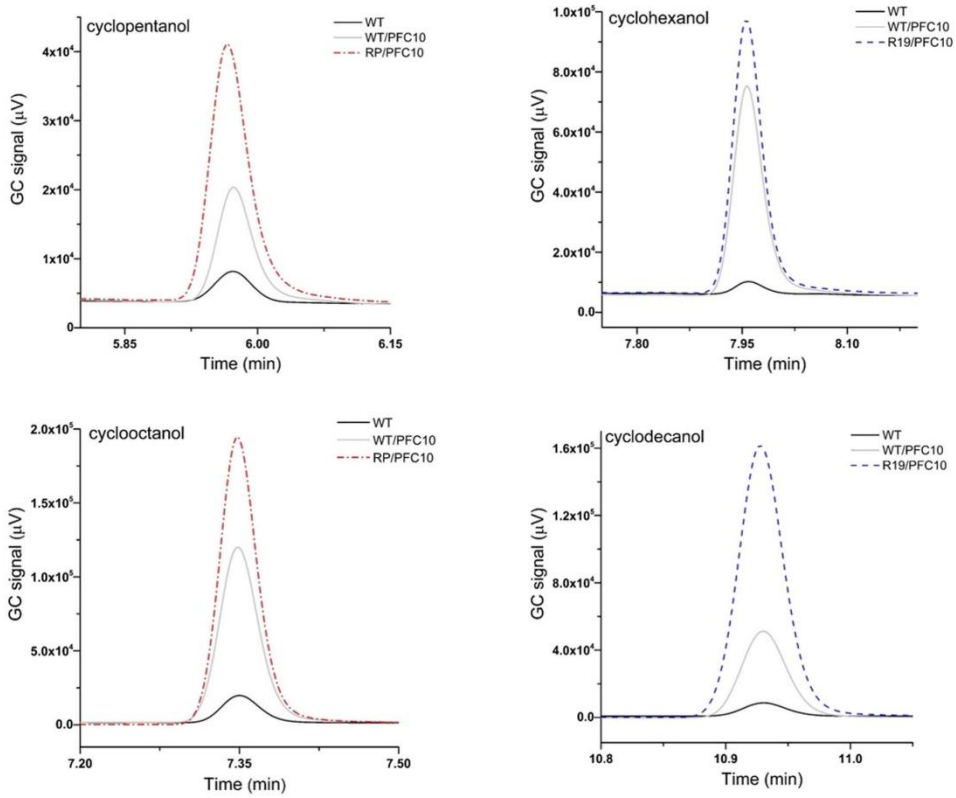

Fig. 2. GC analysis of turnovers of cyclopentane, cyclohexane, cyclooctane and cyclodecane with WT (solid black), WT/PFC10 (grey) and the optimised variant/PFC for each substrate. The optimal biocatalyst combination for cyclopentane and cyclooctane is RP/PFC10 (red dash dot) while R19/PFC10 (blue dash) generated more products with cyclohexane and cyclodecane (full data provided in Table 1). (For interpretation of the references to color in this figure legend, the reader is referred to the web version of this article.)

all the substrates were observed with PFC9 and PFC10. It is of note that the catalytic turnover with PFC10 was substantially higher than that achieved when using PFC9 for the smaller cycloalkanes (Table 1). The results obtained with these two decoy molecules and the larger cyclooctane and cyclodecane substrates were comparable (Table 1). The overall product formation rates obtained for the WT enzyme combined with these first generation decoy molecules was lower than with the mutant forms of CYP102A1, e.g. 204 min^{-1} for cyclooctane oxidation by the WF/PFC10 combination versus 1050 min^{-1} for the RP variant alone (Table 1).

The addition of these fatty acid based PFC decoy molecules also upgraded cycloalkane oxidation with the KT2, R19 and the RP variants. With the R19 and RP variants the PFC10 decoy molecule also resulted in the highest turnover rates. The KT2/PFC9 combination was better than that with PFC10 for all the cycloalkanes (Fig. 3 and Table 1). This suggested that changes in the conformation or structure of the mutant enzymes may affect the decoy molecule/substrate preference and therefore the overall activity.

The addition of the decoy molecules resulted in differing levels of enhancement with each CYP102A1 mutant compared to the oxidation activity of the variant itself. In all instances the magnitude of the upturn in the product formation rates was lower than those observed with the WT enzyme (Table 1). Across all substrates the improvement observed with KT2 was greater than that of the R19 and RP variants. The latter two CYP102A1 mutants contain the RLYF double mutation at the entrance to the substrate access channel and also have higher innate product formation activities with the cycloalkanes. Despite the lower relative levels of enhancement compared to WT and KT2, the combination of the decoy molecules with the R19 or RP variants resulted in the highest oxidation rates (Fig. 3 and Table 1). The R19/PFC10 combination generated the maximum rate of hydroxylation with cyclodecane and cyclohexane while the addition of PFC10 to the RP variant brought about the highest activities with cyclopentane and cyclooctane (Fig. 3 and Table 1).

As with the WT enzyme the majority of the CYP102A1 variant and decoy molecule combinations hydroxylated cyclooctane more effectively than the other cycloalkanes. Cyclopentane or cyclodecane oxidation occurred with the lowest efficiency depending on the combination used. The exception was the KT2 variant, which when coupled with certain decoy molecules, catalysed cyclohexane oxidation more rapidly than cyclooctane under the assay conditions (Table 1). Cyclopentane oxidation peaked at 200 min^{-1}, a > 3000-fold improvement over the WT enzyme. Cyclohexane oxidation with the R19 and PFC10 decoy molecule occurred at a rate of 938 min^{-1}. The improvements achieved with cyclodecane and cyclooctane were more modest being, 300-fold (524 min^{-1}) and 560-fold (1700 min^{-1}), respectively. Importantly, for the best CYP102A1 variant/decoy molecule combinations the coupling efficiency, which is a measure of the productive use of the NADPH

Table 1
NADPH consumption and product formation rates of cycloalkane turnovers with WT CYP102A1 and the rate accelerating variants with and without the presence of the first generation of decoy molecules (PFC8, PFC9 and PFC10 are abbreviated to 8, 9 and 10 respectively). Coupling efficiency which is the percentage of NADPH utilised for the formation of cycloalkanol products are also provided. NADPH oxidation rate (NADPH) and product formation rate (PFR) are reported as mean ± S.D. ($n \geq 3$) and given in nmol(nmol-CYP)$^{-1}$ min^{-1}. The optimal decoy molecule has been highlighted for each enzyme/cycloalkane combination in bold.

	Cyclopentane			Cyclohexane[a]			Cyclooctane			Cyclodecane		
	NADPH	Coupling	PFR	NADPH	Coupling	PFR	NADPH	Coupling	PFR	NADPH	Coupling	PFR
WT	17 ± 0.7	1 ± 0.1	0.15 ± 0	20 ± 2	1.2 ± 0.2	0.3 ± 0.1	53 ± 3	6 ± 1	3 ± 0.8	61 ± 1	3 ± 0.6	1.7 ± 0.1
WT/8	77 ± 1	2 ± 0.1	1.76 ± 0.1	94 ± 3	35 ± 2	33 ± 2	145 ± 17	63 ± 5	91 ± 4	83 ± 1	25 ± 0.1	20 ± 1
WT/9	87 ± 3	5 ± 1	4 ± 0.2	175 ± 6	49 ± 2	85 ± 6	309 ± 12	64 ± 0.5	197 ± 7	118 ± 4	29 ± 2	34 ± 1
WT/10	**257 ± 2**	**13 ± 0.4**	**45 ± 1**	**443 ± 10**	**33 ± 3**	**144 ± 10**	**438 ± 23**	**47 ± 4**	**204 ± 18**	**249 ± 10**	**15 ± 1**	**37 ± 2**
R19	76 ± 4	5 ± 1	3 ± 0.1	594 ± 21	60 ± 2	355 ± 18	964 ± 7	74 ± 1	708 ± 3	196 ± 18	37 ± 2	72 ± 2
R19/8	133 ± 6	7 ± 1	9 ± 0.9	741 ± 34	56 ± 1	416 ± 24	1170 ± 13	76 ± 3	885 ± 26	656 ± 9	41 ± 2	271 ± 20
R19/9	205 ± 4	15 ± 0.4	32 ± 1.5	710 ± 35	56 ± 2	402 + 22	1260 ± 21	72 ± 1	906 ± 18	835 ± 24	44 ± 2	367 ± 18
R19/10	**575 ± 7**	**25 ± 2**	**142 ± 9**	**1620 ± 10**	**58 ± 1**	**938 ± 20**	**1700 ± 10**	**75 ± 1**	**1280 ± 20**	**1180 ± 10**	**44 ± 1**	**524 ± 9**
RP	352 ± 14	18 ± 0.3	62 ± 3	1210 ± 20	34 ± 1	411 ± 2	1570 ± 46	67 ± 1	1050 ± 20	807 ± 11	35 ± 2	283 ± 16
RP/8	965 ± 28	37 ± 3	359 ± 17	1490 ± 6	42 ± 2	631 ± 26	2060 ± 24	74 ± 0.3	1530 ± 20	932 ± 18	38 ± 2	357 ± 26
RP/9	1140 ± 43	42 ± 2	481 ± 40	1520 ± 40	40 ± 0.4	609 ± 15	2030 ± 17	75 ± 0.2	1520 ± 10	1100 ± 14	39 ± 1	423 ± 14
RP/10	**1180 ± 40**	**42 ± 1**	**501 ± 33**	**1940 ± 20**	**38 ± 1**	**741 ± 15**	**2100 ± 30**	**81 ± 2**	**1700 ± 30**	**1200 ± 30**	**38 ± 3**	**451 ± 42**
KT2	131 ± 8	17 ± 0.7	23 ± 2	244 ± 4	29 ± 1	70 ± 2.7	231 ± 6	45 ± 2	104 ± 1	116 ± 1	27 ± 1	31 ± 1
KT2/8	341 ± 10	34 ± 0.2	117 ± 8	912 ± 36	52 ± 2	478 ± 27	909 ± 14	57 ± 2	518 ± 18	595 ± 21	39 ± 1	233 ± 1
KT2/9	**901 ± 16**	**44 ± 3**	**426 ± 27**	**1590 ± 40**	**45 ± 2**	**714 ± 54**	**1160 ± 20**	**54 ± 2**	**627 ± 24**	**1090 ± 20**	**28 ± 2**	**308 ± 15**
KT2/10	1340 ± 30	34 ± 0.4	397 ± 4	1960 ± 20	27 ± 3	538 ± 51	1450 ± 10	33 ± 0.3	473 ± 4	1740 ± 20	11 ± 0	185 ± 4
GVQ	100 ± 4	4 ± 0.4	3.3 ± 0.1	323 ± 28	25 ± 2	81 ± 9	**660 ± 22**	**51 ± 1**	**339 ± 9**	**1010 ± 40**	**24 ± 1**	**241 ± 8**
GVQ/8	862 ± 15	5 ± 0.1	40 ± 1	855 ± 21	19 ± 1	166 ± 14	988 ± 24	32 ± 2	319 ± 19	1050 ± 30	20 ± 1	208 ± 15
GVQ/9	**1490 ± 30**	**4 ± 0.3**	**159 ± 3**	**1980 ± 50**	**9 ± 0.4**	**183 ± 7**	1310 ± 10	12 ± 0.5	164 ± 8	1180 ± 60	9 ± 0.6	110 ± 4
GVQ/10	1530 ± 50	2 ± 0.1	27 ± 1	1660 ± 30	5 ± 0.7	75 ± 10	1760 ± 20	6 ± 1	110 ± 11	1580 ± 20	5 ± 0.1	72 ± 1

[a] The oxidation of cyclohexane by the WT and KT2 variants PFC decoy molecule have been reported previously [39].

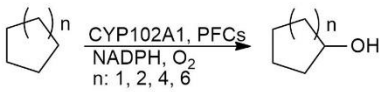

Scheme 1. Production of cyclic alcohols by CYP102A1.

cofactor, was high e.g. 81% for cyclooctane and RP/PFC10. The coupling efficiency of cyclooctane oxidation tended to be higher than for the other cycloalkanes inferring this substrate was able to bind in the active site so that the C–H bonds are readily available for abstraction. The concerted effect of the CYP102A1 variants and decoy molecules resulted in a greater degree of enhancement with the smaller substrates. This increased the product formation rate of cyclohexane (> 3000-fold improvement) to surpass that of cyclodecane in their best turnovers (Table 1).

3.3. The effect of PFC decoy molecules on cycloalkane oxidation by the GVQ variant

The effect of the decoy molecules with the GVQ mutant differed from those observed with the other variants. The addition of all three decoy molecules resulted in a modest enhancement of cyclopentane oxidation, with the GVQ/PFC9 combination yielding the highest product formation rate (59 ± 3.3 min^{-1}, Table 1). Only PFC8 and PFC9 improved the catalytic performance of cyclohexane oxidation but in these instances the coupling efficiency of the turnover decreased (Table 1). The decoy molecules diminished the amount of product generated with cyclooctane (Fig. 3 and Fig. S1) and cyclodecane. With these larger substrates the shorter PFC8 decoy molecule had less of a detrimental effect on the levels of product formation (Table 1).

The GVQ variant is the only form of CYP102A1 tested in this work which has mutations in the substrate binding pocket/access channel of the enzyme close to the heme. This could have a significant effect on how the fatty acid based decoy molecules interact and therefore bind to the enzyme. The Phe87 residue has been shown to have a prominent role in substrate binding in CYP102A1 [28,46,54,55]. To assess if the GVQ variant alters the binding of the fatty acid molecules we investigated the oxidation of decanoic, dodecanoic and tetradecanoic acids. The GVQ variant altered the product distribution of dodecanoic and tetradecanoic acids compared to the WT enzyme (Table 2 and Fig. S2). In the GVQ variant the hydroxylation was shifted away from the ω-terminus which suggested that the fatty acids were bound differently compared to the WT enzyme and that a greater proportion of the subterminal carbons of the fatty acid chain were located over the heme iron. This mutant was also able to oxidise decanoic acid whereas the WT enzyme was only capable of generating a trace amount of the hydroxylated metabolites (Table 2 and Fig. S2).

These results confirm that the GVQ variant binds fatty acid like molecules in a different manner than the WT enzyme. Therefore one plausible explanation for the different effect of the decoy molecules with the GVQ variant is that the altered PFC binding orientation results in the decoy molecules, which contain strong unreactive C–F bonds, being positioned in between the cycloalkane substrate and the heme. While this enabled turnover of the P450 catalytic cycle it reduced productive cycloalkanol formation (Table S1). In an effort to assess if other decoy molecules could improve the productivity of the GVQ mutant we examined the oxidation of cyclooctane with PFC3 through to PFC7 as well as 4-fluoro- and pentafluoro-benzoic acid (Fig. 4). None of these molecules stimulated the NADPH oxidation rate or the level of product formation above that of the GVQ variant alone (Table S1).

3.4. The effect of second generation decoy molecules on cycloalkane oxidation

It is worth noting that PFC8 to PFC10 have been shown to be the optimal fatty acid derived decoy molecules and that shorter and longer versions, such as PFC11 (perfluoroundecanoic), reduce the activity of oxidation [37]. In an effort to explore how the structure of the coadditive effects cycloalkane hydroxylation in more detail we utilised second generation decoy molecules which are based on PFCs modified with L-amino acids, PFC9-L-Ala, PFC9-L-Leu and PFC9-L-Phe (*N*-perfluorononanoyl-L-alanine, *N*-perfluorononanoyl-L-leucine and *N*-perfluorononanoyl-L-phenyalanine Fig. 4) [42]. These molecules bind to WT CYP102A1 with higher affinity than the PFC decoys and their use allowed CYP102A1 to catalytically hydroxylate the small gaseous

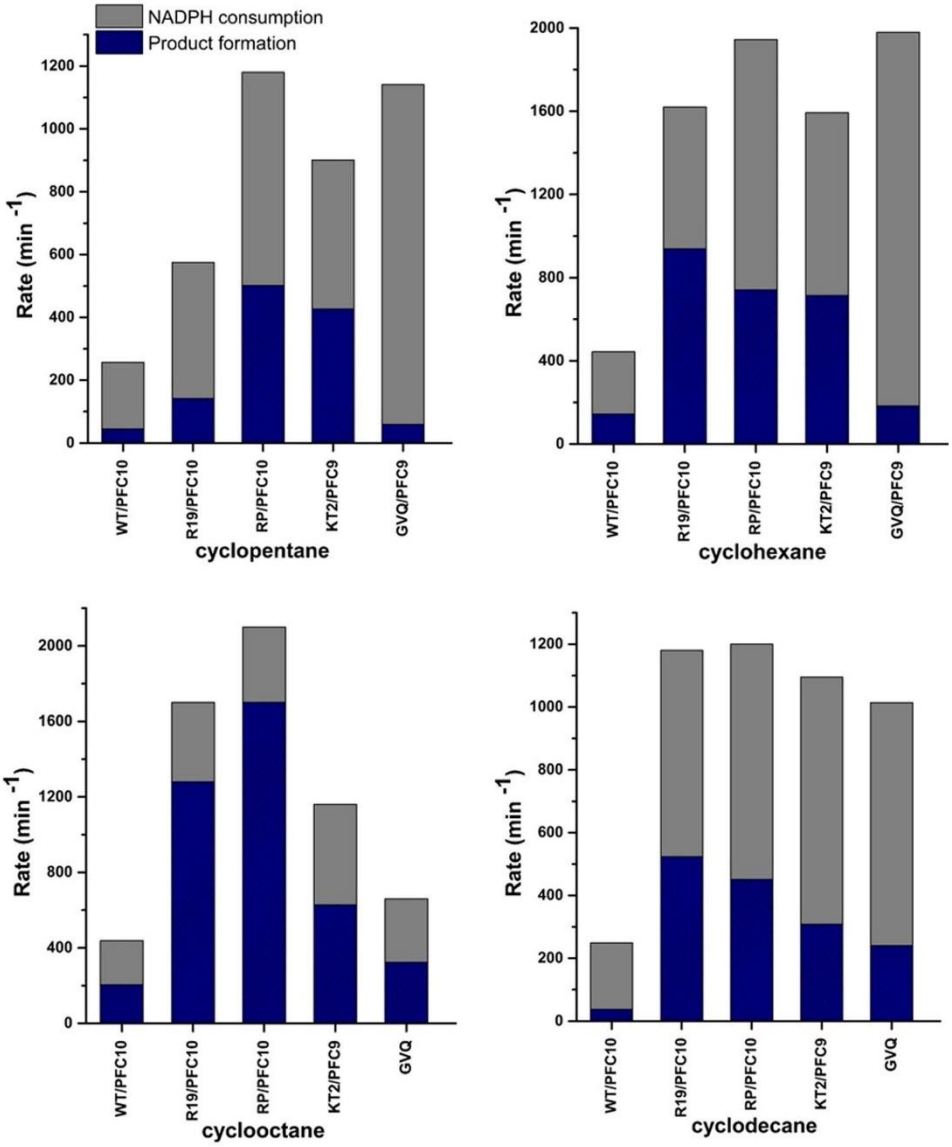

Fig. 3. NADPH oxidation (grey) and product formation rates (blue-lined) of the optimal combination of the PFC decoy molecules with CYP102A1 WT and its variants for cyclopentane, cyclohexane, cyclooctane and cyclodecane hydroxylation. NADPH oxidation and product formation rates are reported as the mean ($n \geq 3$) and given in nmol(nmol-CYP)$^{-1}$ min^{-1} (full data provided in Table 1). (For interpretation of the references to color in this figure legend, the reader is referred to the web version of this article.)

alkanes ethane and propane [42]. When combined with the WT enzyme these second generation molecules also enhanced the rate of NADPH oxidation in the cycloalkane turnovers above those obtained with the first generation PFC decoy molecules (Table S2). The improvements in the coupling efficiency and the product formation rate with the larger C8 and C10 cycloalkanes were modest (Table S2). However, a marked upturn in the coupling efficiency, and therefore the overall product formation rate, was observed with cyclopentane and cyclohexane (Fig. 5). The rate of product formation when the PFC9-L-Phe decoy molecule was added to the WT enzyme was the greatest for both of these cycloalkanes (Fig. 5 and Table S2), resulting in a 21-fold improvement over the PFC10 decoy molecule with cyclopentane (PFR 949 ± 35 min^{-1}) and a 5-fold enhancement with cyclohexane (PFR 725 ± 46 min^{-1}).

Table 2
Product distribution of fatty acids oxidation by CYP102A1 WT and GVQ variants. Very little product was formed with the WT and decanoic acid (Fig. S2).

Fatty acid	%Product	WT	GVQ
Tetradecanoic acid	ω-1	48	7
	ω-2	25	16
	ω-3	24	31
	ω-4	1	16
	ω-5	0.5	25
	ω-6	1	5
Dodecanoic acid	ω-1	37	26
	ω-2	28	37
	ω-3	35	34
	ω-4	0	1
	ω-5	0	2
Decanoic acid	ω-1	–	55
	ω-2	–	22
	ω-3	–	23

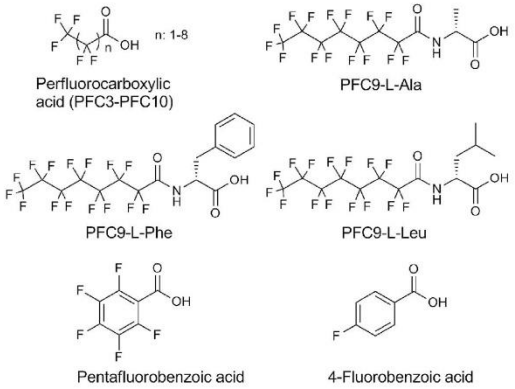

Fig. 4. The structures of the decoy molecules used in this study.

The second generation decoy molecules were also combined with the RP and KT2 variants to assess if they could enhance cycloalkane oxidation. The results were mixed and with cyclohexane the RP/PFC9-L-Ala couple was marginally better than the R19/PFC10 combination (1010 ± 10 versus 938 ± 20 min^{-1}, Fig. 5, Table 1 and S2). The hydroxylation of cyclopentane with RP was also improved using the second generation decoys over the best fluorinated fatty acid derived molecules (845 ± 21 versus 501 ± 33 min^{-1}, Table 1 and S2). Due to reduced coupling efficiency, the product formation rate with RP/PFC9-L-Ala (845 ± 21 min^{-1}) was lower than achieved with the WT/PFC9-L-Phe combination (Fig. 5 and Table S2). With the RP variant and the cyclooctane and cyclodecane substrates all the turnovers with the second generation decoys showed lower product formation than PFC10, with PFC9-L-Ala being the best. The difference between the productivity of the RP variant for cyclooctane and cyclodecane when partnered with the second generation decoy molecules compared to the smaller cycloalkanes is perhaps due to the bulkier nature of the decoy which may hamper access of the larger substrate in the narrow access channel of the enzyme (Fig. 1, Fig. S3 and Table S2). The crystal structure of the heme domain of CYP102A1 with the second generation decoy molecule PFC9-L-Trp bound revealed that Tyr51 formed a hydrogen bond with the amide carbonyl group of the decoy (Fig. 1). In the RP variant Tyr51 has been mutated to a phenylalanine and as a result the decoy molecule may bind in a different way. The second generation decoy molecules bind to WT CYP102A1 with different affinities which strengthen as the bulk of the side chain increases. With the removal of the Tyr51 residue the binding affinities with the variants may change [42]. Overall, PFC9-L-Ala was the best decoy molecule for all the cycloalkanes with RP in contrast to the WT enzyme which was better with PFC9-L-Phe or PFC9-L-Leu.

When the second generation decoy molecules were used with the KT2 variant the product formation rate for the oxidation of the smaller cycloalkanes increased dramatically. This was predominantly due to superior turnover the catalytic cycle, as measured by the NADPH oxidation rate. The upturn for the larger substrates was not as significant. As with the WT enzyme the PFC9-L-Phe combined with KT2 gave rise to the highest product formation rates for smaller cycloalkanes with PFC9-L-Leu being better with the larger. The formation rate of cyclopentanol and cyclohexanol with PFC9-L-Phe partnered with KT2 were the highest observed in this study, with the smaller substrates, and were

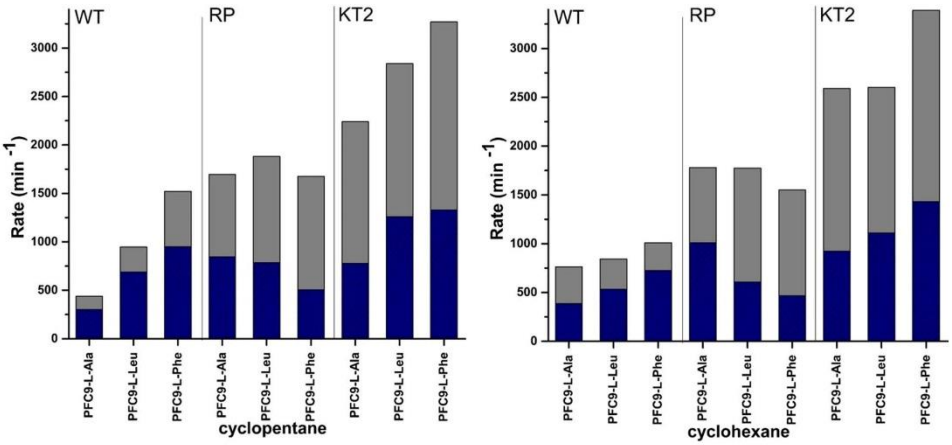

Fig. 5. NADPH oxidation (grey) and product formation rates (blue-lined) of turnovers of cyclopentane and cyclohexane with WT, RP and KT2 variants in combination with the second generation of decoy molecules. NADPH oxidation rate and product formation rate are reported as mean ($n \geq 3$) and given in nmol(nmol-CYP) $^{-1}$ min^{-1} (full data provided in Table S2). (For interpretation of the references to color in this figure legend, the reader is referred to the web version of this article.)

1330 ± 70 min^{-1} and 1430 ± 80 min^{-1}, respectively (Fig. 5 and Table S2). The combination of the second generation decoy molecules with the GVQ variant also diminished the oxidation activity of the enzyme (Table S1).

Overall our results show that combining decoy molecules and CYP102A1 variants resulted in increased rates and efficiency of cycloalkane oxidation. The rate accelerating variants and the decoy molecules are both hypothesised to, and have been shown by crystal structure analysis to, enable the enzyme to more readily access catalytically ready conformations resulting in increased productivity. They also appear to facilitate a favourable binding position for the cycloalkane substrate in relation to the heme which often resulted in an elevated coupling efficiency. The second generation decoy molecules seem to induce a greater effect on the WT and KT2 enzymes which resulted in more frequent turnover of the catalytic cycle. However with the RP variant these decoys were often not as effective as the PFC molecules or as they were with the WT and KT2 enzymes. Second generation decoy molecules of different size were more effective with the KT2 and WT enzymes compared to the RP and GVQ variants suggesting that they interact differently across the mutant forms of CYP102A1.

3.5. Substrate docking experiments in the presence of a second generation decoy molecule

We have hypothesised that the decoy molecules enable the cycloalkane substrates to bind closer to the heme-iron therefore enhancing their oxidation. To assess the validity of this hypothesis we performed docking experiments with WT CYP102A1 (PDB: 1BU7) and the available crystal structure of the *N*-perfluorononanoyl-L-tryptophan (PFC9-L-Trp) bound enzyme (PDB: 3WSP). In the WT enzyme the cyclohexane and cyclooctane preferentially bound in the substrate access channel close to the Ala74, Leu75 and Leu436 residues. The closest carbons of each were 5.9 Å and 6.8 Å from where the likely position of the oxygen of the reactive compound I intermediate would be located (Fig. 6 and Table S3). When the decoy molecule was present in the substrate access channel this position is no longer available and the cyclohexane molecule preferred to bind close to the heme in the active site between Ala264 and Phe87 (Fig. 6). The closest carbon of the cyclohexane and cyclohexane substrates were both now only 2.2 Å from the modelled position of the compound I oxygen and in an ideal position for C—H bond activation. Docking experiments with a model of the GVQ variant also showed that the position of the cyclohexane would be closer to the heme than in the WT. Both cyclohexane and cyclooctane occupied the space vacated by the F87V mutation and the closest carbon of each to the reactive oxygen for both was 3.4 Å. The docking experiments provide a rationale for the improved oxidation activity and coupling efficiency of the cycloalkane substrates in the presence of the decoy molecules and with the GVQ variant.

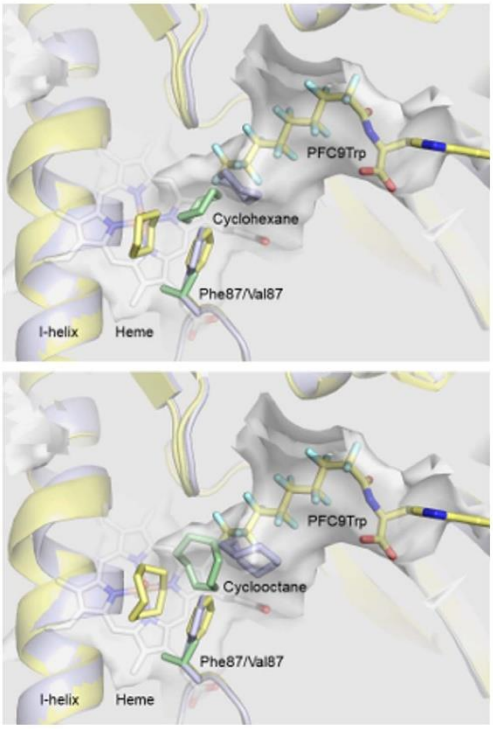

Fig. 6. Docking studies of cyclohexane (top) and cyclooctane (bottom) with WT CYP102A1 (purple), the GVQ variant of CYP102A1 (green) and the WT CYP102A1-PFC9-L-Trp complex (yellow). The location of the PFC9-L-Trp decoy molecule (PFC9Trp), the heme, the residue at 87 and the I-helix are highlighted.

4. Conclusion

Cycloalkanes bear little resemblance to the fatty acid based natural substrates of CYP102A1 but the activity of CYP102A1 towards these unnatural substrates was enhanced by utilising rate accelerating variants and decoy molecules. The best variants contained the R47L/Y51F mutations at the entrance of the substrate access channel (R19 and RP). Their combination with the first generation PFC10 decoy molecule provided high rates of hydroxylation. The addition of the decoy molecules to the R19 and RP variants had less of an impact compared to the innate product formation rate but still resulted in a significant enhancement in monooxygenase activity. The larger second generation decoy molecule PFC9-L-Phe boosted the productivity of the cyclopentane and cyclohexane turnovers of the WT enzyme and KT2 variant even further when compared to PFC10. The GVQ variant showed contradictory results and addition of decoy molecules reduced the level of product formation. This is most likely due to a different binding orientation of the PFC decoy molecule which hampers hydroxylation. That the highest productivity with larger substrates, such as cyclooctane and cyclodecane, could be achieved with the first generation decoys suggests that the CYP102A1 variants can accept molecules of moderate size in conjunction with the PFC molecules. The larger second generation decoy molecules enhanced biocatalysis with the smaller substrates to a significantly greater degree inferring that the active site is more restricted when these are bound to the enzyme. This work highlights that careful consideration and fine tuning of the enzyme variant, decoy molecule and substrate are required to optimise the catalytic activity. The combination of CYP102A1 variants and decoy molecules used here boosted the efficiency of cycloalkane oxidation by up to 8000-fold for the substrates tested.

Acknowledgements

S.G.B. acknowledges the ARC for a Future Fellowship (FT140100355). The authors also acknowledge the University of Adelaide International Postgraduate Award (for S.D.) and for a Priority Partner Grant (University of Nagoya). The authors thank Prof. Luet-Lok Wong (University of Oxford, UK) for the gene constructs of the CYP101A1 and CYP102A1 variants.

Abbreviations

CYP	cytochrome P450
PFC	perfluorocarboxylic acid
PFC8	perfluorooctanoic acid
PFC9	perfluorononanoic acid
PFC10	perfluorodecanoic acid
WT	wild-type CYP102A1
GVQ	A74G/F87V/L188Q mutant of CYP102A1
R19	R47L/Y51F/H171L/Q307H/N319Y mutant of CYP102A1
RP	R47L/Y51F/I401P mutant of CYP102A1
KT2	A191T/N239H/I259V/A276T/L353I mutant of CYP102A1
PFR	product formation rate
PFC9-L-Ala	*N*-perfluorononanoyl-L-alanine
PFC9-L-Leu	*N*-perfluorononanoyl-L-leucine
PFC9-L-Phe	*N*-perfluorononanoyl-L-phenylalanine

Appendix A. Supplementary data

Supplementary data to this article can be found online at https://doi.org/10.1016/j.jinorgbio.2018.03.001.

References

[1] U. Schuchardt, D. Cardoso, R. Sercheli, R. Pereira, R.S. da Cruz, M.C. Guerreiro, D. Mandelli, E.V. Spinacé, E.L. Pires, Appl. Catal. A 211 (2001) 1–17.
[2] R. Jevtic, P.A. Ramachandran, M.P. Dudukovic, Chem. Eng. Res. Des. 88 (2010) 255–262.
[3] R.H. Crabtree, Dalton Trans. (2001) 2437–2450.
[4] T. Newhouse, P.S. Baran, Angew. Chem. Int. Ed. Eng. 50 (2011) 3362–3374.
[5] A.E. Shilov, G.B. Shul'pin, Chem. Rev. 97 (1997) 2879–2932.
[6] N.M.F. Carvalho, A. Horn Jr., O.A.C. Antunes, Appl. Catal., A, 305 (2006) 140–145.
[7] M.D. Godbole, M.P. Puig, S. Tanase, H. Kooijman, A.L. Spek, E. Bouwman, Inorg. Chim. Acta 360 (2007) 1954–1960.
[8] F. Hollmann, I.W.C.E. Arends, K. Buehler, A. Schallmey, B. Bühler, Green Chem. 13 (2011) 226–265.
[9] S.C. Maurer, K. Kühnel, L.A. Kaysser, S. Eiben, R.D. Schmid, V.B. Urlacher, Adv. Synth. Catal. 347 (2005) 1090–1098.
[10] E. Weber, A. Seifert, M. Antonovici, C. Geinitz, J. Pleiss, V.B. Urlacher, Chem. Commun. 47 (2011) 944–946.
[11] A.R.H. Narayan, G. Jiménez-Osés, P. Liu, S. Negretti, W. Zhao, M.M. Gilbert, R.O. Ramabhadran, Y.-F. Yang, L.R. Furan, Z. Li, L.M. Podust, J. Montgomery, K.N. Houk, D.H. Sherman, Nat. Chem. 7 (2015) 653–660.
[12] E. Churakova, M. Kluge, R. Ullrich, I. Arends, M. Hofrichter, F. Hollmann, F. Angew, Chem. Int. Ed. Engl. 50 (2011) 10716–10719.
[13] A. Wells, H.-P. Meyer, vol. 6, Wiley-Blackwell, 2014, pp. 918–920.
[14] W.-D. Woggon, Acc. Chem. Res. 38 (2005) 127–136.
[15] E.M. Isin, F.P. Guengerich, Biochim. Biophys. Acta 1770 (2007) 314–329.
[16] D. Mansuy, Comp. Biochem. Physiol. C Pharmacol. Toxicol. Endocrinol. 121 (1998) 5–14.
[17] C.-H. Yun, K.-H. Kim, D.-H. Kim, H.-C. Jung, J.-G. Pan, Trends Biotechnol. 25 (2007) 289–298.
[18] V.B. Urlacher, S. Eiben, Trends Biotechnol. 24 (2006) 324–330.
[19] F.P. Guengerich, Nat. Rev. Drug Discov. 1 (2002) 359–366.
[20] R. Bernhardt, J. Biotechnol. 124 (2006) 128–145.
[21] M. Sono, M.P. Roach, E.D. Coulter, J.H. Dawson, Chem. Rev. 96 (1996) 2841–2888.
[22] J. Rittle, M.T. Green, Science 330 (2010) 933–937.
[23] I.G. Denisov, T.M. Makris, S.G. Sligar, I. Schlichting, Chem. Rev. 105 (2005) 2253–2277.
[24] C.M. Krest, E.L. Onderko, T.H. Yosca, J.C. Calixto, R.F. Karp, J. Livada, J. Rittle, M.T. Green, J. Biol. Chem. 288 (2013) 17074–17081.
[25] D. Appel, S. Lutz-Wahl, P. Fischer, U. Schwaneberg, R.D. Schmid, J. Biotechnol. 88 (2001) 167–171.
[26] Edgardo T. Farinas, U. Schwaneberg, A. Glieder, Frances H. Arnold, Adv. Synth. Catal. 343 (2001) 601–606.
[27] A. Glieder, E.T. Farinas, F.H. Arnold, Nat. Biotechnol. 20 (2002) 1135–1139.
[28] C.J. Whitehouse, S.G. Bell, H.G. Tufton, R.J. Kenny, L.C. Ogilvie, L.L. Wong, Chem. Commun. (2008) 966–968.
[29] C.J. Whitehouse, S.G. Bell, L.L. Wong, Chem. Soc. Rev. 41 (2012) 1218–1260.
[30] H. Schwalb, L. Owers Narhi, A.J. Fulco, Biochim. Biophys. Acta Gen. Subj. 838 (1985) 302–311.
[31] A.J. Fulco, Annu. Rev. Pharmacol. Toxicol. 31 (1991) 177–203.
[32] S.T. Jung, R. Lauchli, F.H. Arnold, Curr. Opin. Biotechnol. 22 (2011) 809–817.
[33] J.A. McIntosh, C.C. Farwell, F.H. Arnold, Curr. Opin. Chem. Biol. 19 (2014) 126–134.
[34] C.F. Oliver, S. Modi, M.J. Sutcliffe, W.U. Primrose, L.-Y. Lian, G.C.K. Roberts, Biochemistry 36 (1997) 1567–1572.
[35] J.B.Y.H. Behrendorff, W. Huang, E.M.J. Gillam, Biochem. J. 467 (2015) 1–15.
[36] M.W. Peters, P. Meinhold, A. Glieder, F.H. Arnold, J. Am. Chem. Soc. 125 (2003) 13442–13450.
[37] O. Shoji, T. Kunimatsu, N. Kawakami, Y. Watanabe, Angew. Chem. Int. Ed. Eng. 52 (2013) 6606–6610.
[38] O. Shoji, T. Fujishiro, H. Nakajima, M. Kim, S. Nagano, Y. Shiro, Y. Watanabe, Angew. Chem. Int. Ed. Eng. 46 (2007) 3656–3659.
[39] S.D. Munday, O. Shoji, Y. Watanabe, L.L. Wong, S.G. Bell, Chem. Commun. 52 (2016) 1036–1039.
[40] S.D. Munday, S. Dezvarei, S.G. Bell, ChemCatChem 8 (2016) 2789–2796.
[41] S.D. Munday, S. Dezvarei, I.C.K. Lau, S.G. Bell, ChemCatChem 9 (2017) 2512–2522.
[42] Z. Cong, O. Shoji, C. Kasai, N. Kawakami, H. Sugimoto, Y. Shiro, Y. Watanabe, ACS Catal. 5 (2015) 150–156.
[43] C.J. Whitehouse, S.G. Bell, W. Yang, J.A. Yorke, C.F. Blanford, A.J. Strong, E.J. Morse, M. Bartlam, Z. Rao, L.L. Wong, Chembiochem 10 (2009) 1654–1656.
[44] C.J. Whitehouse, W. Yang, J.A. Yorke, B.C. Rowlatt, A.J. Strong, C.F. Blanford, S.G. Bell, M. Bartlam, L.L. Wong, Z. Rao, Chembiochem 11 (2010) 2549–2556.
[45] H.M. Li, L.H. Mei, V.B. Urlacher, R.D. Schmid, Appl. Biochem. Biotechnol. 144 (2008) 27–36.
[46] Q.S. Li, U. Schwaneberg, P. Fischer, R.D. Schmid, Chem. Eur. J. 6 (2000) 1531–1536.
[47] C.-H. Chiang, R. Ramu, Y.-J. Tu, C.-L. Yang, K.Y. Ng, W.-I. Luo, C.H. Chen, Y.-Y. Lu, C.-L. Liu, S.S.F. Yu, Chem. Eur. J. 19 (2013) 13680–13691.
[48] S.D. Munday, N.K. Maddigan, R.J. Young, S.G. Bell, Biochim. Biophys. Acta 1860 (2016) 1149–1162.
[49] G.M. Sastry, M. Adzhigirey, T. Day, R. Annabhimoju, W. Sherman, J. Comput. Aided Mol. Des. 27 (2013) 221–234.
[50] G.M. Morris, R. Huey, W. Lindstrom, M.F. Sanner, R.K. Belew, D.S. Goodsell, A.J. Olson, J. Comput. Chem. 30 (2009) 2785–2791.
[51] O. Trott, A.J. Olson, J. Comput. Chem. 31 (2010) 455–461.
[52] L. Capoferri, R. Leth, E. ter Haar, A.K. Mohanty, P.D. Grootenhuis, E. Vottero, J.N. Commandeur, N.P. Vermeulen, F.S. Jorgensen, L. Olsen, D.P. Geerke, Proteins 84 (2016) 383–396.
[53] I. Geronimo, C.A. Denning, W.E. Rogers, T. Othman, T. Huxford, D.K. Heidary, E.C. Glazer, C.M. Payne, Biochemistry 55 (2016) 3594–3606.
[54] S. Graham-Lorence, G. Truan, J.A. Peterson, J.R. Falck, S. Wei, C. Helvig, J.H. Capdevila, J. Biol. Chem. 272 (1997) 1127–1135.
[55] M.A. Noble, C.S. Miles, S.K. Chapman, D.A. Lysek, A.C. MacKay, G.A. Reid, R.P. Hanzlik, A.W. Munro, Biochem. J. 339 (Pt 2) (1999) 371–379.

Efficient hydroxylation of cycloalkanes by co-addition of decoy molecules to variants of the cytochrome P450 CYP102A1

Shaghayegh Dezvarei,[a] Hiroki Onoda,[b] Osami Shoji,[b] Yoshihito Watanabe,[b] and Stephen G. Bell[a,*]

[a] *Department of Chemistry, University of Adelaide, Adelaide, 5005, Australia*

[b] *Department of Chemistry, Graduate School of Science, Nagoya University, Furo-cho, Chikusa-ku, Nagoya, 464-8602, Japan*

Supplementary Information

Protein production and purification

E. coli BL21 (DE3) transformed with pET28 which contains the relative gene for WT, KT2, R19 and RP variants and with pET11d containing GVQ gene. Plasmids (pET28 and pET11d) containing the relevant gene were transformed into *E. coli* BL21(DE3) competent cells and grown on an LB plate containing the relevant antibiotic. A single colony was used to inoculate 500 mL of 2xYT media containing trace elements solution ($CaCl_2$, $ZnSO_4.7H_2O$, $MnSO_4.H_2O$, Na_2-EDTA, $FeCl_3.6H_2O$, $CuSO_4.5H_2O$, and $CoCl_2.6H_2O$) and grown at 37 °C and 110 rpm. The incubation temperature was lowered to 18 °C for 30 min before the addition of 0.02 % v/v benzyl alcohol and 2 % v/v ethanol. After a further 30 min, protein expression was induced by the addition of 0.1 mM IPTG and the growth was continued for 18 – 24 h. The cell pellet was then harvested by centrifugation (5000 *g*, 10 min, 4 °C) and resuspended in 40 mM phosphate buffer (pH 7.4, 1 mM DTT) and lysed by sonication on ice (30 cycles with 20 s on, 40 s off). Cell debris was removed by centrifugation (37000 *g*, 20 min, 4 °C) and the protein containing supernatant was loaded onto a DEAE Sepharose column (XK50, 200 mm × 40 mm; GE Healthcare) and eluted using a linear salt gradient of 80 – 400 mM $(NH_4)_2SO_4$ in phosphate buffer. The red-coloured fractions were combined and concentrated by centrifugation (1900 *g*, 4 °C) using ultrafiltration (30 kDa membrane, Vivacell 100, Sartorius). The protein was then desalted using a Sephadex G-25 medium grain column (250 mm × 40 mm; GE Healthcare). After desalting the protein was concentrated to approximately 10 ml by ultrafiltration and was loaded onto a Source-Q ion-exchange column (XK26, 80 mm × 30 mm; GE Healthcare) using an AKTA purifier (GE Healthcare) and eluted using a linear salt gradient of 16 × phosphate buffer (0 – 35 %). Fractions giving an $A_{419}/A_{280} > 0.5$ were combined and concentrated by ultrafiltration. An equivalent volume of 80 % glycerol was added before the protein was filter-sterilised and stored at -20 °C.

Decoy	NADPH	% Coupling	PFR
GVQ	660 ± 22	51 ± 0	339 ± 9
PFC3	552 ± 5	46 ± 4	260 ± 21
PFC4	627 ± 46	49 ± 1	277 ± 42
PFC5	655 ± 20	49 ± 2	321 ± 14
PFC6	663 ± 28	46 ± 1	319 ± 7
PFC7	705 ± 24	45 ± 1	321 ± 17
PFC8	988 ± 24	32 ± 2	319 ± 19
PFC9	1310 ± 7	12 ± 1	164 ± 8
PFC10	1760 ± 24	6 ± 1	110 ± 11
4-fluorobenzoic acid	663 ± 28	42 ± 1	290 ± 7
perfluorobenzoic acid	621 ± 28	48 ± 1	297 ± 14
PFC9-L-Ala	1430 ± 16	5 ± 1	67 ± 11
PFC9-L-Leu	1050 ± 34	17 ± 1	179 ± 13
PFC9-L-Phe	1100 ± 23	19 ± 1	213 ± 10

Table S1 NADPH oxidation and product formation rate of cyclooctane oxidation with the GVQ variant combined with different decoy molecules. The coupling efficiency which is the percentage of NADPH utilised for the formation of cyclooctanol is also provided. NADPH oxidation rate (NADPH) and product formation rate (PFR) are reported as mean ± S.D. ($n \geq 3$) and given in nmol(nmol-CYP)$^{-1}$min^{-1}. The larger decoy molecule increased the NADPH rate but decreases the coupling efficiency reducing the PFR.

	cyclopentane			cyclohexane			cyclooctane			cyclodecane		
	NADPH	coupling	PFR	NADPH	coupling	PFR	NADPH	coupling	PFR	NADPH	coupling	PFR
WT/9-Ala	438 ± 31	69 ± 1	302 ± 23	763 ± 43	50 ± 1	388 ± 36	544 ± 44	34 ± 1	169 ± 34	418 ± 16	33 ± 1	33 ± 0.3
WT/9-Leu	948 ± 81	73 ± 2	687 ± 40	843 ± 50	63 ± 2	533 ± 24	560 ± 30	46 ± 4	267 ± 38	372 ± 8	53 ± 4	53 ± 3
WT/9-Phe	1520 ±16	62 ± 2	949 ± 35	1010 ± 33	72 ± 3	725 ± 47	724 ± 64	37 ± 2	257 ± 4	582 ± 13	52 ± 4	52 ± 4
RP/9-Ala	1700 ± 30	50 ± 1	845 ± 21	1780 ± 67	57 ± 3	1010 ± 10	**1690 ± 50**	**61 ± 1**	**1020 ± 10**	**1280 ± 10**	**20 ± 0.4**	**253 ± 4**
RP/9-Leu	1880 ± 4	42 ± 2	785 ± 36	1770 ± 47	34 ± 1	606 ± 11	1700 ± 40	18 ± 1	310 ± 22	1550 ± 20	6 ± 0.2	89 ± 3
RP/9-Phe	1680 ± 100	31 ± 1	505 ± 19	1550 ± 92	30 ± 2	466 ± 11	1550 ± 80	20 ± 2	296 ± 51	1450 ± 10	4 ± 0.1	56 ± 2
KT2/9-Ala	2240 ± 30	35 ± 2	777 ± 59	2590 ± 100	36 ±1	922 ± 31	2320 ± 80	24 ± 2	564 ± 85	~2250	~4	~100
KT2/9-Leu	2840 ± 10	49 ± 4	1260 ± 10	2600 ± 40	43 ± 1	1110 ± 20	2750 ± 20	31 ± 1	860 ± 18	~2430	~6	~150
KT2/9-Phe	**3270 ± 20**	**41 ± 2**	**1330 ± 70**	**3390 ± 10**	**42 ± 2**	**1430 ± 80**	2640 ± 100	22 ± 1	580 ± 7	~2560	~5	~130

Table S2 Product formation rate, NADPH oxidation rate and coupling efficiency of turnovers of cyclopentane, cyclohexane, cyclooctane and cyclodecane with WT CYP102A1, RP and KT2 variants in combination of the second generation of decoy molecules. NADPH oxidation rate (NADPH) and product formation rate (PFR) are reported as mean ± S.D. ($n \geq 3$) and given in nmol(nmol-CYP)$^{-1}$min^{-1}. The optimal mutant/decoy molecule combination for each substrate has been highlighted in bold. For cyclooctane and cyclodecane the product formation rates were lower than for the best mutant/PFC decoy molecule combinations.

Cyclohexane	WT	PFC9-L-Trp	GVQ
Fe=O–H-C (Å)	5.2	1.7	2.4
Fe=O–C (Å)	5.9	2.2	3.4
Fe–C (Å)	7.1	3.7	4.6
affinity (kcal mol^{-1})	-3.8	-2.8	-4.2
Cyclooctane	**WT**	**PFC9-L-Trp**	**GVQ**
Fe=O–H-C (Å)	5.8	1.1	2.5
Fe=O–C (Å)	6.8	2.2	3.4
Fe–C (Å)	7.7	3.6	4.6
Affinity (kcal mol^{-1})	-5.0	-2.9	-5.5

Table S3 Distances of the cycloalkane atoms from the heme iron and likely position of Compound I oxygen. Docking experiments are with WT CYP102A1 (PDB: 1BU7) and the the N-perfluorononanoyl-L-tryptophan (PFC9-L-Trp) bound enzyme (PDB: 3WSP). A model of the GVQ mutant (A84G/F87V/L188Q) was prepared by mutation of the WT structure (PDB: 1BU7) using PyMol mutagenesis wizard as outlined in the experimental section.

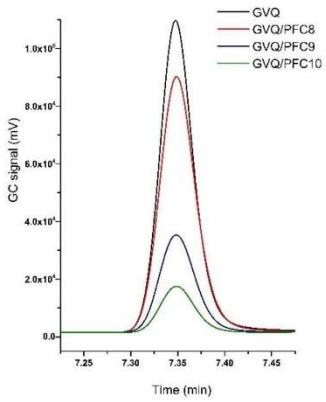

Figure S1 GC analysis of the levels of cyclooctanol formation arising from the addition of different PFC decoy molecules in the turnovers of cyclooctane by the GVQ variant.

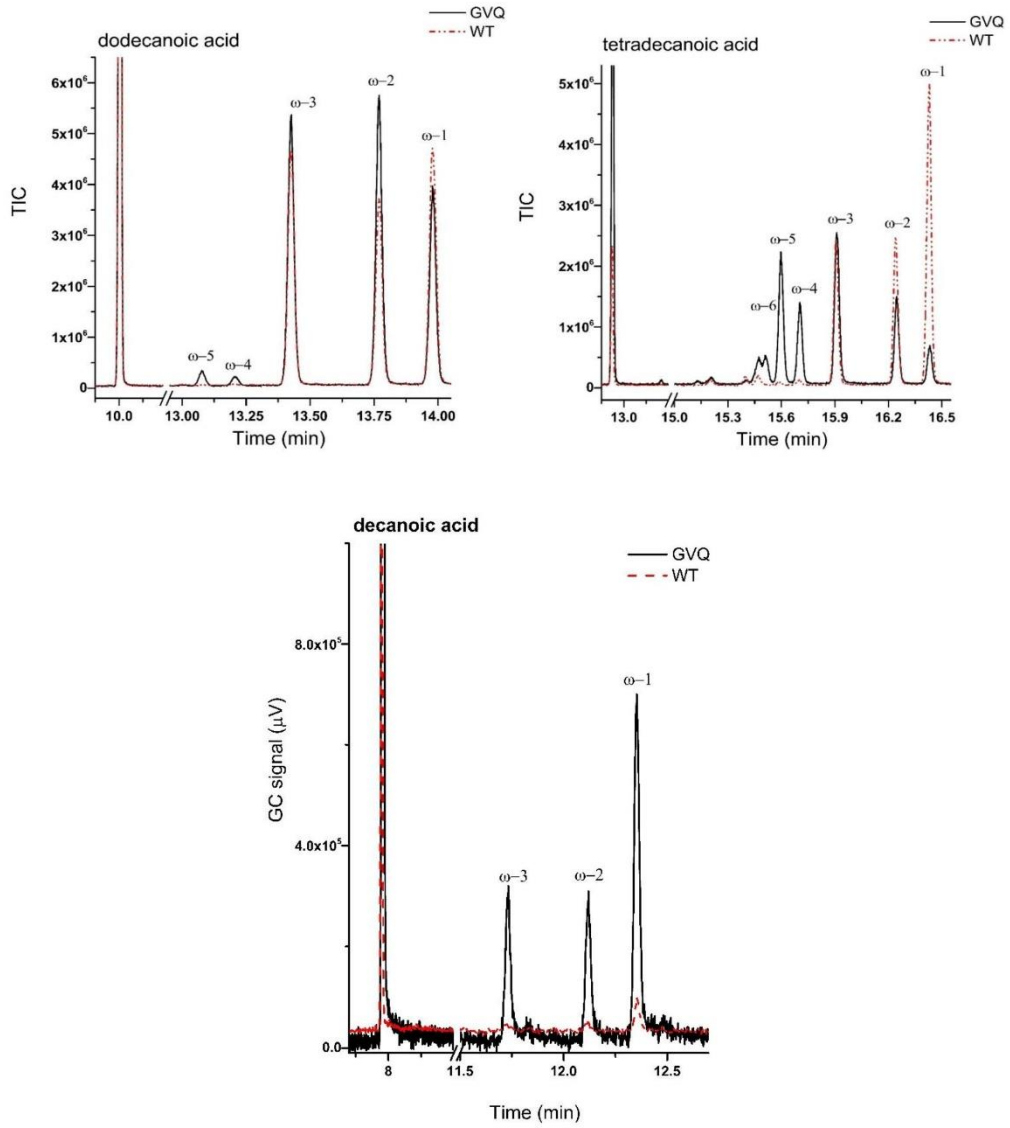

Figure S2 GC-MS analysis of the turnovers of dodecanoic, tetradecanoic and decanoic acids with CYP102A1 WT and GVQ variants (derivatised with BSTFA/TMSCl).

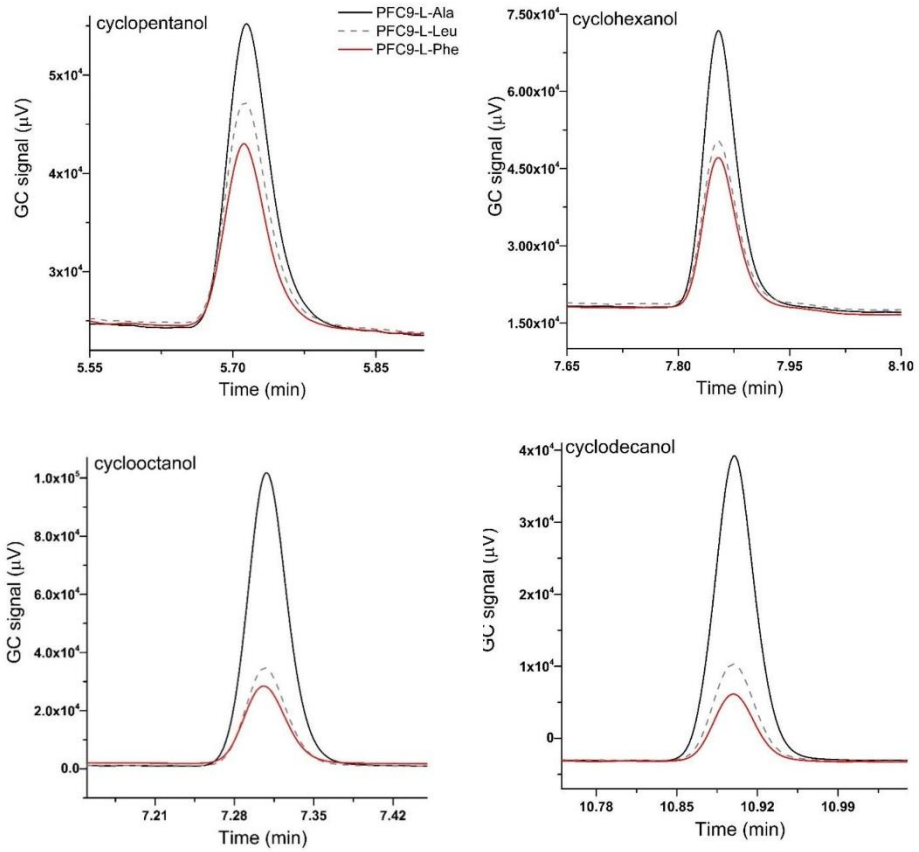

Figure S3 GC analysis of turnovers of the RP variant in combination with the second generation of decoy molecules. PFC9-L-Ala (solid black), PFC9-L-Leu (grey dash) and PFC9-L-Phe (solid red). (full data provided in Table S2).

Chapter 7

The effect of decoy molecules on the activity of the P450Bm3 holoenzyme and a heme domain peroxygenase variant

Citation:

Dezvarei, S.; Shoji, O.; Watanabe, Y.; Bell, S. G., Catal Commun 2019, 124, 97-102.

Statement of Authorship

Title of Paper	The effect of decoy molecules on the activity of the P450Bm3 holoenzyme and a heme domain peroxygenase variant
Publication Status	☑ Published ☐ Accepted for Publication ☐ Submitted for Publication ☐ Unpublished and Unsubmitted work written in manuscript style
Publication Details	Dezvarei, S.; Shoji, O.; Watanabe, Y.; Bell, S. G., The effect of decoy molecules on the activity of the P450Bm3 holoenzyme and a heme domain peroxygenase variant. Catalysis Communications 2019, 124, 97-102.

Principal Author

Name of Principal Author (Candidate)	Shaghayegh Dezvarei
Contribution to the Paper	Enzyme preparation, product formation via turnovers, products characterisation, analysis of substrates and products, interpreted data and discussion, wrote manuscript.
Overall percentage (%)	85
Certification:	This paper reports on original research I conducted during the period of my Higher Degree by Research candidature and is not subject to any obligations or contractual agreements with a third party that would constrain its inclusion in this thesis. I am the primary author of this paper.
Signature	Date 08/04/19

Co-Author Contributions

By signing the Statement of Authorship, each author certifies that:

i. the candidate's stated contribution to the publication is accurate (as detailed above);
ii. permission is granted for the candidate in include the publication in the thesis; and
iii. the sum of all co-author contributions is equal to 100% less the candidate's stated contribution.

Name of Co-Author	Osami Shoji
Contribution to the Paper	Providing the second generation of decoy molecules and Bm3TE plasmid.
Signature	Date 28th March 2019

Name of Co-Author	Yoshihito Watanabe
Contribution to the Paper	Providing the second generation of decoy molecules and Bm3TE plasmid.
Signature	Date Mar 25, 2019

Name of Co-Author	Stephen G. Bell		
Contribution to the Paper	Experimental design, supervision, manuscript preparation and review.		
Signature		Date	8/04/2019

Catalysis Communications 124 (2019) 97–102

Contents lists available at ScienceDirect

Catalysis Communications

journal homepage: www.elsevier.com/locate/catcom

Short communication

The effect of decoy molecules on the activity of the P450Bm3 holoenzyme and a heme domain peroxygenase variant

Shaghayegh Dezvarei[a], Osami Shoji[b], Yoshihito Watanabe[b], Stephen G. Bell[a,*]

[a] Department of Chemistry, University of Adelaide, Adelaide 5005, Australia
[b] Department of Chemistry, Graduate School of Science, Nagoya University, Furo-cho, Chikusa-ku, Nagoya 464-8602, Japan

ARTICLE INFO

Keywords:
Cytochrome P450 monooxygenase
Hydroxylation
Peroxygenase
Epoxidation
Sulfoxidation
Biocatalysis

ABSTRACT

Perfluorinated decoy molecules based on a combination of fatty and amino acids were used to enhance hydroxylation, epoxidation and sulfoxidation reactions of P450Bm3. The combination of amino acid derived second generation decoy molecules, with the rate accelerating variant R19 (R47L/Y51F/H171L/Q307H/N319Y) displayed the highest oxidation rates. Mutation of Thr268 to Glu (Bm3TE) converted the heme domain to a H_2O_2 utilising peroxygenase. This Bm3TE variant displayed significant peroxygenase activity towards all the substrates tested with a preference for methylthiobenzene sulfoxidation. However, the addition of decoy molecules did not improve the efficiency of this variant.

1. Introduction

Cytochromes P450 (P450s) are a family of enzymes that carry out oxidative transformations including hydroxylations, epoxidations, sulfoxidation and other more complex reactions [1]. As a result these enzymes offer advantages over traditional methods of synthesis for carbon-hydrogen bond hydroxylation in that the reaction occurs with high regio- and stereoselectivity in a single step under mild conditions [2]. Most P450s catalyse C–H bond hydroxylation via a high-valent iron-oxo radical cation intermediate which abstracts a hydrogen from the substrate before undergoing an oxygen rebound step, labelled the radical rebound mechanism [3,4]. The key steps of the catalytic cycle are, in order, substrate binding, first electron transfer, dioxygen binding, activation of the oxygen by delivery of a second electron and proton delivery to enable O–O bond cleavage to generate Cpd I (Fig. 1). The electrons are sourced from a nicotinamide cofactor (NADH or NADPH) and delivered via specific electron transfer partners. [5] These reducing cofactors are expensive and many attempts have been made to replace them with simpler alternatives or to do away the requirement for electron transfer proteins by using hydrogen peroxide (H_2O_2) as a source of oxygen via a shunt mechanism (Fig. 1) [6–12].

The cytochrome P450Bm3 from *Bacillus megaterium* rapidly oxidises long chain fatty acid substrates (C12 to C16) close to the omega terminus [13,14]. It, along with other members of the CYP102A subfamily, is unusual compared to other bacterial counterparts in that it is fused to a domain which contains the organic electron transfer cofactors FAD and FMN. This results in the enzyme being self-sufficient in that it requires no other external proteins [14]. P450Bm3 is soluble, easy to produce and sources its electrons from NADPH over NADH [15]. It has been adapted for the selective hydroxylation of a broad range of substrates through rational protein engineering [16,17]. Directed evolution has also been used to expand the substrate range of P450Bm3 as well as increase its thermostability and to improve its activity with H_2O_2 [6,14,18]. In addition it has recently been modified to enable to it to carry out non-physiological P450 chemistry, for example isoforms which enable the cyclopropanation, amination and aziridination of various substrates have been reported [19].

These directed evolution studies have highlighted that P450Bm3 can be enhanced by making alterations outside of the active site. These mutations alter the conformation of the enzyme to enhance its activity but do not alter the active site architecture and so maintain the product regio-selectivity, of the WT enzyme [20–23]. The conformations adopted by these variants more closely resembles those of the fatty acid bound form of the enzyme and lengthens the heme-iron axial water

Abbreviations: P450, cytochrome P450; P450Bm3, CYP102A1 from *Bacillus megaterium*; IPTG, Isopropyl β-D-1-thiogalactopyranoside; BID, Barrier discharge Ionization Detector; WT, wild-type; R19, (R47L/Y51F/H171L/Q307H/N319Y); Bm3TE, Thr268 to Glu variant of the CYP102A1 heme domain; NADPH, reduced nicotinamide adenine dinucleotide phosphate; NADH, reduced nicotinamide adenine dinucleotide; FAD, flavin adenine dinucleotide; FMN, flavin mononucleotide; mCPBA, *meta*-chloroperoxybenzoic acid; PFC, perfluorocarboxcylic acid; PFC9-L-Ala, N-perfluorononanoyl-L-alanine; PFR, product formation rate; tBuOOH, *tert*-butyl hydroperoxide

* Corresponding author.
E-mail address: stephen.bell@adelaide.edu.au (S.G. Bell).

https://doi.org/10.1016/j.catcom.2019.03.004
Received 7 January 2019; Received in revised form 26 February 2019; Accepted 4 March 2019
Available online 06 March 2019

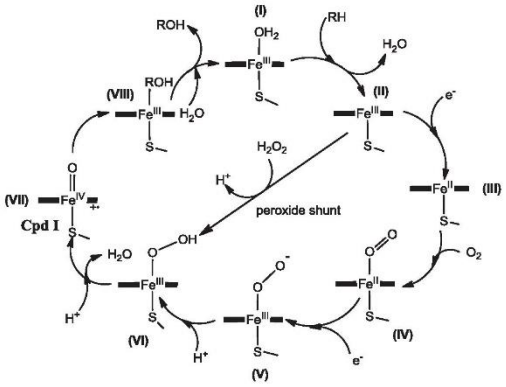

Fig. 1. Catalytic cycle of P450 monooxygenases including the H_2O_2 shunt pathway.

bond [21,23]. One example of such a rate accelerating mutant is the R47L/Y51F/H171L/Q307H/N319Y (R19) variant of P450Bm3, which enhanced the oxidation of hydrophobic unnatural substrates [24,25].

Chemically inert decoy molecules have also been used to improve the activity of P450Bm3 [26]. These promote the oxidation of unnatural substrates such as benzenes, xylenes and short chain alkanes by the wild-type (WT) enzyme [25–28]. They work as the fluorinated alkyl chain of the decoy molecule is used to fill the substrate access channel of the enzyme and this leads to conformational changes. However, they are short enough that sufficient space remains in the active site of the enzyme over the heme to allow a substrate to bind [28]. One consequence of this is, as with the rate accelerating mutants described above, the regioselectivity of oxidation is largely unaffected. We have shown that it is possible to use decoy molecules, in conjugation with the rate accelerating mutants of P450Bm3 to significantly enhance the rates of product formation for cycloalkane and benzene-derived substrates and improve the productivity of regio- and stereo-selective biocatalysis reactions [24,25].

More recently, inspired by the H_2O_2 utilising CYP152 family of enzymes including CYP152A1 (P450BSβ) [29], CYP152A2 (P450CLA) [30] and CYP152B1 (P450SPα) [31], a single mutation at threonine 268 was introduced to alter the activity of the P450Bm3 heme domain. Threonine 268 is part of the highly conserved acid-alcohol pair used to activate dioxygen. Replacing the threonine alcohol side chain with the acidic glutamate residue allowed the heme domain of P450Bm3 to hydroxylate fatty acids using hydrogen peroxide as the oxidant [32].

For the first time we show that the combination of second generation decoy molecules and mutated variants of the holoenzyme result in large increases in the efficiency of benzylic hydroxylation, epoxidation and sulfoxidation reactions. We also demonstrate that the threonine 268 to glutamate heme domain variant (Bm3TE) can catalyse these reactions using hydrogen peroxide but that no improvement in oxidation is observed when the decoy molecules are added.

2. Experimental

2.1. General

General reagents and organics were purchased from Sigma-Aldrich, Tokyo Chemical Industry, Chem-Supply or Fluorochem. Isopropyl-β-D-thiogalactopyranoside (IPTG) and buffer components were obtained from Astal Scientific (Australia). UV/Vis spectroscopy was performed on an Agilent Cary 60 spectrophotometer. Gas chromatography was carried out on a Shimadzu Tracera GC with Barrier discharge Ionization Detector (BID) detector using an Rt-βDEXse column (30 m × 0.32 mm × 0.25 um). Gas Chromatography-Mass Spectrometry was carried out on a Shimadzu GC-2010 with GC–MS-QP2010S detector. The GC methods are provided in the Supplemental section.

2.2. Protein expression and purification

Plasmids, pT7 containing the gene encoding the P450Bm3 heme domain Thr268Glu mutant (Bm3TE) or pET28 with the WT and R19 holoenzyme genes, were transformed into *E. coli* BL21 (DE3) competent cells and grown on LB plate in the presence of ampicillin or kanamycin, respectively [20,32]. A single colony was added to 500 mL of LB media containing trace elements solution ($CaCl_2$, $ZnSO_4.7H_2O$, $MnSO_4.H_2O$, Na_2-EDTA, $FeCl_3.6H_2O$, $CuSO_4.5H_2O$, and $CoCl_2.6H_2O$) in presence of the relevant antibiotic and incubated at 37 °C and 110 rpm. After 14 h incubation the temperature was lowered to 18 °C followed by the addition of 0.02% v/v benzyl alcohol and 2% v/v ethanol after 30 min. IPTG (100 μM) was then added to induce protein expression. Cells were harvested after 24 h by centrifugation (5000 *g*, 10 min, 4 °C) and resuspended in 50 mM buffer pH 7.4 (Tris buffer for Bm3TE and phosphate buffer for holoenzymes; both contained 1 mM DTT). The cells were lysed by sonication on ice for 30 min (20 s on, 40 s off) and cell debris was removed by centrifugation (37,000 *g*, 20 min, 4 °C). The supernatant was loaded onto a DEAE Sepharose column (XK50, 200 mm × 40 mm; GE Healthcare) and eluted using a salt linear gradient (100–400 mM KCl in Tris buffer for Bm3TE and 80–400 mM $(NH_4)_2SO_4$ in phosphate buffer for holoenzymes). The red coloured fractions which contain the P450 enzyme were combined and concentrated by ultrafiltration (1900 *g*, 4 °C) using 10 and 30 kDa membranes for Bm3TE and holoenzymes, respectively, (Vivacell 100, Sartorius). Concentrated protein was desalted using a Sephadex G-25 medium grain column (250 mm × 40 mm; GE Healthcare). This was concentrated by ultrafiltration as described above to approximately 10 mL before being loaded onto a Source-Q ion-exchange column (XK26, 80 mm × 30 mm; GE Healthcare). The proteins were purified on an AKTA purifier (GE Healthcare) and eluted using a salt gradient (100–400 mM KCl in Tris buffer for Bm3TE and 0–35% 16 × phosphate buffer for Bm3 holoenzymes). Fractions with $A_{418}/A_{280} > 0.5$ (for both holoenzymes and Bm3TE variant) were collected and concentrated, afterwards an equivalent volume of 80% glycerol was added to the protein and filter sterilised before storage at −20 °C.

2.3. Activity assays

The peroxygenase turnover assays for the Bm3TE variant were run in 1 mL Tris buffer (pH 7.4, 100 mM) at room temperature containing 3 μM enzyme. Substrate (5 mM) and decoy molecule (100 μM if present) were added. The reaction was started by addition of 60 mM H_2O_2 and quenched after 5 min by addition of 400 μL ethyl acetate. The NADPH monooxygenase turnover assays on the holoenzymes were carried out as reported previously (see Supplemental section) [24,33].

2.4. Product analysis

After the NADPH consumption or hydrogen peroxide assays were completed, 990 μL of the reaction mixture was mixed with 10 μL of an internal standard solution (*p*-cresol, 20 mM stock solution in DMSO). These mixtures were extracted with 400 μL of ethyl acetate and the organic extracts were used directly for GC–MS or GC analysis. Products were initially identified by GC-coelution experiments and matching the GC–MS spectra to those of the products (styrene oxide, 1-phenylethanol and methyl phenylsulfoxide; see supplementary material). Products were calibrated against authentic product standards using the assumption that isomeric products would give comparable responses e.g. phenylacetaldehyde and styrene oxide were presumed to give the same

Table 1
Enzyme turnover and coupling efficiency data for WT and the R19 variant of P450Bm3 with ethylbenzene, styrene and methylthiobenzene. Activities are expressed as the NADPH oxidation rate (N) and were measured using a concentration of 0.2 μM CYP enzyme, 50 mM Tris, pH 7.4). The coupling efficiency (C) is the percentage efficiency of NADPH utilization for the formation of organic products. N and the product formation rates (PFR) are reported as mean ± S.D. ($n \geq 3$) and given in nmol(nmol-CYP)$^{-1}$ min^{-1}.

	Ethylbenzene			
	N	C	PFR	*ee (R)*
WT[a]	71 ± 4	5.3 ± 1.5	3.8 ± 1.2	48
WT/PFC9[a]	1106 ± 19	74 ± 2	814 ± 33	56
WT/PFC10[a]	1311 ± 13	49 ± 2	645 ± 33	62
WT/PFC9-Phe	1560 ± 8	61 ± 2	962 ± 32	39
WT/PFC9-Leu	1040 ± 24	58 ± 2	563 ± 13	28
WT/PFC9-Ala	947 ± 17	51 ± 1	482 ± 4	38
R19[a]	702	52	366	16
R19/PFC10[a]	1460	71	1030	30
R19/PFC9-Phe	2240 ± 85	61 ± 3	1420 ± 26	12
R19/PFC9-Leu	2830 ± 69	66 ± 6	1860 ± 100	12
R19/PFC9-Ala	2760 ± 96	63 ± 5	1720 ± 180	20
	Styrene			
	N	C	PFR	*ee (R)*
WT[a]	41 ± 1	4.0 ± 0.6	1.6 ± 0.2	18
WT/PFC9[a]	457 ± 11	32 ± 1	146 ± 4	32
WT/PFC10[a]	691 ± 7	17 ± 1	117 ± 7	32
WT/PFC9-Phe	932 ± 25	21 ± 3	194 ± 28	15
WT/PFC9-Leu	665 ± 10	38 ± 5	255 ± 31	18
WT/PFC9-Ala	601 ± 14	43 ± 4	255 ± 14	18
R19[a]	976	63	611	22
R19/PFC10[a]	1530	76	1160	28
R19/P9-Phe	1620 ± 20	63 ± 4	1030 ± 70	18
R19/P9-Leu	2210 ± 130	67 ± 3	1480 ± 20	18
R19/P9-Ala	2020 ± 65	78 ± 1	1580 ± 42	26
	Methylthiobenzene			
	N	C	PFR	*ee (R)*
WT[f]	39 ± 1.4	12 ± 2	3 ± 1	2
WT/PFC10	267 ± 18	22 ± 3	58 ± 6.6	0
WT/PFC9-Phe	1770 ± 18	28 ± 1	502 ± 21	1
WT/PFC9-Leu	1410 ± 23	30 ± 2	423 ± 24	0
WT/PFC9-Ala	934 ± 31	23 ± 1	213 ± 13	10
R19	1060 ± 75	31 ± 2	317 ± 15	0
R19/PFC10	1440 ± 40	32 ± 2	466 ± 27	0
R19/P9-Phe	2080 ± 14	32 ± 1	660 ± 29	0
R19/P9-Leu	2880 ± 62	32 ± 0.5	905 ± 11	0
R19/P9-Ala	2330 ± 3.5	36 ± 3	831 ± 72	2

[a] These results are in line with what was reported previously for these substrate/enzyme/decoy combinations [24].

detector response.

3. Results

3.1. P450Bm3 catalysed oxidation of ethylbenzene, styrene and methylthiobenzene

The rates of NADPH oxidation, product formation and the coupling efficiency for different P450Bm3 variants, in the presence and absence of different polyfluorinated carboxylic acids (PFCs), were obtained for ethylbenzene, styrene and methylthiobenzene oxidation (Table 1). All the combinations tested gave rise to a single major oxidation metabolite which could be identified by GC–MS coelution experiments with authentic product standards (Scheme 1). In turnovers of styrene, there was an additional minor product which coeluted with and had a MS spectra consistent of an aldehyde (< 11%) arising from a rearrangement reaction (phenylacetaldehyde, Scheme 1). There was also a small amount of a sulfone further oxidation product (< 15%) in the turnovers of methylthiobenzene. In turnovers of ethylbenzene two minor products were observed and were assigned as acetophenone and 2-ethylphenol (Scheme 1) [24].

The activity of WT Bm3 for oxidation of all three substrates, as measured by the product formation rate, was low (PFR; ≤4 nmol (nmol-CYP)$^{-1}$ min^{-1}; henceforth abbreviated to min^{-1}). In line with what has been reported previously for ethylbenzene and styrene the addition of first generation decoy molecules perfluorononanoic acid (PFC9) and perfluorodecanoic acid (PFC10) improved the activity (ranging from 17- to 214-fold) with all the substrates, while the regio- and stereo-selectivity was predominantly maintained (Table 1) [24,33]. Based on these previous studies, PFC9 and PFC10 were the optimal compounds in the first generation of decoy molecules, therefore longer and shorter PFCs were not examined [33].

The rate accelerating variant, R19 increased the activity of substrate oxidation over the WT enzyme (Table 1) and its combination with a first generation decoy molecules generated even higher product formation activities (466 to 1160 min^{-1} an up to 3-fold improvement over the R19 variant alone; Table 1, Fig. S1). The 725-fold improvement in PFR of the WT enzyme observed with styrene oxidation by the R19 variant in combination with PFC10 was greater than those observed for ethylbenzene and methylthiobenzene (271- and 155-fold, respectively). The regioselectivity of R19-catalysed oxidation of all substrates in the presence or absence of the decoy molecules were similar to those of the WT enzyme (Scheme 1). There were no significant changes in the stereoselectivity of styrene and methylthiobenzene oxidation. However, the R19 variant was less selective for the *(R)*-enantiomer of 1-phenylethanol compared to the WT enzyme with the enantiomeric excess (*ee*) dropping from 48 to 62 to 16–30% across the turnovers.

Second generation decoy molecules have been developed to explore the effect of amino acid derived compounds for small molecule oxidation by P450Bm3 [28]. The oxidation activity of the P450Bm3 WT and R19 variants were tested in presence of PFC9-L-Ala, PFC9-L-Leu and PFC9-L-Phe (N-perfluorononanoyl-L-alanine, N-perfluorononanoyl-L-leucine and N-perfluorononanoyl-L-phenyalanine, see supplementary section for structures). The oxidation rates in turnovers of ethylbenzene and methylthiobenzene were found to be the greatest when the PFC9-L-Phe decoy molecule was added to the WT enzyme (Table 1, Fig. S1). This resulted in a 248-fold improvement with ethylbenzene (PFR 962 ± 32 min^{-1}) and a 146-fold enhancement with methylthiobenzene (PFR 502 ± 21 min^{-1}). In terms of styrene oxidation, the highest production rate with the WT was observed with addition of PFC9-L-Leu or PFC9-L-Ala (both had a PFR of 255 min^{-1}, 159-fold improvement over the WT by itself). As with the first generation decoys, the addition of these second generation molecules to the WT enzyme resulted in small changes in the stereoselectivity of the overall reactions (Table 1, Fig. S2). For example, that of ethylbenzene benzylic hydroxylation was slightly reduced (Table 1).

The combination of the second generation of decoy molecules with the R19 variant was also studied. All three substrates were oxidised with their maximum product formation rates (PFR) with R19/PFC9-L-Leu or R19/PFC9-L-Ala. This arose predominantly due to a superior NADPH rate with little or no increase in the coupling efficiency over the R19 variant alone or the WT enzyme with the decoy molecules. The greatest PFR was found for the PFC9-L-Leu/R19 combination for the oxidation reaction with ethylbenzene (PFR 1860 ± 100 min$^{-1;}$ 490-fold improvement over WT alone). For styrene epoxidation PFC9-L-Ala/R19 was the optimal combination (PFR 1580 ± 100 min^{-1}; 980-fold improvement). The coupling efficiency of methylthiobenzene oxidation was not enhanced to the same degree as the other two substrates but its oxidation rate increased 300-fold with the PFC9-L-Leu/R19 combination to yield a PFR of 905 ± 11 min^{-1}. As with the other decoy molecule turnovers the combination of the second generation of decoy

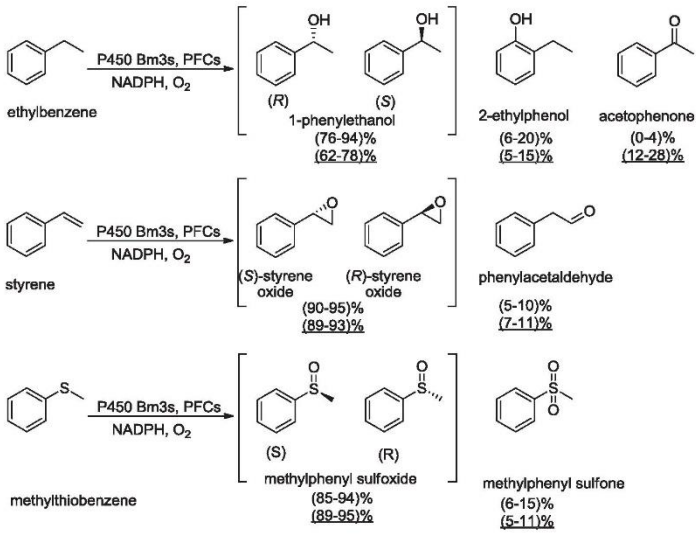

Scheme 1. Product distributions for the catalysed oxidation of ethylbenzene, styrene and methylthiobenzene in the presence and absence of decoy molecules. The products from ethylbenzene: 1-phenylethanol and 2-ethylphenol, from styrene: styrene oxide and phenylacetaldehyde and from methylthiobenzene: methylphenyl sulfoxide and methylphenyl sulfone. Values in black represent the percentage of products with WT and R19 variant. The values obtained with the Bm3TE variant are underlined.

molecules maintained the regio- and stereo-selectivity of the turnovers (Table 1).

3.2. Peroxygenase activity of the Thr268Glu variant of the heme domain of P450Bm3

A single mutation of threonine 268 to glutamic acid converts the heme domain of P450Bm3 (Bm3TE) into a H_2O_2 utilising peroxygenase variant [32]. The activity of Bm3TE variant was tested for the oxidation of ethylbenzene, styrene, and methylthiobenzene. The P450Bm3 holoenzyme displayed little peroxygenase activity with these substrates (Fig. 2). With styrene and ethylbenzene the Bm3TE variant generated 640 nmoles of styrene oxide and 199 nmoles of α-EtOH after addition of H_2O_2. Analysis of the methylthiobenzene turnovers was more complex as H_2O_2 by itself can lead to sulfoxidation. However in the presence of the Bm3TE variant a significant increase in sulfoxidation was observed. The oxidation of methylthiobenzene produced of 914 nmols of methyl phenyl sulfoxide (versus 80 nmols in the no P450 control). In these peroxygenase turnovers the addition of the first or the second generation of decoy molecules showed little to no improvement on the oxidation of the substrates. For styrene and ethylbenzene the highest productivity was observed in the absence of decoy molecules and significant decreases in the amount of product were found when the second generation decoy molecules were used. Small increases in product formation were observed in certain instances with methylthiobenzene (Table S1). In order to assess if the decoy molecule might be blocking H_2O_2 access to the heme we modified the order of addition of the H_2O_2 before the decoy molecule and the substrate but this did not alter the amount of product generated (Fig. S3). We also tested alternative peroxides (tBuOOH and mCPBA) with the BM3TE peroxygenase variant for the oxidation of ethylbenzene and the levels of product generated by each of these was significantly lower than obtained with H_2O_2 (tBuOOH 22% and mCPBA 2% of the levels of product formation of H_2O_2 (Fig. S4).

While the regioselectivity of the peroxygenase turnovers were similar to those of the holoenzyme monoxygenase activities differences in metabolite formation were observed (Scheme 1). In the turnovers of ethylbenzene with Bm3TE variant 15% of the further oxidation product acetophenone was detected which was higher than the monooxygenase reactions (0–4%; Scheme 1). Changes were observed in the stereoselectivity of the peroxygenase reactions. Oxidation of styrene with Bm3TE was less in favor of the *R*-enantiomer (10–20% *ee*) compared to the holoenzymes (15–32%). The stereoselectivity for oxidation of methylthiobenzene with the T268E variant towards the *R* enantiomer increased up to 20% (Table S1). The most dramatic change was observed for the hydroxylation of ethylbenzene where the peroxygenase reactions favoured the (*S*)-enantiomer in contrast to the holoenzyme monooxygenase turnovers which were more *R*-selective (Fig. 3).

4. Discussion

The rates of product formation for ethylbenzene, styrene and methylthiobenzene oxidation with P450Bm3 holoenzymes were significantly increased by using decoy molecules. The highest activities were observed with the second generation of decoy molecules with the R19 variant. The regioselectivity and the stereoselectivity was maintained across both variants in the presence of the decoy molecules.

The Bm3TE heme domain variant was capable of oxidising all of the substrates using H_2O_2 instead of molecular dioxygen and NADPH. This variant was more active for the sulfoxidation of methylthiobenzene over the epoxidation of styrene and benzylic hydroxylation of ethylbenzene. This contrasted with the holoenzyme turnovers which were most effective for ethylbenzene oxidation suggesting a potential change in the rate determining step for these reactions. The coupling efficiency of methylthiobenzene sulfoxidation, the most reactive functional group to be tested, was lowest for the monooxygenase turnovers using the holoenzyme. This infers that there may be a change in the rate determining step and perhaps the proportion of potential reactive oxidants during the hydrogen peroxide driven turnovers is different from that of the monoxygenase catalytic cycle of the holoenzyme (Fig. 1). This is in line with observations by De Voss and coworkers with the WT P450Bm3 and sulfur containing fatty acid probes and the variations in coupling efficiency with different length fatty acids and the T268A holoenzyme variant [34,35].

The addition of decoy molecules induced no improvement in the oxidation efficiency of Bm3TE. It is hypothesised that the decoy molecules enhance the activity by binding to the enzyme together with the substrate overcoming the substrate gate, inducing a conformation

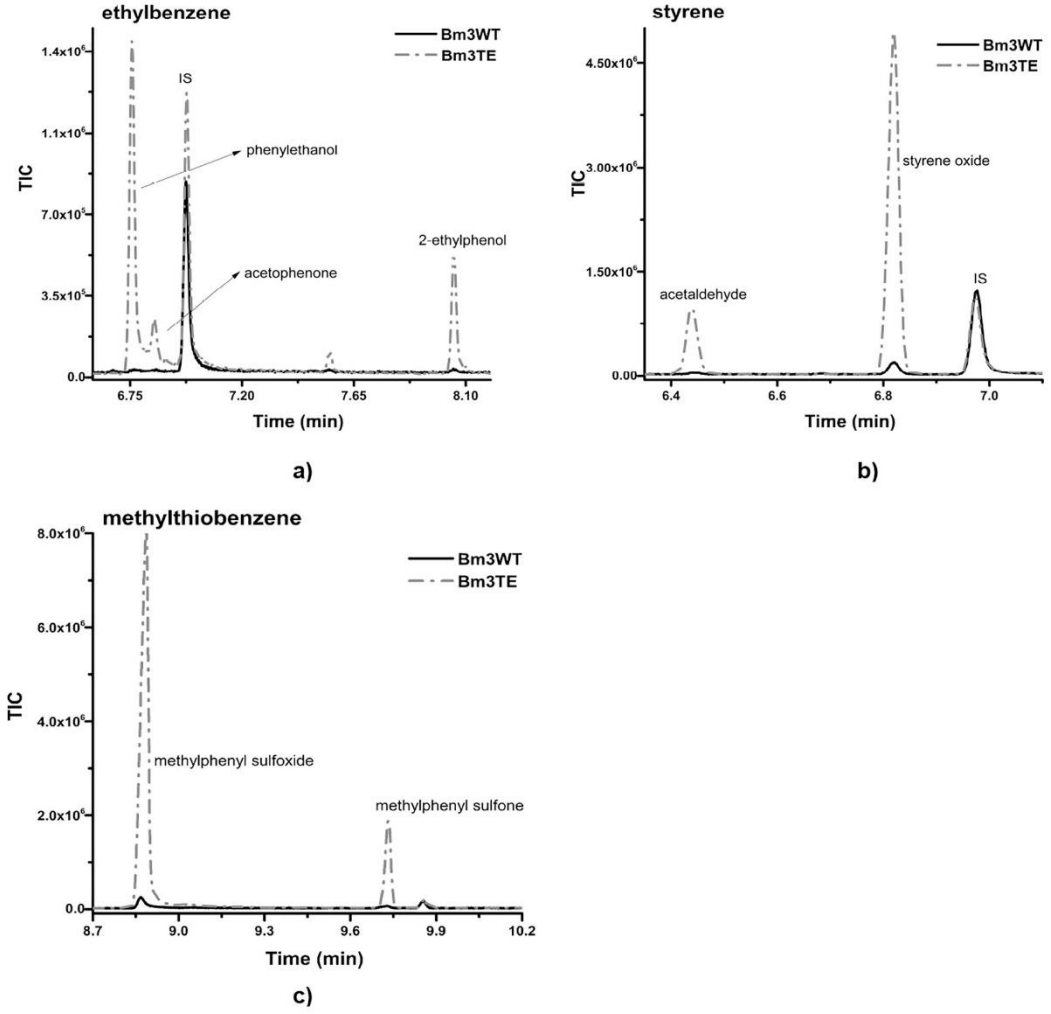

Fig. 2. GC–MS analysis the hydrogen peroxide driven turnovers of a) ethylbenzene, b) styrene and c) methylthiobenzene with WT Bm3 holoenzyme (black) and the Bm3TE (T268E) variant (grey). The WT holoenzyme displayed little to no activity in the presence of H_2O_2 compared to the Bm3TE variant.

change which triggers the first electron transfer, subsequent oxygen binding and faster turnover of the catalytic cycle. The second generation of decoy molecules have been shown to bind tightly to P450Bm3 and to alter the conformation of the enzyme. The crystal structure of PFC9-L-Trp-bound P45Bm3 highlights modification in the position of F and G helices, the G/F loop and the I helix [28].

The switch in the stereoselectivity of ethylbenzene hydroxylation towards the *(S)*-enantiomer for the peroxygenase mutant compared to the monooxygenase turnovers of the holoenzyme is intriguing. This change could be due to an altered binding orientation of the substrate in the mutant, though the regioselectivity of the reaction was similar. In addition minimal changes were observed for the epoxidation of styrene and sulfoxidation of methylthiobenzene inferring their positions relative to the heme iron may not be altered. The double bond in styrene may provide a more rigid structure leading to less opportunity for movement.

5. Conclusion

The results highlight the important role that decoy molecules can play in accelerating the productive oxidation of non-physiological substrates by P450Bm3. They also back up the hypothesis that these decoy molecules work by inducing conformational changes which boost the monooxygenase catalytic cycle by enhancing the rate of electron transfer. The peroxygenase variant could also efficiently oxidise the substrates. Further optimisation of this system could result in simpler and larger scale green biocatalytic oxidation processes.

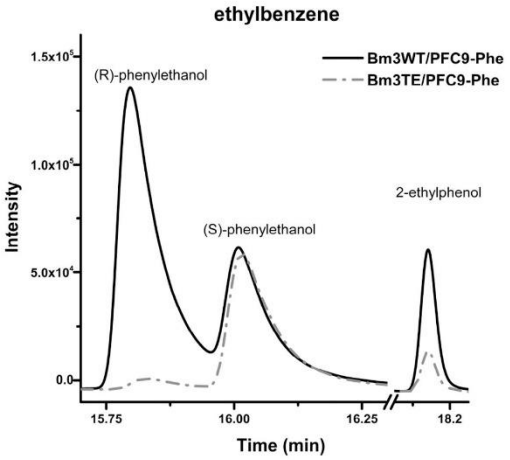

Fig. 3. Chiral GC analysis of ethylbenzene oxidation illustrating a change in stereo-selectivity of the Bm3TE variant versus the holoenzymes for 1-phenylethanol. While WT and R19 variant are more (*R*) selective the Bm3TE variant is more (*S*) selective.

Acknowledgements

S.G.B. acknowledges the Australian Research Council for a Future Fellowship (FT140100355). The authors also acknowledge the University of Adelaide International Postgraduate Award (for S.D.) and a Nagoya Priority Grant. The authors thank Prof. Luet-Lok Wong (University of Oxford, UK) for the gene constructs of the P450Bm3 holoenzymes.

Appendix A. Supplementary data

Supplementary data to this article can be found online at https://doi.org/10.1016/j.catcom.2019.03.004.

References

[1] P.R. Ortiz de Montellano, Cytochrome P450: Structure, Mechanism, and Biochemistry Cytochrome P450: Structure, Mechanism, and Biochemistry, Springer International Publishing, Switzerland, 2015.
[2] G.D. Roiban, M.T. Reetz, Expanding the toolbox of organic chemists: directed evolution of P450 monooxygenases as catalysts in regio- and stereoselective oxidative hydroxylation, Chem. Commun. 51 (2015) 2208–2224.
[3] J. Rittle, M.T. Green, Cytochrome P450 compound I: capture, characterization, and C-H bond activation kinetics, Science 330 (2010) 933–937.
[4] J.T. Groves, G.A. McClusky, Aliphatic hydroxylation via oxygen rebound - oxygen-transfer catalyzed by iron, J. Am. Chem. Soc. 98 (1976) 859–861.
[5] F. Hannemann, A. Bichet, K.M. Ewen, R. Bernhardt, Cytochrome P450 systems–biological variations of electron transport chains, Biochim. Biophys. Acta 1770 (2007) 330–344.
[6] P.C. Cirino, F.H. Arnold, A self-sufficient peroxide-driven hydroxylation biocatalyst, Angew. Chem. Int. Ed. Eng. 42 (2003) 3299–3301.
[7] I. Zachos, C. Nowak, V. Sieber, Biomimetic cofactors and methods for their recycling, Curr. Opin. Chem. Biol. 49 (2019) 59–66.
[8] F.E. Zilly, A. Taglieber, F. Schulz, F. Hollmann, M.T. Reetz, Deazaflavins as mediators in light-driven cytochrome P450 catalyzed hydroxylations, Chem. Commun. (2009) 7152–7154.
[9] K. Jensen, P.E. Jensen, B.L. Møller, Light-driven cytochrome p450 hydroxylations, ACS Chem. Biol. 6 (2011) 533–539.
[10] S. Krishnan, D. Wasalathanthri, L. Zhao, J.B. Schenkman, J.F. Rusling, Efficient bioelectronic actuation of the natural catalytic pathway of human metabolic cytochrome P450s, J. Am. Chem. Soc. 133 (2011) 1459–1465.
[11] A.K. Udit, F.H. Arnold, H.B. Gray, Cobaltocene-mediated catalytic monooxygenation using holo and heme domain cytochrome P450 BM3, J. Inorg. Biochem. 98 (2004) 1547–1550.
[12] N.H. Tran, D. Nguyen, S. Dwaraknath, S. Mahadevan, G. Chavez, A. Nguyen, T. Dao, S. Mullen, T.A. Nguyen, L.E. Cheruzel, An efficient light-driven P450 BM3 biocatalyst, J. Am. Chem. Soc. 135 (2013) 14484–14487.
[13] P.P. Ho, A.J. Fulco, Involvement of a single hydroxylase species in the hydroxylation of palmitate at the omega-1, omega-2 and omega-3 positions by a preparation from bacillus megaterium, Biochim. Biophys. Acta 431 (1976) 249–256.
[14] C.J. Whitehouse, S.G. Bell, L.L. Wong, P450(BM3) (CYP102A1): connecting the dots, Chem. Soc. Rev. 41 (2012) 1218–1260.
[15] M.G. Joyce, I.S. Ekanem, O. Roitel, A.J. Dunford, R. Neeli, H.M. Girvan, G.J. Baker, R.A. Curtis, A.W. Munro, D. Leys, The crystal structure of the FAD/NADPH-binding domain of flavocytochrome P450 BM3, FEBS J. 279 (2012) 1694–1706.
[16] R.J. Sowden, S. Yasmin, N.H. Rees, S.G. Bell, L.L. Wong, Biotransformation of the sesquiterpene (+)-valencene by cytochrome P450cam and P450BM-3, Org. Biomol. Chem. 3 (2005) 57–64.
[17] V.B. Urlacher, S.G. Bell, L.L. Wong, The bacterial cytochrome P450 monooxygenases: P450cam and P450BM-3, in: R.D. Schmid, V.B. Urlacher (Eds.), Modern Biooxidation, Wiley, New York, 2007, pp. 99–122.
[18] S. Kille, F.E. Zilly, J.P. Acevedo, M.T. Reetz, Regio- and stereoselectivity of P450-catalysed hydroxylation of steroids controlled by laboratory evolution, Nat. Chem. 3 (2011) 738–743.
[19] O.F. Brandenberg, R. Fasan, F.H. Arnold, Exploiting and engineering hemoproteins for abiological carbene and nitrene transfer reactions, Curr. Opin. Biotechnol. 47 (2017) 102–111.
[20] C.J. Whitehouse, S.G. Bell, H.G. Tufton, R.J. Kenny, L.C. Ogilvie, L.L. Wong, Evolved CYP102A1 (P450(BM3)) variants oxidise a range of non-natural substrates and offer new selectivity options, Chem. Commun. (2008) 966–968.
[21] C.J. Whitehouse, S.G. Bell, W. Yang, J.A. Yorke, C.F. Blanford, A.J. Strong, E.J. Morse, M. Bartlam, Z. Rao, L.L. Wong, A highly active single-mutation variant of P450(BM3) (CYP102A1), ChemBioChem (10) (2009) 1654–1656.
[22] C.J. Whitehouse, W. Yang, J.A. Yorke, B.C. Rowlatt, A.J. Strong, C.F. Blanford, S.G. Bell, M. Bartlam, L.L. Wong, Z. Rao, Structural basis for the properties of two single-site proline mutants of CYP102A1 (P450(BM3)), ChemBioChem 11 (2010) 2549–2556.
[23] C.J. Whitehouse, W. Yang, J.A. Yorke, H.G. Tufton, L.C. Ogilvie, S.G. Bell, W. Zhou, M. Bartlam, Z. Rao, L.L. Wong, Structure, electronic properties and catalytic behaviour of an activity-enhancing CYP102A1 (P450(BM3)) variant, Dalton Trans. 40 (2011) 10383–10396.
[24] S.D. Munday, S. Dezvarei, S.G. Bell, Increasing the activity and efficiency of stereoselective oxidations by using decoy molecules in combination with rate-enhancing variants of P450Bm3, ChemCatChem 8 (2016) 2789–2796.
[25] S.D. Munday, O. Shoji, Y. Watanabe, L.L. Wong, S.G. Bell, Improved oxidation of aromatic and aliphatic hydrocarbons using rate enhancing variants of P450Bm3 in combination with decoy molecules, Chem. Commun. 52 (2016) 1036–1039.
[26] N. Kawakami, O. Shoji, Y. Watanabe, Use of perfluorocarboxylic acids to trick cytochrome P450BM3 into initiating the hydroxylation of gaseous alkanes, Angew. Chem. Int. Ed. Eng. 50 (2011) 5315–5318.
[27] O. Shoji, T. Kunimatsu, N. Kawakami, Y. Watanabe, Highly selective hydroxylation of benzene to phenol by wild-type cytochrome P450BM3 assisted by decoy molecules, Angew. Chem. Int. Ed. Eng. 52 (2013) 6606–6610.
[28] Z. Cong, O. Shoji, C. Kasai, N. Kawakami, H. Sugimoto, Y. Shiro, Y. Watanabe, Activation of wild-type cytochrome P450BM3 by the next generation of decoy molecules: enhanced hydroxylation of gaseous alkanes and crystallographic evidence, ACS Catal. 5 (2015) 150–156.
[29] I. Matsunaga, A. Ueda, T. Sumimoto, K. Ichihara, M. Ayata, H. Ogura, Site-directed mutagenesis of the putative distal helix of peroxygenase cytochrome P450, Arch. Biochem. Biophys. 394 (2001) 45–53.
[30] M. Girhard, S. Schuster, M. Dietrich, P. Durre, V.B. Urlacher, Cytochrome P450 monooxygenase from Clostridium acetobutylicum: a new alpha-fatty acid hydroxylase, Biochem. Biophys. Res. Commun. 362 (2007) 114–119.
[31] I. Matsunaga, T. Sumimoto, A. Ueda, E. Kusunose, K. Ichihara, Fatty acid-specific, regiospecific, and stereospecific hydroxylation by cytochrome P450 (CYP152B1) from Sphingomonas paucimobilis: substrate structure required for alpha-hydroxylation, Lipids 35 (2000) 365–371.
[32] O. Shoji, T. Fujishiro, K. Nishio, Y. Kano, H. Kimoto, S.-C. Chien, H. Onoda, A. Muramatsu, S. Tanaka, A. Hori, A substrate-binding-state mimic of H 2 O 2-dependent cytochrome P450 produced by one-point mutagenesis and peroxygenation of non-native substrates, Catal. Sci. Technol. 6 (2016) 5806–5811.
[33] S. Dezvarei, H. Onoda, O. Shoji, Y. Watanabe, S.G. Bell, Efficient hydroxylation of cycloalkanes by co-addition of decoy molecules to variants of the cytochrome P450 CYP102A1, J. Inorg. Biochem. 183 (2018) 137–145.
[34] M.J. Cryle, J.J. De Voss, Is the ferric hydroperoxy species responsible for sulfur oxidation in cytochrome p450s? Angew. Chem. Int. Ed. Eng. 45 (2006) 8221–8223.
[35] M.J. Cryle, J.J. De Voss, The role of the conserved threonine in P450 BM3 oxygen activation: substrate-determined hydroxylation activity of the Thr268Ala mutant, ChemBioChem 9 (2008) 261–266.

The effect of decoy molecules on the activity of the P450Bm3 holoenzyme and a heme domain peroxygenase variant

Shaghayegh Dezvarei,[a] Osami Shoji,[b] Yoshihito Watanabe,[b] and Stephen G. Bell[a,*]

[a] *Department of Chemistry, University of Adelaide, Adelaide, 5005, Australia*

[b] *Department of Chemistry, Graduate School of Science, Nagoya University, Furo-cho, Chikusa-ku, Nagoya, 464-8602, Japan*

Supplemental section

Chromatography methods

GC-MS

For styrene and ethylbenzene the oven temperature was held at 60 °C for 3 min then increased at 10 °C min $^{-1}$ to 200 °C and maintained at this temperature for 5 min. For methylthiobenzene the initial oven temperature was 80 °C (held for 3 min) which was increased at 5 °C min $^{-1}$ to 200 °C and maintained at this temperature for 3 min The injector and interface temperature were 250 and 280 °C, respectively. A Shimadzu GC-2010 coupled to a GC-MS-QP2010S detector equipped with a ZebronDB-5 MS fused silica column (30 m x 0.25 mm x 0.25 µm) was used.

Chiral GC

Chiral chromatography was undertaken on a Shimadzu Tracera GC coupled to Barrier Discharge Ionization Detector (BID) equipped with a RT®- BDEXse chiral silica column (Restek; 30 m x 0.32 mm x 0.25 µm). For styrene and ethylbenzene the oven temperature was held at 60 °C for 3 min then increased at 5 °C min $^{-1}$ to 140 °C and maintained at this

1

temperature for 5 min and then raised at 20 °C min $^{-1}$ to 200 °C (2 min). For methylthiobenzene the oven temperature was maintained at 80 °C for 3 min then raised at 5 °C min $^{-1}$ to 200 °C and maintained at this temperature for 3 min. The injector and detector temperature were 230 °C. Ethylbenzene turnovers were also analysed on a Shimadzu Nexus GC system equipped Supelcowax column (Supelco, 30 m x 0.32 mm x 0.25 µm) a using the method above

NADPH turnovers

The Bm3 holoenzyme *in vitro* NADPH turnovers were run at 30 °C in 1200 µL of 50 mM Tris, pH 7.4 at 30 °C, containing 0.2 µM enzyme and 120 µg bovine liver catalase. The buffer was saturated with oxygen gas just before use and the assays were allowed to equilibrate for 1 min prior to the addition of the decoy molecule (100 µM from a 10 mM stock in DMSO) if present, and substrate (1 mM substrate from a 100 mM stock in DMSO). Finally NADPH was added, from a 20 mg mL^{-1} stock, to a final concentration of ~320 µM (equivalent to 2 AU). After NADPH addition before the rate of absorbance decay at 340 nm was measured. The reactions were allowed to run until all the NADPH was consumed. The NADPH turnover rate was derived using $\varepsilon_{340} = 6.22\ mM^{-1}\ cm^{-1}$.

2

The chromatographic retention times of substrates and the relevant products

Product	m/z	GC-MS RT	GC RT
ethylbenzene	105	3.0	
1-phenylethanol	122	6.75	*R*:15.8, *S*:16.0
acetophenone	120	6.8	
2-ethylphenol	122	8.1	
styrene	105	2.9	
phenylacetaldehyde	120	6.4	
styrene oxide	119	6.8	*R*:12.6, *S*:12.9
methylthiobenzene	124	< 3	
methylphenyl sulfoxide	132	8.9	*R*:17.9, *S*:18
methylphenyl sulfone	150	9.75	

3

Table S1 Enzyme turnover data for the Bm3TE heme domain variant of P450Bm3 with ethylbenzene, styrene and methylthiobenzene. The total amount of product (nmoles) in the 1 ml reactions are reported. A concentration of 5mM substrate, 3 μM CYP enzyme, in 50 mM Tris, pH 7.4 and 60 mM H_2O_2 was used.

	Bm3 TE	PFC10	PFC9-L-Ala	PFC9-L-Val	PFC9-L-Leu	PFC9-L-Gly	PFC9-L-Met	PFC9-L-Phe	PFC9-L-Trp
ethylbenzene									
ethylphenol	199	118	120	168	127	111	117	108	184
2-ethylphenol	42	23	16	19	11	21	11	11	19
acetophenone	44	29	30	39	52	38	50	43	39
% acetophenone	15	17	18	17	27	22	28	27	16
ee (S)	59	46	48	62	55	42	69	61	62
styrene									
styrene oxide	640	472	495	287	206	298	153	127	130
aldehyde	52	48	43	27	23	35	16	13	17
% aldehyde	8	9	8	9	10	11	9	9	12
ee (R)	11	19	13	10	12	16	16	20	15
methylthiobenzene									
sulfoxide	914	937	1300	957	1010	712	700	695	863
sulfone	119	92	72	75	63	79	39	31	71
sulfone%	12	9	5	7	6	10	5	4	8
ee (R)	14	15	14	24	25	18	31	26	22

Note: Methylthiobenzene oxidation in absence of enzyme and the presence of H_2O_2 generated 79 nmoles of methylphenyl sulfoxide

4

The structures of the second generation decoy molecules used in this work.

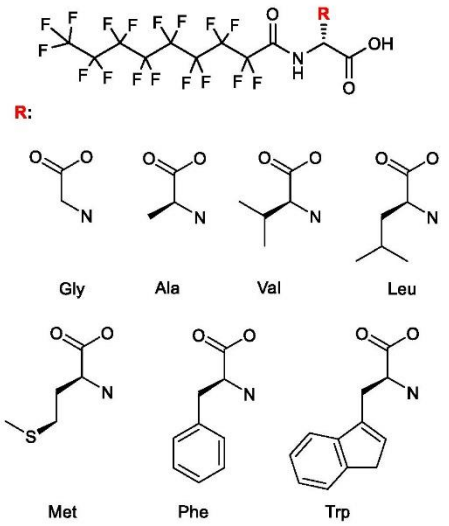

5

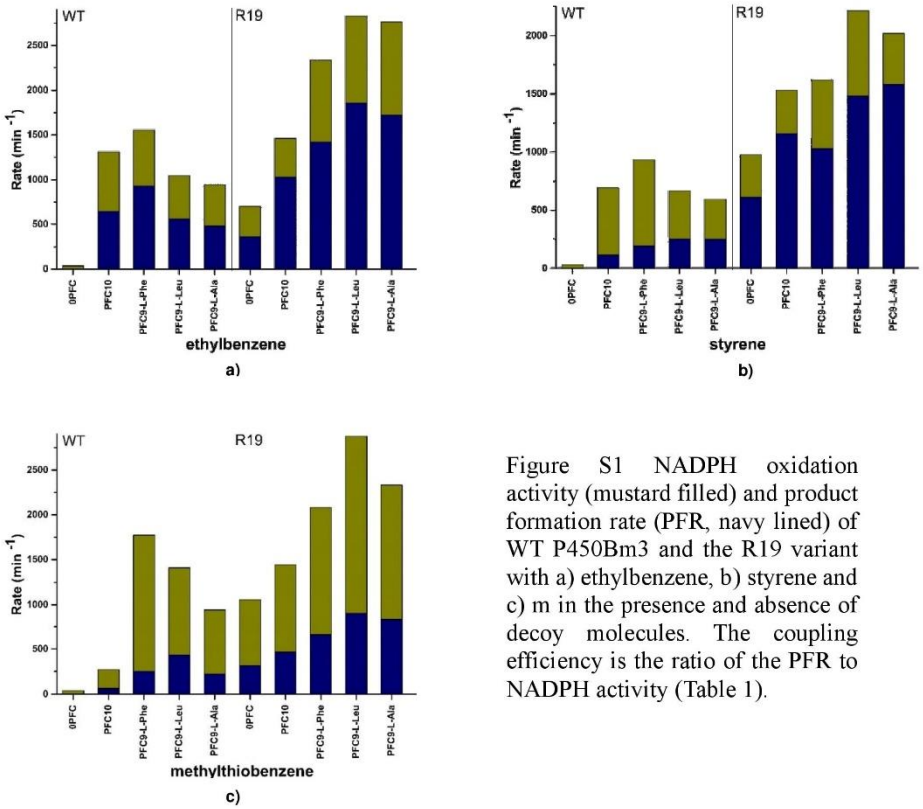

Figure S1 NADPH oxidation activity (mustard filled) and product formation rate (PFR, navy lined) of WT P450Bm3 and the R19 variant with a) ethylbenzene, b) styrene and c) m in the presence and absence of decoy molecules. The coupling efficiency is the ratio of the PFR to NADPH activity (Table 1).

6

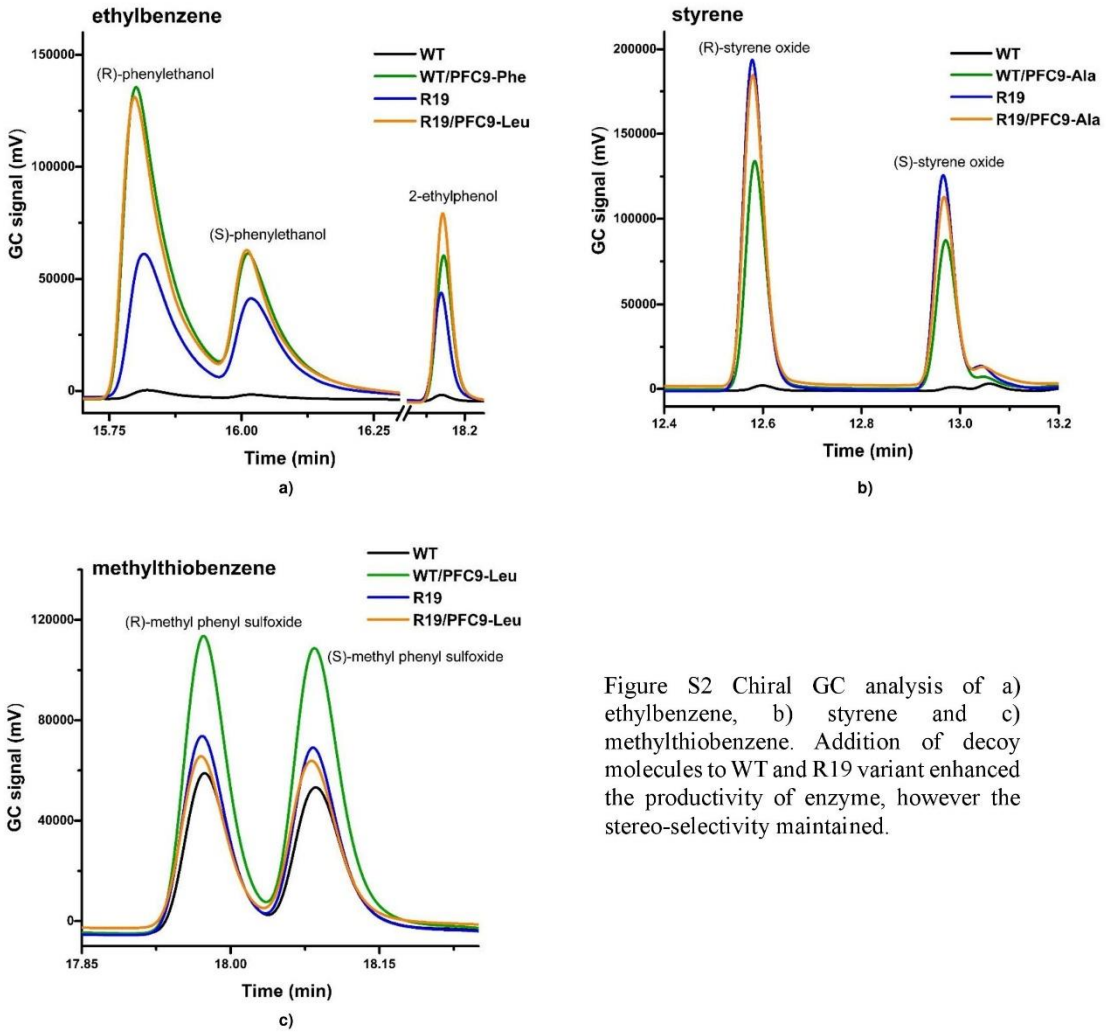

Figure S2 Chiral GC analysis of a) ethylbenzene, b) styrene and c) methylthiobenzene. Addition of decoy molecules to WT and R19 variant enhanced the productivity of enzyme, however the stereo-selectivity maintained.

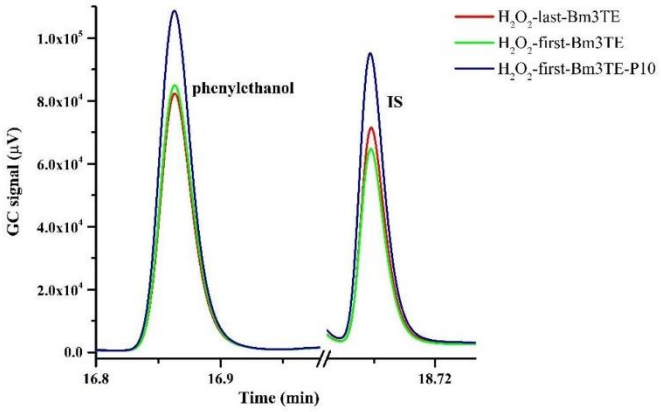

Figure S3 A comparison of 1-phenylethanol formation from the oxidation of ethylbenzene by Bm3TE with H_2O_2 added before or after substrate addition and decoy molecule (P10; PFC10, when present). This highlights that the level of product is not significantly increased when the order changes.

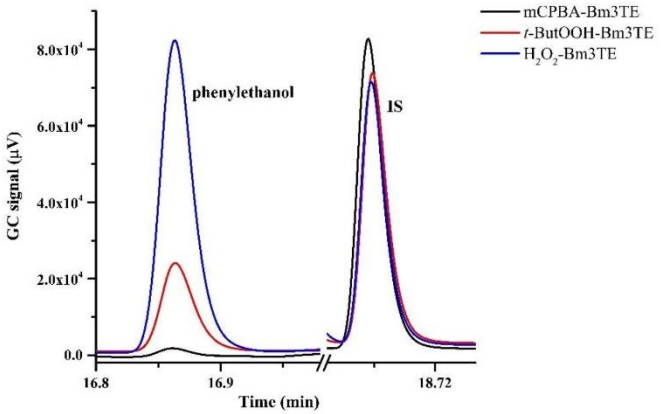

Figure S4 A comparison of 1-phenylethanol formation from the oxidation of ethybenzene by Bm3TE with H_2O_2, t-ButOOH (*t*-butylhydroperoxide) and mCPBA (*meta*-chloroperoxybenzoic acid)

8

GC-MS data

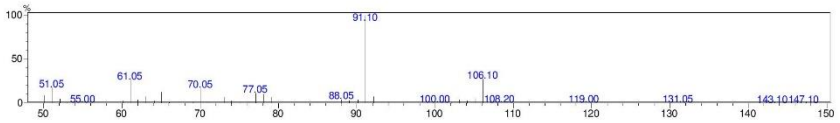

ethylbenzene GCMS RT: 3 min

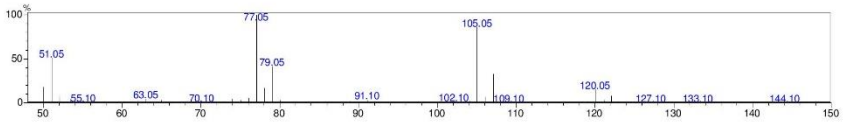

acetophenone GCMS RT: 6.75 min

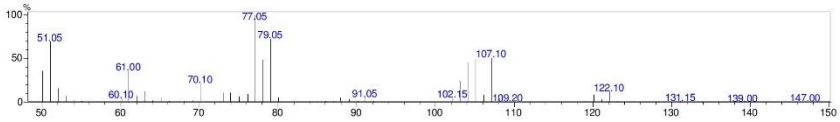

ethylphenol GCMS RT: 6.8 min

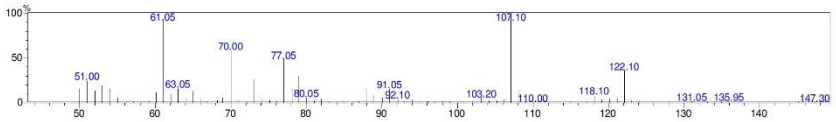

2-ethylphenol GCMS RT: 8.1 min

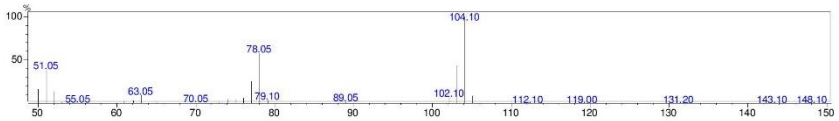

styrene GCMS RT: 2.9 min

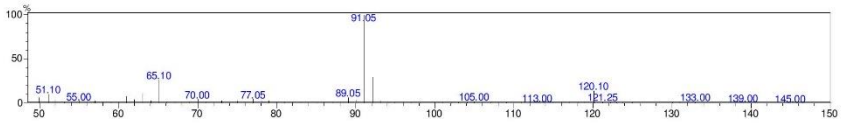

acetaldehyde GCMS RT: 6.4 min

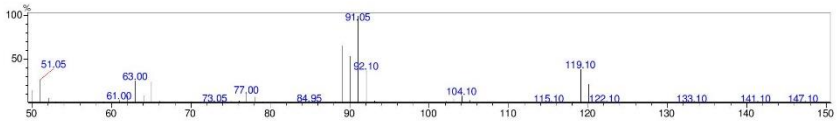

styrene oxide GCMS RT: 6.8 min

9

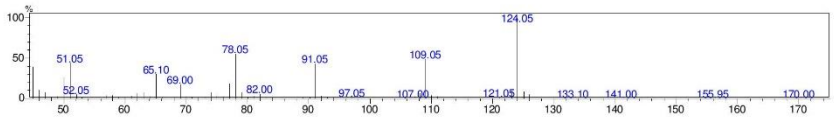

methylthiobenzene GCMS RT: < 3 min

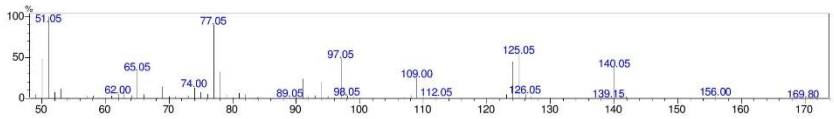

methylphenyl sulfoxide GCMS RT: 8.9 min

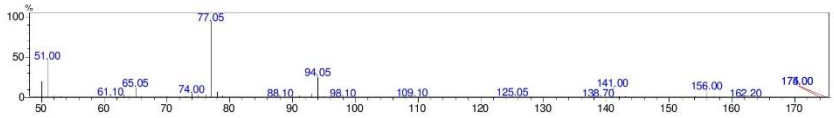

methylphenyl sulfone GCMS RT: 9.75 min

Chapter 8

Immobilisation of Bm3TE in ZIF-8, ZIF-90 crystals and nanobacterial compartments (encapsulins)

8.1 *In situ* encapsulation of Bm3TE@ZIF-8

The lower cost of using H_2O_2 for oxidation reactions with Bm3T268E (Bm3TE) make this variant a promising biocatalyst for oxidation reactions (Chapter 7). However, there are drawbacks using free enzymes which hamper their applications for efficient processes. The inability to separate the homogenous enzyme from the product and low thermal and chemical stability restrict the recycling of enzymes after a reaction, which can lead to an increase in the expense[257-261]. The regio- and stereoselectivity potential of enzymes has led to many studies to improve their functional properties like recyclability and higher stability[262-264]. Zeolitic imidazolate frameworks (ZIFs), are suitable candidates for the immobilisation of enzymes because they can be synthesised under biologically compatible conditions (1.9.1 Zeolitic imidazolate frameworks (ZIFs)). In this chapter, immobilisation of Bm3TE in ZIF-8 and ZIF-90 crystals and nanobacterial compartments (encapsulin) (1.9.2 Bacterial compartments) is studied in an attempt to increase the stability of the enzyme.

Encapsulation of P450Bm3TE was carried out using a method adapted from the work of Liang et al.[205]. P450Bm3TE in water (high concentration of phosphate buffer in Bm3 purification might decompose ZIF-8[202], therefore prior to encapsulation a buffer exchange step is employed) was added to an aqueous solution of 2-methylimidazole (HMIM, 160 mM, 2ml) and mixed with an aqueous solution of zinc acetate dihydrate ($Zn(OAc)_2.2H_2O$, 40 mM, 2ml)

(Figure 8. 1) resulting in a molar ratio of HMIM:Zn of 4:1[205] (2.3 Encapsulation of Bm3TE@ZIF-8). All reactions were carried out at room temperature with no stirring and the pH after mixing the protein, HMIM and Zn was 9.5.

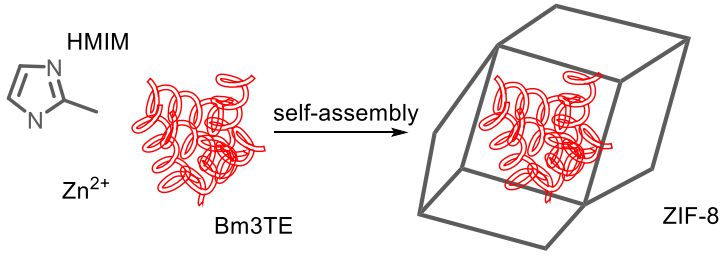

Figure 8. 1 Encapsulation of Bm3TE within ZIF-8 crystals.

After 30 min the synthesis solution started to turn cloudy, indicating the formation of a Bm3TE@ZIF-8 biocomposite (2.3 Encapsulation of Bm3TE@ZIF-8). The presence of protein therefore facilitates the seeding process in ZIF-8 crystals growth. The solution was left overnight to enable completion of the reaction. After 24 hours the product was collected by centrifugation, washed with ethanol and water and vacuum dried at room temperature (2.3 Encapsulation of Bm3TE@ZIF-8). The particles obtained were analysed by powder X-ray diffraction (PXRD) (Figure 8. 2).

The absence of the characteristic peak of ZIF-8 at 2θ values of 7.29 and 12.83 ° in the PXRD pattern indicated that the formed precipitate did not have the sodalite topology of ZIF-8[221]. The experiment was repeated at the same ratio of HMIM:Zn (160:40 mM) and this time left for 72 hours to check whether longer ageing the solution assists the formation of ZIF-8[201]. The obtained crystals were centrifuged, washed and characterised with PXRD. However, again, the PXRD pattern did not demonstrate the formation of ZIF-8 (Figure A. 1).

The use of 4:1 ratio of HMIM to Zn in aqueous solution did not form ZIF-8, and an unknown crystalline phase was observed in PXRD (Figure 8. 2). Previously ZIF-8 formation has been

shown to require the presence of some organic solvent or the use of the higher ratio of HMIM:Zn in an aqueous system[255]. Therefore, the concentration of the HMIM ligand was increased, while the rest of the conditions of the reaction were maintained. Higher ratios of HMIM:Zn (8:1, 16:1 and 30:1) were assessed to see if these would result in the formation of ZIF-8 in the presence of the Bm3TE protein. The resulting crystals in these experiments were centrifuged, washed (2.3 Encapsulation of Bm3TE@ZIF-8), analysed by PXRD (Figure 8. 2) and scanning electron microscopy (SEM) (Figure 8. 3). The PXRD patterns of Bm3TE@ZIF-8 crystals that precipitated out using the higher concentrations of HMIM (16:1 and 30:1 ratios of HMIM:Zn) were in good agreement with the pattern reported in the literature for ZIF-8 (Figure 8. 2). The characteristic peaks of ZIF-8 at 2θ values of 7.4, 10.4, 12.7, 14.7, 16.4, 18.0, 22.1, 24.5, 26.7 and 29.6° corresponded to the (011), (002), (112), (022), (013), (222), (114), (233), (134) and (044) index planes, respectively[203, 265, 266].

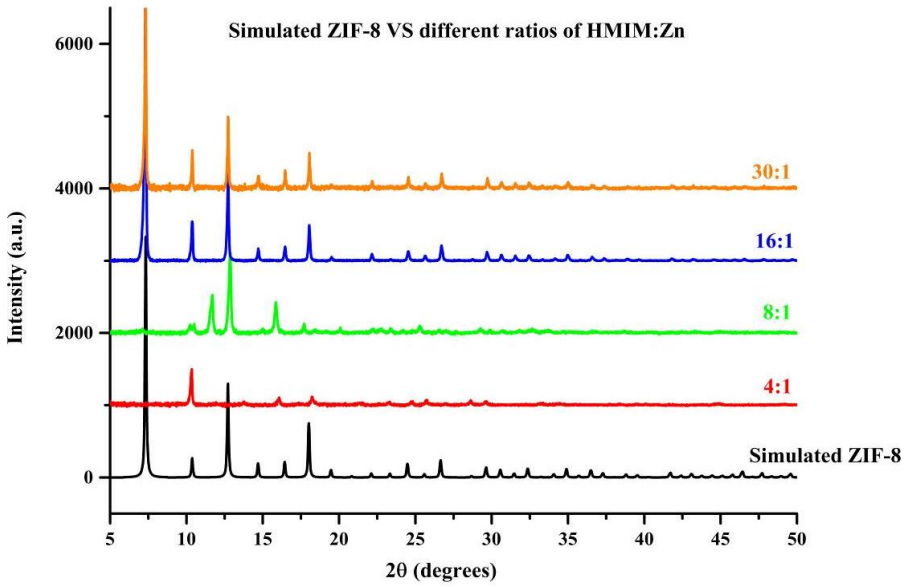

Figure 8. 2 PXRD patterns of the simulated ZIF-8 (black) and the crystals obtained through encapsulation of Bm3TE with various molar ratio of HMIM:Zn; 4:1 (red), 8:1 (green), 16:1 (blue) and 30:1 (orange).

To check the morphology and crystal size of ZIF-8, the scanning electron microscopy images were studied (2.8 Scanning electron microscopy (SEM). Rhombic dodecahedron crystals were obtained for the 16:1 and 30:1 ratios of HMIM:Zn with diameter size of 1.2 µm and 0.6 µm respectively. This further evidenced the successful formation of ZIF-8 in the presence of Bm3TE. However, the scanning electron microscopy image of 8:1 ratio showed a mixture of other crystals with different morphology (Figure 8. 3).

Encapsulation of Bm3TE was therefore carried out using a 16:1 ratio of HMIM:Zn overnight. To confirm the success of Bm3TE immobilisation in ZIF-8 crystals, the reaction mixture was centrifuged, and the UV-vis absorbance of the supernatant was measured to check for the presence of P450Bm3 in the solution. The supernatant after centrifugation did not show the characteristic P450 Soret peak at 418 nm, which inferred the absence of the P450Bm3TE haem domain protein.

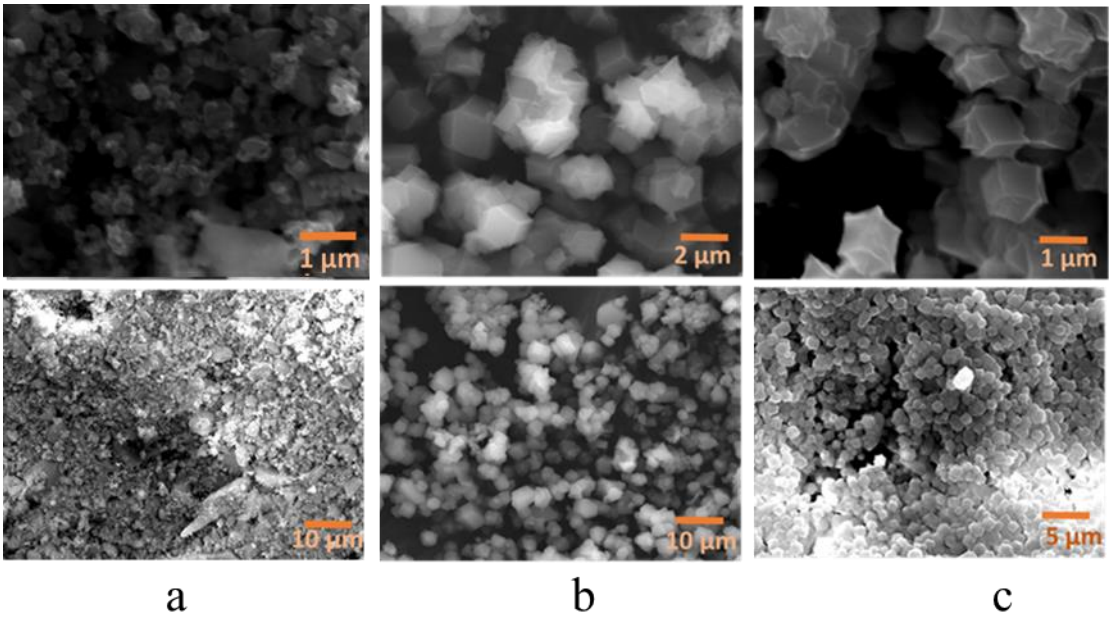

Figure 8. 3 Different resolutions of scanning electron microscopy images of crystals obtained by a) 8:1, b) 16:1 and c) 30:1 ratio of HMIM:Zn. The top images are at a higher magnification that demonstrates the rhombic dodecahedron crystals and the low magnification images on below imaged show the uniformity of crystals at 16:1 and 30:1 ratio of HMIM:Zn.

To determine the spatial distribution of Bm3TE within the ZIF-8 crystals, Bm3TE was labelled with fluorescein isothiocyanate (FITC) and analysed by confocal laser microscopy (CLSM) (2.9 Fluorescein isothiocyanate-tagged Bm3TE). FITC labelled P450 Bm3TE (FITC-Bm3TE) molecules were synthesised and encapsulated in ZIF-8 crystals using a previously reported method[255]. In a typical experiment, FITC and Bm3TE were dissolved in carbonate-bicarbonate aqueous buffer and left at room temperature in the dark (2.9 Fluorescein isothiocyanate-tagged Bm3TE). After 12 hours the FITC tagged Bm3TE (FITC-Bm3TE) was recovered, concentrated and washed to remove the excess FITC. Samples prepared using labelled protein were analysed by confocal laser microscopy (2.10 Confocal laser scanning microscopy (CLSM)). The images showed that the FITC-Bm3TE molecules were associated with the ZIF-8 crystals (Figure 8. 4)

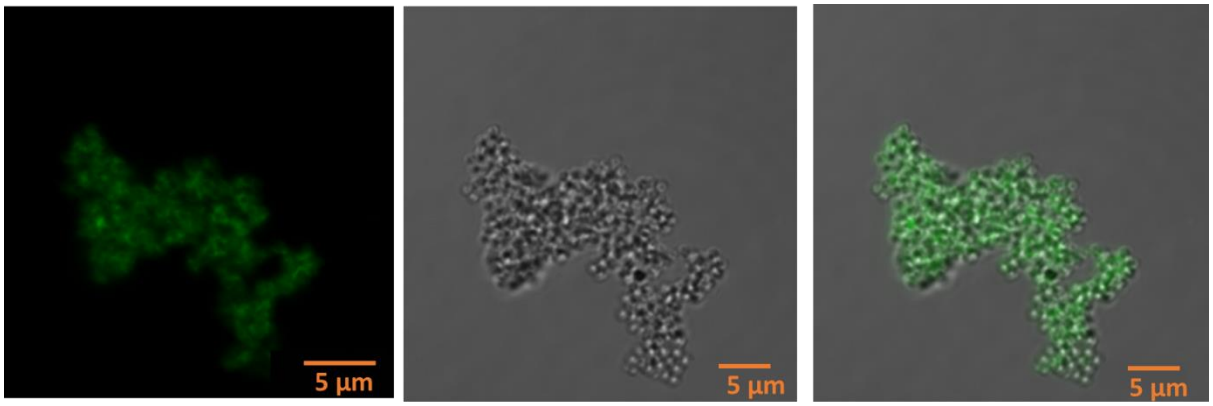

Figure 8. 4 Confocal laser scanning microscopy images demonstrate the co-location of FITC-Bm3TE and the rhombic dodecahedron ZIF-8 crystals after a Milli-Q H_2O and EtOH wash. From left to right; fluorescence, bright field, and overlay images of the FITC-Bm3TE@ZIF-8.

To check the activity of the Bm3TE@ZIF-8, samples were washed with Milli-Q H_2O and EtOH to remove the loosely adsorbed protein on the crystal surface. Certain P450 enzymes can oxidise indole to indigo in the presence of the H_2O_2 [267] therefore, the activity of the encapsulated Bm3TE as an H_2O_2-dependent P450 enzyme was investigated with indole in the presence of H_2O_2 as a simple colourimetric assay (Figure 8. 5). The free Bm3TE oxidised indole

to indigo at pH above 8.0, generating a blue colour in the reaction solution (Figure 8. 5). However, Bm3TE@ZIF-8 showed no colour changes in indole turn over.

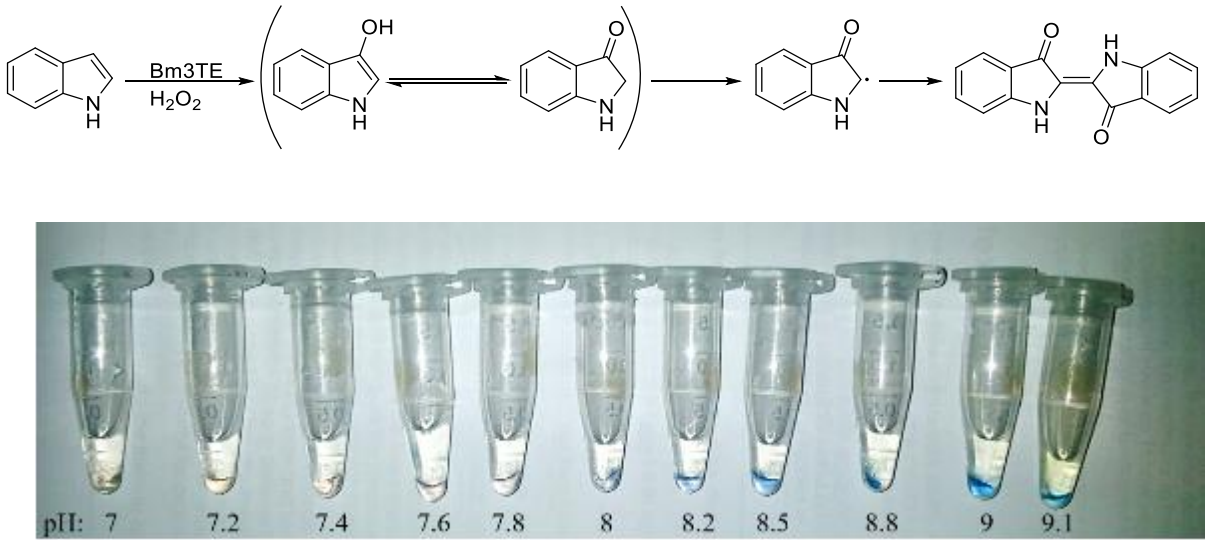

Figure 8. 5 The indole turnover with Bm3TE in the presence of H_2O_2 at different pHs. A blue colour was observed at pH above 8.

Considering that ZIF-8 has small pore aperture (3.4 Å)[167] for substrate diffusion, the large size of indole (6.7-6.8 Å) might inhibit its diffusion through the ZIF-8 to reach the active site of Bm3TE or product release. Chapter 6 has shown that Bm3TE variant can successfully produce styrene oxide. Styrene was chosen as a more reactive substrate to investigate its oxidation with Bm3TE@ZIF-8. The encapsulated Bm3TE was washed with Milli-Q H_2O and then EtOH to remove the excess enzyme from the surface of ZIF-8 before its activity was tested with styrene. The H_2O_2-driven turnover with free Bm3TE oxidised styrene to styrene oxide but the encapsulated Bm3TE displayed no activity (Figure 8. 6).

We then considered two possibilities regarding the lack of enzymatic activity of encapsulated Bm3TE with styrene: the first reason could be the inactivation of the enzyme during the encapsulation process, and the other reason could be the inaccessibility of enzyme to styrene due to the small pore aperture size in ZIF-8 as discussed above.

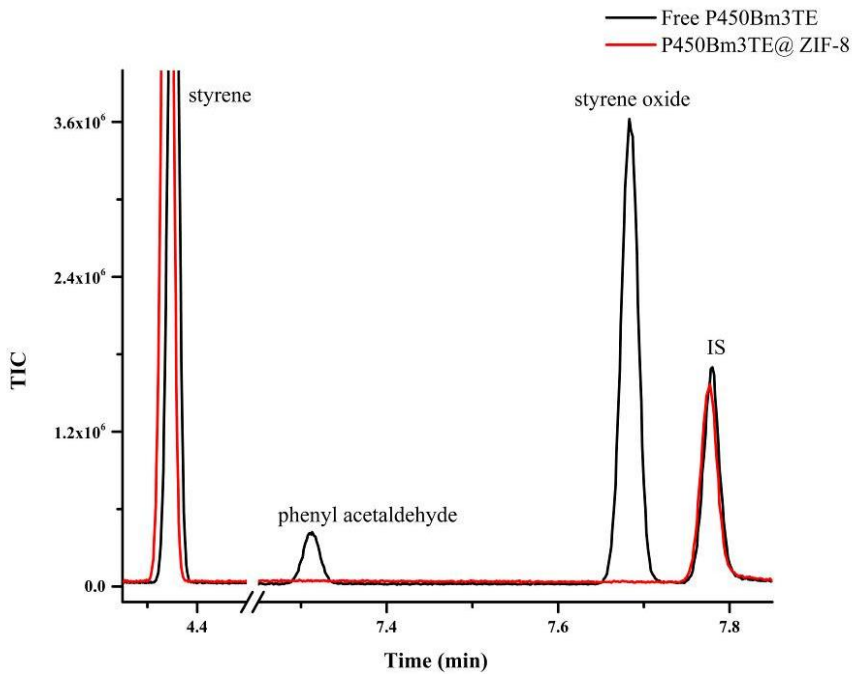

Figure 8. 6 GC-MS analysis the hydrogen peroxide driven turnovers of styrene with free Bm3TE and Bm3TE@ZIF-8 showed that the encapsulated Bm3@ZIF-8 is not active.

In terms of inactivation, one hypothesis is that the imidazole based ligands of the ZIF-8 could bind to the enzyme haem moeity and inhibit the oxidation activity of Bm3TE. When imidazole ligands bind to haem, a type II binding spectrum arises[268]. Therefore the spin state of Bm3TE was measured in the presence of the HMIM ligand (160 mM). No red-shift to ~420 nm was observed to indicate that type II binding has occurred (Figure A. 2). However, in order to minimise the effect of the high concentration of HMIM (640 mM) used, instead of adding Bm3TE to an aqueous solution of HMIM, it was added to the Zn acetate dihydrate solution. Also to eliminate the possibility that the deactivation of Bm3TE@ZIF-8 is derived from high pH, in this experiment pH of the solution mixture was adjusted to 8.0. Using this alternative method, the formation of ZIF-8 was confirmed by PXRD (Figure 8. 7), but no product with styrene was observed. This enzymatic assay data demonstrated that pH did not inhibit Bm3TE activity. The high concentration of HMIM present in the solution before ZIF-8 formation might

have deactivated the enzyme or the loss of activity could be due to hydrophobicity of ZIF-8 which could interact with Bm3TE and resulted in irreversible deactivation[283, 284].

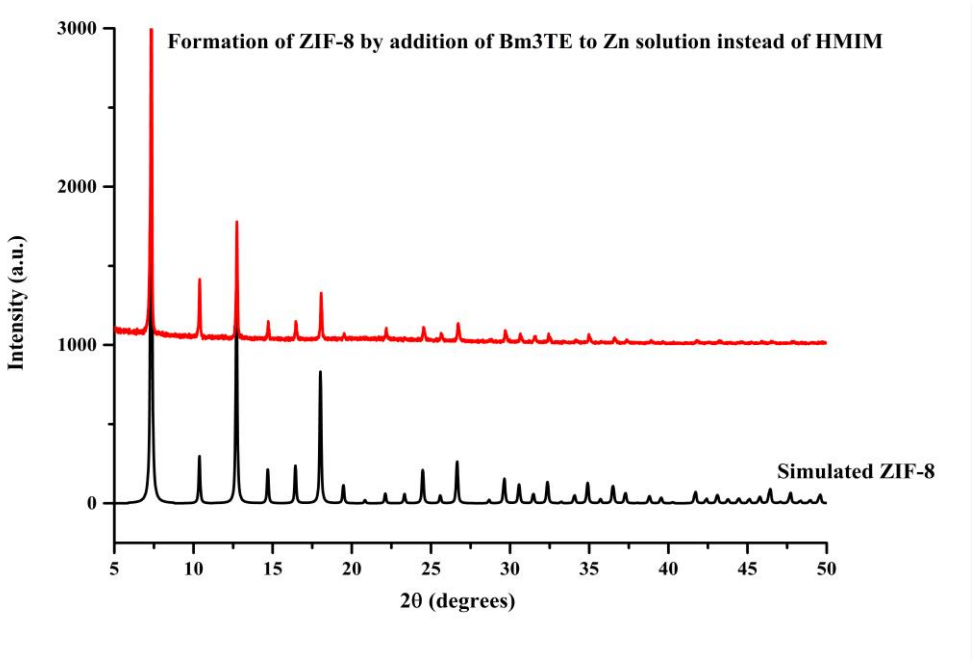

Figure 8. 7 PXRD patterns of Bm3TE@ZIF-8. In this encapsulation process, Bm3TE was added to the aqueous Zn solution instead of HMIM to investigate whether the effect of high concentration HMIM (640 mM) on inactivation of the enzyme can be reduced.

ZIF-8 crystals are not stable at pH below 7.0, and they dissociate in solution[202]. Therefore, to investigate whether the encapsulated enzyme was active or the small pore size prohibited substrate accessibility, the crystals of Bm3TE@ZIF-8 were dissolved using 0.1 M citric acid/sodium citrate aqueous buffer (pH 5.0) to release the enzyme into solution[255]. The dissolved solution of Bm3TE@ZIF-8 passed through a PD-10 desalting column. After washing the sample with Milli-Q H_2O followed by centrifugation, a red pellet was observed. The red colour indicates that denatured haem protein may be present in the pellet. This suggested the denaturation of the Bm3TE during the encapsulation or release process may be occurring. For further confirmation, the oxidation activity of the released enzyme (supernatant) was tested with styrene and no activity was observed (Figure 8. 8). Overall the results suggest that the

protein could be denatured during the biocomposite synthesis process and this is the reason we do not observe activity.

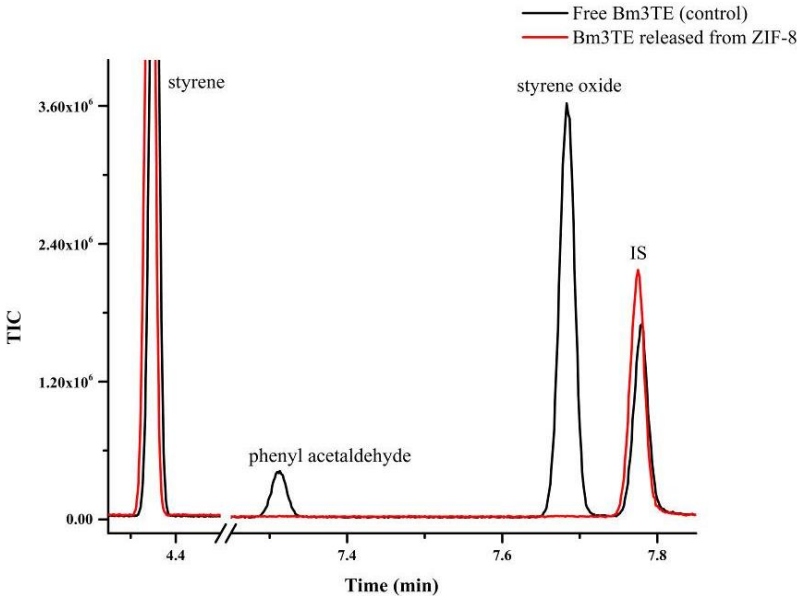

Figure 8. 8 GC-MS analysis of the hydrogen peroxide driven turnovers of styrene with Bm3TE free enzyme and the supernatant, which could contain Bm3TE released from ZIF-8.

In a control experiment the activity of Bm3TE was tested in the presence of 640 mM HMIM aqueous solution, the initial pH of this solution was 11.0 which was then adjusted to 9.5 before the addition of enzyme using HCl to simulate the condition of ZIF-8 formation. The colour of the initial solution of Bm3TE and HMIM is pale red, which arise from the P450 enzyme colour. This red colour disappeared after ~2 hours which could indicate denaturation of the enzyme. The activity of Bm3TE was tested for the oxidation of styrene, and a lower activity was observed after 2 hours treatment of Bm3TE with 640 mM HMIM (Figure 8. 9).

Another possible reason for inactivation of the enzyme is the hydrophobic nature of ZIF-8. It has been shown that enzymes have good affinity for hydrophobic surfaces, this can result in conformational changes and their denaturation[269, 270]. Liang et al. studies showed that encapsulated catalase within ZIF-8 crystals is inactive because of these interactions[256].

Therefore, the hydrophobic interaction of ZIF-8 with Bm3TE could result in denaturation and activity loss[269, 270].

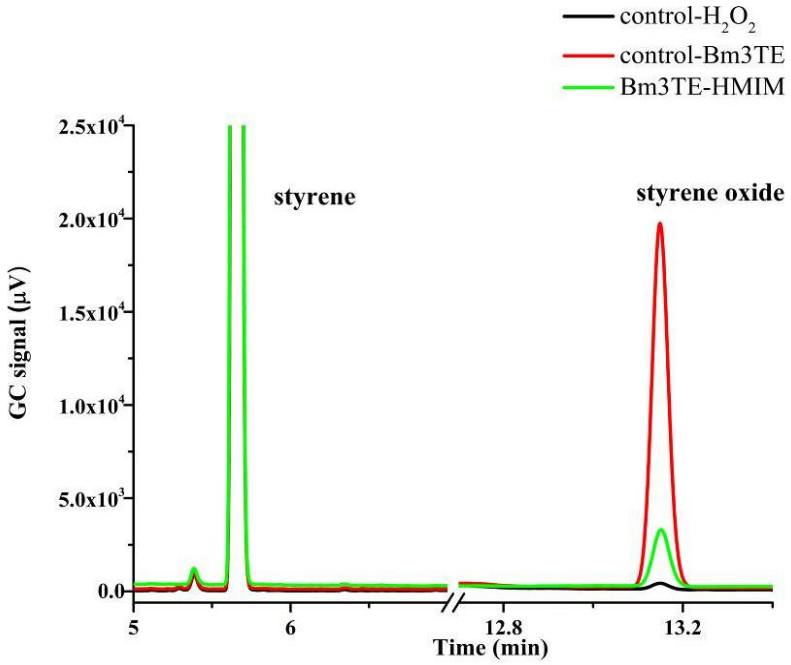

Figure 8. 9 GC analysis of styrene oxidation with Bm3TE showed that enzyme almost lost its activity in the presence of 640 mM HMIM

Encapsulation of Bm3TE in ZIF-8 crystals was investigated, and the PXRD patterns showed the successful formation of ZIF-8 in the presence of Bm3TE. However, the encapsulated enzyme showed no activity, and it was hypothesised that Bm3TE denatured during the biocomposite synthesis process presumably because of either the hydrophobic interaction with ZIF-8[269, 270] or deactivation in the presence of the high concentration of HMIM. Therefore to eliminate the effect of high concentration of HMIM, different ZIFs could be tested. ZIF-90, which has a more hydrophilic 2-imidazole carboxaldehyde (HICA) ligands, was studied for encapsulation of Bm3TE. Changing the ligand from HMIM to HICA could affect the conditions of formation, and reduce the hydrophobicity of the crystals (which has been shown to be an issue with other enzymes[21, 22]).

8.2 *In situ* encapsulation of P450 Bm3@ZIF-90

Given that Bm3TE appeared to lose its activity in a high concentration of HMIM and the hydrophobic interactions with ZIF-8 may be problematic, an alternative encapsulation method using ZIF-90 was investigated[165, 271]. The difference between ZIF-8 and ZIF-90 is in the choice of the imidazole ligands. While 2-methylimidazole is employed in the synthesis of ZIF-8, the formation of ZIF-90 occurs with HICA and the resulting MOF is more hydrophilic (Equation 8. 2). The pH of HICA ligand solution is around 6.0 which is significantly lower than HMIM (11.0).

Equation 8. 2 ZIF-8 forms with HMIM and for ZIF-90 formation HICA ligands are used.

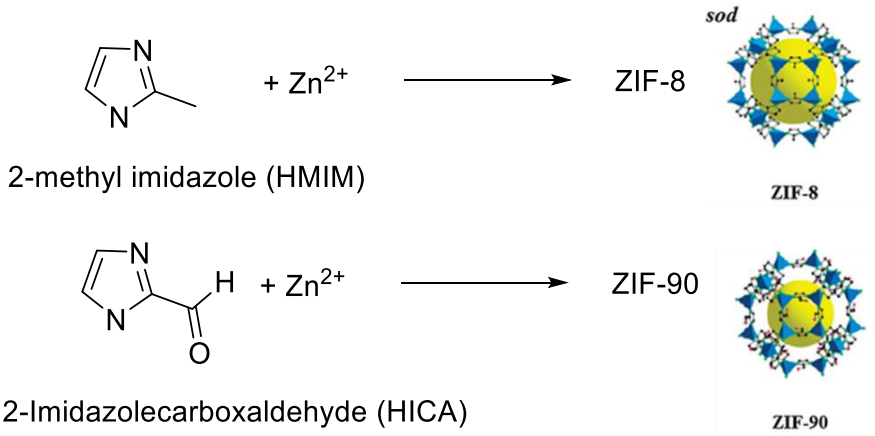

In a typical experiment, HICA (160 mM) and Zn $(NO_3)_2.6H_2O$ (40mM) were dissolved in 1:1 v/v of glycerol/water separately. The enzyme was added to the HICA solution followed by addition of the aqueous Zn solution (2.4 Encapsulation of Bm3TE@ZIF-90). The pH of the reaction mixture was 7.0. The solution turned cloudy immediately after mixing the HICA/enzyme and Zn solution indicating formation Bm3TE/ZIF-90 biocomposite. The resulting precipitates were centrifuged and collected after 2 hours. The formed crystals were washed with H_2O and EtOH to remove the loosely adsorbed protein on the crystal surface. ZIF-90 crystals were prepared using a 1:4 ratio of Zn: HICA, which was confirmed by the PXRD

(Figure 8. 10). The 2θ values of 7.4°, 10.4°, 12.7°, 14.7°, 16.4°, 18.0°, 22.1°, 24.5°, 26.7° and 29.6° corresponded to the (011), (002), (112), (022), (013), (222), (114), (233), (134) and (044) index planes respectively, were in a good agreement with the reported literature[209, 272, 273] (Figure 8. 10).

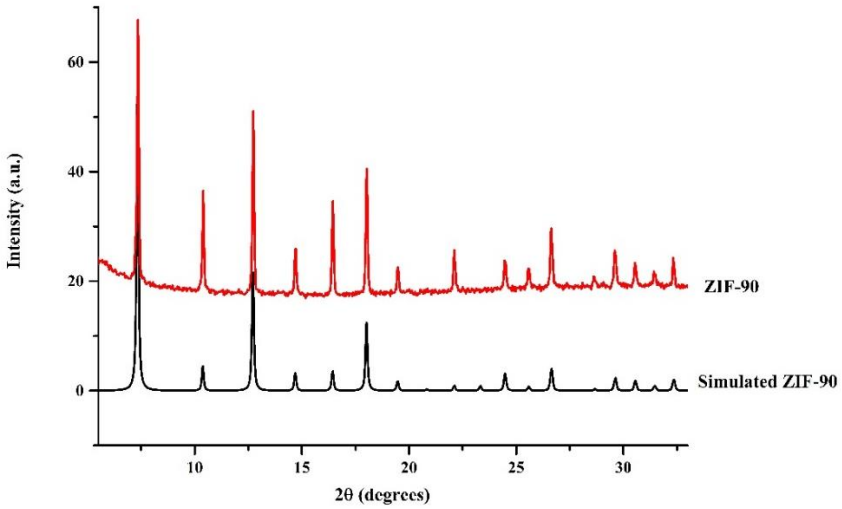

Figure 8. 10 The identical PXRD patterns of Bm3TE@ZIF-90 to the simulated patterns shows the successful formation of ZIF-90 in the presence of the enzyme.

The morphology and size of Bm3TE@ZIF-90 was assessed by scanning electron microscopy (2.8 Scanning electron microscopy (SEM). The images showed the rhombic dodecahedral crystals ZIF-90 in presence of Bm3TE with an average size of 1.4 μm diameter (Figure 8. 11).

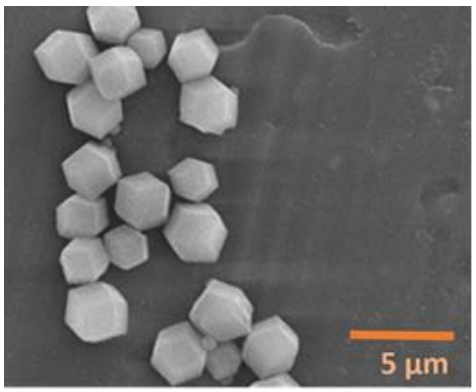

Figure 8. 11 Scanning electron microscopy images of Bm3TE@ZIF-90 showed the rhombic dodecahedral crystals with 1.41 μm diameter.

The location of the enzyme within the ZIF-90 was studied by confocal laser scanning microscopy. The FITC labelled Bm3TE (FITC-Bm3TE) molecules were synthesised as before (2.9 Fluorescein isothiocyanate-tagged Bm3TE) and encapsulated in ZIF-90 crystals using the same method. The confocal laser scanning microscopy images highlighted the distribution of FITC-Bm3TE molecules through the ZIF-90 crystals (Figure 8. 12).

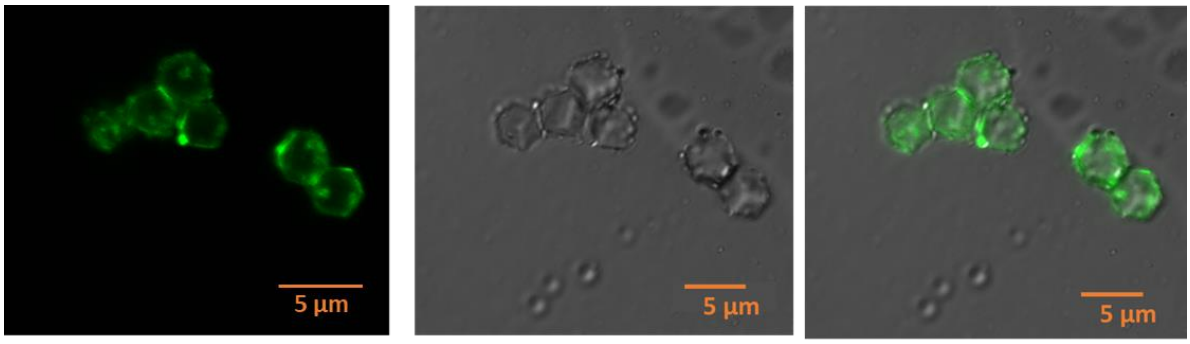

Figure 8. 12 Confocal laser scanning microscopy images demonstrate the FITC-Bm3TE in rhombic dodecahedron ZIF-90 crystals after Milli-Q H_2O, and EtOH wash. Left to right; fluorescence, bright field, and overlay images of the FITC-Bm3TE@ZIF-90.

The activity of Bm3TE@ZIF-90 was evaluated for the oxidation of styrene, but no product formation activity was observed (Figure 8. 14). Therefore, polyvinylpyrrolidone (PVP) was added to the reaction mixture during the encapsulation process to investigate whether PVP stabilises Bm3TE. PVP is an amphiphilic and non-ionic surfactant[274]. It acts as a MOF nucleating agent and has been used to stabilise nanoparticles against aggregation and to control their size and shape within encapsulation process[275-277]. PVP has been reported to stabilise. gold and silver nanoparticles in polar solvents during the formation of MOFs[189]. It has also been used in encapsulation of cytochrome (Cyt c), as a biological agent, in MOFs[168, 189]. The PVP was added to the protein solution prior to adding the HICA ligand solution followed by the addition of zinc nitrate, Zn $(NO_3)_2.6H_2O$, solution to initiate encapsulation of

Bm3TE@ZIF-90. The PXRD pattern of Bm3TE@ZIF-90 in the presence of PVP was analysed and confirmed the successful formation of ZIF-90 (Figure 8. 13).

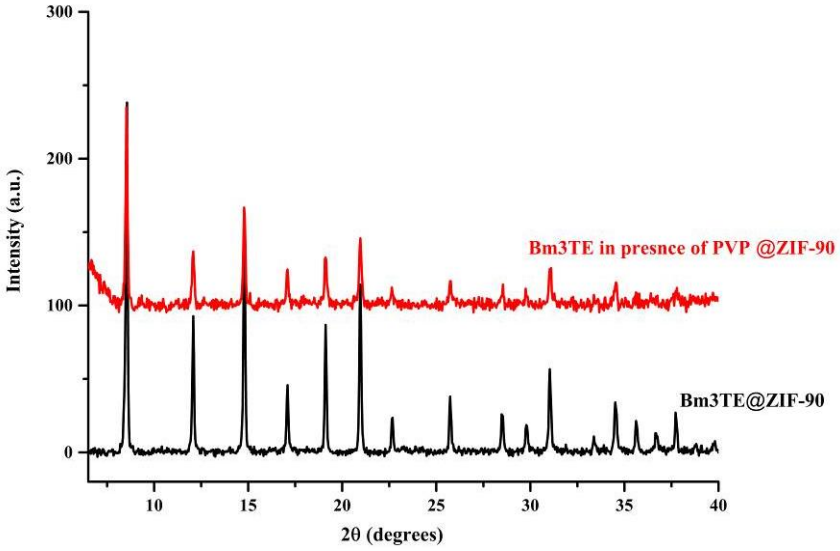

Figure 8. 13 PXRD patterns of Bm3TE in presence and absence of PVP in ZIF-90. The run time for the Bm3E@ZIF-90 in the presence of PVP was shorter than that shown in Figure 8.10, which contributes to the noisier baseline in this PXRD.

The activity of encapsulated Bm3TE@ZIF-90 in presence and absence of PVP was tested for styrene oxidation, and a small peak was observed at 7.68 min (Figure 8. 14). This retention time was the same as that of styrene oxide. To confirm the activity of the enzyme, the encapsulation of Bm3TE in ZIF-90 was repeated with double concentration of the enzyme and its oxidation activity for styrene was tested. In this experiment, the peak at RT: 7.68 min did not increase as expected, and no phenylacetaldehyde product was observed. Therefore a control experiment was performed to check whether this peak could be a background signal from ZIF-90. In similar turnover experiments, styrene was added to the buffer in the presence of ZIF-90 crystals and H_2O_2 (60 mM) without any Bm3TE, and in another experiment, styrene was added to buffer without any ZIF-90 crystals. The peak at 7.68 min was observed in the presence of ZIF-90 crystals but not in the styrene and H_2O_2 control (Figure 8. 15).

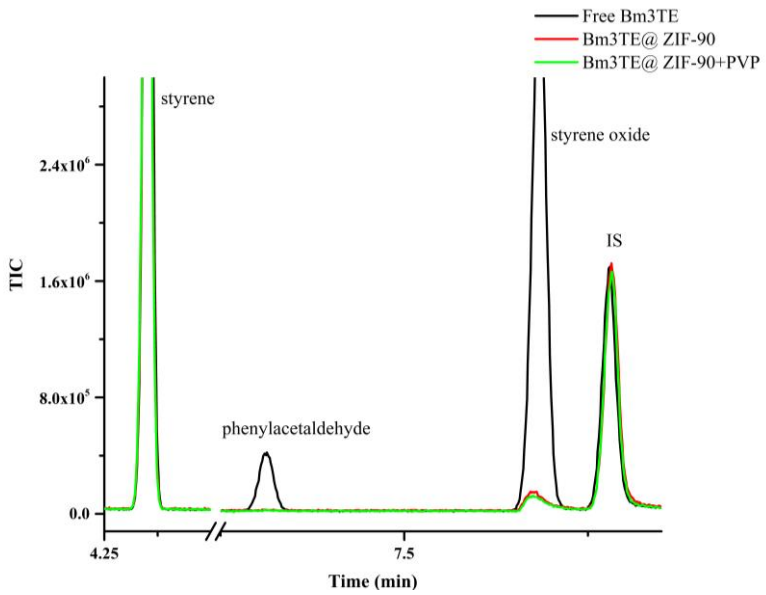

Figure 8. 14 The GC-MS of free enzyme vs the Bm3TE@ZIF-90 in the presence and absence of PVP.

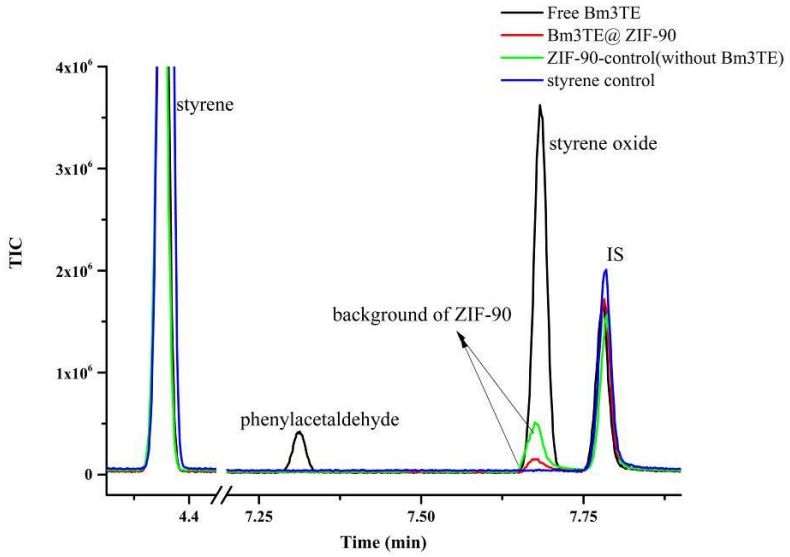

Figure 8. 15 The GC-MS analysis of free Bm3TE vs the Bm3TE@ZIF-90 and control of styrene turnover with ZIF-90 without enzyme in the presence of H_2O_2. A peak at 7.68 min was observed in all the three experiments concluding ZIF-90.

The control experiment suggested that the aforementioned peak arises from ZIF-90 and not from the oxidation of styrene. A comparison between the mass spectra of the peak from styrene oxidant and the ZIF-90 background confirmed that the peak at 7.68 min is not the expected

product as the m/z at 119 from the styrene oxide was not observed (Figure 1. 16). The m/z at 96 correlates to the molecular weight of the HICA ligand which could be present from the material decomposition or residual ligand from insufficient washing (2.4 Encapsulation of Bm3TE@ZIF-90). The mass spectra from the turnover showed a very small peak at m/z 91, which could suggest a very low level of product (Figure 1. 16 b). The inability of Bm3TE@ ZIF-90 to oxidise styrene in the presence of PVP demonstrated that PVP does not have a significant stabilising effect on Bm3TE.

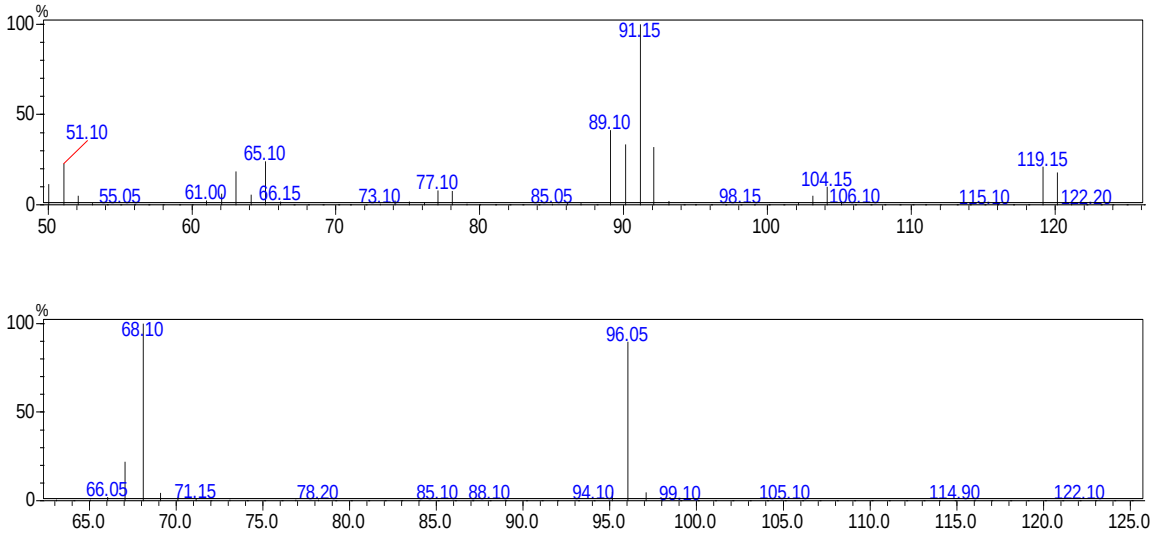

Figure 8. 16 The mass spectra of styrene oxide (top) vs the mass spectra of ZIF-90 background peak (bottom) with 7.68 min retention time.

In a control reaction, the encapsulated Bm3TE@ZIF-90 was treated with citrate buffer (pH:5.5) to break down ZIF-90 structure and release Bm3TE[255]. ZIF-90 crystals were left to fully dissolve in the buffer resulting in a clear solution. Similar to the released Bm3TE from ZIF-8, after centrifugation a red pellet was observed that inferred the presence of Bm3TE haem The supernatant of this mixture was tested with styrene but no oxidation activity was observed from the released enzyme (Figure 8. 17).

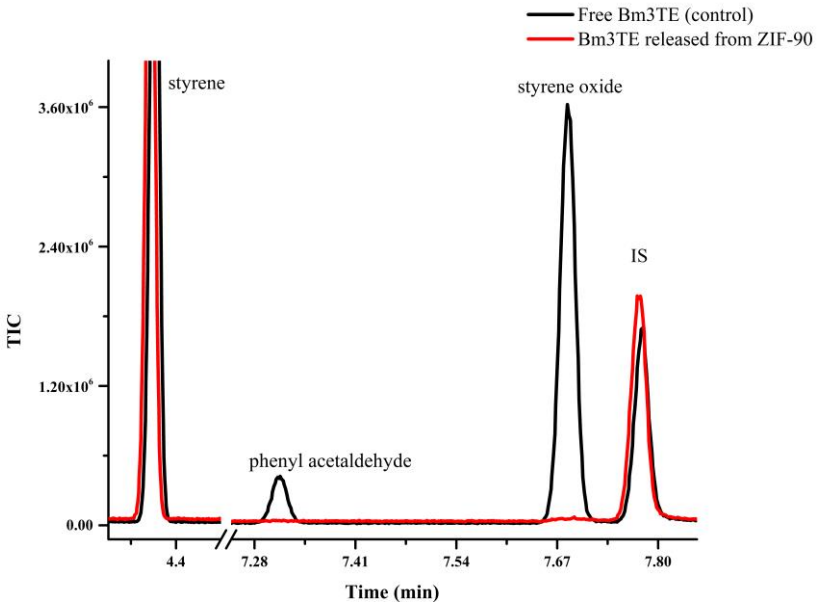

Figure 8. 17 GC-MS analysis of free Bm3TE compared to the supernatant which would contain Bm3TE released from ZIF-90. The latter showed no activity, which suggests denaturation of the Bm3TE enzyme.

As Bm3TE activity was significantly reduced in the presence of HMIM (Figure 8. 18), the activity of free P450 Bm3TE in the presence of zinc acetate dehydrate ($Zn(CH_3COO)_2$), and HICA in solutions was also tested to check if the existence of this organic ligand affects its activity. The concentrations of the $Zn(CH_3COO)_2$ and HICA were kept the same as in the encapsulation experiment. The oxidation activity of Bm3TE was tested on styrene turnover, and after 2 hours only a small amount of product was observed in the presence of the $Zn(CH_3COO)_2$ and more than half of the activity was lost in the presence of the HICA. This inferred the reduction of enzyme activity in the presence of $Zn(CH_3COO)_2$ and HICA ligand (Figure 8. 18).

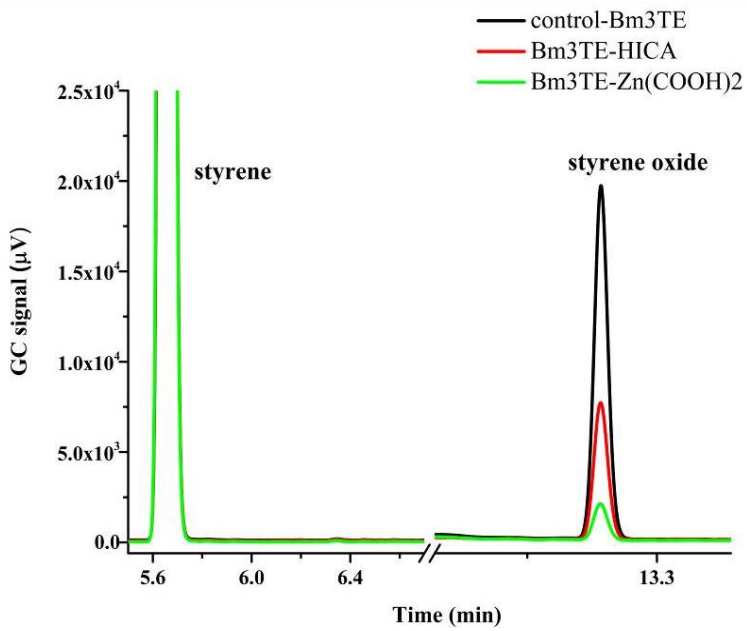

Figure 8. 18 GC analysis of styrene oxidation with Bm3TE in the presence of the $Zn(CH_3COO)_2$ salt (green) and HICA ligands (red) showed that enzyme had lost most of its activity.

Considering that Bm3TE lost its activity during the encapsulation process, the ZIF-90 and ZIF-8 crystals were then synthesised in advance for the adsorption of P450 Bm3TE on the external surface instead of in-situ encapsulation to limit the effect of Zn salts and ligands (HMIM and HICA) also assess if the enzyme was active after surface immobilisation.

8.3 Surface attachment of Bm3TE on ZIF-8 and ZIF-90

ZIF-8 and ZIF-90 particles were synthesised in advance using their published methods (2.5 Pre-synthesised ZIF-8 crystals, 2.6 Pre-synthesised ZIF-90 crystals)[253, 254]. The PXRD pattern of synthesised ZIF-8 and ZIF-90 were in good agreement with the literature[165, 203, 265, 266, 278] (Figure 8. 19). In a typical synthesis, ZIF-8 crystals with a diameter of 100 nm were prepared via a mild and facile route reported previously; the zinc nitrate solution (40 mM in methanol) was added to the methanol solution of HMIM (160 mM) and the mixture aged at room

temperature overnight under static conditions. The obtained crystals were washed with excess methanol and vacuum dried[253]. For surface adsorption, the prepared ZIF-8 crystals were added to the solution of Bm3TE in H_2O and left on ice while was gently shaking. To test the activity of the enzyme, after 1 hour, a 500 µl sample was taken from the solution and centrifuged to remove the supernatant, which would include any unadsorbed enzyme solution. However, the ZIF-8 crystals were floating in the enzyme solution, and centrifugation was unable to sediment them to check their activity.

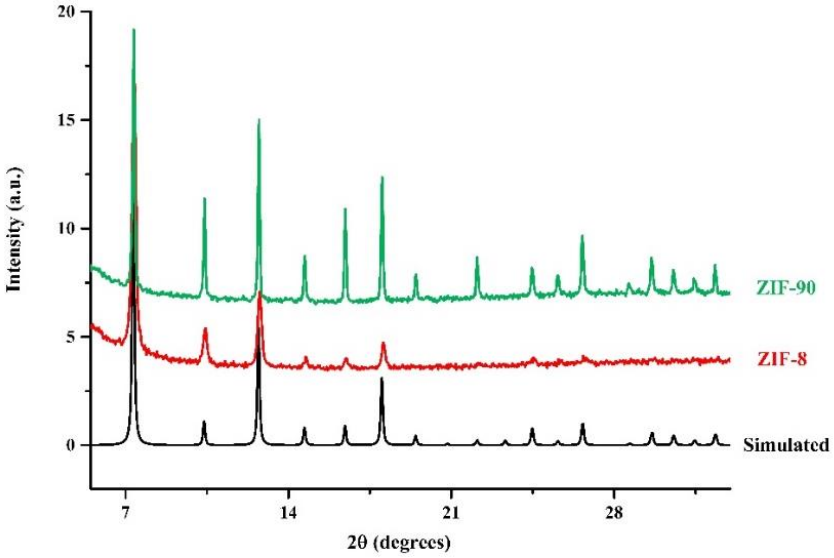

Figure 8. 19 PXRD patterns of pre-synthesised ZIF-8 and ZIF-90 crystals are in good agreement with the simulated patterns.

The confocal laser scanning microscopy images of immobilised Bm3TE on pre-synthesised ZIF-8 showed that the crystals are very small to observe individually (Figure 8. 20). Organic solvents at different concentrations are known to significantly effect on the size of ZIF-8 crystals[199, 279, 280]. Using methanol as a solvent in these pre-synthesised experiments could have led to smaller size crystals which could not be sedimented from the solution[281, 282]. Another reason that MOF crystals float to the surface could be the hydrophobicity of ZIF-8, which

limited its mixing with H_2O. ZIF-8 synthesis in H_2O could help to obtain bigger crystals for the immobilisation of Bm3TE on the surface of ZIF-8[295].

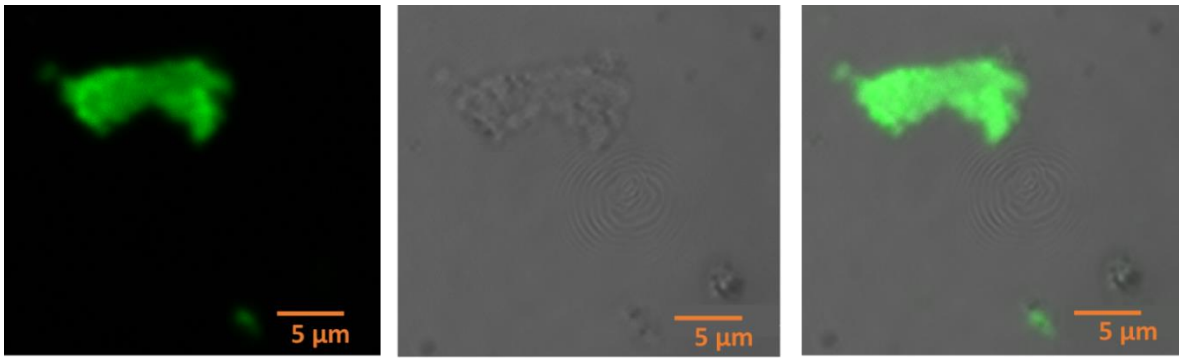

Figure 8. 20 Confocal laser scanning microscopy images demonstrate the FITC-Bm3TE on very small ZIF-8 crystals. Left to right; fluorescence, bright field, and overlay images of the FITC-Bm3TE on ZIF-8.

To immobilise Bm3TE on the surface of ZIF-90, MOF particles were synthesised by mixing a zinc nitrate solution (40 mM, in 1:1, *tert*-butanol: Milli-Q H_2O) with HICA solution (160 mM, in 1:1 glycerol: Milli-Q H_2O) and aging at room temperature overnight without agitation, the obtained particles were washed with excess methanol and vacuum dried[254] (2.6 Pre-synthesised ZIF-90 crystals). The synthesised ZIF-90 particles were added to different concentration of Bm3TE in water (3- 6 µM) and gently mixed on ice. At various time intervals, 500 µl samples of this solution mixture were taken and centrifuged to check the activity of the immobilised protein. The UV/Vis analysis of supernatant of these samples after centrifugation showed a strong absorbance at 418 nm (Figure 8. 21), which suggested the presence of the Bm3TE in the supernatant. To check if Bm3TE is adsorbed on the ZIF-90 crystals, Bm3TE was labelled with FITC, and its spatial distribution within the ZIF-90 crystals was analysed using confocal laser microscopy (Figure 8. 22).

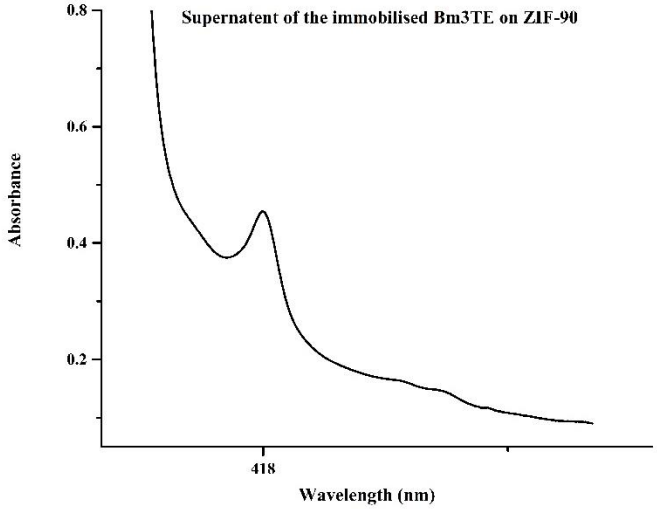

Figure 8. 21 The UV/Vis of the supernatant of Bm3TE solution after shaking in the presence of ZIF-90 (2 hours) showed that most of the protein remained in the solution and was not adsorbed on ZIF-90 crystals.

The confocal laser microscopy images of the ZIF-90 particles after 2h in FITC-Bm3TE solution showed the low interaction of Bm3TE on ZIF-90 crystals (Figure 8. 22), suggesting that most, if not all the protein remained in the solution and was not absorbed on the surface of ZIF-90. This experiment was repeated with more vigorous shaking of the reaction mixture, and the same results were obtained.

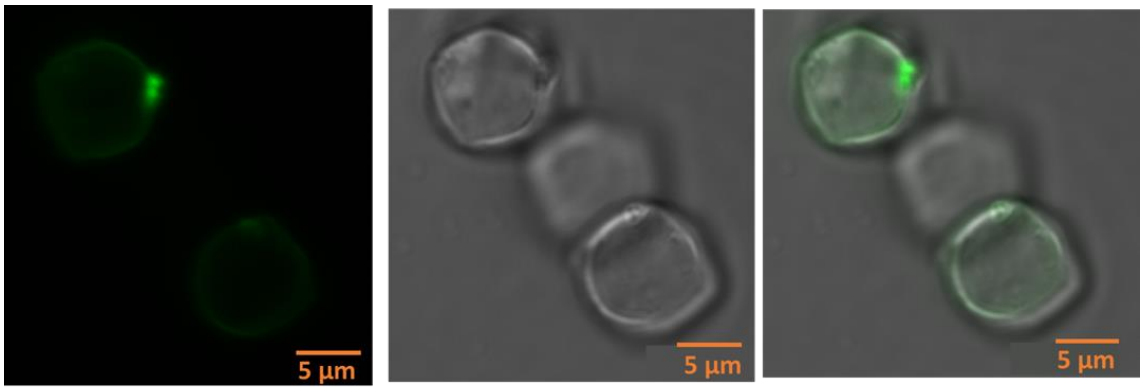

Figure 8. 22 Confocal laser scanning microscopy images demonstrate that the FITC-Bm3TE did not adsorb on ZIF-90 crystals. Left to right; fluorescence, bright field, and overlay images of the FITC-Bm3TE on ZIF-90.

The reaction mixture of Bm3TE and ZIF-90 crystals was centrifuged, and the collected crystals were tested with styrene no styrene oxide or phenylacetaldehyde product was observed (Figure 8. 23).

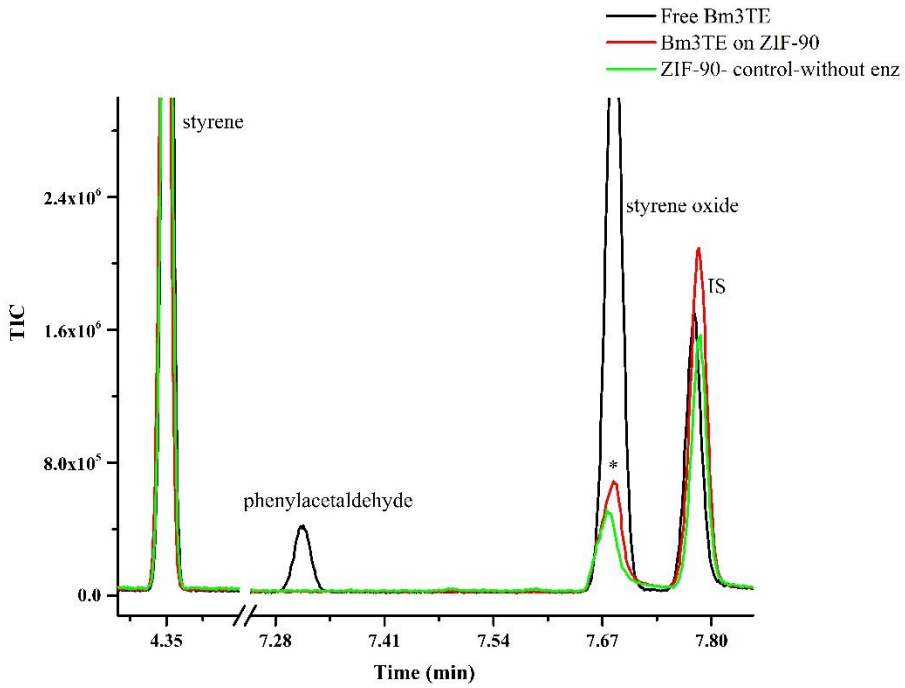

Figure 8. 23 GC analysis of styrene oxidation with immobilised Bm3TE on ZIF-90 shows no product (red).* is the signal from HICA in ZIF-90 as discussed earlier.

Overall our experiments for in-situ encapsulation of Bm3TE in ZIF-8 and ZIF-90 crystals did not appear to be successful for the oxidation of styrene. In the future substrates with a smaller molecular diameter than styrene could be employed to check if diffusion through the ZIF-8 pores was problematic. Some modification on Bm3TE may be required to enable its encapsulation without deactivation of the enzyme. Functionalisation of ZIF-8 particles may increase their interaction with Bm3TE to assist immobilisation. Studies of Madigan et al. showed that the increasing negative charge of the surface facilitates the encapsulation of Haemogolobin and Myoglobin in ZIF-8[283]. The reaction of lysine residues with succinic or acetic anhydride decreased the pI value and induced the formation of ZIF-8 due to an increase in the concentration of zinc at the surface to seed crystal growth[283]. For surface attachment of

Bm3TE on ZIF-8, larger crystals of ZIF-8 may be required to adsorb Bm3TE and help the surface adsorption[270]. Alternatively, to avoid imidazole ligands, metal azolate framework (MAF-7) can be employed. MAF-7 are Zn^{2+} based framework and has 3-methyl-1,2,4-triazole ($C_3H_5N_3$) as ligands. MAF-7 is more hydrophilic than ZIF-8 therefore hydrophobic interactions with the enzyme are reduced[256]. Hydrogen bonded organic frameworks (HOFs) are a new class of frameworks that can be employed for encapsulation. HOFs form by the self-assembly of organic molecules via hydrogen-bonding interactions[284]. The metal-free, low-density porous media and biocompatibility make HOFs suitable candidates for immobilisation of enzyme[284].

Overall the inactivation of Bm3TE in the process of encapsulation appears to be one reason for lack of activity. Therefore, instead of using organic/inorganic materials, bacterial compartments were studied in an attempt to encapsulate P450Bm3.

8.4 Encapsulation of P450Bm3R19 in bacterial encapsulins

Because P450Bm3 was thought to be deactivated in the presence of organic ligands during previous attempts at encapsulation using MOFs, we sought an alternative method for encapsulating these enzymes that could be performed under non-denaturing biocompatible conditions. Encapsulins are the smallest members of bacterial microcompartments composed of protein cages, which have a very flexible assembly mechanism that has previously been used for encasing enzymes[285] (1.9.2 Bacterial compartments). Encapsulins have a conserved peptide sequence at C-terminal that composed of 30-40 amino acids. This peptide sequence interacts with a hydrophobic binding pocket inside the encapsulin, which acts as an anchor for orientation of the native cargo protein. This peptide sequence can be used to package non-native cargo protein inside encapsulin (Figure 8. 24). Therefore, non-native cargo proteins can be packaged into encapsulins via fusion of this C-terminal peptide to their C-terminal[285, 286]. The encapsulation of two cargo proteins has been described previously: dye-decolourising

peroxidase (DyP) and ferritin-like protein (Flp)[240], both of which have a C-terminal peptide consisting of 10-40 amino acids. These targeting regions are rich in alanine, proline and glycine; and most have a single or double glycosphingolipid (GSL)-binding motif as an anchor sequence[251]. The interactions between the C-terminal extension and encapsulin include salt bridges, shape complementarity and hydrophobic interactions [240](Figure 8. 24).

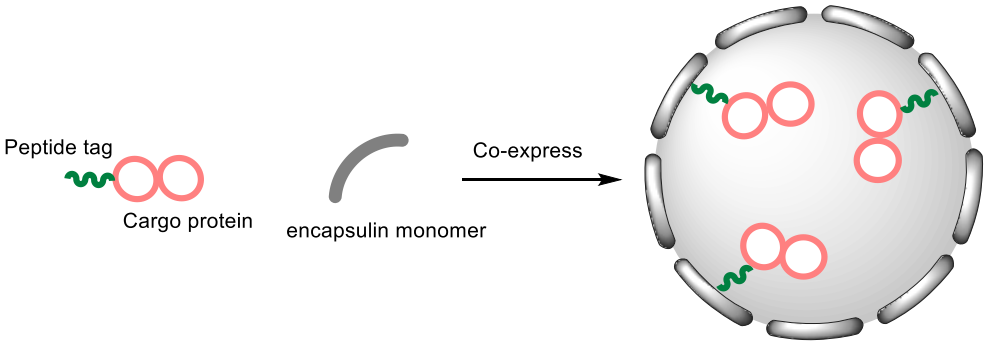

Figure 8. 24 Fusion of a peptide tag on the C-terminal of a non-native cargo protein leads to its *in vivo* packaging inside encapsulin compartments.

In the present study, two encapsulin proteins expressed in *Thermotoga maritima* (Tm) and *Myxococcus xanthus* (Mx) were employed to package the P450Bm3R19 variant (1.9.2 Bacterial compartments, Figure 8. 25). To achieve this, the Bm3R19 plasmid was tagged with short targeting peptides (TPs) of the natural cargo protein for Tm and Mx encapsulins by Dr Yu Heng Lau.

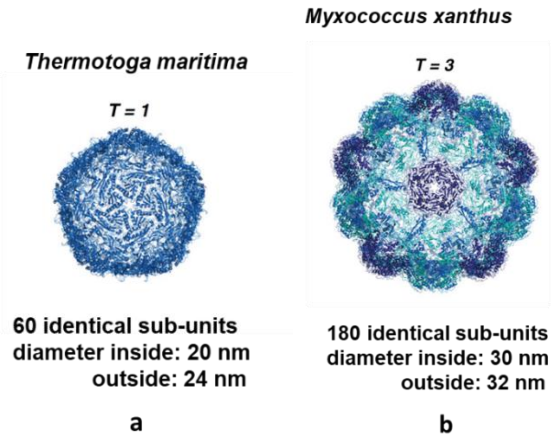

Figure 8. 25 *Thermotoga maritima* (Tm) and *Myxococcus xanthus* (Mx) are employed for the packaging of P450Bm3R19. This figure is from "Encapsulins: microbial nanocompartments with applications in biomedicine, nanobiotechnology and materials science" by Giessen[251].

Co-expression and self-assembly of Bm3R19 and Tm encapsulin was achieved using two plasmids: one containing the Bm3R19 gene tagged with the natural cargo targeting peptide of the Tm encapsulin, and the other containing the gene coding for the Tm encapsulin protein itself (Bm3R19TmTP and TmEnc plasmids, respectively). The modified form of the enzyme Bm3R19TmTP was assessed as a whole-cell biocatalyst using the oxidation of isophorone. It was found to successfully generate 4-hydroxyisophorone to similar levels to those reported in Chapter 5 suggesting that this P450Bm3 variant was active. In a typical experiment, cells containing both plasmids were grown on an LB plate in the presence of ampicillin and streptomycin (2.12 Encapsulation of Bm3R19 in Mx and Tm encapsulins). LB media was inoculated with a single colony, and after 6 hours, isopropyl-β-D-thiogalactopyranoside (IPTG) added to induce expression of tagged Bm3R19. Cells were incubated for 3 hours before pelleting by centrifugation. The cell pellet was then resuspended in LB and induced with arabinose to express TmEnc as capsids which would package the Bm3R19 enzyme. The overnight culture was pelleted and cells lysed as described in (2.12 Encapsulation of Bm3R19 in Mx and Tm encapsulins). Polyethylene glycol is commonly used for the precipitation of biological microstructures from cells by removing the protective water layer surrounding the plasmid[287-289]. Therefore, Tm encapsulin compartments were precipitated by the addition of 12 % PEG 8000 to the cell lysate after 30 min[252]. The resulting precipitate, which presumably contained Bm3R19TmTP encapsulated in TmEnc, was isolated by centrifugation and the supernatant kept for subsequent activity tests. The isolated encapsulin compartments were washed with Tris buffer and centrifuged to remove excess PEG 8000 (2.12 Encapsulation of Bm3R19 in Mx and Tm encapsulins). The washed pellet was then purified by size exclusion

chromatography (SEC) and the UV-absorbing fractions that eluted after the void volume were concentrated and washed for further purification via anion exchange chromatography (IEX).

The fractions containing protein obtained after size exclusion chromatography did not bind to the anion exchange column and we assumed that a high concentration of salt (presumably residual NaCl and PEG 8000) might have inhibited the encapsulin's binding. Therefore, the crude enzyme was washed with additional Tris buffer (×3) to remove all the adsorbed salt from the surface of enzyme before reattempting anion exchange chromatography. After these steps, the enzyme showed lower conductivity (less than 1 mS cm^{-1}) during the chromatography steps, which infers lower salt in the protein solution. However, the protein again failed to bind the column. Therefore, its activity for the oxidation of isophorone was tested without further purification, but very low activity was observed (Figure 8. 26). However, the supernatant, which was kept after the addition of PEG 8000 to cell generated the isophorone oxidation product 4-hydroxyisophorone (4-HIP), suggesting it contained Bm3R19 (Figure 8. 26).

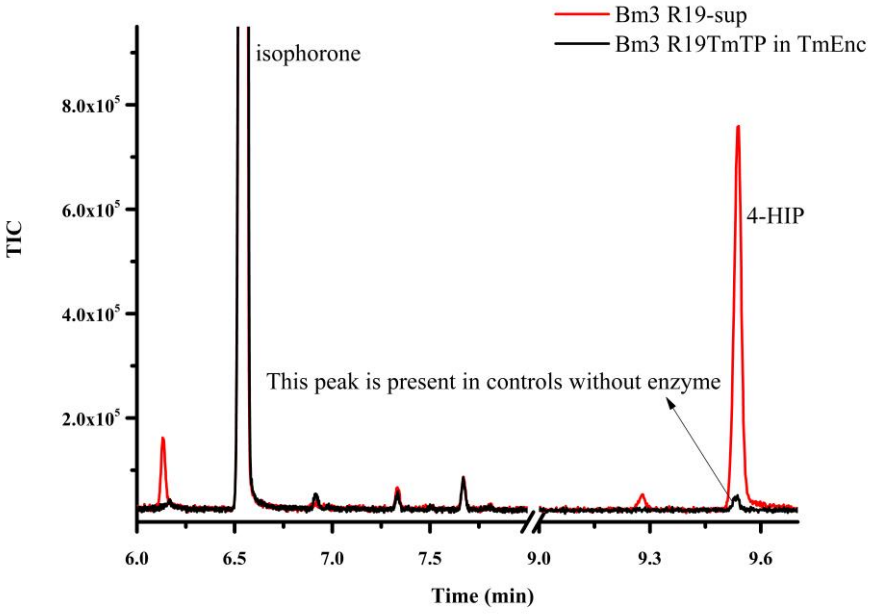

Figure 8. 26 GC-MS analysis of isophorone oxidation by Bm3R19 encapsulated in TmEnc (black) showed almost no activity (this small peak is also present in the control of isophorone),

whereas incubation of isophorone with the supernatant collected after addition of PEG 8000 (red) generated significant quantities of 4-hydroxyisophorone (4-HIP).

The observation of oxidation activity towards 4-HIP by the PEG 8000 supernatant but not the precipitate suggests that Bm3R19 was successfully expressed but not encapsulated by TmEnc. Therefore, attempted co-expression of Bm3R19 and TmEnc was repeated to check if an increase in the ratio of encapsulin to cargo could improve the efficiency of enzyme packaging. This was achieved by decreasing the concentration of added IPTG (to induce less Bm3R19 as cargo protein) with otherwise identical experimental conditions. PEG 8000 was again added to the cell lysate but the mixture incubated for a longer time (50 min) to maximise the amount of encapsulin precipitated. Following centrifugation and washing to remove the excess PEG 8000, the resulting encapsulin fraction was purified by size exclusion chromatography and its oxidation activity towards isophorone determined. However, changing the concentration of Bm3R19 appeared to have no effect on its encapsulation as again no oxidation activity was observed.

It is possible that the small compartment size of Tm (20 nm diameter) (Figure 8. 25) inhibited packaging of Bm3R19 into the encapsulin. Therefore, we attempted to employ the Mx encapsulin (MxEnc), which has a larger size (30 nm diameter) (Figure 8. 25), for the encapsulation of Bm3R19. The Bm3R19 plasmid was tagged with the MxEnc TP (Bm3R19MxTP) and co-expressed with the MxEnc plasmid in cells grown on an LB plate in the presence of ampicillin and streptomycin. In a similar method to the encapsulation of Bm3R19 in TmEnc, cells were first induced with IPTG (to express Bm3R19) followed by arabinose induction to express the encapsulin protein. The overnight growth was centrifuged, and PEG 8000 was added to the cell lysate. Because MxEnc is a larger encapsulin it required the use of 10 % PEG 8000, rather than the 12 % employed for the precipitation of the TmEnc

variant. The precipitated encapsulin compartments were isolated by centrifugation and washed to remove adsorbed salts before purification via size exclusion chromatography (Figure 8.27)

All fractions with UV absorbance at 280 nm, excluding the void volume of the column were collected (Figure 8.27), washed with Tris buffer (×3) and concentrated for further purification. The concentrated enzyme was loaded to the anion exchange column but did not bind to the column.

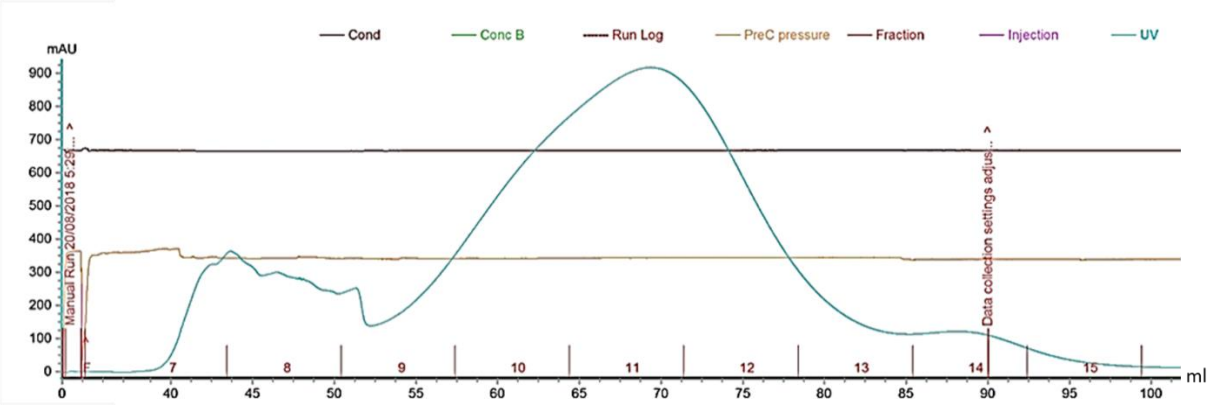

Figure 8.27 Fast protein liquid chromatography purification of encapsulated Bm3R19MxTP in MxEnc with size exclusion chromatography (S500 column). Fractions 10-12 were collected for further purification via IEX chromatography.

The SDS-PAGE analysis of collected fractions (10-12), which were assumed to contain Bm3R19 encapsulated in MxEnc, was performed) after size exclusion purification (2.13 Sodium dodecyl sulfate polyacrylamide gel electrophoresis (SDS-PAGE)). In all fractions, a clear band was observed at 32 kDa, which corresponded to the encapsulin monomer. However, no band corresponding to the 119 kDa Bm3R19 enzyme was observed (Figure 8. 28), which suggests that there was an absence, or a negligible amount, of Bm3R19 inside the encapsulin compartments. However, the PEG 8000 supernatant demonstrated a band at 119 kDa, which indicates the presence of Bm3R19 that was not encapsulated by MxEnc.

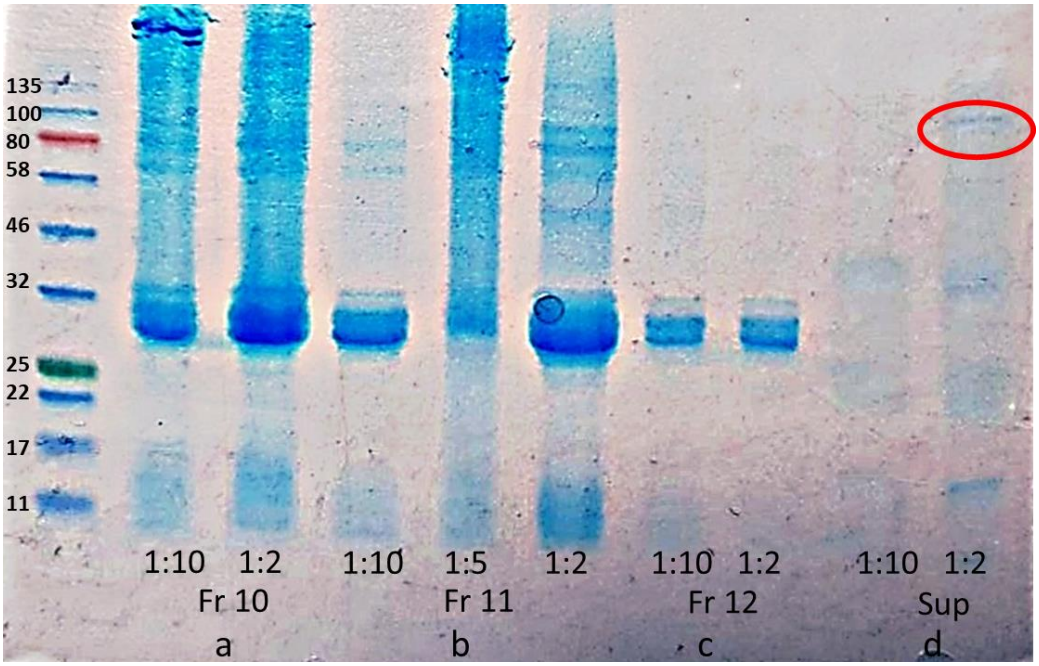

Figure 8. 28 SDS-PAGE of collected fractions (Fr 10-12) after attempted encapsulation of Bm3R19 in MxEnc. a) 1:10 and 1:2 dilution of Fr 10, b) 1:10, 1:5, 1:2 dilution of Fr 11, c) 1:10 and 1:2 dilution of Fr 12 and d) 1:10 and 1:2 dilution of the supernatant. All fractions showed the same pattern with a clear band at 32kDa corresponding to encapsulin monomers. The 1:2 dilution of the supernatant demonstrated a band at 119 kDa, which indicated the presence of Bm3R19.

Since further purification of the enzyme by anion exchange column was not possible, the oxidation activity of the crude enzyme after size exclusion chromatography purification was tested with isophorone. Very low levels of activity were observed that could be from the control. However, the supernatant (after PEG 8000 incubation and centrifugation) generated the oxidation product (4-HIP) in significantly higher quantities (Figure 8. 29).

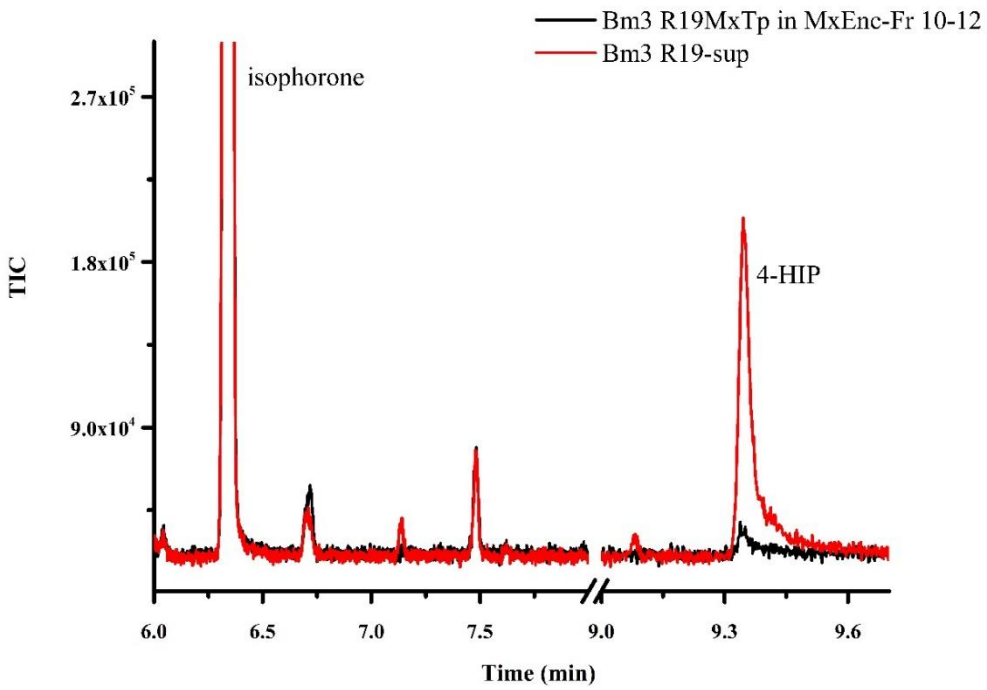

Figure 8. 29 GC-MS analysis of the isophorone oxidation by combined size exclusion chromatography fractions thought to contain Bm3R19MxTP encapsulated in MxEnc showed almost no 4-HIP generation (black), whereas the supernatant (red) generated more product.

The low level of activity, which might be from the control, could indicate that only a small portion of Bm3R19MxTP was encapsulated in MxEnc. Another reason could be the early dissociation of encapsulin compartments that may lead to the release of cargo[285]. Furthermore, this observation is in agreement with the SDS-PAGE analysis as no clear band corresponding to Bm3R19 was observed in the fractions, which could suggest an inefficient encapsulation process.

In a control experiment, Bm3R19MxTP was expressed without MxEnc to assess its effect on the composition of the PEG precipitate. After expression of tagged Bm3R19, 10 % PEG 8000 was added to the cell lysate, and the mixture centrifuged after incubating for 40 min. The isolated enzyme was purified by size exclusion chromatography, and the fractions with UV absorbance, which therefore contained protein, (fractions 12-14) were collected (Figure 8. 30).

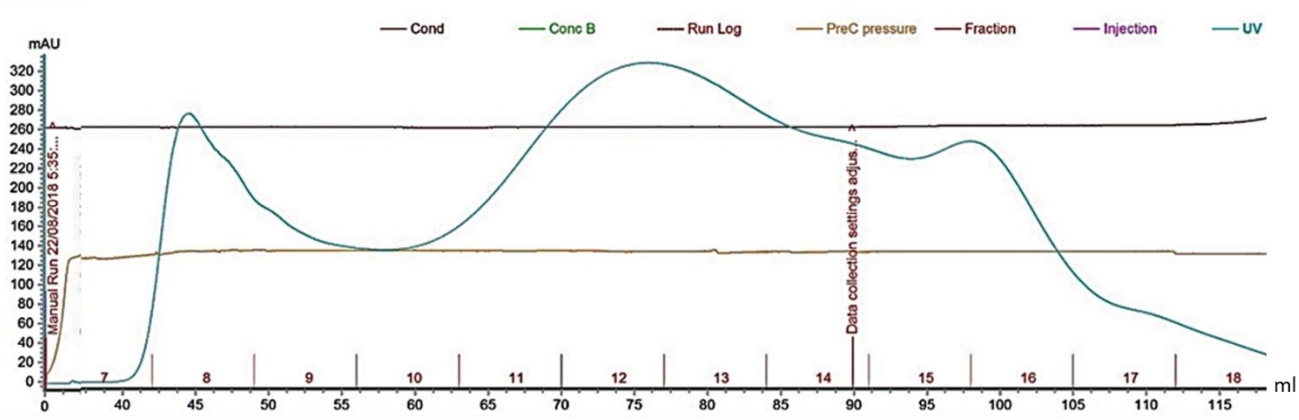

Figure 8. 30 Fast protein liquid chromatography purification of Bm3R19 (without MxEnc co-expression) using size exclusion chromatography. Fractions with UV absorbance (Fr 12-14) were collected to test their oxidation activity towards isophorone.

The activity of these fractions was tested individually, to identify which fractions contained Bm3R19. Almost no activity was observed for any of the collected fractions. However, low levels of product was observed for the crude Bm3R19 prior to size exclusion chromatography purification, which suggests that the observed activity could arise from Bm3R19 adsorbed on the PEG 8000 particles (Figure 8. 31).

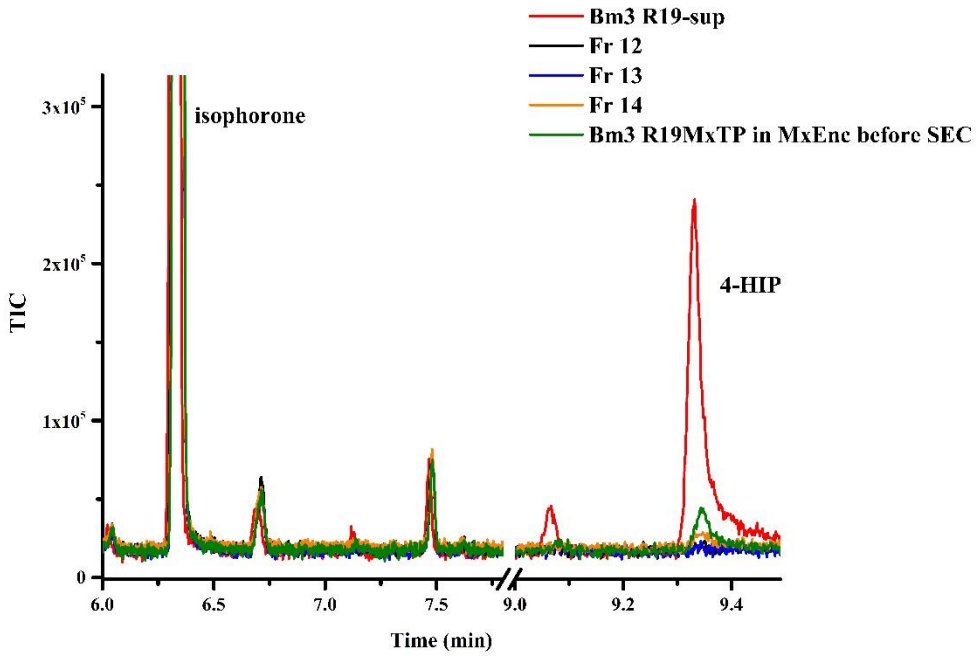

Figure 8. 31 GC-MS analysis of isophorone oxidation by individual fractions after size exclusion purification (Fr 12-14). Fractions 12 (black), 13 (blue) and 14 (orange) generated almost no product. A low level of 4-HIP was observed for the crude enzyme before size exclusion chromatography (green). However, the supernatant (red) showed good activity. (Crude enzyme is the PEG precipitation before size exclusion chromatography and supernatant is the supernatant after addition of PEG 8000 and centrifugation).

The 5-10 Å sized pores in encapsulins should enable the diffusion of small substrates into and out of the compartment[252]. Considering that the interaction between the cargo and shell could destabilize encapsulin compartments[290], early dissociation of capsid could happen.

The active supernatant after PEG precipitation showed that Bm3R19 was successfully expressed. Therefore, one probable reason for not observing activity is the absence of Bm3R19 in the encapsulin compartments, due to inefficient encapsulation of the enzyme. Hence, further investigation is required to determine an effective method for the encapsulation of Bm3R19 using this strategy. For example, the peptide tag of MxEnc on Bm3R19 may require

modification to provide a better anchoring effect. The expression conditions could also be altered to assist in encasing the enzyme. The large size of Bm3 as a dimer may be prohibited its packaging inside Mx encapsulin, or the required interactions for active Bm3 dimer formation may be perturbed. Another reason for not observing activity might be the effect of PEG precipitation on the activity of Bm3. To limit this effect, other purification methods could be used. Alternatively, larger encapsulins could be employed for encasing Bm3R19.

Conclusion

The rate accelerating variants KT2 (A191T/N239H/I259V/A276T/L353I), RLYFIP (R47L/Y51F/I401P), and R19 (R47L/Y51F/H171L/Q307H/N319Y) increased product formation compared to the WT enzyme, presumably because of their catalytically ready conformations. Likewise, the addition of decoy molecules to the WT enzyme improved formation rates by inducing a catalytically ready conformation and the combination of decoy molecules with the rate accelerating variants further increased productivity, while maintaining the regioselectivity. In general the best decoy molecule evaluated was PFC10; however, the KT2 variant showed higher coupling efficiency with PFC9. In certain instances the stereoselectivity was slightly improved with addition of decoy molecules; for example, during the oxidation of ethylbenzene by WT Bm3, the addition of PFC10 enhanced the enantiomeric excess from 48 % to 68 % *(R)*. The highest activity was observed in the oxidation of n-propylbenzene, presumably because the longer chain of n-propylbenzene assisted in the correct positioning of the substrate within the active site. Therefore, the addition of decoy molecules was not as effective in increasing turnover activity of this substrate, compared to ethylbenzene. The major product for ethylbenzene and n-propylbenzene was oxidation of the benzylic C-H bond. Despite the higher activity of alkenes compared to alkanes, less epoxide formation was observed predominantly due to a lower coupling efficiency. Given that epoxidation is more energetically favourable than hydroxylation, this reduced activity could be due to the rigid structure of the double bond, which limits substrate mobility in the active site.

The results presented here showed how the different positions and properties of substituents on the benzene ring affect the regioselectivity of P450Bm3 in the oxidation of substituted benzene. All enzyme variants increased product formation rate compared to the WT P450Bm3, with

those containing R47L/Y51F mutations showing the highest oxidation activity because of improved uptake of hydrophobic substrates into the access channel. Regioselectivity was almost maintained for the variants; however, the for 3-ethyltoluene oxidation, the R47L/Y51F/A330P variant provided different product distributions compared to the other enzymes and generated 2-ethyl-4-methylphenol as a single product, despite the presence of the more reactive benzylic C-H bonds.

Variants of P450Bm3 were able to regio- and stereoselectively oxidise isophorone to *(R)*-4-hydroxyisophorone. The RLYFIP and GVQ (A74G/F87V/L188Q) variants provided the highest product formation and showed a 280-fold increase in oxidation activity over the WT enzyme. The combination of decoy molecules with these variants further improved product formation. However decoy molecules inhibited the activity of the GVQ variant due to the F87V mutation in the substrate access channel, which must alter the binding of the decoy molecules resulting in lower activity

The formation of cyclic alcohols from the corresponding cycloalkanes (C5-C10) using WT P450Bm3 was very low; however, the addition of decoy molecules significantly improved their formation rates. By increasing the size of the decoy molecule, higher activity was achieved with both WT and PFC10, including a more than 3000-fold increase in cyclohexane hydroxylation by the latter. Cyclooctane demonstrated the highest product formation, its size must be optimal for the access channel of the enzyme. The combination of the RLYFIP enzyme variant with the PFC10 decoy was the best biocatalyst for the hydroxylation of all cycloalkanes. However, results for the GVQ variant were contradictory to those of the other variants in that, as with isophorone, its activity was reduced by the addition of decoy molecules. These findings likely result from a different substrate binding orientation above the haem in the substrate access channel. The combination of second generation decoy molecules with the WT and R19

for the hydroxylation of smaller substrates (cyclopentane and cyclohexane) generated more product, which provides an insight as to how the combination of different sizes of decoy and substrate influence the activity of these enzymes. These results highlight that optimal catalytic activity requires the tuning of enzyme mutations along with the size of substrate and decoy molecules.

Oxidation of ethylbenzene, styrene and methylthiobenzene in the presence of H_2O_2 was successful using the Bm3TE variant, whereas the WT and R19 holoenzymes showed no activity with the peroxide shunt mechanism. Selectivity was almost maintained for the oxidation of these substrates by Bm3TE, with the exception of ethylbenzene, which showed different stereoselectivity and favoured formation of the *(S)* enantiomer (in contrast to the holoenzymes, which generated more of the *(R)* enantiomer). This variant presented higher activity in the oxidation of methylthiobenzene over ethylbenzene and styrene. In contrast, the holoenzymes were more active in the hydroxylation of ethylbenzene, which infers the involvement of a different rate-determining step in the H_2O_2 shunt mechanism. Furthermore, the addition of decoy molecules did not improve the product formation rate, which again suggests a different pathway, however further studies are required to fully understand the differences in oxidation activity. Second-generation decoy molecules significantly improved the formation rates of all products and their combination with the R19 holoenzyme variant providing the highest formation rates.

To improve the the catalytic efficiency of Bm3TE, its immobilisation in ZIF-8 and ZIF-90 was studied. The formation of ZIF-8 crystals in the presence of the Bm3TE was successful; however, the enzyme lost almost all activity, presumably because of the high concentration of HMIM and its interaction with the hydrophobic ZIF-8 molecules. Hence, ZIF-90 with HICA ligands, which is a more hydrophilic ZIF, was employed for encapsulation of Bm3TE but again

no activity was observed, which suggests that Bm3TE was deactivated during the encapsulation process. The enzyme's immobilisation on the surface of pre-synthesised ZIF-8 and ZIF-90 was tested and it was found that immobilisation of Bm3TE on the surface of ZIF-8 was inefficient and that ZIF-90 crystals showed no affinity for the enzyme. Further studies that involve functionalisation of Bm3TE may provide a route to its efficient immobilisation on ZIF-8 and ZIF-90 crystals. Alternatively, the application of more hydrophilic frameworks, such as MAF-7 with 3-methyl-1,2,4-triazolate ligands, or metal-free HOFs could provide more effective platforms for an encapsulation strategy.

Since the organic ligands in MOFs affect the activity of enzyme, its encapsulation under biocompatible conditions was performed. As an alternative approach to molecular frameworks, we investigated the application of bacterial compartments for the encapsulation of Bm3R19. *Thermotoga maritima* (Tm) and *Myxococcus xanthus* (Mx) encapsulins were employed as capsids with Bm3R19 as a cargo. Based on the absence of oxidation activity of Bm3R19TmTP towards isophorone, we postulated that the small size of the TmEnc encapsulin inhibited encasing of Bm3R19. Encapsulation using MxEnc, which forms encapsulins with a larger pore size, was therefore attempted; however, almost no isophorone oxidation by Bm3R19MxTP was observed, indicating similarly inefficient encapsulation of enzyme. Further studies are therefore required to determine the factors that influence the encapsulation of Bm3R19 using encapsulins and to establish methods, such as modification of the C-terminal peptide tag, for their effective encapsulation and isolation of active complexes.

Overall, the catalytic activity of P450Bm3 was improved by employing enzyme mutagenesis and addition of decoy molecules. It has been demonstrated that rate accelerating variants significantly increased product formation while maintaining selectivity. With the exception of the GVQ variant, the combination of decoy molecules with these variants further increased their

activity. A single T268E mutation converted P450Bm3 to a H_2O_2- dependent variant and subsequently reduced the expense associated with using NADPH. Lastly, to improve thermal and chemical stability of P450Bm3, we investigated its potential immobilisation.

References

1. D. Nelson, *The Cytochrome P450 Homepage*, 2009, **4**.
2. M. Klingenberg, *Arch. Biochem. Biophys.*, 1958, **75**, 376-386.
3. D. Garfinkel, *Arch. Biochem. Biophys.*, 1958, **77**, 493-509.
4. T. Omura and R. Sato, *J. Biol. Chem*, 1962, **237**, 1375-1376.
5. D. R. Nelson, *Biochim. Biophys. Acta*, 2018, **1866**, 141-154.
6. D. W. Nebert, D. R. Nelson, M. Adesnik, M. J. Coon, R. W. Estabrook, F. J. Gonzalez, F. P. Guengerich, I. C. Gunsalus, E. F. Johnson, B. Kemper and et al., *DNA (Mary Ann Liebert, Inc.)*, 1989, **8**, 1-13.
7. D. W. Nebert, M. Adesnik, M. J. Coon, R. W. Estabrook, F. J. Gonzalez, F. P. Guengerich, I. C. Gunsalus, E. F. Johnson, B. Kemper, W. Levin and et al., *DNA (Mary Ann Liebert, Inc.)*, 1987, **6**, 1-11.
8. D. W. Nebert, D. R. Nelson, M. J. Coon, R. W. Estabrook, R. Feyereisen, Y. Fujii-Kuriyama, F. J. Gonzalez, F. P. Guengerich, I. C. Gunsalus, E. F. Johnson and et al., *DNA Cell Biol.*, 1991, **10**, 1-14.
9. T. L. Poulos, B. Finzel, I. Gunsalus, G. C. Wagner and J. Kraut, *J. Biol. Chem.*, 1985, **260**, 16122-16130.
10. T. L. Poulos, B. C. Finzel and A. J. Howard, *J. Mol. Biol.*, 1987, **195**, 687-700.
11. P. R. O. De Montellano, *Cytochrome P450: structure, mechanism, and biochemistry*, Springer Science & Business Media, 2005.
12. B. Meunier, S. P. de Visser and S. Shaik, *Chem. Rev.*, 2004, **104**, 3947-3980.
13. M. Sono, M. P. Roach, E. D. Coulter and J. H. Dawson, *Chem. Rev.*, 1996, **96**, 2841-2888.
14. F. P. Guengerich, *Chem. Res. Toxicol.*, 2001, **14**, 611-650.

15. M. Coon and A. Vaz, *Chemica Scripta*, 1987, **27**, 17-19.

16. D.-S. Lee, A. Yamada, H. Sugimoto, I. Matsunaga, H. Ogura, K. Ichihara, S.-i. Adachi, S.-Y. Park and Y. Shiro, *J. Biol. Chem.*, 2003, **278**, 9761-9767.

17. J. Belcher, K. J. McLean, S. Matthews, L. S. Woodward, K. Fisher, S. E. Rigby, D. R. Nelson, D. Potts, M. T. Baynham and D. A. Parker, *J. Biol. Chem.*, 2014, **289**, 6535-6550.

18. D. F. Lewis and J. M. Pratt, *Drug Metab. Rev.*, 1998, **30**, 739-786.

19. J. Rittle and M. T. Green, *Science*, 2010, **330**, 933-937.

20. I. G. Denisov, T. M. Makris, S. G. Sligar and I. Schlichting, *Chem. Rev.*, 2005, **105**, 2253-2278.

21. C. M. Krest, E. L. Onderko, T. H. Yosca, J. C. Calixto, R. F. Karp, J. Livada, J. Rittle and M. T. Green, *J. Biol. Chem.*, 2013, **288**, 17074-17081.

22. P. R. O. de Montellano and J. J. De Voss, *Nat. Prod. Rep.*, 2002, **19**, 477-493.

23. C. Aldag, I. A. Gromov, I. García-Rubio, K. von Koenig, I. Schlichting, B. Jaun and D. Hilvert, *Proc. Natl. Acad. Sci.*, 2009, **106**, 5481-5486.

24. H. B. Gray and J. R. Winkler, *Annu. Rev. Biochem*, 1996, **65**, 537-561.

25. H. B. Gray and J. R. Winkler, *Biochim. Biophys. Acta. Bioeng.*, 2010, **1797**, 1563-1572.

26. F. Hannemann, A. Bichet, K. M. Ewen and R. Bernhardt, *Biochim. Biophys. Acta. Gen. Subj.*, 2007, **1770**, 330-344.

27. R. Bernhardt, *J. Biotechnol.*, 2006, **124**, 128-145.

28. J. Lambeth, *Frontiers in biotransformation*, 1990, **3**, 58-100.

29. R. Bernhardt, in *Reviews of Physiology Biochemistry and Pharmacology*, *127*, Springer, 1995, 137-221.

30. S. D. Black and S. T. Martin, *Biochem.*, 1994, **33**, 12056-12062.

31. R. Neeli, H. M. Girvan, A. Lawrence, M. J. Warren, D. Leys, N. S. Scrutton and A. W. Munro, *FEBS Lett.*, 2005, **579**, 5582-5588.

32. T. L. Poulos, *Chem. Rev.*, 2014, **114**, 3919-3962.

33. R. Raag, S. A. Martinis, S. G. Sligar and T. L. Poulos, *Biochem.*, 1991, **30**, 11420-11429.

34. R. Davydov, R. Perera, S. Jin, T.-C. Yang, T. A. Bryson, M. Sono, J. H. Dawson and B. M. Hoffman, *J. Am. Chem. Soc*, 2005, **127**, 1403-1413.

35. P. R. Ortiz de Montellano, *Chem. Rev.*, 2009, **110**, 932-948.

36. S. Jin, T. M. Makris, T. A. Bryson, S. G. Sligar and J. H. Dawson, *J. Am. Chem. Soc*, 2003, **125**, 3406-3407.

37. M. J. Cryle and J. J. De Voss, *Angew. Chem. Int. Ed.*, 2006, **45**, 8221-8223.

38. W. D. Kerber, B. Ramdhanie and D. P. Goldberg, *Angew. Chem. Int. Ed.*, 2007, **46**, 3718-3721.

39. F. P. Guengerich and T. L. Macdonald, *Acc. Chem. Res.*, 1984, **17**, 9-16.

40. P. R. O. de Montellano and J. J. De Voss, in *Cytochrome P450*, Springer, 2005, pp. 183-245.

41. M. J. Cryle, J. E. Stok and J. J. De Voss, *Aust. J. Chem.*, 2003, **56**, 749-762.

42. F. P. Guengerich, *J. Biol. Chem.*, 1991, **266**, 10019-10022.

43. J. T. Groves and M. Van der Puy, *J. Am. Chem. Soc*, 1976, **98**, 5290-5297.

44. J. T. Groves and D. V. Adhyam, *J. Am. Chem. Soc*, 1984, **106**, 2177-2181.

45. D. Dolphin, in *Oxygen radicals in biology and medicine*, Springer, 1988, pp. 491-500.

46. J. I. Manchester, J. P. Dinnocenzo, L. Higgins and J. P. Jones, *J. Am. Chem. Soc*, 1997, **119**, 5069-5070.

47. M. Newcomb and P. H. Toy, *Acc. Chem. Res.*, 2000, **33**, 449-455.

48. J. K. Atkinson and K. Ingold, *Biochem.*, 1993, **32**, 9209-9214.

49. P. H. Toy, M. Newcomb and P. F. Hollenberg, *J. Am. Chem. Soc*, 1998, **120**, 7719-7729.

50. M. Newcomb, R. Shen, Y. Lu, M. J. Coon, P. F. Hollenberg, D. A. Kopp and S. J. Lippard, *J. Am. Chem. Soc*, 2002, **124**, 6879-6886.

51. M. Newcomb, R. Shen, S.-Y. Choi, P. H. Toy, P. F. Hollenberg, A. D. Vaz and M. J. Coon, *J. Am. Chem. Soc*, 2000, **122**, 2677-2686.

52. M. Newcomb, M.-H. Le Tadic-Biadatti, D. L. Chestney, E. S. Roberts and P. F. Hollenberg, *J. Am. Chem. Soc*, 1995, **117**, 12085-12091.

53. S. Shaik, S. Cohen, S. P. de Visser, P. K. Sharma, D. Kumar, S. Kozuch, F. Ogliaro and D. Danovich, *Eur. J. Inorg. Chem.*, 2004, **2004**, 207-226.

54. A. D. N. Vaz, D. F. McGinnity and M. J. Coon, *Proc. Natl. Acad. Sci.*, 1998, **95**, 3555-3560.

55. F. Ogliaro, S. P. de Visser, S. Cohen, P. K. Sharma and S. Shaik, *J. Am. Chem. Soc*, 2002, **124**, 2806-2817.

56. S. P. de Visser, F. Ogliaro, P. K. Sharma and S. Shaik, *J. Am. Chem. Soc*, 2002, **124**, 11809-11826.

57. S. P. de Visser, F. Ogliaro, P. K. Sharma and S. Shaik, *Angew. Chem. Int. Ed.*, 2002, **41**, 1947-1951.

58. T. Kamachi, Y. Shiota, T. Ohta and K. Yoshizawa, *Bull. Chem. Soc. Jpn.*, 2003, **76**, 721-732.

59. S. P. de Visser, F. Ogliaro and S. Shaik, *Angew. Chem.*, 2001, **113**, 2955-2958.

60. B. Meunier, *Biomimetic oxidations catalyzed by transition metal complexes*, Imperial College Press, 2000.

61. H. Sato and F. P. Guengerich, *J. Am. Chem. Soc*, 2000, **122**, 8099-8100.

62. G. Guroff, J. W. Daly, D. M. Jerina, J. Renson, B. Witkop and S. Udenfriend, *Science*, 1967, **157**, 1524-1530.

63. S. P. de Visser and S. Shaik, *J. Am. Chem. Soc*, 2003, **125**, 7413-7424.

64. D. Boyd, J. Daly and D. Jerina, *Biochem.*, 1972, **11**, 1961-1966.

65. R. P. Hanzlik, K. Hogberg and C. M. Judson, *Biochem.*, 1984, **23**, 3048-3055.

66. C. M. Bathelt, L. Ridder, A. J. Mulholland and J. N. Harvey, *J. Am. Chem. Soc*, 2003, **125**, 15004-15005.

67. B. Wang, C. Li, K.-B. Cho, W. Nam and S. Shaik, *J. Chem. Theory Comput.*, 2013, **9**, 2519-2525.

68. L. Ji, A. S. Faponle, M. G. Quesne, M. A. Sainna, J. Zhang, A. Franke, D. Kumar, R. van Eldik, W. Liu and S. P. de Visser, *Chem.: Eur. J.*, 2015, **21**, 9083-9092.

69. D. Kumar, S. P. de Visser and S. Shaik, *J. Am. Chem. Soc*, 2004, **126**, 5072-5073.

70. W. Lai, H. Chen, S. Cohen and S. Shaik, *J. Phys. Chem. Lett.*, 2011, **2**, 2229-2235.

71. A. J. Fulco, *Annu. Rev. Pharmacool. Toxicol.*, 1991, **31**, 177-203.

72. J.-S. He, Q. Liang and A. J. Fulco, *J. Biol. Chem.*, 1995, **270**, 18615-18625.

73. J.-S. He, R. T. Ruettinger, H.-M. Liu and A. J. Fulco, *Biochim. Biophys. Acta. Gene Struc. Express*, 1989, **1009**, 301-303.

74. H. Schwalb, L. O. Narhi and A. J. Fulco, *Biochim. Biophys. Acta. Gen. Sub.* 1985, **838**, 302-311.

75. L. O. Narhi and A. J. Fulco, *J. Biol. Chem.*, 1986, **261**, 7160-7169.

76. L. O. Narhi, B. H. Kim, P. M. Stevenson and A. J. Fulco, *Biochem. Biophys. Res. Commun.*, 1983, **116**, 851-858.

77. L. O. Narhi and A. J. Fulco, *J. Biol. Chem.*, 1987, **262**, 6683-6690.

78. A. W. Munro, J. G. Lindsay, J. R. Coggins, S. M. Kelly and N. C. Price, *Biochim. Biophys. Acta. Protein Struc. and Molecul. Enzymol.* 1996, **1296**, 127-137.

79. S. Govindaraj and T. L. Poulos, *Protein Sci.*, 1996, **5**, 1389-1393.

80. S. Govindaraj and T. L. Poulos, *Biochem.*, 1995, **34**, 11221-11226.

81. R. T. Ruettinger and A. Fulco, *J. Biol. Chem.*, 1981, **256**, 5728-5734.

82. Y. Miura and A. J. Fulco, *Biochim. Biophys. Acta. Lipids and Lipid Metabolism*, 1975, **388**, 305-317.

83. S. S. Boddupalli, R. W. Estabrook and J. A. Peterson, *J. Biol. Chem.*, 1990, **265**, 4233-4239.

84. S. Black, *Biochem. Biophys. Res. Commun.*, 1994, **203**, 162-168.

85. T. Oster, S. Boddupalli and J. A. Peterson, *J. Biol. Chem.*, 1991, **266**, 22718-22725.

86. C. J. Whitehouse, S. G. Bell and L. L. Wong, *Chem. Soc. Rev.*, 2012, **41**, 1218-1260.

87. T. D. Porter, *Trends Biochem. Sci*, 1991, **16**, 154-158.

88. I. Sevrioukova, C. Shaffer, D. P. Ballou and J. A. Peterson, *Biochem.*, 1996, **35**, 7058-7068.

89. S. C. Hanley, T. W. B. Ost and S. Daff, *Biochem. Biophys. Res. Commun.*, 2004, **325**, 1418-1423.

90. S. Daff, S. Chapman, K. Turner, R. Holt, S. Govindaraj, T. Poulos and A. Munro, *Biochem.*, 1997, **36**, 13816-13823.

91. I. Sevrioukova and J. Peterson, *Biochimie*, 1995, **77**, 562-572.

92. D. Appel, S. Lutz-Wahl, P. Fischer, U. Schwaneberg and R. D. Schmid, *J. Biotechnol.*, 2001, **88**, 167-171.

93. I. Sevrioukova and J. Peterson, *Biochimie*, 1996, **78**, 744-751.

94. P. A. Williams, J. Cosme, D. M. Vinković, A. Ward, H. C. Angove, P. J. Day, C. Vonrhein, I. J. Tickle and H. Jhoti, *Science*, 2004, **305**, 683-686.

95. H. Li and T. L. Poulos, *Nat. Struct. Biol.*, 1997, **4**, 140.

96. M. A. Noble, C. S. Miles, S. K. Chapman, D. A. Lysek, A. C. MacKay, R. P. Hanzlik and A. W. Munro, *Biochem. J*, 1999, **339**, 371-379.

97. F. C. Oliver, M. Sandeep, U. W. Primrose, L. Lu-Yun and C. G. Roberts, *Biochem. J*, 1997, **327**, 537-544.

98. T. W. Ost, C. S. Miles, J. Murdoch, Y.-F. Cheung, G. A. Reid, S. K. Chapman and A. W. Munro, *FEBS Lett.*, 2000, **486**, 173-177.

99. H. Li and T. L. Poulos, *Biochim. Biophys. Acta. Molecular and Cell Biology of Lipids*, 1999, **1441**, 141-149.

100. H. Li and T. Poulos, *Biochimie*, 1996, **78**, 695-699.

101. C. J. Whitehouse, W. Yang, J. A. Yorke, B. C. Rowlatt, A. J. Strong, C. F. Blanford, S. G. Bell, M. Bartlam, L. L. Wong and Z. Rao, *ChemBioChem*, 2010, **11**, 2549-2556.

102. E. G. Hrycay and S. M. Bandiera, in *Monooxygenase, Peroxidase and Peroxygenase Properties and Mechanisms of Cytochrome P450*, Springer, 2015, pp. 1-61.

103. H. Yeom and S. G. Sligar, *Arch. Biochem. Biophys.*, 1997, **337**, 209-216.

104. H. Yeom, S. G. Sligar, H. Li, T. L. Poulos and A. J. Fulco, *Biochem.*, 1995, **34**, 14733-14740.

105. S. A. Martinis, W. M. Atkins, P. S. Stayton and S. G. Sligar, *J. Am. Chem. Soc*, 1989, **111**, 9252-9253.

106. G. Truan and J. A. Peterson, *Arch. Biochem. Biophys.*, 1998, **349**, 53-64.

107. D. C. Haines, D. R. Tomchick, M. Machius and J. A. Peterson, *Biochem.*, 2001, **40**, 13456-13465.

108. M. J. Cryle and J. J. De Voss, *ChemBioChem*, 2008, **9**, 261-266.

109. F. Hollmann, I. W. Arends, K. Buehler, A. Schallmey and B. Bühler, *Green Chem*, 2011, **13**, 226-265.

110. Z. Li, J. B. van Beilen, W. A. Duetz, A. Schmid, A. de Raadt, H. Griengl and B. Witholt, *Curr. Opin. Chem. Biol.*, 2002, **6**, 136-144.

111. F. van Rantwijk and R. A. Sheldon, *Curr. Opin. Biotechnol.*, 2000, **11**, 554-564.

112. I. C. Gunsalus and G. C. Wagner, in *Methods Enzymol.*, Elsevier, 1978, vol. 52, pp. 166-188.

113. K. Darwish, H. Li and T. Poulos, *Protein Engineering, Design and Selection*, 1991, **4**, 701-708.

114. J. Peterson, J.-Y. Lu, J. Geisselsoder, S. Graham-Lorence, C. Carmona, F. Witney and M. Lorence, *J. Biol. Chem.*, 1992, **267**, 14193-14203.

115. A. W. Munro, D. G. Leys, K. J. McLean, K. R. Marshall, T. W. Ost, S. Daff, C. S. Miles, S. K. Chapman, D. A. Lysek and C. C. Moser, *Trends Biochem. Sci*, 2002, **27**, 250-257.

116. S. C. Maurer, K. Kühnel, L. A. Kaysser, S. Eiben, R. D. Schmid and V. B. Urlacher, *Adv. Synth. Catal.*, 2005, **347**, 1090-1098.

117. S. T. Jung, R. Lauchli and F. H. Arnold, *Curr. Opin. Biotechnol.*, 2011, **22**, 809-817.

118. E. T. Farinas, U. Schwaneberg, A. Glieder and F. H. Arnold, *Adv. Synth. Catal.*, 2001, **343**, 601-606.

119. C. J. Whitehouse, S. G. Bell, W. Yang, J. A. Yorke, C. F. Blanford, A. J. Strong, E. J. Morse, M. Bartlam, Z. Rao and L. L. Wong, *ChemBioChem*, 2009, **10**, 1654-1656.

120. P. C. Cirino and F. H. Arnold, *Curr. Opin. Chem. Biol.*, 2002, **6**, 130-135.

121. B. M. A. van Vugt-Lussenburg, E. Stjernschantz, J. Lastdrager, C. Oostenbrink, P. E. Vermeulen and J. N. M. Commandeur, *J. Med. Chem.*, 2007, **50**, 455-461.

122. A. B. Carmichael and L. L. Wong, *Eur. J. Biochem.*, 2001, **268**, 3117-3125.

123. C. J. Whitehouse, S. G. Bell, H. G. Tufton, R. J. Kenny, L. C. Ogilvie and L.-L. Wong, *Chem. Commun.*, 2008, 966-968.

124. C. J. Whitehouse, W. Yang, J. A. Yorke, H. G. Tufton, L. C. Ogilvie, S. G. Bell, W. Zhou, M. Bartlam, Z. Rao and L.-L. Wong, *Dalton Trans.*, 2011, **40**, 10383-10396.

125. C. R. Otey, G. Bandara, J. Lalonde, K. Takahashi and F. H. Arnold, *Biotechnol. Bioeng.*, 2006, **93**, 494-499.

126. B. M. A. van Vugt-Lussenburg, M. C. Damsten, D. M. Maasdijk, N. P. E. Vermeulen and J. N. M. Commandeur, *Biochem. Biophys. Res. Commun.*, 2006, **346**, 810-818.

127. J. C. Lewis, S. M. Mantovani, Y. Fu, C. D. Snow, R. S. Komor, C. H. Wong and F. H. Arnold, *ChemBioChem*, 2010, **11**, 2502-2505.

128. V. Rea, A. J. Kolkman, E. Vottero, E. J. Stronks, K. Ampt, M. Honing, N. P. Vermeulen, S. Wijmenga and J. Commandeur, *Biochem.*, 2012, **51**, 750-760.

129. P. Le-Huu, T. Heidt, B. Claasen, S. Laschat and V. B. Urlacher, *ACS Catalysis*, 2015, **5**, 1772-1780.

130. H. Venkataraman, S. B. d. Beer, D. P. Geerke, N. P. Vermeulen and J. N. Commandeur, *Adv. Synth. Catal.*, 2012, **354**, 2172-2184.

131. P. Meinhold, M. W. Peters, A. Hartwick, A. R. Hernandez and F. H. Arnold, *Adv. Synth. Catal.*, 2006, **348**, 763-772.

132. E. Weber, A. Seifert, M. Antonovici, C. Geinitz, J. Pleiss and V. B. Urlacher, *Chem. Commun.*, 2011, **47**, 944-946.

133. I. Matsunaga, M. Yamada, E. Kusunose, Y. Nishiuchi, I. Yano and K. Ichihara, *FEBS Lett.*, 1996, **386**, 252-254.

134. T. L. Poulos and J. Kraut, *J. Biol. Chem.*, 1980, **255**, 8199-8205.

135. J. Wang, J. M. Mauro, S. L. Edwards, S. J. Oatley, L. A. Fishel, V. A. Ashford, N. H. Xuong and J. Kraut, *Biochem.*, 1990, **29**, 7160-7173.

136. M. Gajhede, D. J. Schuller, A. Henriksen, A. T. Smith and T. L. Poulos, *Nat. Struct. Mol. Biol.*, 1997, **4**, 1032.

137. M. Sundaramoorthy, J. Terner and T. L. Poulos, *Chem. Biol.*, 1998, **5**, 461-473.

138. O. Shoji, T. Fujishiro, H. Nakajima, M. Kim, S. Nagano, Y. Shiro and Y. Watanabe, *Angew. Chem.*, 2007, **119**, 3730-3733.

139. T. Fujishiro, O. Shoji, S. Nagano, H. Sugimoto, Y. Shiro and Y. Watanabe, *J. Biol. Chem.*, 2011, **286**, 29941-29950.

140. H. Onoda, O. Shoji and Y. Watanabe, *Dalton Transactions*, 2015, **44**, 15316-15323.

141. O. Shoji, T. Fujishiro, K. Nishio, Y. Kano, H. Kimoto, S.-C. Chien, H. Onoda, A. Muramatsu, S. Tanaka and A. Hori, *Catal. Sci. Technol*, 2016, **6**, 5806-5811.

142. N. Kawakami, O. Shoji and Y. Watanabe, *Angew. Chem.*, 2011, **123**, 5427-5430.

143. D. C. Haines, B. Chen, D. R. Tomchick, M. Bondlela, A. Hegde, M. Machius and J. A. Peterson, *Biochem.*, 2008, **47**, 3662-3670.

144. M. Noble, L. Quaroni, G. D. Chumanov, K. Turner, S. Chapman, R. Hanzlik and A. Munro, *Biochem.*, 1998, **37**, 15799-15807.

145. P. Meinhold, M. W. Peters, M. M. Chen, K. Takahashi and F. H. Arnold, *ChemBioChem*, 2005, **6**, 1765-1768.

146. N. Kawakami, O. Shoji and Y. Watanabe, *Chem. Sci*, 2013, **4**, 2344-2348.

147. O. Shoji and Y. Watanabe, *Isr. J. Chem.*, 2015, **55**, 32-39.

148. Z. Cong, O. Shoji, C. Kasai, N. Kawakami, H. Sugimoto, Y. Shiro and Y. Watanabe, *ACS Catalysis*, 2015, **5**, 150-156.

149. M. Mohammadi, M. Ashjari, S. Dezvarei, M. Yousefi, M. Babaki and J. Mohammadi, *RSC Advances*, 2015, **5**, 32698-32705.

150. M. Mohammadi, Z. Habibi, S. Dezvarei, M. Yousefi, S. Samadi and M. Ashjari, *Process Biochem.*, 2014, **49**, 1314-1323.

151. M. Mohammadi, Z. Habibi, S. Dezvarei, M. Yousefi and M. Ashjari, *Food Bioprod. Process.*, 2015, **94**, 414-421.

152. J. M. Nelson and E. Griffin, *J. Am. Chem. Soc.*, 1916, **38**, 1109-1115.

153. T. Laird, *Org. Process Res. Dev.*, 2002, **6**, 86-86.

154. A. Sassolas, L. J. Blum and B. D. Leca-Bouvier, *Biotechnol. Adv.*, 2012, **30**, 489-511.

155. P. Adlercreutz, *Chem. Soc. Rev.*, 2013, **42**, 6406-6436.

156. A. K. Cheetham, C. Rao and R. K. Feller, *Chem. Commun.*, 2006, 4780-4795.

157. X. Wu, M. Hou and J. Ge, *Catal. Sci. Technol* 2015, **5**, 5077-5085.

158. L. Cao, L. van Langen and R. A. Sheldon, *Curr. Opin. Biotechnol.*, 2003, **14**, 387-394.

159. M. Arroyo, J. M. a. Sánchez-Montero and J. V. Sinisterra, *Enzyme Microb. Technol.*, 1999, **24**, 3-12.

160. J. M. Moreno and J. V. Sinisterra, *J. Mol. Catal.*, 1994, **93**, 357-369.

161. T. J. Pisklak, M. Macías, D. H. Coutinho, R. S. Huang and K. J. Balkus, *Top. Catal.*, 2006, **38**, 269-278.

162. G. Férey, C. Mellot-Draznieks, C. Serre, F. Millange, J. Dutour, S. Surblé and I. Margiolaki, *Science*, 2005, **309**, 2040-2042.

163. A. G. Wong-Foy, A. J. Matzger and O. M. Yaghi, *J. Am.Chem. Soc*, 2006, **128**, 3494-3495.

164. J. H. Cavka, S. Jakobsen, U. Olsbye, N. Guillou, C. Lamberti, S. Bordiga and K. P. Lillerud, *J. Am.Chem. Soc*, 2008, **130**, 13850-13851.

165. K. S. Park, Z. Ni, A. P. Côté, J. Y. Choi, R. Huang, F. J. Uribe-Romo, H. K. Chae, M. O'Keeffe and O. M. Yaghi, *Proc. Natl. Acad. Sci.*, 2006, **103**, 10186-10191.

166. H. Furukawa, K. E. Cordova, M. O'Keeffe and O. M. Yaghi, *Science*, 2013, **341**, 1230444.

167. A. Phan, C. J. Doonan, F. J. Uribe-Romo, C. B. Knobler, M. O'keeffe and O. M. Yaghi, *Acc. Chem. Res*, 2010, **43**, 58-67.

168. C. Doonan, R. Riccò, K. Liang, D. Bradshaw and P. Falcaro, *Acc. Chem. Res.*, 2017, **50**, 1423-1432.

169. U. Mueller, M. Schubert, F. Teich, H. Puetter, K. Schierle-Arndt and J. Pastré, *J. Mater. Chem.*, 2006, **16**, 626-636.

170. P. Horcajada, T. Chalati, C. Serre, B. Gillet, C. Sebrie, T. Baati, J. F. Eubank, D. Heurtaux, P. Clayette, C. Kreuz, J.-S. Chang, Y. K. Hwang, V. Marsaud, P.-N. Bories, L. Cynober, S. Gil, G. Férey, P. Couvreur and R. Gref, *Nat. Mater*, 2009, **9**, 172.

171. J. Lei, R. Qian, P. Ling, L. Cui and H. Ju, *TrAC, Trends Anal. Chem.*, 2014, **58**, 71-78.

172. M. R. Ryder and J.-C. Tan, *Mater. Sci. Technol.*, 2014, **30**, 1598-1612.

173. A. U. Czaja, N. Trukhan and U. Müller, *Chem. Soc. Rev.*, 2009, **38**, 1284-1293.

174. S. Keskin and S. Kızılel, *Ind. Eng. Chem. Res*, 2011, **50**, 1799-1812.

175. J. Mehta, N. Bhardwaj, S. K. Bhardwaj, K.-H. Kim and A. Deep, *Coord. Chem. Rev.*, 2016, **322**, 30-40.

176. O. K. Farha, I. Eryazici, N. C. Jeong, B. G. Hauser, C. E. Wilmer, A. A. Sarjeant, R. Q. Snurr, S. T. Nguyen, A. O. z. r. Yazaydın and J. T. Hupp, *J. Am. Chem. Soc*, 2012, **134**, 15016-15021.

177. P. Horcajada, C. Serre, M. Vallet-Regí, M. Sebban, F. Taulelle and G. Férey, *Angew. Chem. Int. Ed.*, 2006, **45**, 5974-5978.

178. J.-R. Li, R. J. Kuppler and H.-C. Zhou, *Chem. Soc. Rev.*, 2009, **38**, 1477-1504.

179. J. A. Mason, M. Veenstra and J. R. Long, *Chemical Science*, 2014, **5**, 32-51.

180. Y. Peng, V. Krungleviciute, I. Eryazici, J. T. Hupp, O. K. Farha and T. Yildirim, *J. Am. Chem. Soc*, 2013, **135**, 11887-11894.

181. J. Lee, O. K. Farha, J. Roberts, K. A. Scheidt, S. T. Nguyen and J. T. Hupp, *Chem. Soc. Rev.*, 2009, **38**, 1450-1459.

182. D. E. Williams and N. B. Shustova, *Chem.: Eur. J.*, 2015, **21**, 15474-15479.

183. X. Lian, Y. Fang, E. Joseph, Q. Wang, J. Li, S. Banerjee, C. Lollar, X. Wang and H.-C. Zhou, *Chem. Soc. Rev.*, 2017, **46**, 3386-3401.

184. H. M. Marques, *Dalton Trans.*, 2007, 4371-4385.

185. V. Lykourinou, Y. Chen, X.-S. Wang, L. Meng, T. Hoang, L.-J. Ming, R. L. Musselman and S. Ma, *J. Am. Chem. Soc.*, 2011, **133**, 10382-10385.

186. P. Li, Justin A. Modica, Ashlee J. Howarth, E. Vargas L, Peyman Z. Moghadam, Randall Q. Snurr, M. Mrksich, Joseph T. Hupp and Omar K. Farha, *Chem*, 2016, **1**, 154-169.

187. Y. Cao, Z. Wu, T. Wang, Y. Xiao, Q. Huo and Y. Liu, *Dalton Trans.*, 2016, **45**, 6998-7003.

188. S. Jung, Y. Kim, S.-J. Kim, T.-H. Kwon, S. Huh and S. Park, *Chem. Commun.*, 2011, **47**, 2904-2906.

189. F. Lyu, Y. Zhang, R. N. Zare, J. Ge and Z. Liu, *Nano Lett.*, 2014, **14**, 5761-5765.

190. C. Yim, H. Lee, S. Lee and S. Jeon, *RSC Advances*, 2017, **7**, 1418-1422.

191. K. Liang, C. J. Coghlan, S. G. Bell, C. Doonan and P. Falcaro, *Chem. Commun.*, 2016, **52**, 473-476.

192. C. Zhang, Y. Dai, J. R. Johnson, O. Karvan and W. J. Koros, *J. Membr. Sci.*, 2012, **389**, 34-42.

193. X. C. Huang, Y. Y. Lin, J. P. Zhang and X. M. Chen, *Angew. Chem. Int. Ed.*, 2006, **45**, 1557-1559.

194. H.-Y. Cho, J. Kim, S.-N. Kim and W.-S. Ahn, *Microporous Mesoporous Mater.*, 2013, **169**, 180-184.

195. Q. Bao, Y. Lou, T. Xing and J. Chen, *Inorg. Chem. Commun.*, 2013, **37**, 170-173.

196. P. J. Beldon, L. Fábián, R. S. Stein, A. Thirumurugan, A. K. Cheetham and T. Friščić, *Angew. Chem.*, 2010, **122**, 9834-9837.

197. S. Bhattacharjee, M.-S. Jang, H.-J. Kwon and W.-S. Ahn, *Catal. Surv. Asia*, 2014, **18**, 101-127.

198. Y. Pan, Y. Liu, G. Zeng, L. Zhao and Z. Lai, *Chem. Commun.*, 2011, **47**, 2071-2073.

199. K. Kida, M. Okita, K. Fujita, S. Tanaka and Y. Miyake, *CrystEngComm*, 2013, **15**, 1794-1801.

200. J. Cui, Y. Feng, T. Lin, Z. Tan, C. Zhong and S. Jia, *ACS Appl. Mater. Interfaces*, 2017, **9**, 10587-10594.

201. A. Polyzoidis, T. Altenburg, M. Schwarzer, S. Loebbecke and S. Kaskel, *Chem. Eng. J.*, 2016, **283**, 971-977.

202. C.-Y. Sun, C. Qin, X.-L. Wang, G.-S. Yang, K.-Z. Shao, Y.-Q. Lan, Z.-M. Su, P. Huang, C.-G. Wang and E.-B. Wang, *Dalton Trans.*, 2012, **41**, 6906-6909.

203. A. Tiwari, A. Singh, N. Garg and J. K. Randhawa, *Sci. Rep.*, 2017, **7**, 12598.

204. L. Wang, H. Guan, Z. Wang, Y. Xing, J. Zhang and K. Cai, *Mol. Pharm.*, 2018.

205. K. Liang, R. Ricco, C. M. Doherty, M. J. Styles, S. Bell, N. Kirby, S. Mudie, D. Haylock, A. J. Hill and C. J. Doonan, *Nat. Commun.*, 2015, **6**, 7240.

206. V. Gascón, E. Castro-Miguel, M. Díaz-García, R. M. Blanco and M. Sanchez-Sanchez, *J. Chem. Technol. Biotechnol.*, 2017, **92**, 2583-2593.

207. V. Gascón, C. Carucci, M. B. Jiménez, R. M. Blanco, M. Sánchez-Sánchez and E. Magner, *ChemCatChem*, 2017, **9**, 1182-1186.

208. F. Pitzalis, C. Carucci, M. Naseri, L. Fotouhi, E. Magner and A. Salis, *ChemCatChem*, 2018, **10**, 1578-1585.

209. W. Morris, C. J. Doonan, H. Furukawa, R. Banerjee and O. M. Yaghi, *J. Am. Chem. Soc.*, 2008, **130**, 12626-12627.

210. F. K. Shieh, S. C. Wang, S. Y. Leo and K. C. W. Wu, *Chem.: Eur. J.*, 2013, **19**, 11139-11142.

211. F.-K. Shieh, S.-C. Wang, C.-I. Yen, C.-C. Wu, S. Dutta, L.-Y. Chou, J. V. Morabito, P. Hu, M.-H. Hsu and K. C.-W. Wu, *J. Am. Chem. Soc.*, 2015, **137**, 4276-4279.

212. W. Martin, *Philos. Trans. R. Soc. Lond. B. Biol. Sci.*, 2010, **365**, 847-855.

213. E. Cornejo, N. Abreu and A. Komeili, *Curr. Opin. Cell Biol.*, 2014, **26**, 132-138.

214. M. Uchida, M. Terashima, C. H. Cunningham, Y. Suzuki, D. A. Willits, A. F. Willis, P. C. Yang, P. S. Tsao, M. V. McConnell and M. J. Young, *Magn. Reson. Med.*, 2008, **60**, 1073-1081.

215. Y. Ma, R. J. Nolte and J. J. Cornelissen, *Adv. Drug Del. Rev.*, 2012, **64**, 811-825.

216. B. Maity, K. Fujita and T. Ueno, *Curr. Opin. Chem. Biol.*, 2015, **25**, 88-97.

217. M. L. Flenniken, L. O. Liepold, B. E. Crowley, D. A. Willits, M. J. Young and T. Douglas, *Chem. Commun.*, 2005, 447-449.

218. I. J. Minten, L. J. A. Hendriks, R. J. M. Nolte and J. J. L. M. Cornelissen, *J. Am. Chem. Soc.*, 2009, **131**, 17771-17773.

219. J. D. Fiedler, S. D. Brown, J. L. Lau and M. Finn, *Angew. Chem. Int. Ed.*, 2010, **49**, 9648-9651.

220. J. E. Glasgow, S. L. Capehart, M. B. Francis and D. Tullman-Ercek, *ACS nano*, 2012, **6**, 8658-8664.

221. T. Douglas and M. Young, *Nature*, 1998, **393**, 152.

222. J. A. Speir, S. Munshi, G. Wang, T. S. Baker and J. E. Johnson, *Structure*, 1995, **3**, 63-78.

223. F. D. Sikkema, M. Comellas-Aragones, R. G. Fokkink, B. J. Verduin, J. J. Cornelissen and R. J. Nolte, *Org. Biomol. Chem.*, 2007, **5**, 54-57.

224. T. O. Yeates, M. C. Thompson and T. A. Bobik, *Curr. Opin. Struct. Biol.*, 2011, **21**, 223-231.

225. C. A. Kerfeld, S. Heinhorst and G. C. Cannon, *Annu. Rev. Microbiol.*, 2010, **64**, 391-408.

226. G. Drews and W. Niklowitz, *Arch. Mikrobiol.*, 1956, **24**, 147-162.

227. E. Gantt and S. Conti, *J. Bacteriol.*, 1969, **97**, 1486-1493.

228. J. Shively, G. Decker and J. Greenawalt, *J. Bacteriol.*, 1970, **101**, 618-627.

229. G. Cannon, R. English and J. Shively, *J. Bacteriol.*, 1991, **173**, 1565-1568.

230. M. Held, M. B. Quin and C. Schmidt-Dannert, *J. Mol. Microbiol. Biotechnol.*, 2013, **23**, 308-320.

231. D. Amichay, R. Levitz and M. Gurevitz, *Plant Mol. Biol.*, 1993, **23**, 465-476.

232. F. C. Hartman and M. R. Harpel, *Annu. Rev. Biochem*, 1994, **63**, 197-232.

233. G. C. Cannon, C. E. Bradburne, H. C. Aldrich, S. H. Baker, S. Heinhorst and J. M. Shively, *Appl. Environ. Microbiol.*, 2001, **67**, 5351-5361.

234. M. F. Schmid, A. M. Paredes, H. A. Khant, F. Soyer, H. C. Aldrich, W. Chiu and J. M. Shively, *J. Mol. Biol.*, 2006, **364**, 526-535.

235. C. A. Kerfeld, M. R. Sawaya, S. Tanaka, C. V. Nguyen, M. Phillips, M. Beeby and T. O. Yeates, *Science*, 2005, **309**, 936-938.

236. Y. Tsai, M. R. Sawaya, G. C. Cannon, F. Cai, E. B. Williams, S. Heinhorst, C. A. Kerfeld and T. O. Yeates, *PLoS Biol.*, 2007, **5**, e144.

237. T. O. Yeates, C. A. Kerfeld, S. Heinhorst, G. C. Cannon and J. M. Shively, *Nat. Rev. Microbiol.*, 2008, **6**, 681.

238. P. Chen, D. I. Andersson and J. R. Roth, *J. Bacteriol.*, 1994, **176**, 5474-5482.

239. G. D. Havemann, E. M. Sampson and T. A. Bobik, *J. Bacteriol.*, 2002, **184**, 1253-1261.

240. M. Sutter, D. Boehringer, S. Gutmann, S. Günther, D. Prangishvili, M. J. Loessner, K. O. Stetter, E. Weber-Ban and N. Ban, *Nat. Struct. Mol. Biol.*, 2008, **15**, 939.

241. N. Winter, J. A. Triccas, B. Rivoire, M. C. V. Pessolani, K. Eiglmeier, E.-M. Lim, S. W. Hunter, P. J. Brennan and W. J. Britton, *Mol. Microbiol.*, 1995, **16**, 865-876.

242. N. Valdés-Stauber and S. Scherer, *Appl. Environ. Microbiol.*, 1994, **60**, 3809-3814.

243. H. Moon, J. Lee, J. Min and S. Kang, *Biomacromolecules*, 2014, **15**, 3794-3801.

244. H. Contreras, M. S. Joens, L. M. McMath, V. P. Le, M. V. Tullius, J. M. Kimmey, N. Bionghi, M. A. Horwitz, J. A. Fitzpatrick and C. W. Goulding, *J. Biol. Chem.*, 2014, jbc. M114. 570119.

245. C. A. McHugh, J. Fontana, D. Nemecek, N. Cheng, A. A. Aksyuk, J. B. Heymann, D. C. Winkler, A. S. Lam, J. S. Wall and A. C. Steven, *EMBO J.*, 2014, **33**, 1896-1911.

246. M. Sutter, D. Boehringer, S. Gutmann, S. Günther, D. Prangishvili, M. J. Loessner, K. O. Stetter, E. Weber-Ban and N. Ban, *Nat. Struct. Mol. Biol.*, 2008, **15**, 939.

247. W. F. Rurup, J. Snijder, M. S. Koay, A. J. Heck and J. J. Cornelissen, *J. Am. Chem. Soc*,. 2014, **136**, 3828-3832.

248. R. Rahmanpour and T. D. Bugg, *FEBS J.*, 2013, **280**, 2097-2104.

249. C. Cassidy-Amstutz, L. Oltrogge, C. C. Going, A. Lee, P. Teng, D. Quintanilla, A. East-Seletsky, E. R. Williams and D. F. Savage, *Biochem.*, 2016, **55**, 3461-3468.

250. F. Akita, K. T. Chong, H. Tanaka, E. Yamashita, N. Miyazaki, Y. Nakaishi, M. Suzuki, K. Namba, Y. Ono and T. Tsukihara, *J. Mol. Biol.*, 2007, **368**, 1469-1483.

251. T. W. Giessen, *Curr. Opin. Chem. Biol.*, 2016, **34**, 1-10.

252. Y. H. Lau, T. W. Giessen, W. J. Altenburg and P. A. Silver, *Nat Commun*, 2018, **9**, 1311.

253. O. M. Linder-Patton, T. J. de Prinse, S. Furukawa, S. G. Bell, K. Sumida, C. J. Doonan and C. J. Sumby, *CrystEngComm*, 2018, **20**, 4926-4934.

254. W.-S. Lo, S.-M. Liu, S.-C. Wang, H.-P. Lin, N. Ma, H.-Y. Huang and F.-K. Shieh, *RSC Advances*, 2014, **4**, 52883-52886.

255. W. Liang, R. Ricco, N. K. Maddigan, R. P. Dickinson, H. Xu, Q. Li, C. J. Sumby, S. G. Bell, P. Falcaro and C. J. Doonan, *Chem. Mater.*, 2018, **30**, 1069-1077.

256. W. Liang, H. Xu, F. Carraro, N. K. Maddigan, Q. Li, S. G. Bell, D. M. Huang, A. Tarzia, M. B. Solomon, H. Amenitsch, L. Vaccari, C. J. Sumby, P. Falcaro and C. J. Doonan, *J. Am. Chem. Soc.*, 2019, **141**, 2348-2355.

257. M. Hartmann and D. Jung, *J. Mater. Chem.*, 2010, **20**, 844-857.

258. L. Cao and R. Schmid, *Journal*, 2005.

259. F. López-Gallego, T. Montes, M. Fuentes, N. Alonso, V. Grazu, L. Betancor, J. M. Guisán and R. Fernández-Lafuente, *J. Biotechnol.*, 2005, **116**, 1-10.

260. C. J. Gray, M. J. Weissenborn, C. E. Eyers and S. L. Flitsch, *Chem. Soc. Rev.*, 2013, **42**, 6378-6405.

261. R. DiCosimo, J. McAuliffe, A. J. Poulose and G. Bohlmann, *Chem. Soc. Rev.*, 2013, **42**, 6437-6474.

262. C. Mateo, J. M. Palomo, G. Fernandez-Lorente, J. M. Guisan and R. Fernandez-Lafuente, *Enzyme Microb. Technol.*, 2007, **40**, 1451-1463.

263. R. Fernandez-Lafuente, *Enzyme Microb. Technol.*, 2009, **45**, 405-418.

264. C. Garcia-Galan, Á. Berenguer-Murcia, R. Fernandez-Lafuente and R. C. Rodrigues, *Adv. Synth. Catal.*, 2011, **353**, 2885-2904.

265. M. Zhu, S. R. Venna, J. B. Jasinski and M. A. Carreon, *Chem. Mater.*, 2011, **23**, 3590-3592.

266. S. Aleksandra, L. Balan, V. Falk and R. Schneider, presented in part at the International Symposium of Metal-Mediated Chemistry, Strasbourg, France, 2013-11-22, 2013.

267. J. Xu, O. Shoji, T. Fujishiro, T. Ohki, T. Ueno and Y. Watanabe, *Catal. Sci. Technol.*, 2012, **2**, 739-744.

268. C. W. Locuson, J. M. Hutzler and T. S. Tracy, *Drug Metab. Disposition*, 2007, **35**, 614-622.

269. T. Zoungrana, G. H. Findenegg and W. Norde, *J. Colloid Interface Sci.*, 1997, **190**, 437-448.

270. M. Rabe, D. Verdes and S. Seeger, *Adv. Colloid Interface Sci.*, 2011, **162**, 87-106.

271. R. Banerjee, A. Phan, B. Wang, C. Knobler, H. Furukawa, M. O'keeffe and O. M. Yaghi, *Science*, 2008, **319**, 939-943.

272. K. Eum, K. C. Jayachandrababu, F. Rashidi, K. Zhang, J. Leisen, S. Graham, R. P. Lively, R. R. Chance, D. S. Sholl, C. W. Jones and S. Nair, *J. Am. Chem. Soc*, 2015, **137**, 4191-4197.

273. T. Yang and T.-S. Chung, *J. Mater. Chem., A*, 2013, **1**, 6081-6090.

274. G. Lu, S. Li, Z. Guo, O. K. Farha, B. G. Hauser, X. Qi, Y. Wang, X. Wang, S. Han, X. Liu, J. S. DuChene, H. Zhang, Q. Zhang, X. Chen, J. Ma, S. C. Loo, W. D. Wei, Y. Yang, J. T. Hupp and F. Huo, *Nat Chem*, 2012, **4**, 310-316.

275. Z. Li and Y. Zhang, *Angew. Chem.*, 2006, **118**, 7896-7899.

276. Y. Sun and Y. Xia, *Science*, 2002, **298**, 2176-2179.

277. R. Si, Y. W. Zhang, L. P. You and C. H. Yan, *J. Phys. Chem. B.*, 2006, **110**, 5994-6000.

278. Y. Zhang, Y. Jia, M. Li and L. a. Hou, *Sci. Rep.*, 2018, **8**, 9597.

279. D. N. Ta, H. K. D. Nguyen, B. X. Trinh, Q. T. N. Le, H. N. Ta and H. T. Nguyen, *Can. J.Chem. Eng.*, 2018, **96**, 1518-1531.

280. J. Cravillon, R. Nayuk, S. Springer, A. Feldhoff, K. Huber and M. Wiebcke, *Chem. Mater.*, 2011, **23**, 2130-2141.

281. M. Jian, B. Liu, R. Liu, J. Qu, H. Wang and X. Zhang, *RSC Advances*, 2015, **5**, 48433-48441.

282. A. Parulkar and N. A. Brunelli, *Ind. Eng. Chem. Res.*, 2017, **56**, 10384-10392.

283. N. K. Maddigan, A. Tarzia, D. M. Huang, C. J. Sumby, S. G. Bell, P. Falcaro and C. J. Doonan, *Chem. Sci.*, 2018, **9**, 4217-4223.

284. R.-B. Lin, Y. He, P. Li, H. Wang, W. Zhou and B. Chen, *Chem. Soc. Rev.*, 2019, **48**, 5, 1362-1389.

285. J. Snijder, O. Kononova, I. M. Barbu, C. Uetrecht, W. F. Rurup, R. J. Burnley, M. S. Koay, J. J. Cornelissen, W. H. Roos and V. Barsegov, *Biomacromolecules*, 2016, **17**, 2522-2529.

286. W. F. Rurup, J. Snijder, M. S. T. Koay, A. J. R. Heck and J. J. L. M. Cornelissen, *J. Am. Chem. Soc.*, 2014, **136**, 3828-3832.

287. W. Honig and M. R. Kula, *Anal. Biochem.*, 1976, **72**, 502-512.

288. K. R. Yamamoto, B. M. Alberts, R. Benzinger, L. Lawhorne and G. Treiber, *Virology*, 1970, **40**, 734-744.

289. J. T. Lis, *Methods Enzymol.*, 1980, **65**, 347-353.

290. A. Llauro, D. Luque, E. Edwards, B. L. Trus, J. Avera, D. Reguera, T. Douglas, P. J. Pablo and J. R. Caston, *Nanoscale*, 2016, **8**, 9328-9336.

Appendix

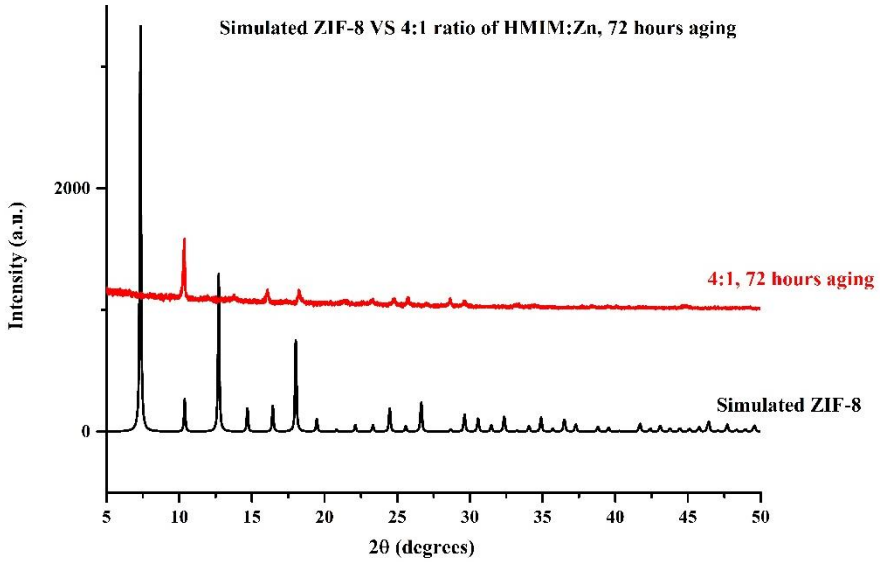

Figure A. 1 PXRD patterns of the simulated ZIF-8 (black) vs the crystals obtained through encapsulation of Bm3TE with 4:1 molar ratio of HMIM:Zn, after 72 hours aging (red).

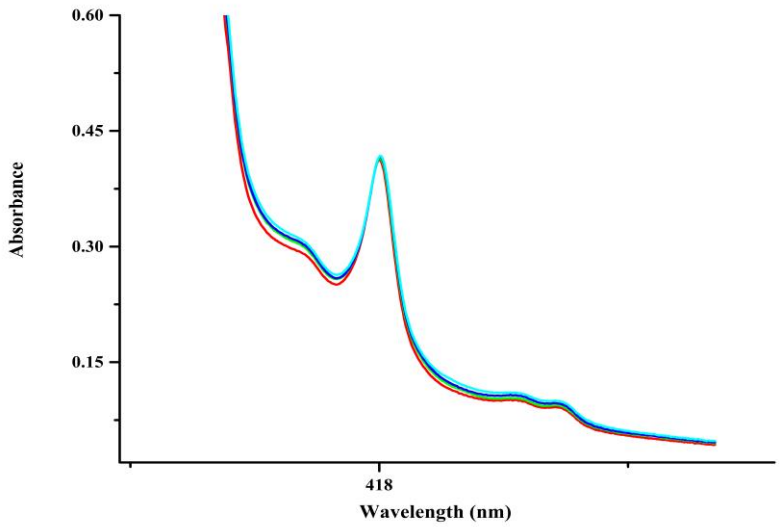

Figure A. 2 Spin state shift of P450Bm3TE in the presence of HMIM (160 mM)